Optimization of rAAV mediated targeted suicide gene therapy,

rAAV manufacturing and downstream processing

Dissertation

Zur Erlangung des akademischen Grades

Doctor rerum naturalium (Dr. rer. nat.)

Zelluläre und Molekulare Biotechnologie

Technische Fakultät

Universität Bielefeld

vorgelegt von

Kathrin Erika Teschner

Bielefeld

2019

Die vorliegende Arbeit entstand in der Zeit von

Juni 2014 bis Juli 2019

in der Arbeitsgruppe

- Zelluläre und Molekulare Biotechnologie -

an der Technische Fakultät der Universität Bielefeld

unter Leitung von

Herrn Prof. Dr. Kristian M. Müller

1. Gutachter: Prof. Dr. Kristian M. Müller
   Arbeitsgruppe Zelluläre und Molekulare Biotechnologie,
   Technische Fakultät, Universität Bielefeld

2. Gutachter: Prof. Dr. Thomas Noll
   Arbeitsgruppe Zellkulturtechnik,
   Technische Fakultät, Universität Bielefeld

Danksagung

An erster Stelle gilt mein herzlicher Dank meinem Doktorvater Prof. Dr. Kristian M. Müller für seine wissenschaftliche und methodische Unterstützung während der gesamten Bearbeitungsphase meiner Dissertation. Deinen zahlreiche Ratschläge und fachlichen Anmerkungen, sowie das Gefühl mit jeder Frage zu dir kommen zu können haben einen ganz besonderen Beitrag zum Gelingen dieser Arbeit geleistet.

Prof. Dr. Thomas Nollmöchte ich herzlich für seine Bereitschaft bedanken meine Dissertation zu begutachten. Gleichzeitig danke ich Prof. Dr. Karl Friehs für die Übernahme des Vorsitzes der Prüfungskommission sowie Dr. Dominik Cholewa für die Bereitschaft Mitglied in meiner Prüfungskommission zu werden.

Den gesamten Mitgliedern der Arbeitsgruppe Zelluläre und Molekulare Biotechnologie danke ich für eine ganz besondere Arbeitsatmosphäre. Die vielen gemeinsamen Stunden im Labor und Büro werden unvergessen bleiben. Besonders danken möchte ich in diesem Zusammenhang Philipp Borchert, der jederzeit auch spontan meine Ideen im Labor umgesetzt und mich bei den unterschiedlichsten Experimenten unterstützt hat. An meine Labor-und Bürokollegen Rebecca Feiner, Marco Radukic, Dinh To Le, Georg Falck und Julian Teschner ein großes Danke für die gemeinsam verbrachten lustigen Stunden. Ein besonderer Dank geht an Rebecca und Marco für die Korrektur dieser Arbeit und gesondert Rebecca für die tolle Unterstützung auch neben dem Arbeitsalltag.

Der größte Dank geht an meine Familie. Mein Mann Julian, der nicht nur während der Promotion eine verlässliche Unterstützung, sondern ein toller Ehemann und Vater ist, der gerade in Zeiten intensiver Arbeit mir viel Freiräume geschaffen und unsere Kinder liebevoll betreut hat. Meinen beiden Kindern Felix und Max ein großes Dankeschön, die obwohl doch noch so klein schon Verständnis für lange Arbeitstage aufbringen und mir durch ihr Lächeln jeden Tag aufs neue Energie geben. Meinen Eltern, auf die ich mich jederzeit verlassen kann, möchte ich vom tiefsten Herzen danken. Ihr habt mich in allen Phasen meines Lebens bestärkt und unterstützt und ohne euch wären viele wunderschöne Erlebnisse nicht möglich gewesen.

Veröffentlichungen im Rahmen der Dissertation

Teschner KE, Leppin M, Teschner J, Müller KM; Generating a quick, easy and low-cost affinity purification method for rAAV based on adeno-associated virus receptor′s PKD domain, Vorlage zum Patent.

Teschner KE, Teschner J, Müller KM, Comparison of viral mediated suicide gene therapy targeting by promoters and de-targeting by miRNA in tumor and primary cells, in Vorbereitung.

Feiner RC, Teschner K, Schierbaum I, Teschner J, Müller KM, AAV production in suspension: evaluation of different cell culture media and scale-up potential. *BMC Proceedings* 12 (Suppl 1):P-349, (2018) doi: 10.1186/s12919-018-0097-x.

Feiner RC, Teschner J, Teschner KE, Radukic MT, Baumann T, Hagen S, Hannappel Y, Biere N, Anselmetti D, Arndt KM, Müller KM, rAAV engineering for capsid-protein enzyme insertions and mosaicism reveals resilience to mutational, structural and thermal perturbations. IJMS (2019) eingereicht.

Feiner RC, Teschner KE, Teschner J, Müller KM, HEK293-KARE1, a cell line with stably integrated adenovirus helper sequences simplifies rAAV production. BMC Biotechnology (2019), eingereicht.

Poster

Feiner RC, Schlicht K, Teschner J, Arndt KM, Müller KM, Recombinant Adeno-associated virus (rAAV) for tumor therapy: engineering of capsid and genetic modifications. 67. Mosbacher Kolloquium - "Protein Design: From First Principles to Biomedical Applications", Mosbach, 30.03.2016 - 02.04.2016.

Feiner RC, Teschner K, Schierbaum I, Teschner J, Müller KM, AAV production in suspension: Evaluation of different cell culture media and scale-up potential. 25th ESACT Meeting: Cell technologies for innovative therapies, Lausanne, 14-17.05.2017.

Feiner RC, Teschner K, Teschner J, Scheiner O, Müller KM, Recombinant adeno-associated virus for tumor therapy – capsid and genetic engineering. 4th Global Synthetic Biology & Gene Editing, London, 04.-05.12.2017.

Teschner J, Feiner RC, Teschner KE, Radukic MT, Hertle Y, Biere N, Anselmetti D, Müller KM, "rAAV2 capsid protein modification, expression and stability", DECHEMA, Frankfurt am Main, "Gene Therapy – Ready for the Market?", 30-31 January 2019

Contents

List of abbreviations

5-FC	5-fluorocytosine
5-FU	5-fluorouracil
AA	arachidonic acid
AAP	assembly activating protein
AAV	adeno-associated virus
AAVR	Adeno-associated virus receptor
AAVS1	Adeno-associated virus integration site 1 (AAV safe-harbor locus)
ABTS	2,2'-azino-bis(3-ethylbenzothiazoline-6-sulphonic acid)
AD5	Adenovirus type 5
AFM	Atomic force microscopy
AFP	alpha fetal protein
AGO2	Argonaute protein 2
APS	Ammonium persulfate
ATP	Adenosine triphosphate
bp	base pair
BSA	bovine serum albumin
bsd	blasticidin deaminase
CCKAR	cholecystokinin type A receptor
CEA	carcinoma embryonic antigen
CHAPS	3-[(3-Cholamidopropyl)dimethylammonio]-1-propanesulfonate hydrate
CMV	Cytomegalovirus (promoter)
COX-2	cyclooxygenase-2 (promoter)
CRISPR/Cas9	Clustered Regularly Interspaced Short Palindromic Repeats/CRISPR-associated protein 9
cryo-EM	cryogenic electron microscopy
CV	column volume
Cx	Connexin protein
CXCR-4	chemokine receptor 4 (promoter)
Da	Dalton
DARPin	designed ankyrin repeat proteins
dGTP	deoxyguanosine triphosphate
DMSO	Dimethyl sulfoxide
DNA	deoxyribonucleic acid
dNTP	deoxyribonucleotide triphosphate
DTT	Dithiothreitol
DVS	divinyl sulfone
EDTA	Ethylenediaminetetraacetic acid
eGFP	enhanced green fluorescent protein
EGFR	epidermal growth factor receptor
ELISA	enzyme-linked immunosorbent assay

FACS	fluorescence activated cell sorting
Fc	fragment crystallizable
FCS	Fetal Calf Serum
FDA	(U.S.) Food and Drug Administration
FGFR-1	fibroblast growth factor 1
FRT	Flippase Recognition Target (flipase recombinase recognition site)
FS	feed solution
FSC	forward scatter diode
gc	genomic copies
GCV	Ganciclovir
GCV-DP	GCV diphosphate
GCV-MP	GCV monophosphate
GCV-TP	GCV triphosphate
GJIC	gap junctions
GMK	guanylate kinase
HDFa	adult human dermal fibroblasts (cell line)
HEK-293	human embryonic kidney 293 (cell line)
HEK-F	human embryonic kidney 'Freestyle' (cell line)
HeLa	Henrietta Lacks (cell line)
HEPES	4-(2-hydroxyethyl)-1-piperazineethanesulfonic acid
HER2	human epidermal growth factor receptor 2
HGFR	hepatocyte growth factor
hGH	human growth hormone
His_6	polyhistidine-tag
HRP	horseradish peroxidase
HSPG	heparan sulfate proteoglycan
HSV	herpes simplex virus
HSV-tk	herpes simplex virus thymidine kinase
HSV-tk30	herpes simplex virus thymidine kinase (clone number 30)
hTERT	human telomerase reverse transcriptase
IAP	inhibitor of apoptosis
IgG-Fc	Immunoglobulin G-fragment crystallizable
IMAC	immobilized metal ion affinity chromatography
IPTG	Isopropyl β-D-1-thiogalactopyranoside
ITR	inverted terminal repeats
kb	Kilo bases
kDa	Kilo Dalton
KDR	kinase insert domain receptor
LamR	laminin receptor
LB (liquid/solid) medium	lysogeny broth (liquid/solid) medium
M1FS	human fibroblasts from foreskin (cell line)

mAB	monoclonal antibody
mAU	milli absorbance units
MBP	Maltose-binding protein
mGMK	mouse guanylate kinase
miRNA	micro RNA
MOI	multiplicity of infection
mRNA	messenger RNA
MW	molecular weight
Nab	neutralizing antibodies
Ni-NTA	nickel (-charged) nitrilotriacetic acid (resin)
nt	nucleotides
NTA	nitrilotriacetic acid
OD_{600}	optical density at 600 nm
ORF	Open reading frame
pA	poly adenylation
PAM	protospacer adjacent motif
PBS (buffer)	phosphate buffer saline (buffer)
PCR	Polymerase chain reaction
PDB ID	Protein Data Bank Identity
PEG	polyethylene glycol
PEI_{max}	Polyethylenimine (max)
PG	prostaglandin
PKD2	polycystic kidney disease 2
PLA2	harbors phospholipase A2
pri-miRNA	long precursor RNA
pZMB	Plasmid from the working group of Cellular and Molecular Biotechnology
qPCR	quantitative Polymerase chain reaction
rAAV	recombinant adeno-associated virus
RISC	RNA-induced silencing complex
RNA	ribonucleic acid
ROI	region of interest
rpm	revolutions per minute
scFv	single chain variable fragment
SDS-PAGE	sodium dodecyl sulfate–polyacrylamide gel electrophoresis
SMA	spinal muscular atrophy
SMN1	*survival motor neuron 1*
SOC	Super Optimal broth with Catabolite repression
SSC	side scatter
ssDNA	single-stranded DNA
SUR	survivin (promoter)
T7	Phage T7

TAE (buffer)	Tris-acetate-EDTA (buffer)
TCD	total cell density
TEMED	Tetramethylethylenediamine
TSP	tumor-specific promoters
UC	Ultracentrifugation (UZ: german Ultrazentrifugation)
UTR	untranslated region
UV	Ultraviolet
VDEPT	virus-directed enzyme prodrug therapy
VP (1-3)	virus protein
VSV	vesicular stomatitis virus
wt	wild type
ZMB	Zelluläre und Molekulare Biotechnologie

Commonly used abbreviations and SI units are not separately listed.

1. Zusammenfassung

Rekombinante adeno-assoziierter Viren (rAAV) weisen aufgrund ihrer geringen Immunogenität, hohen Stabilität und langfristigen Genexpression in Zielzellen ein großes Potential für den Einsatz in der Gentherapie auf. Jedoch fehlt es bisher sowohl an effizienten als auch kostengünstigen rAAV Herstellungsverfahren, um eine Erweiterung der Verwendung von rAAVs auch auf weitere medizinische Indikationen, wie zum Beispiel die Tumortherapie zu ermöglichen da hier weitaus höhere rAAV Dosen benötigt werden. Zusätzlich sind durch den breiten Tropismus des AAV schädliche Auswirkungen in einer Tumorgentherapie mit einem letalen Transgen auch auf gesunde Zellen zu erwarten. Daher wurde in dieser Arbeit der Einsatz von tumorspezifischen Promotoren (TSP) und mikroRNA (miRNA) Zielsequenzen analysiert, um eine selektive Abtötung von Tumorzellen zu erreichen. Darüber hinaus wurden eine in diesem Labor erzeugte rAAV-Produktionszelllinie, eine neue Affinitätschromatographie und die Möglichkeit der rAAV-Produktion in Suspensionszellen analysiert.

Eine neue Zelllinie mit integrierten adenoviralen Helfersequenzen wurde hinsichtlich effizienter Produktion analysiert. Ein Transfektionprotokoll wurde etabliert, mit dem es möglich wurde ausschließlich das RepCap- und ein ITR/Vektor-Plasmid in die Produktionszellen einzubringen, wodurch die während der Produktion benötigte Menge an DNA um die Hälfte reduziert werden konnte. Die biologischen Eigenschaften der so produzierten rAAV sowie die Ausbeute wurden analysiert und waren vergleichbar mit Ergebnissen des Dreiplasmid-Transfektionsprotokolls in der Standard HEK-293 Zelllinie. Demnach konnte gezeigt werden, dass die neue Zelllinie rAAVs in gleichbleibender Qualität und Ausbeute produziert bei gleichzeitiger Kosten- und Zeitersparnis durch den Wegfall der Bereitstellung der sonst benötigten-Helfer-Plasmid DNA.

Die begrenzte Wachstumsfläche in dem auf adhärent wachsenden HEK-293 Zellen beruhendem Standardprozess erschwert die Bereitstellung großer Mengen an rAAV. Daher wurde in einer kommerziell erhältlichen, suspensionsadaptierten Zelllinie das für die rAAV Produktion benötigte Dreiplasmid-System etabliert und die Kultivierungsbedingungen vor und während der Transfektion optimiert, wodurch eine deutliche Erhöhung der rAAV Ausbeute verglichen zu dem Ursprungsprotokoll erzielt werden konnte. Generell konnte durch die Kultivierung der Suspensionszellen mit hoher Zelldichte eine höhere volumetrischen Ausbeute als das Verfahren auf Basis adhärent wachsender Zellen erzielt werden und eröffnet dabei die Möglichkeit den Produktionsmaßstab zu erhöhen.

Die Aufreinigung von rAAV2 durch die Verwendung der *polycystic kidney disease* 2 (PKD2) Domäne des natürlichen AAV-Rezeptors (AAVR) als Affinitätsliganden wurde etabliert. Die Analyse verschiedener Trägermaterialien zur kovalenten Bindung des Liganden wurden getestet, wobei Cellulosepapier die einfachste Handhabung ermöglichte, sowie eine hohe Reinheit und zeitgleich eine hohe rAAV Ausbeute erzielt werden konnte. Die biologische Aktivität der so

aufgereinigten rAAVs war vergleichbar mit solchen die mittels Ultrazentrifugation (UZ) aufgereinigt wurden. Jedoch konnte mit der entwickelten Affinitätschromatographie eine deutlich höhere Reinheit der Endprobe bei gleichzeitiger Reduktion der Arbeitszeit von mehr als einem Tag für die UZ-Reinigung auf wenige Stunden für die Affinitätschromatographie erzielt werden, u.a. durch den Wegfall des der UZ vorgeschalteten Ankonzentrierungsschrittes.

Die Vorteile von TSP und miRNA vermitteltem De-targeting in einer virusgesteuerten Enzym-Prodrug-Therapie (VDEPT) wurden untersucht. Als Selbstmordgen wurde das Thymidinkinasegen (HSV-*tk*) des Herpes-Simplex-Virus verwendet und die Umwandlung des prodrugs Ganciclovir (GCV) in seinen toxischen Metaboliten indirekt durch einen Zytotoxizitätstest gemessen. Die Aktivität von drei zuvor als tumorspezifischen beschriebenen Promotoren (Survivin (SUR), Cyclooxygenase-2 (COX-2) und C-X-C-Motiv Chemokin-Rezeptor 4 (CXCR-4)) wurde mit der Aktivität des Cytomegalievirus *immediate early* promoters (CMV) in vier Tumor- und zwei gesunden Zelllinien verglichen. Für die SUR- und CMV-promotorgetriebene Expression des Suizidgens wurde zusätzlich die let-7a miRNA-Zielsequenz in die Transgenexpressionskassette integriert. Je nach betrachteter Zelllinie konnte eine Tumorspezifität der TSP nachgewiesen werden, wobei mit der vom CMV Promotor getriebene Genexpression in Kombination mit der let-7a miRNA-Zielsequenz eine hohe Tumorspezifität in allen untersuchten Krebszelllinien erreicht werden konnte.

Die Ergebnisse dieser Studie bilden die Grundlage für weitere Verbesserungen des rAAV-Produktionsprozesses und zeigen zusätzliche Strategien zur Erzielung einer Tumorspezifität in VDEPT-Ansätzen. So könnte in Zukunft eine Adaption der neuen rAAV-Produktionszelllinie an die Kultivierung in Suspension, sowie weitere Kombinationen von CMV-Promotor-gesteuerter Genexpression mit unterschiedlichen miRNA-Zielsequenzen getestet werden. Darüber hinaus sollte zusätzlich transkriptionelles Targeting und miRNA-vermitteltes De-Targeting mit Tumormarker-basiertem Re-Targeting kombiniert werden, um in Zukunft eine noch spezifischere Suizidgentherapie zu ermöglichen.

2. Abstract

Recombinant adeno-associated viruses (rAAV) have gained an outstanding reputation in gene therapy due to their low immunogenicity, high stability and long-term gene expression in target cells. However, there is a lack of efficient and cost-effective manufacturing processes to enable the expansion of AAVs into therapeutic indications such as tumor therapy where higher doses are needed. Additionally, in tumor therapy, the broad tropism of the AAV is problematic since harmful effects on healthy cells can be expected during cancer gene therapy with lethal transgenes. In this work, the use of tumor-specific promoters (TSPs) and microRNA (miRNA) target sequences have been analyzed to allow selective eradication of tumor cells. Moreover, the use of a rAAV production cell line generated in our laboratory, a new affinity chromatography and the possibility of rAAV production in suspension cells have been analyzed.

For efficient rAAV production, a new cell line with integrated adenoviral helper sequences was analyzed during this work. Providing a RepCap and an ITR/vector plasmid during transient transfection was established, leading to a significant reduction in the amount of plasmid DNA required for production. Biological characteristics and the yield were analyzed and were comparable to those obtained with the triple transfection protocol in the HEK-293 standard cell line. This result demonstrates that the new producer ensures constant quality of viral particles produced while reducing costs and time, as providing of the helper plasmid is no longer required.

Upscaling of the production is very restricted due to the limited growth area in the standard adherent growing HEK-293 cells. Therefore, a triple transfection protocol for the rAAV production was established, in a commercially available suspension adapted cell line and the medium conditions for cell propagation and production were adjusted and resulted in a protocol with increased yields compared to the starting conditions. The high cell density cultivation in the suspension-based process led to a higher volumetric yield than the process based on adherent growing cells and at the same time allows for up-scaling.

The use of single domains of the natural AAV receptor (AAVR) as an affinity ligand for rAAV purification was established in this work. Different carrier materials for covalent binding were tested, with cellulose paper showing the best characteristics regarding the ease of handling as well as final purity and yield of the rAAV sample. The biological activity of rAAV purified by this affinity chromatography was comparable to those purified by the standard ultracentrifugation (UC) method but with a superior purity. Furthermore, the processing time was reduced from more than one day for UC purification to a few hours for the affinity chromatography, since the affinity chromatography was optimized for the application of directly capturing rAAVs from the crude cell extract contrary to UC purification where a concentrating step is necessary.

The benefits of TSPs and miRNA mediated de-targeting in a virus-directed enzyme prodrug therapy (VDEPT) were investigated in this work. As a suicide gene, the herpes simplex virus thymidine

kinase (HSV-*tk*) was used, and the conversion of the prodrug Ganciclovir (GCV) to its toxic metabolite was indirectly measured by a cytotoxicity assay. The activity of three tumor-specific promoters (survivin (SUR), cyclooxygenase-2 (COX-2) and C-X-C motif chemokine receptor 4 (CXCR-4)) was compared to the cytomegalovirus immediate early promoter (CMV) in four cancer and two healthy cell lines. For SUR and CMV promoter driven HSV-tk expression, a let-7a miRNA target sequence was included. Depending on the cell line investigated, tumor specificity was enabled, with the CMV promoter driven gene expression in combination with the let-7a miRNA target sequence reaching, the highest tumor specificity in all investigated cancer cell lines.

The results of this study provide a starting point for further improvements of the rAAV manufacturing process and strategies for de-targeting of healthy cells in VDEPT approaches. For example, an adaption of the new rAAV production cell line to suspension and combinations of CMV promoter driven gene expression with distinct miRNA target sequences could be tested. In addition, combinations of transcriptional targeting and miRNA mediated de-targeting should be tested together with tumor marker-based re-targeting of rAAVs, which may enable more specific suicide gene therapy in the future.

3. Introduction

3.1. Biology of adeno-associated viruses

The adeno-associated virus is a single-stranded DNA virus and belongs to the family of parvoviruses. Even though most humans show a high seroprevalence of neutralizing antibodies (NAb) for at least one serotype, AAV has not been associated with any human or animal disease.[1,2] The 4.7 kb genome contains three open reading frames (ORFs) which are flanked by inverted terminal repeats (ITRs) (Figure 1). The T-shaped palindromic ITRs are 145 bases long and serve as origins for DNA replication. They are the only *cis*-acting elements and are required for packaging, integration and rescue of the AAV genome, while all other viral sequences are supplied *in trans*.[3] The four Rep proteins (Rep78, Rep 68, Rep52, Rep40) responsible for replication, are located in the left ORF and are synthesized from mRNAs initiated from the p5 and p19 promoter. Rep78 and Rep68 are required for DNA replication, whereas Rep52 and Rep40 are necessary for packaging DNA into the AAV capsid.[4–6]

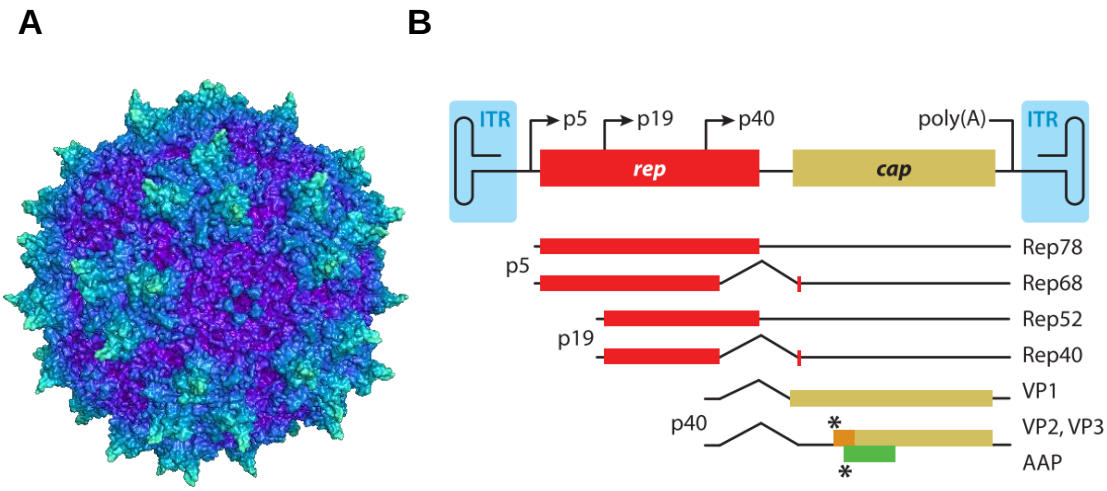

Figure 1: Representation of the surface and of the AAV genomic structure.(A) Surface structure of AAV2 based on the PDB-ID (Protein Data Bank Identity) 1LP3 using PyMOL. Amino-acids are colored by their relative distance to the center from dark blue in the center to cyan. The 5-fold axes are located in the center of the dark blue canyon. The cyan colored protrusions are surrounding the 3-fold axes in the center. (B) AAV genomic structure. The open reading frame for the four Rep proteins is colored in red. Expression is driven by the p5 promoter for Rep78, Rep68 and from p19 promoter for Rep52, Rep40.[5,6] The open reading frame for the Cap proteins is colored in beige. The p40 promoter drives the expression of the mRNA which is then alternatively spliced and by this generating the three capsid proteins VP1, VP2 and VP3.[7] A third ORF in the VP2/VP3 mRNA codes for the assembly activating protein (green) and the x protein (not shown).[8,9] Asterisks marks the VP2 start codon and the AAP start codon. Inverted terminal repeats are highlighted in blue. Figure 1B adopted from Samulski, R. J.; Muzyczka, N., 2014.[10]

The right ORF encodes the three capsid proteins VP1, VP2 and VP3 whose expression is initiated by the p40 promoter from one single gene. By alternative splicing, the VP1 and the VP2/VP3 containing transcript arise.[7,11] The shorter VP2/VP3 mRNA codes for VP3 from a conventional initiation codon (AUG) and for VP2 by a weak noncanonical ACG start codon upstream of the VP3

start. As a result, VP1, VP2 and VP3 proteins have the same *C*-terminus and only differ from each other in their *N*-terminus with VP1 being the largest and VP3 the smallest protein.[12] The additional *N*-terminal sequence of VP1 harbors phospholipase A2 (PLA2) activity and nuclear localization signals which are also located inVP2 N-terminus. These sequences are conserved among all AAV serotypes and are required for the translocation of the AAV genome to the nucleus.[13,14] From a weak noncanonical CTG start codon in the VP2/VP3 mRNA, a third ORF is located, which codes for the assembly activating protein (AAP). AAP plays an essential role in the assembly of the viral capsid for some serotypes.[8] In the same reading frame at the 3'-end of AAV2, the sequence of the x gene was found and the transcript is supposed to support AAV DNA replication.[9]

To assemble the 25 nm sized icosahedral capsid shell, a total of 60 proteins are required. The stoichiometry of V1, VP2 and VP3 in AAV particles of 1:1:10 is thought to be the consequence of the relative abundance of the proteins caused by splice product abundance and the efficiency of translation initiation at the different start codons.[15] After capsid assembly, the AAV DNA is selectively encapsulated by protein-protein interactions between the pre-formed empty capsid and Rep78/ Rep68 which are complexed with the newly synthesized AAV DNA.[16,17] The capsid shell is the main determinant of AAV tropism and transduction characteristics and several naturally occurring AAV variants were discovered.[18] Depending on the capsid serotype, different cellular receptors and co-receptors are necessary for AAV transduction.

In the past, AAV2 has been extensively studied and heparan sulfate proteoglycane (HSPG) was found to be the primary receptor for initial cell membrane binding.[19] The basic amino acids R484, R487, K532, R585 and R588 (VP1 numbering) in the three-fold spike region of the capsid interact through electrostatic interactions with the negatively charged sulfate and carboxyl groups of the abundantly expressed HSPG. In the multistep infectious entry pathway fibroblast growth factor 1 (FGFR-1)[20], hepatocyte growth factor (HGFR)[21], 37/67 kDa laminin receptor (LamR)[22] and integrins (α5β1 and αvβ5)[23,24] were identified as secondary receptors which stabilize virus attachment or participate during internalization.[25] Further processes include receptor-mediated endocytosis via the formation of clathrin-coated pits and endosomal escape through a pH-dependent process by inducing a conformational change, leading to the exposure of PLA2.[14,26] Upon entry into the nucleus, AAVs can either follow the lytic or lysogenic pathway. In the absence of a helper virus, the AAV genome integrates specifically in human chromosome 19 designated as AAV safe-harbor locus (AAVS1).[27,28] The integrated genome can then be rescued from the latent infection by superinfection with helper virus which induces expression of AAV Rep and Cap genes *in trans.*[29]

In 2016, a new cellular factor, the so-called AAVR was identified.[30] In a haploid genetic screen, the KIAA0319L gene showed to be essential for multiple AAV serotypes for efficient transduction. KIAA0319L codes for a type I transmembrane protein containing a motif at *N*-terminus with eight cysteines (MANEC domain), five Ig-like poly-cystic kidney disease (PKD) domains, and a C6 re-

gion near the *N*-terminus (Figure 2A).[31] The AAVR is a *N*-linked glycosylated protein, but glycosylation is not required for AAV binding or functional transduction. Dominant interactions of certain domains with specific serotypes have been described. AAV2 interacts predominantly with the second PKD domain, whereas PKD1 promotes transduction for AAV5. For AAV1 and AAV8 a combination of PKD1 and PKD2 is necessary for optimal transduction.[32] By cryogenic electron microscopy (cryo-EM) the interaction of AAV2 with the AAVR was shown and the interacting amino acids bound to the capsid were identified as belonging to AAVR PKD2. One AAVR PKD2 interacts with the right edge of the spike which surrounds the icosahedral three-fold axis, making contact with two AAV2 capsid protomers (Figure 2B,C).[33] For the other AAV serotypes, interaction with the AAVR has not been clarified so far.

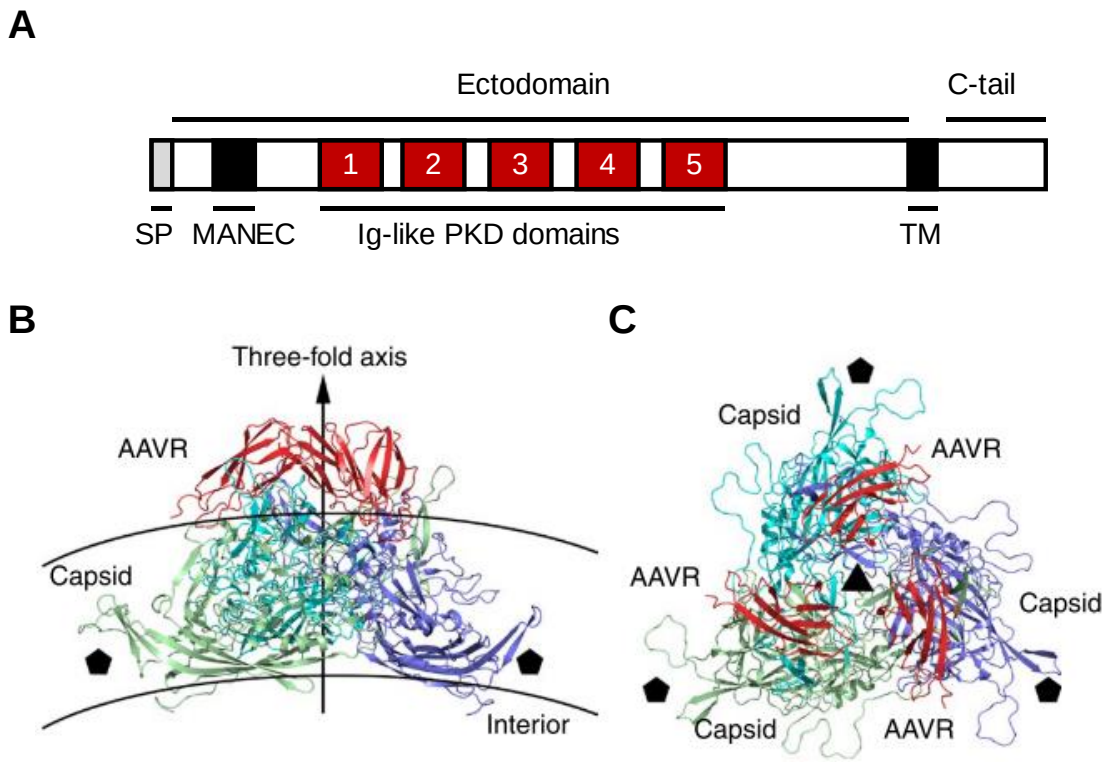

Figure 2: Schematic view of the AAVR domains and their interaction with the AAV2 capsid. (A) The domains of the KIAA0319L protein. (B, C) Structure of trimeric AAV2 protomers in complex with AAVR from the side (B) and from the top (C). The protomers are shown blue, green and cyan, the AAVR is shown in red. The five-fold axes are indicated by pentagons and the triangle indicates the three-fold axis.
SP, signal peptide; MANEC, motif with eight cysteines; TM, transmembrane. Figure 2A: modified from Pillay et al. 2016.[30] *Figure 2B, C: Adopted from Zhang et al. 2019.*[33]

3.2. Cancer gene therapy

Cancer is one of the leading causes of death in the world. In 2018, 18.1 million new cases and 9.6 million deaths worldwide were estimated.[34,35] The clinical effectiveness of conventional chemo- and radiotherapy is limited due to a lack of tissue specificity, which causes serious side effects. Gene therapy offers the possibility to target a therapeutic transgene directly to tumor cells so that normal tissue toxicity might be avoided. So far, gene therapy has mainly referred to the transfer of

human normal genes or therapeutically interesting genes into human target cells, to correct gene defects.[36] By now, gene therapy is also being researched for the treatment of a variety of other diseases including cancer, cardiovascular disease, and neurodegenerative diseases with cancer as the most frequent clinical trial representative.[37] Regardless of the disease to be treated, the transport of a transgene into target cells is required.

For this purpose, viral and non-viral vectors are available.[38] Transfection of non-viral vectors into cells can be accomplished with physical methods like electroporation of naked DNA and chemical-mediated transfer for example with cationic liposomes.[39,40] Their advantages of safety and modifiability as well as simple large-scale production offset the disadvantages of low transfection efficiency and low transgene expression. In contrast, viral vectors own the highly evolved mechanism of the parental viruses to efficiently transduce cells with prolonged gene expression and by this offer advantages over non-viral delivery systems. Despite challenges in the introduction of modifications, the majority of clinical studies are conducted with viral vectors.[37] Here, adenoviruses are the most commonly used vectors, followed by retrovirus, lentivirus and adeno-associated virus. Most of them trigger extensive immune responses to the vector, or randomly integrate into the host cell genome with the risk of insertional mutation.[37,38] The adeno-associated virus emerged as an outstanding option for gene therapy. It provides long-term target gene expression, is not associated with any disease and is unable to replicate autonomously which results in a high safety profile. They transduce a wide range of dividing and non-dividing cells and are able to penetrate the stroma of solid tumors due to their small size, which ensures adequate distribution of the transgene throughout the tumor.[41,42] Until today, seven gene therapies although not in the field of tumor therapy, have received approval, with three based on AAV. The latest, *onasemnogene abeparvovecxioi* (Zolgensma) was approved in 2019 by the U.S. Food and Drug Administration (FDA) and is based on rAAV9. It delivers a functional variant of the *survival motor neuron 1 (SMN1)* gene and is used to treat children less than two years old with spinal muscular atrophy (SMA) with bi-allelic mutations.

3.3. Capsid engineering of AAV in cancer gene therapy

AAVs offer the potential to serve as a gene delivery vehicle for cancer gene therapy. Systemic application of AAV allows for targeting of the primary tumor and metastases but requires a strict control of gene expression to prevent harm to normal tissue.[43] A number of natural AAV serotypes, which differ in their tropism, provide optimal transduction for particular cell types. Though, challenges in the use of AAV vectors remain. The use is limited by prior exposure of most people to natural AAVs and by this a reduction of vector delivery efficiency by anti-AAV neutralizing antibodies, as well as poor vector bio distribution to important tissue targets and limited spread within those tissues. Therefore, great effort in the engineering of AAV capsids as well as the engineering of genetic cargos has been made.[44]

The amino acid sequence of the proteins that constitute the viral capsid determines the tropism of AAV vectors. Thus, engineering the capsid can generate novel AAV phenotypes with higher potency and selective expression. Such vector engineering efforts can be grouped into two categories: directed evolution, and rational design of the capsid proteins.[45]

Directed evolution offers the possibility to generate enhanced AAV variants, even without knowledge of viral structure function. Here, large libraries of AAV cap genes are created by methods like DNA shuffling, random point mutagenesis and random peptide insertions.[46–48] In a suitable number of selection rounds, optimized AAV vectors with altered tissue tropism, enhanced tissue spread and infection of non-permissive cells are isolated.[49,50] Directed evolution therefore potentially enables the development of new AAV vectors for improved gene transfer.

In cancer gene therapy, changes in the expression profile of degenerated cells and the associated presentation of tumor-specific antigens on the cell surface allows for a rational design of AAV capsid proteins.[51,52] In 2008, Zhong *et al.* showed that mutations of surface exposed tyrosine residues on AAV2 capsids towards phenylalanine resulted in high-efficient transduction of cells.[53] By site-directed mutagenesis of AAV2 serine, threonine and lysine residues Gabriel *et al.* were able to show optimized transduction efficiency and higher packaging titer.[54] To obtain not only a general improvement in transduction efficiency but also increased tumor specificity, peptide motifs were introduced into the AAV capsid. By introducing an NGR peptide motif into the AAV2 capsid, Grifman *et al.* changed the tropism from HSPG to CD13, a membrane-bound enzyme strongly expressed in tumor tissue.[55] Also RGD peptides have been successfully incorporated into surface-exposed VP areas to target integrin expressing cancer cells.[56]. By insertions of larger binding proteins e.g. designed ankyrin repeat proteins (DARPins), variants of known AAV serotypes have been produced to ensure greater cell specificity.[57,58] Transcriptional control of transgene expression can further increase targeting efficiency. This can prevent toxicity to normal cells and will be an essential part of systemic cancer therapy.[43,59]

3.4. Payload engineering for cancer-specific gene expression

The key factors for successful application of gene therapy in the treatment of cancer lie within its targeting efficiency and safety. In addition to tissue specificity, AAV vectors may have regulatory elements which can be used to achieve a tumor-specific gene expression and by this reducing the damage to normal cells. One of these regulatory elements is the promoter, located near the transcription start sites of genes, upstream on the DNA 5' region of a gene. Promoters are DNA sequences that direct accurate initiation of transcription by the RNA polymerase II machinery.[60] Conventionally, the CMV promoter is used to drive transgene expression. However, the CMV promoter but is ubiquitously active and by this of limited use to increase vector specificity, as it can cause serious side effects in normal human cells. In the past, genes have been identified which are turned

on or are upregulated in certain types of tumors and by this attracted attention in cancer gene therapy. Promoters of such upregulated genes are ideal candidates for the use in tumor-specific gene expressions and were extensively studied in the past. Examples of previously studied promotors are shown in Table 1.

Table 1: Promoters used in cancer gene therapy with their advantages and disadvantages.

Promoter	Target	Advantages	Disadvantages
hTERT[61,62]	lung cancer, liver cancer, gastrointestinal cancer, breast cancer, etc.	suitable for a variety of cancer cells	varying outcome
KDR[63,64]	lung cancer, liver cancer, gastrointestinal cancer, breast cancer, etc.		
Survivin[65–67]	liver cancer, gastrointestinal cancer, gallbladder cancer, etc.		
HER2[68,69]	prostate cancer, breast cancer, pancreatic cancer, etc.		
COX-2[70–72]	colorectal cancer, endometrial cancer, breast cancer, etc.		
CXCR-4[73,74]	breast cancer, skin cancer		
CCKAR[75,76]	pancreatic cancer	effect on specific tumor is relatively certain	only for specific tumors
AFP[77,78]	liver cancer		
CEA[79,80]	gastrointestinal cancer		

AFP, alpha fetal protein; CCKAR, cholecystokinin type A receptor; CEA, carcinoma embryonic antigen; COX-2, cyclooxygenase 2; CXCR-4, C-X-C chemokine receptor 4; HER2, human epidermal growth factor receptor 2; hTERT, human telomerase reverse transcriptase; KDR, kinase insert domain receptor

Depending on the type of cancer, different genes are overexpressed due to their upregulated promoters. Thus, these promoters offer the possibility to increase specificity of transcriptional regulation in therapy approaches. The telomerase reverse transcriptase (TERT) promoter serves as an example, approximately 90% of human cancers show TERT activity, which is considered to be a critical step in cancer progression due to its role in cellular immortalization.[81] The hTERT promoter has therefore widely been used as a cancer-specific promoter but often showed weak transcriptional activity.[82]

Next to promoters like CCKAR, AFP and CEA which are targeting specific tumor cells, there are also promoters that can be widely used for various tumors. One of these, is the promoter of survivin gene (*BIRC5*). Survivin belongs to the inhibitor of apoptosis (IAPs) family, which have an important role in the regulation of programmed cell death. Survivin is expressed during mitosis and is essential for the completion of various stages of cell division. Inhibition of the intrinsic (mitochondrial) pathway of apoptosis via interference with caspase-9 processing, allows survivin to contribute to the inhibition of apoptosis.[83,84] Compared to normal human tissue, the survivin expression is highly upregulated in several cancer types like breast, colorectal, melanoma, pancreatic and non-small-cell lung cancer.[85] Here it is involved in the critical determinants of tumor progression such

as cell proliferation, evasion of apoptosis, resistance to growth-inhibitory signals and angiogenesis.[86] Transgene expression based on plasmid transfection or adenovirus transduction, had shown that the survivin promoter was predominantly achieved in tumor cells *in vitro* and *in vivo*.[85,87,88]

Other promising promoters in the context of cancer gene therapy are the COX-2 and the CXCR-4 promoter. The cyclooxygenase (COX) isoenzymes catalyze the metabolism of arachidonic acid (AA) to prostaglandin (PG).[89] Three isoforms of Cyclooxygenases have been identified. COX-1 is constitutively expressed and plays a role in tissue homeostasis by modulating several cellular processes. COX-2 expression is induced by growth factors and cytokines during inflammation and modulates cell proliferation, cell death, and tumor invasion in many types of cancer including colon, breast, and lung, but it is rarely detected in most normal adult tissues.[70] In 2009, Wang *et al.* showed that adenoviral expression of the HSV-*tk* gene under the transcriptional control of COX-2 promoter induced a significant *in vitro* and *in vivo* growth inhibition of cancer cells.[72] Furthermore, Yamamoto *et al*. demonstrated selective killing of COX-2 positive cells in the context of adenoviral transduction.[71] CXCR-4 is a chemokine receptor which is highly expressed in cancer cells, but repressed in normal tissue. For example, in tumor cells from breast, prostate, pancreatic, lung and ovarian carcinomas, CXCR-4 overexpression was detected. Chemokines belong to the family of cytokine-like proteins, which play an important role in cytoskeletal rearrangement, adhesion to endothelial cells and directional migration.[90] In tumor cells they regulate the growth of primary and metastatic tumors through chemokine gradients.[91] In the context of AAV2 and adenoviral gene transfer, it had been shown that expression of the transgene was preferential achieved in tumor cells.[73,74,92]

An additional layer of tumor specificity is advisable as residual activity of tumor-specific promoters in normal human cells was observed.[93,94] Post-transcriptional repression of transgene expression has been an emerging approach to improve vector targeting. MicroRNAs (miRNAs) are single-stranded, non-coding RNA molecules that anneal with complementary sequences in the 3'- UTR of target mRNAs triggering either translational repression or mRNA degradation.[95] As depicted in Figure 3, the ~ 22 nucleotide (nt) long mature miRNAs are transcribed by RNA-polymerase II as long precursor RNAs (pri-miRNAs) which are then further processed in the nucleus and finally shortened in the cytoplasm by RNase III Endonuclease Dicer to give rise to mature miRNA. The miRNAs associate with mRNAs within a multiprotein complex of Argonaute (AGO2) proteins. This RNA-induced silencing complex (RISC) facilitates and stabilizes miRNA–mRNA interactions.[96] The sequence with which miRNAs bind their RNA targets is known as the 'seed sequence', which is typically 6–8 nt long, and is located at the 5′-end of the miRNA. The degree of complementarity determines whether RISC-mediates translational inhibition or target mRNA degradation.[97]

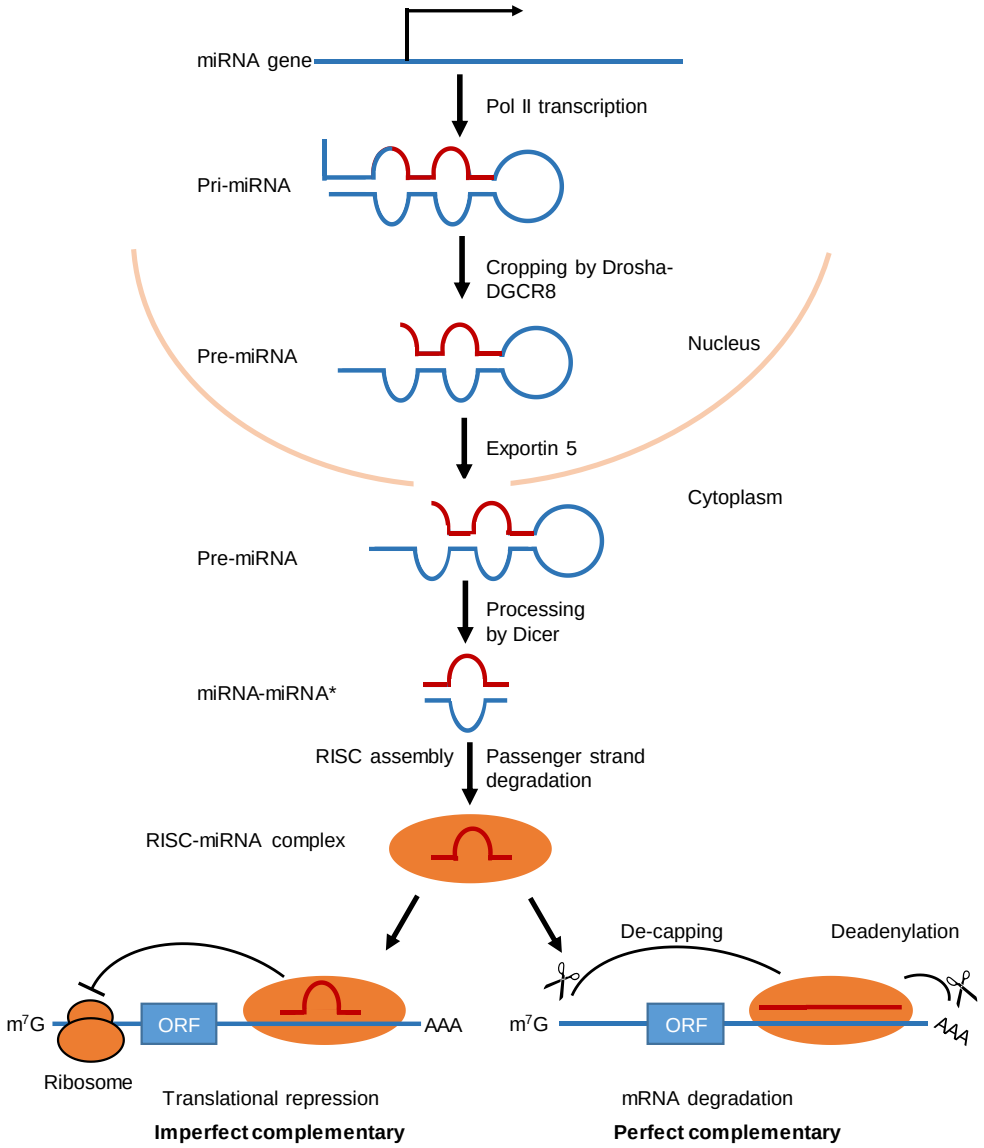

Figure 3: MicroRNA biogenesis and mechanism of action. RNA polymerase II (Pol II) generates a capped and polyadenylated transcript, the primary miRNA (pri-miRNA). The RNase III Drosha and DiGeorge syndrome critical region 8 (DGCR8)., cleaves the pri-miRNA to produce the precursor-miRNA (pre-miRNA). The pre-miRNA is exported from the nucleus into the cytoplasm by Exportin5/RanGTP, where it is further cleaved by the RNase III enzyme Dicer, which yields in an imperfect miRNA–miRNA duplex that is about 22 nucleotides in length. Finally, the 5' or 3' strand of the mature miRNA duplex is incorporated into the RNA-induced silencing complex (RISC). Association of a miRNA-RISC complex with its mRNA target results in translational repression as well as in degradation of the mRNA.*
m^7G, 7-methylguanosine; ORF, open reading frame. Modified from van Rooij et al..[98]

Lethal-7 (let-7) was one of the first miRNAs to be discovered. In humans, the let-7 family is composed of nine mature let-7 miRNAs which generally function as tumor suppressors and promote differentiation during development. Reduced levels of let-7 were observed in lung, breast, gastric and colon cancer.[99] This downregulation is possibly explained by a delayed or inhibited processing by Dicer and/or a failure at the Drosha-processing step.[100] The downregulation of let-7 upregulates some cell cycle regulators such as cyclin A2, cyclin D1/2 as well as Aurora A and B kinases, which results in the activation of cell cycle and by this promotes unregulated tumor growth.[101] In the past, incorporation of let-7 microRNA complementary sequences to-mediate post-transcriptional gene

silencing has proven to be an effective and tissue-specific approach to regulate gene expression. In suicide gene therapy, utilizing vesicular stomatitis virus (VSV) and adenovirus vectors, miRNA regulated gene expression prevented toxicity to normal tissue and by this can further increase the safety profile of AAV vectors in cancer gene therapy.[102–104]

3.5. Suicide gene therapy in cancer

By introducing a viral or bacterial suicide transgene to a tumor cell, activation of a non-toxic pro-drug into a toxic metabolite by the expressed transgene is enabled and elimination of targeted cells is possible. The resulting cytotoxic substance can then expand into neighboring cells and creates a so called bystander effect (Figure 4).[105]

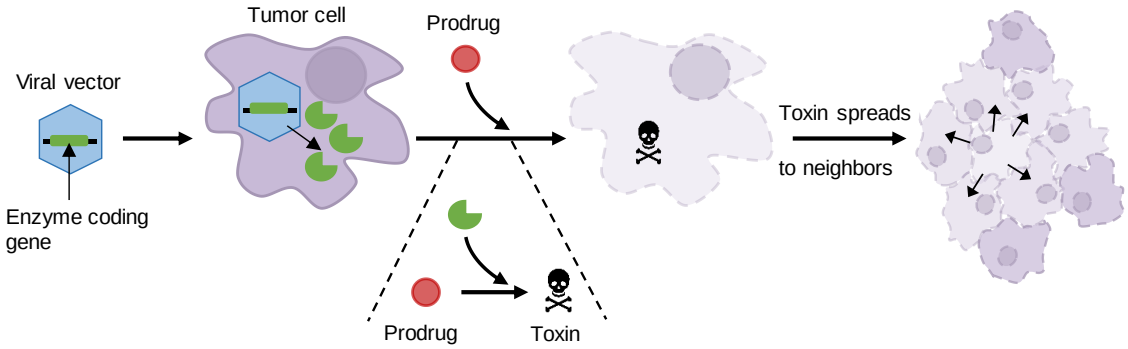

Figure 4: Schematic illustration of suicide gene therapy. Upon transduction, the transgene that codes for a prodrug-converting enzyme is expressed. Cell death is induced by local or systematic delivery of the non-toxic prodrug and the conversion of the prodrug to a toxic metabolite. The activated drug expands from the tumor cell to neighboring cells in the so called bystander effect. Modified from McCormick.[106]

For suicide gene therapy the gene for cytosine-deaminase (CD) from *E. coli* and the herpes simplex virus type 1 thymidine kinase (HSV-tk) are most commonly used. CD converts the non-toxic 5-fluorocytosine (5-FC) to 5-fluorouracil (5-FU), whereas HSV-tk converts Ganciclovir (GCV) into the metabolite GCV-monophosphate.[107] The elaborately studied HSV-tk gene/prodrug system relies on the phosphorylation of GCV to GCV monophosphate (GCV-MP) by thymidine kinase expressed in transduced tumor cells. GCV-MP is further processed by cellular guanylate kinase (GMK) to the diphosphate and by guanosine diphosphate kinase to the toxic triphosphate (GCV-TP) (Figure 5).[108,109] GCV-TP is an analogue of deoxyguanosine triphosphate (dGTP), and once bound to the DNA polymerase, inhibition of the polymerase or incorporation into the DNA is causing chain termination, S-phase delay as well as G2-phase arrest and is finally leading to apoptosis.[110–113] Limitations in the intracellular conversion pathway are located in the phosphorylation step of GCV-MP to GCV-DP by the guanosine monophosphate kinase, thus leading to the accumulation of ineffective intermediate products.[114] To overcome these limitations, a fusion protein was generated consisting of mouse guanylate kinase (mGMK) and HSV-TK30, which showed an improved turnover rate.[115] Also HSV-tk mutants with increased activity were generated which enhanced cell sensitivity to GCV by a factor of 200.[116,117]

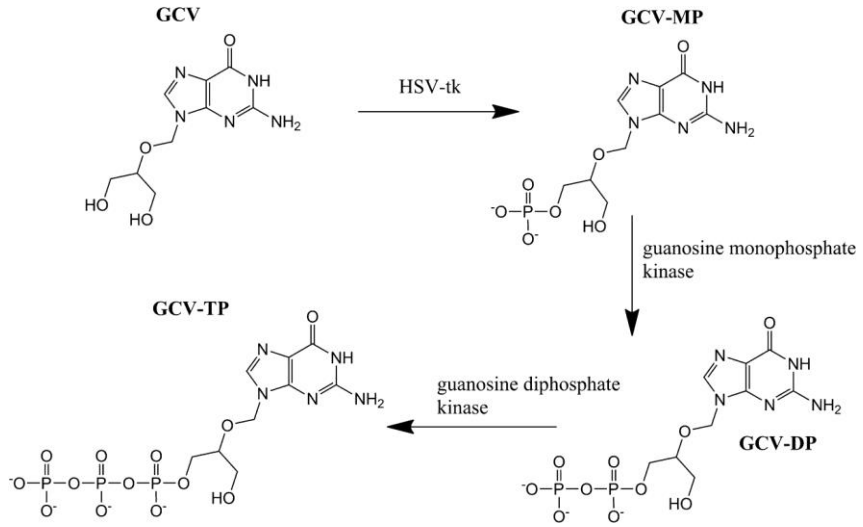

Figure 5: Structure and conversion of Ganciclovir (GCV) to GCV triphosphate (GCV-TP). HSV-tk converts GCV to GCV-MP. Subsequently, GCV-MP is further processed by cellular guanylate kinase (GMK) to the diphosphate and by guanosine diphosphate kinase to the toxic GCV-TP. Adopted from Gynther et al., 2015.[109]

The frequently observed bystander effect, where not only HSV-tk positive cells, but also neighboring cells are affected upon GCV treatment, is primarily based on cell-cell contacts. Toxic metabolites are transported between nearby cells through gap junctions (GJIC) in a process called 'metabolic cooperation'. These intercellular channels are composed of six connexin (Cx) protein subunits and form a central pore through which small molecules with a molecular weight (MW) up to 1000 Da (GCV-TP MW: 495 Da) can pass to adjacent cells.[118] Depending on cell type, other mechanisms, independent of GIJC, contribute to the bystander effect as well.[119]

4. Aim

Recombinant adeno associated virus emerged as an outstanding option in the field of gene therapy. However, the prospective success of rAAV relies on efficient and cost-effective manufacturing processes. Thus, one aim of this thesis is to simplify and optimize current rAAV up- and downstream processes.

To increase the yield and quality of viral preparations, a new rAAV producer cell line will be used for rAAV upstream processing. For this cell line, an improved rAAV production protocol will established and biological characteristics of viral particles will be determined, to achieve a time and cost advantage over the standard HEK-293 producer cells.

For further optimization of the upstream process, the production procedure will be converted to a suspension-based process to enable simple upscaling. To this end, the transfection protocol and the medium conditions will be analyzed in small batches before being transferred to a bioreactor cultivation.

In rAAV downstream processing, purification strategies suitable for future up-scale requirements are needed. Thus, an affinity chromatography based on the AAV receptor will be established. Optimal formulation of the affinity resin, amount of affinity ligand and rAAV elution conditions will be examined in order to obtain sufficient purity and biological functionality in a one-step purification process.

Analyzing transcriptional and translational targeting strategies for rAAV based suicide gene therapy will be another fundamental issue in this thesis. Different tumor-specific promoters will be examined for their ability of selective gene expression in cancerous cell lines. Additionally, a detargeting strategy by miRNA will be implemented. To analyze tumor selectivity, rAAV variants, delivering a transgene coding for a suicide gene, will be generated and upon transduction cell toxicity assays will be conducted.

5. Results and Discussion

5.1. Transcriptional and translational targeting of cancer cells

Results of this project were summarized in a manuscript with the title 'Comparison of viral mediated suicide gene therapy targeting by promoters and de-targeting by miRNA in tumor and primary cells'. The original manuscript is included in the appendix and a summary of the work is presented in the following chapter.

The regulation of transgene expression after rAAV2 transduction was one of the main goals in this work. For this purpose, the HSV-tk/GCV system was selected as a reporter. To facilitate cell killing, a HSV-tk mutant (HSV-tk30) was used which shows higher kinase activity and by this an increased GCV sensitivity.[117]

5.1.1. Choice of tumor-specific promoters, miRNA target sequence and cell lines

The promoters of survivin (SUR), cyclooxygenase-2 (COX-2) and the C-X-C motif chemokine receptor 4 (CXCR-4) were chosen to drive transgene expression. Survivin was found to be expressed in a variety of human cancers like brain, breast and ovarian tumors and to be absent in most normal tissue.[83,120] In this work, the DNA sequence related to the SUR promoter was chosen as a 521-base-pair (bp) fragment (nucleotides 2283 to 2804, GenBank Accession number U75285.1). The second promoter sequence relies on the COX-2 expression which is upregulated during inflammation and cancers like breast and colorectal cancer.[72] For the COX-2 promoter, a 904 bp fragment (nucleotides 6249 to 7152, GenBank Accession Number AF044206.1) was selected. The third promoter sequence is predicated on the overexpression of CXCR-4 gene which is typical observed in ovarian and breast cancer, as well as for human melanoma.[90,92] For CXCR-4 a 936 bp (nucleotides 1165 to 2100, GenBank Accession Number AY728138.1) fragment was designed during the master thesis of Claudia Curdt.[121] The CMV promoter in contrast shows high expression levels in a variety of mammalian cells without tumor specificity and by this leads to off-target effects in normal human tissue. This promoter was chosen as a positive control for transfection efficiency as well as for comparison of achieved protection of non-tumor cells using tumor specific promoters (TSPs). All promoters were cloned in bicistronic vector constructs by Claudia Curdt and analyzed by transient transfection approaches. Nevertheless, low promoter activities and varying transfection efficiencies were observed.

Within this work, promoters were equipped with a strong Kozak sequence in front of the start codon by overlap-extension PCR. The Kozak consensus sequence 5'-GCCRCC**ATG**G-3' (R = purine A or G), is known to enhance the initiation of translation by improving the recognition of the AUG

start codon through the pre-initiation complex (PIC) and recruitment of the large ribosomal subunit.[122,123] By this, potentially low transcription rate of chosen promoters should be compensated by improved translation.

To reduce unwanted AAV transgene expression in normal human tissue without affecting the expression in various cancer cell lines the let-7a target sequence 5'-ACTATACAACCTACTACCTCA-3' was introduced into the 3' UTR of the CMV and SUR driven transgene expression cassettes. A schematic overview of the bicistronic vectors is shown in Figure 6.

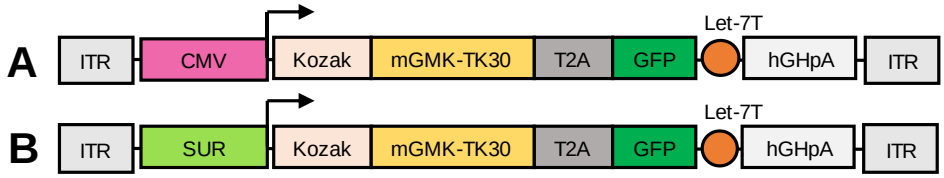

Figure 6: Vector plasmid for translational targeting of cancer cells, where transgene expression is driven by CMV (A) and SUR (B) promoter, respectively. In the 3'-UTR of the transgene, a let7a target sequence (let7-T) was introduced.

The selective expression of the HSV-*tk* suicide gene was studied in two non-cancer (healthy) fibroblast cell lines HDFa (human dermal fibroblasts),[124] and M1FS (GM22143, human fibroblasts from foreskin)[125], as well as in four tumor cell lines. Fibrosarcoma cell line HT-1080 was chosen, because of the high amount of AAV2 primary receptor HSPG on the cell surface, allowing for high transduction efficiencies. For breast cancer cell lines MDA-MB231 and MDA-MB453 previous data suggested high survivin promoter activity,[126,127] and for MDA-MB231 additionally, COX-2 and CXCR-4 promoter activity was reported.[90,120] In the future, a combined transcriptional targeting, miRNA mediated de-targeting and tumor marker-based re-targeting, is from particular interest. Therefore, the epidermoid carcinoma cell line A431 was included showing high amounts of the known tumor-marker epidermal growth factor receptor (EGFR) on the cell surface.[128] Also for MDA-MB231 high EGF-receptor densities were reported, whereas for MDA-MB453 a low EGFR density was known.[129,130] For HT-1080 no data were available for the EGF-receptor status.

5.1.2. Determination of transduction efficiencies and prodrug toxicity

By introducing a viral or bacterial suicide transgene to a tumor cell, activation of a non-toxic prodrug into a toxic metabolite by the expressed transgene is enabled and elimination of targeted cells is possible. This process is named VDEPT when a viral vector is utilized for gene transfer. In this work, the HSV-*tk* as a transgene and GCV as a prodrug were used. To correlate the effect of GCV on transduced cells with the transduction efficiency, the sequence of enhanced green fluorescent protein (eGFP) was introduced into the mGMK-TK30_T2A_eGFP bicistronic vector construct. To obtain two proteins from one promoter a T2A site was introduced in between the two genes (Figure 8A). However, after transduction no eGFP fluorescence was detectable for the tumor specific promoters and minimal fluorescence for the CMV promoter vector was seen (Figure 7A).

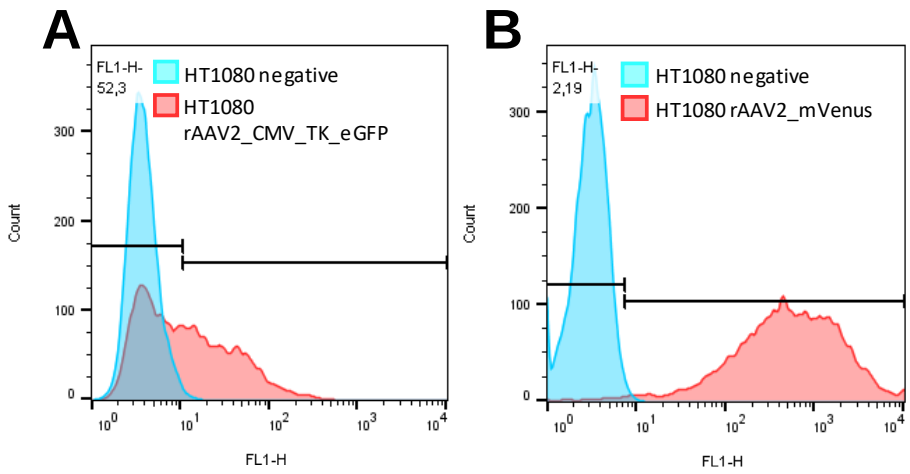

Figure 7: Flow cytometry data for rAAV transduction of HT1080 cells in comparison the negative buffer control. (A) Cells were transduced with rAAV2_CMV_TK_eGFP at a multiplicity of infection (MOI) of 10,000 and analyzed via flow cytometry after incubation in biological duplicates. (B) Cells were transduced with rAAV2_CMV_mVenus at a MOI of 10,000 and analyzed via flow cytometry after incubation in biological duplicates. Data analysis was performed using FlowJo. A gate of 1% false positive cells was selected in the sample of the negative control. This gate is visualized in each diagram.

By this, the eGFP fluorescence signal was not suitable for the determination of transduction efficiency. The T2A site in the bicistronic vector should mediate 'cleavage' of polypeptides during translation. The underlying mechanism relies on a steric hindrance during translation and ribosome skipping leading to two 'cleaved' proteins. More 2A sites exist, but T2A was reported to show the highest level of protein expression at the second gene position.[131] However, a decrease of up to 70 % compared to the first gene in a bicistronic vector construct was observed.[132] Additionally, it was found that cleavage efficiency differs widely between different cell lines.[133] Therefore, a drop in eGFP expression was to be expected, although a decrease of the fluorescence signal below the detection limit was unpredictable. To determine the transduction efficiency of rAAV2 wt on the cell lines despite missing GFP fluorescence, cells were transduced with rAAV2-CMV-mVenus (Figure 8B).

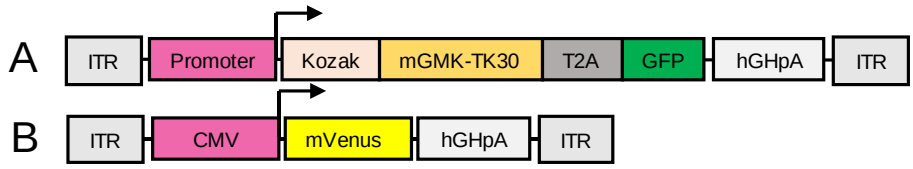

Figure 8: Schematic view of transgene expression cassettes. (A) Vector plasmid for transcriptional targeting of cancer cells, with promoter as placeholder for CMV, COX-2, SUR or CXCR-4 promoter, respectively. (B) CMV_mVenus vector plasmid used as transduction control for the determination of transduction efficiency of rAAV2 and as negative control for the calculation of relative fluorescence.

Successful transduction was detected by the expression of the delivered transgene mVenus using flow cytometry. rAAV2_mVenus was able to transduce all examined cell lines to varying degrees (Table 2).

Table 2:Transduction efficiencies of rAAV2 with CMV_mVenus as reporter for different cell lines transduced with a MOI of 10.000. Mean and standard deviation (SD) of two biological duplicates are shown.

Cell line	**Transduction efficiency in %**
HDFa	58.1 ± 1.5
M1FS	73.5 ± 1.4
HT1080	97.0 ± 1.0
MDA-MB231	64.5 ± 2.6
MDA-MB453	59.3 ± 2.3
A431	77.1 ± 2.3

It was assumed, that this transduction ability should remain if the transgene is changed, since the capsid remains the same. Admittedly, it has been reported that about 10 % of undissolved polypeptides are produced by ribosome read-through.[132] This effect was not taken into account in the following evaluations but should be aware, since individual activity of the two proteins in potentially present fusion proteins is unknown and may cause cells to show no thymidine kinase activity even though they were transduced.

To determine the individual strength of TSPs by the conversion of GCV to its toxic metabolite by a cell viability assay the optimal working concentration of GCV had to be determined. Previous data suggested, that a GCV concentration of 1 mM showed the greatest effect on cell viability after transduction of HT1080 cells with viral particles containing the mGMK-TK30 transgene.[134] Lower concentrations of GCV led to less reduction in cell viability at a constant MOI. However, higher concentrations were not tested in these previous experiments. To control whether even higher concentrations of ganciclovir were tolerated by the cells, a cytotoxicity assay was performed on HT1080 cells. In Figure 9A, a major drop in the fluorescence signal relative to non-incubated HT1080 cells (hereinafter referred to as (relative) cell viability),caused by the increasing GCV concentration was observed while cell viability remained relatively constant up to a concentration of 1 mM. Since healthy cells should be studied, the high impact of GCV in the absence of thymidine-kinase is untenable. Therefore, the concentration of 1 mM GCV was retained and the effect on all other cell lines used was investigated. The decline in cell viability relative to untreated cells was comparable between chosen cells lines with relative viability ranging from 80 % for MDA-MB231 and 100 % for A431 (Figure 9B).

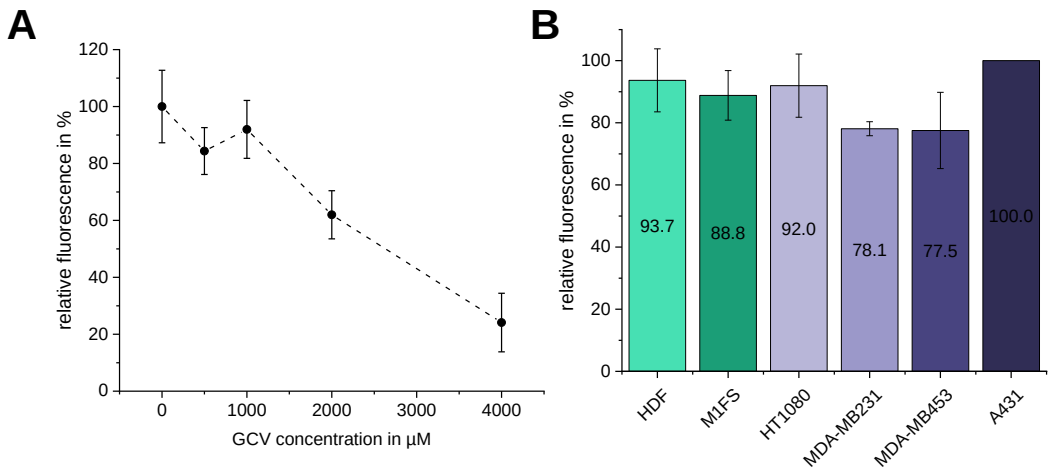

Figure 9: Effect of Ganciclovir on non-transduced cells. (A) Analysis of the effect of increasing GCV concentrations on the viability of HT1080 cells. Relative viability was determined to non-incubated HT1080 cells in biological duplicates and 6-fold technical replicates. For each spot, SD was calculated between biological samples. (B) Cytotoxicity assay to study the effect of 1 mM GCV on the cell viability of HDFa, M1FS, HT1080, MDA-MB231, MDA-MB453 and A431 cells. Relative viability was determined to non-incubated cells in biological duplicates and 6-fold technical replicates. For each column, SD was calculated between biological samples.

In all subsequent analyses, the reference cells were also treated with 1 mM GCV as a precaution to exclude distortions caused by the influence of the prodrug on cell viability. Additionally, reference cells were transduced with rAAV2_mVenus, to exclude effects on cell viability resulting from transduction.

5.1.3. Determination of de-targeting efficiencies by cell viability assays

The effect of the prodrug conversion by thymidine kinase expressing cells was determined by a cytotoxicity assay (Alamar Blue assay). Here, the reduction of the non-fluorescent resazurin by metabolically active cells results in a pink fluorescent dye.[135] This fluorescence can then be measured and was used to determine the cytotoxic effect of the prodrug GCV converted to its toxic metabolite GCV-TP.

At first, cells were transduced with a multiplicity of infection (MOI) of 10'000 and after 24 h, 1 mM GCV was added for another 72 h and an Alamar Blue Assay was performed by adding resazurin and measuring the emerging fluorescence. In Figure 10, results of the Alamar Blue assays for the two non-cancer cell lines HDFa and M1FS are shown. Additionally, the number of non-transduced cells is displayed via a horizontal line (Figure 10A, C). For the calculation of relative fluorescence, the measured fluorescence for the different vector constructs was normalized to the fluorescence obtained from the rAAV-mVenus transduced reference (negative). The resulting relative fluorescence is hereinafter referred to as cell viability. By this, the cell viability of the total population was illustrated. Investigating the total cell population has the advantage to observe possible phenomena such as the bystander effect. A drop of the cell viability below the number of transduced cells (horizontal line) may provide an indication for this effect. However, this was not observed for

HDFa and M1FS cell lines. In previous *in vitro* studies, it was found that cell-cell contact is essential for most cell lines for an efficient bystander effect.[136,137] In this study low plating densities were used in order to circumvent an overgrowing of the culture during the long cultivation in 96-well plates. This also suggests that no bystander effect was achieved. The conversion of GCV to its toxic metabolite was highest for the CXCR-4 promoter driven gene expression in HDFa (Figure 10A, sixth column) and CMV promoter in M1FS cells (Figure 10C, first column) indicated by the lowest cell viability. The addition of the let-7a miRNA target sequence (let-7aT) allowed for a strong protective effect for the CMV promoter construct, whereas the SUR promoter remained virtually unaffected by the translation control in both cell lines (Figure 10A, C columns with banded pattern).

In Figure 10B, D only transduced cells were investigated and the proportion of dead cells in these populations were calculated from the relative fluorescence data. For HDFa and M1FS, the COX-2 promoter led to the lowest number of dead cells in the transduced population if only transcriptional targeting is considered. Overall, CMV promoter driven gene expression in combination with let-7aT, turned out to be the best combination for both non-cancer cell lines, and was able to rescue all transduced HDFa cells and only 12.8 % of M1FS cells died (Figure 10B, D second columns). Interestingly, even if the highest expression rate was achieved under the CMV-promoter, many of the transduced cells were still viable (~ 40 % HDFa, ~30 % M1FS). Since we observed doubling times of up to 48 h for both cell lines, a higher effect of GCV-treatment can probably be achieved by longer exposure times, as cytotoxicity of GCV-TP is induced by its incorporation into the DNA of replicating cells and by this inhibiting DNA synthesis.

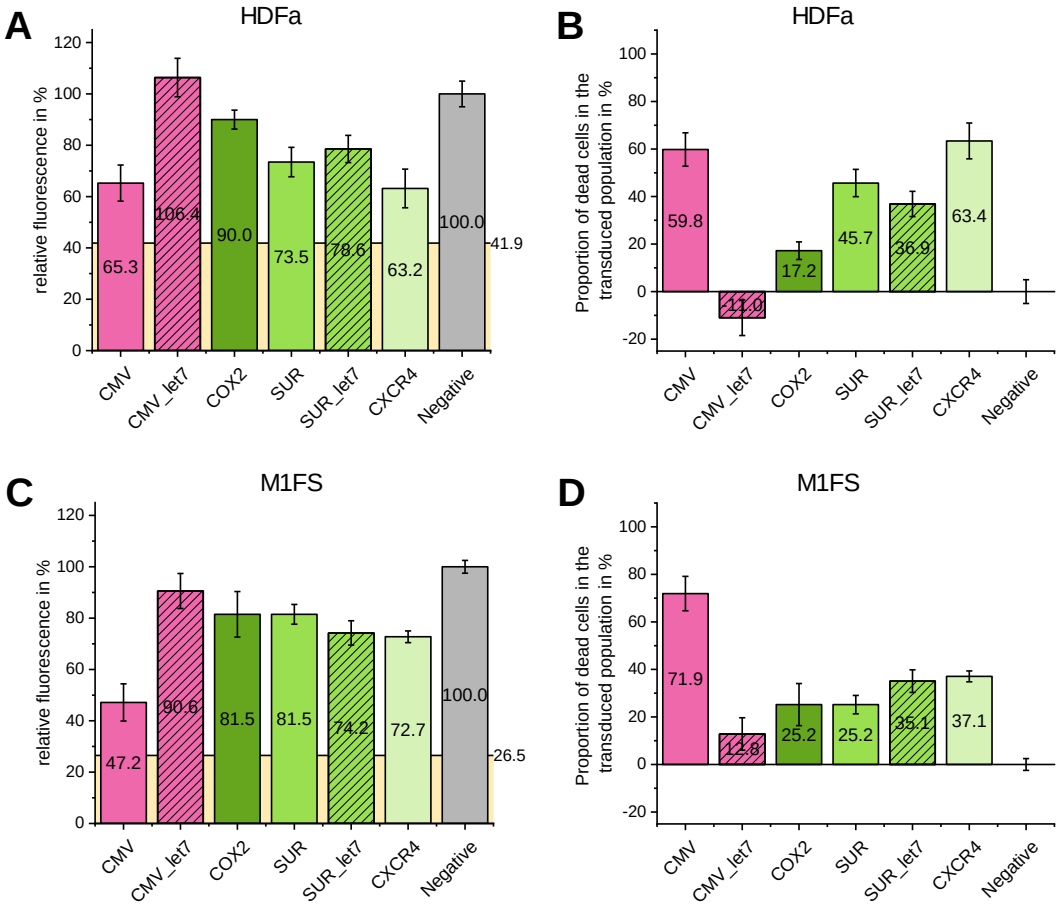

Figure 10: Alamar Blue Assay for determination of thymidine kinase activity in the context of TSPs. The transcriptional activity of CMV, COX-2, SUR and CXCR-4 promoters, driving the transgene expression upon rAAV transduction, was measured in the two non-cancer cell lines HDFa (A, B) and M1FS (C, D). Cells were transduced with a MOI of 10'000 and after 24 h treated with 1 mM GCV for another 72 h before performing the Alamar blue assay. Negative reference cells were transduced with rAAV2_mVenus and treated with 1 mM GCV. (A, C) Calculation of relative fluorescence was performed by normalization of the fluorescence for the different viral vectors to the fluorescence obtained from the rAAV-mVenus transduced reference (negative). The number of non-transduced cells is given as a horizontal line. (B, D) The proportion of dead cells in the transduced population was calculated from the relative fluorescence data and the transduction efficiency determined by rAAV_mVenus transduction of the respective cells. The data shown are the means of two biological duplicates with six technical replicates, with error bars indicating the standard deviation.

The results of the cytotoxicity assay for the four cancer cell lines were displayed in Figure 11. On the left hand side (Figure 11A, C, E, G) an overview of the total populations, and on the right hand side (Figure 11B, D, F, H) only the percentage of dead cells in the transduced fraction were shown. In the transduced population, for HT1080, MDA-MB231 and A431 almost all cells died under CMV promoter driven suicide gene expression (Figure 11B, D, H, first column). For MDA-MB453 (Figure 11E), the high percentage of viable cells is expected to be a result of observed doubling times of approximately 48 h as before for HDFa and M1FS cells. Again, the data indicate that no bystander effect has been achieved as no drop of the relative fluorescence below the number of transduced cells (Figure 11A, C, E, G, horizontal line) was observed. HT1080 cells strongly responded to the treatment with ganciclovir regardless of the promoter and let-7aT and by this HT1080 were not well suited as a control cell line, since differences in targeting efficiency were

not discernible (Figure 11A, B). De-targeting with let-7aT led to an increase in the relative fluorescence for all tumor cells (Figure 11A, C, E, G; columns with banded pattern) indicating that let-7a target sequence may not be the best-possible sequence for selected cell lines. Aberrant miRNA expression is well known for cancer cells.[138–140] However, a general statement about the expression profile cannot be made. For MDA-MB231 and MDA-MB453 cells a high let-7a expression level was detected in miRNA microarrays,[139] which fits to obtained results, at least for the CMV promoter construct. Though, for A431 and HT1080 no published data were found, but the experimental findings indicate that let-7a miRNA is also expressed in this both cell lines. To optimize the regulation of protein translation, other miRNA target sequences are possible or even the use of different targets in one transgene expression cassette to de-target various cells.[94]

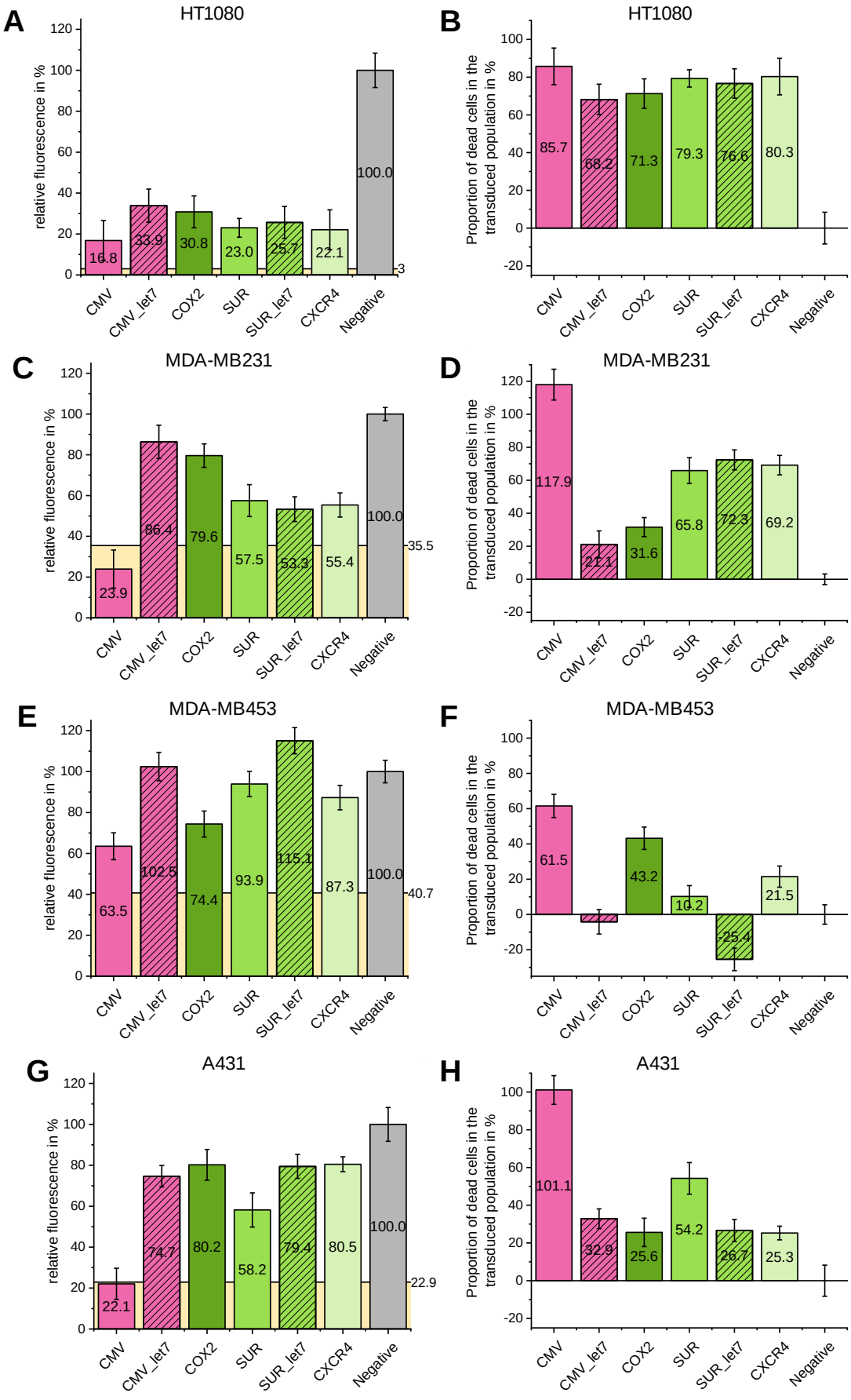

Figure 11: Alamar Blue Assay for determination of thymidine kinase activity in the context of TSPs. The transcriptional activity of CMV, COX-2, SUR and CXCR-4 promoters, driving the transgene expression upon

rAAV transduction, was measured in four cancer cell lines HT1080 (A, B), MDA-MB231 (C, D), MDA-MB453 (E, F) and A431 (G, H). Cells were transduced with a MOI of 10'000 and after 24 h treated with 1 mM GCV for another 72 h before performing the Alamar blue assay. Negative reference cells were transduced with rAAV2_mVenus and treated with 1 mM GCV. (A, C, E, G) Calculation of relative fluorescence was performed by normalization of the fluorescence for the different viral vectors to the fluorescence obtained from the rAAV-mVenus transduced reference (negative). The number of non-transduced cells is given as a horizontal line. (B, D, F, H) The proportion of dead cells in the transduced population was calculated from the relative fluorescence data and the transduction efficiency determined by rAAV_mVenus transduction of the respective cells. The data shown are the means of two biological duplicates with six technical replicates, with error bars indicating the standard deviation.

5.1.4. Calculation of individual tumor specificities

To determine the individual tumor specificity of the promoters used alone, or in combination with the let-7aT, the percentage of dead cells for the given promoter in HDFa (Figure 12A) or M1FS (Figure 12B) cells was divided by the percentage of dead cells of the respective tumor cells with the corresponding promoters. By this a heat map was generated indicating a ratio of zero in green and a ratio of one and more in read. Combinations with a value close to zero or zero, show the highest tumor specificity. Here, no or low numbers of the non-cancer cells and high proportions of the cancer cells died. At a value of one and more at least the same proportion of dead cells was found in the cancer and non-cancer cell lines.

A

HDFa	A431	MDA-MB231	MDA-MB453	HT-1080
CMV	0.59	0.51	0.97	0.70
CMV_let7	0.00	0.00	2.65	0.00
COX2	0.67	0.55	0.40	0.24
SUR	0.84	0.69	4.46	0.58
SUR_let7	1.38	0.51	0.00	0.48
CXCR4	2.51	0.92	2.96	0.79

B

M1FS	A431	MDA-MB231	MDA-MB453	HT-1080
CMV	0.71	0.61	1.17	0.84
CMV_let7	0.39	0.61	0.00	0.19
COX2	0.98	0.80	0.58	0.35
SUR	0.46	0.38	2.46	0.32
SUR_let7	1.32	0.48	0.00	0.46
CXCR4	1.47	0.54	1.73	0.46

Figure 12: Heat map of calculations of individual tumor specificities. The percentage of dead cells of the transduced cell populations for the given promoter in (A) HDFa or (B) M1FS cells was divided by the percentage of dead cells of the transduced cell population of respective tumor cells with the corresponding promoters.

For both reference cell lines (HDFa, M1FS) the same pattern can be seen, with MDA-MB453 showing the only exception for CMV_let-7a. Across all other cell lines, the highest tumor specificity was achieved with the combination of the CMV promoter with the let7a target sequence.

The CXCR-4 promoter showed low tumor specificity in the investigated cell lines. On the contrary, in A431 and MDA-MB453 even more non-tumor than tumor cells died. For breast cancer cell lines MDA-MB231 and MDA-MB453 previous data suggested high survivin promoter activity.[126,127] At least for MDA-MB231 this was proven here as well. For MDA-MB453, both the COX-2 promoter and the SUR_let-7a combination achieve the highest tumor specificity.

In summary these results suggest, that no general statement can be made about the functionality of the individual promoters. Also, for let-7a upregulation rather than downregulation of the miRNA was reported for several types of cancer.[141] Regarding the bystander effect, higher plating densities could potentially lead to an increased killing and needs to be further evaluated. The most promising combination of the strong CMV promoter with the let-7a miRNA target sequence can serve as a good starting point for further optimization e.g. with other or even a combination of several miRNA target sequences in one transgene expression cassette. One optimal promoter and one miRNA target sequence for all types of cancer is unrealistic and a patient-specific adaptation of the transgene expression cassette is probably inevitable.

5.2. Optimization of rAAV production in HEK-F suspension cells

As the demand for high titer rAAV production with superior purity, which is likewise user friendly and cost-efficient increases, great effort was put into the generation of a suspension-based rAAV manufacturing process.

5.2.1. Establishment of a transfection protocol for rAAV production

The most widely used method for the production of rAAV is based on the multi-plasmid transfection of adherent growing HEK-293 cells.[142] By this the possibility for a scalable rAAV manufacturing process is very restricted due to the limited growth area. A suspension-based production system in e.g. bioreactors allows for mammalian production to a scale of many thousands of liters.[143]

In the beginning a transfection protocol had to be established first in small scale. An attempt for the adaption of HEK-293 cells failed as the cells were found to grow not individually but as large grapes. Thus, rAAV2 production was optimized in commercially available Freestyle™ 293-F cells (HEK-F) (Thermo Fisher Scientific) which were derived from adherent growing HEK-293 cells and already adapted for high-density growth as a serum-free suspension culture. In a first step, the transfection protocol had to be adapted. Here, several aspects like the cultivation medium, the transfection reagent, the amount of plasmid DNA and the ratio between the three plasmids must be considered. Good experience was already made with the HEK-TF medium (Xell AG) and an associated standard protocol and served as a starting point. As a transfection reagent linear PEI (MW:25k Polysciences, Inc.) was utilized in the beginning and the DNA:PEI ratio, as well as the best DNA concentration were analyzed. For this reason, HEK-F cells were seeded in 6-well plates

and transfected with the ITR-containing plasmid coding for the transgene mVenus. In a first step, three different DNA amounts were combined with altered DNA:PEI ratios. Overall, a higher excess of PEI to DNA always achieved the best transfection efficiency for all DNA concentrations (Figure 13A, third, sixth and ninth column). With 47.2 % the highest transfection efficiency was reached for 2 µg ml^{-1} plasmid DNA with the four-fold excess of linear PEI (Figure 13A, ninth bar) and was therefore maintained as the best conditions. In a second step the molar ratio between the pHelper:RepCap:ITR plasmids was evaluated. In literature, molar ratios ranging from 1:1:1,[144] 2:1:1,[145,146] 2:1.6:1,[147] 1:1:2 [148] and 1.5:2:1[149] were frequently used. Transient transfection with beforehand optimized DNA amount of 2 µg ml^{-1} and DNA:PEI ratio of 1:4 was performed, and as the proportion of viral particles released into the medium during production was not known, DNase I resistant particles were determined from cell pellet and from spent medium by qPCR three days after transfection. As presented in Figure 13B, three molar ratios were selected for this purpose. Admittedly, the differences were not very pronounced. Overall, most of the vector genomes were found in the cell pellet, regardless of the molar ratio of the individual plasmids. For AAV2, this relationship was already known and is primarily related to the heparin affinity of the capsid, which negatively influences the release of the particles into the medium. It should be considered that during production of other AAV serotypes this ratio could be shifted towards more rAAVs in the soluble fraction.

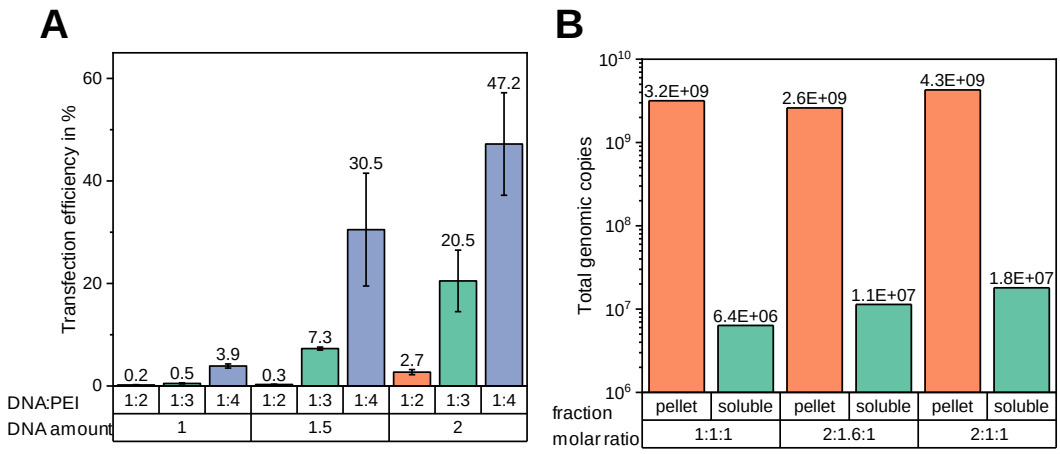

Figure 13: Evaluation of optimal transfection conditions. (A) HEK-F cells were seeded in a 6-well plate with 3·10^6 cells ml^{-1} in a total volume of 3 ml. For transfection 1, 1.5 and 2 µg ml^{-1}of the ITR containing plasmid DNA were incubated with linear PEI in two-, three- or four-fold the amount of the DNA. After three days, transfection efficiency was determined using the expression of the delivered transgene mVenus measured by flow cytometry of 10,000 cells in total. For each column, standard deviation was calculated from two biological duplicates. (B) HEK-F cells were seeded in a 6-well plate with 3·10^6 cells ml^{-1} in a total volume of 4 ml. For transfection, 2 µg ml^{-1}of pHelper:RepCap:ITR in a molar ratio of 1:1:1, 2:1.6:1 or 2:1:1 where complexed with four-fold amount of linear PEI. After three days, cells were pelleted and DNase I resistant particles were determined in the cell pellet after cell disruption in lysis buffer by three freeze-thaw cycles and in the spent medium.

The molar plasmid ratio of 2:1:1 resulted in the highest genomic titer (Figure 13B, the two right columns) and all subsequent optimizations were continued on this basis.

5.2.2. Analysis of the optimal cultivation medium to improve rAAV yields

In cooperation with Xell AG, an optimized manufacturing protocol, primarily regarding the cultivation medium, should be established. To evaluate the productivity of HEK-F cells in HEK-TF medium, an additional commercially available medium, FreeStyle™ F17 Expression Medium (F17) (Thermo Fisher Scientific), was to be used. Besides the transfection medium (HEK-TF) in which the HEK-F cells were propagated and transfected, further media from Xell AG were available. On the one hand a growth medium (HEK-GM) and on the other hand a HEK feeding solution (FS). In Table 3 all tested combinations were summarized.

Table 3: Overview of the different medium conditions tested for rAAV2 production.

Batch number	Growth medium	Transfection medium	Comments
1.1/1.2	HEK-TF	HEK-TF	Fill up with HEK-TF
2.1/2.2	HEK-GM	HEK-TF	Fill up with HEK-GM
3.1/3.2	HEK-TF	HEK-TF	Fill up with HEK-GM
4.1/4.2	HEK-TF	HEK-TF	Fill-up with FS
5.1/5.2	HEK-TF	HEK-TF	Fill-up with HEK-TF+1x FS*
6.1/6.2	HEK-TF	HEK-TF	Fill-up with HEK-TF+xx FS**
7.1/7.2	F17	F17	HEK-TF optimized protocol
8.1/8.2	F17	F17	F17 optimized protocol
*simple feed pulse (3mL) 24 h after filling up; **daily feed pulse (500 µl) starting 24 h after filling up			

The focus of these experiments was to determine the best manufacturing process for the media as well as the required cultivation time for the highest possible titer. In the beginning, HEK-F cells were initially adapted to the respective growth medium for at least three passages. All transfection approaches were conducted in 50 ml TubeSpin® bioreactors with a transfection volume of 6 ml which was then filled up to the final volume of 12 ml 4 h after transfection with the appropriate medium. To determine the best manufacturing process, viable cell density, and viability were measured every day. Two days after transfection, transfection efficiency was further determined by flow cytometry analysis. Additionally, on day one, three and five samples were taken and stored at -80 °C for later analysis of the genomic rAAV2 titer. As a transfection protocol, the beforehand optimized conditions were chosen. For F17 medium, the HEK-TF optimized protocol was chosen (approaches 7.1/7.2) as well as a F17 specific protocol (approaches 8.1/8.2) published by Grieger *et al.*.[149] Here, an optimal cell density of $1 \cdot 10^6$ cells ml^{-1}, 1.5 µg ml^{-1} plasmid DNA and a DNA:PEI ratio of 1:2 is recommended. Furthermore, the suggested plasmid ratio of pHelper:RepCap:ITR of 1.5:2:1 was adopted.

The transfection efficiency, determined by flow cytometry analysis utilizing expression of the mVenus gene, ranged from 66 % for the best Batch 1 to 3.85 % for Batch 2 (Table 4).

Table 4: Transfection efficiency and maximum reached genomic rAAV2 titer for designated batches. Mean and standard deviation (SD) of two biological duplicates are shown for the transfection efficiency.

Batch number	Transfection efficiency	Maximum total genomic titer
1.1/1.2	66.61 ± 2.83	$6.5 \cdot 10^9$
2.1/2.2	3.85 ± 2.03	$1.16 \cdot 10^{10}$
3.1/3.2	62.0 ± 1.63	$1.47 \cdot 10^9$
4.1/4.2	39.96 ± 3.87	$9.14 \cdot 10^8$
5.1/5.2	65.54 ± 4.11	$1.08 \cdot 10^9$
6.1/6.2	64.15 ± 4.15	$7.16 \cdot 10^9$
7.1/7.2	29.64 ± 5.48	$2.15 \cdot 10^9$
8.1/8.2	20.59 ± 1.26	$1.11 \cdot 10^{10}$

Surprisingly, the transfection efficiency did not correlate with maximum total genomic titer. The previously optimized process conditions still resulted in the best transfection efficiency (Batch 1.1/1.2) but not in the overall highest total genomic titer which was highest for Batch 2.1/2.2. There is no simple explanation for this phenomenon. It is possible that the fluorescence intensity in approach 2.1/2.2 was not intense enough, so that the transfection efficiency was underestimated. It is more likely, though that the low transfection efficiency for Batch 2.1/2.2 shows that a more rigorous washing process before transfection is required as media components of the GM medium appear to inhibit transfection. Possibly the number of transfected cells is sufficient for the titer achieved. In the context of the recorded growth curves, the different genomic titers obtained can be partially clarified. For Batch 1.1/1.2 and Batch 2.1/2.2 growth characteristics are comparable. As expected, the maximum viable cell density and the length of cultivation before the decline in viability was higher for Batch 2 (Figure 14B) than for Batch 1 (Figure 14A) as the GM medium should support stable cell growth, whereas the TF medium especially supports transfection.[150,151] For both approaches, the highest total genomic titer was achieved on the third day. By using the growth medium before and after transfection, with $1.2 \cdot 10^{10}$ twice as many total genomic copies as for HEK-TF were yielded. Interestingly, if the HEK-GM medium was used only after transfection and not for cultivation before transfection, an extended cultivation time was also observed before viability fell below 50% (Figure 14C) in Batch 3.1/3.2, but the maximum yield decreased by a factor of about 50 compared to approach 2.1/2.2. Therefore, it seems that the supply of nutrients before transfection is more important than after transfection.

When replenished with 100% FS after transfection (Figure 14D), viable cell density and viability already decreased within the first day, but the maximum genomic titer reached on day 5 was reduced by a factor of only 10 compared to the best batch of 2.1/2.2. This indicates that no cell growth is needed for rAAV2 production. Potentially, the nutrition supply was too high as the protocol recommends the addition up to a ratio of one tenth of the culture volume, which here was clearly exceeded with a ratio of 1:1.[152] For glucose this means a final concentration of more than 100 mM

and thus far more than the physiological 3.9 - 7.8 mM found in human plasma.[153] If productivity per cell is considered, the highest value is even achieved here.

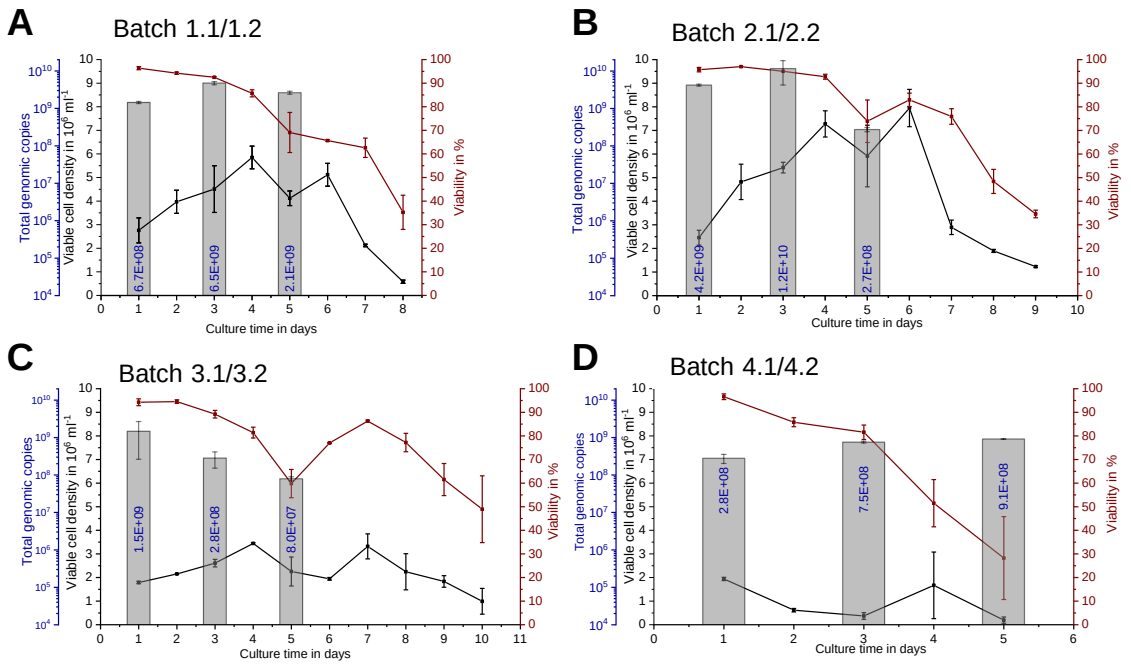

Figure 14: Viability, viable cell density and total genomic copies over the period of cultivation time. $3.0 \cdot 10^6$ ml^{-1} HEK-F cells were transfected, in a total volume of 6 ml, by triple transfection with a molar Ratio of 1:1:1 of pHelper:RepCap:ITR and viable cell density and viability were measured every 24 h. On day 1, 3 and 5 after transfection, produced genomic copies were determined by qPCR analysis from combined spent media and from crude cell lysate after three freeze-thaw cycles. (A) For Batch 1.1/1.2, cells were cultivated in HEK-TF medium. Before transfection medium was exchanged to fresh HEK-TF. 4h after transfection, the cell suspension was filled up with 100 % HEK-TF. (B) For Batch 2.1/2.2, cells were cultivated in HEK-GM medium. Before transfection medium was exchanged to fresh HEK-TF medium. 4 h after transfection, the cell suspension was filled up with 100 % HEK-GM. (C) For Batch 3.1/3.2, cells were cultivated in HEK-TF medium. Before transfection medium was exchanged to fresh HEK-TF. 4 h after transfection, the cell suspension was filled up with 100 % HEK-GM. (B) For Batch 4.1/4.2, cells were cultivated in HEK-TF medium. Before transfection medium was exchanged to fresh HEK-TF medium. 4 h after transfection, the cell suspension was filled up with 100 % FS.

In order to support the observation that a high nutrient supply after transfection does not improve the yield, two approaches were conducted in which the feed solution FS was given once in Batch 5.1/5.2 (Figure 15A) or as a daily feed pulse in Batch 6.1/6.2 (Figure 15B). In either case, viability remained stable for a long time at over 90% and cultivation was stopped because of low culture volume instead of cell death. As before, a prolonged cultivation time did not lead to an increased productivity. For the single feed pulse Batch 5.1/5.2 the highest genomic titer was reached on day one but with a total of $1.1 \cdot 10^9$ vector genomes, the yield was lower than for standard cultivation procedure in Batch 1.1/1.2 or for the variant were HEK-GM medium was used (Figure 14A, B, respectively). For Batch 6.1/6.2 very high cell densities of up to $2.5 \cdot 10^7$ cells ml^{-1} were reached and the total genomic titer was highest on the third day of cultivation. With $7.2 \cdot 10^9$ genomic copies the yield was comparable to those of the standard procedure. this confirmed the suspicion that a

supply of nutrients after transfection, i.e. during production, had no beneficial effect on productivity. A drop in total vector genomes in the end of the cultivation was observed in all cultivations to varying degrees. It should be noted that both the degradation of the rAAVs by enzymes released during cell death, but also an increased inhibition of qPCR by those same enzymes as well as other proteins can provide a possible explanation, since the qPCR was not carried out on purified sample.

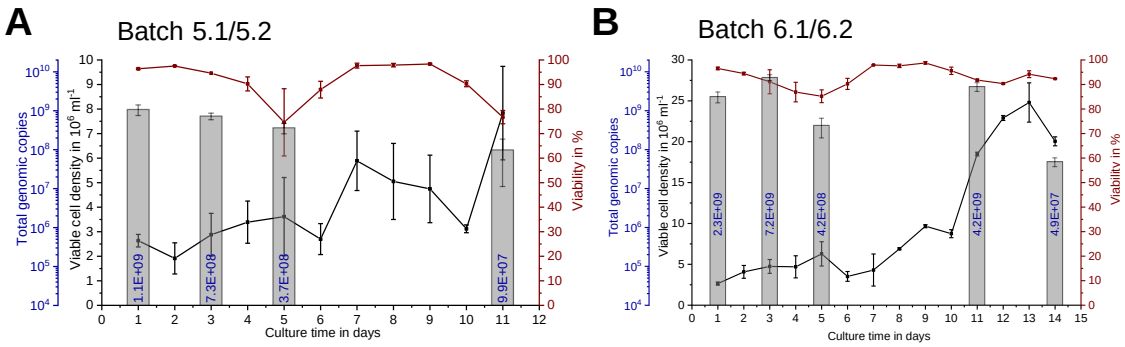

Figure 15: Viability, viable cell density and total genomic copies over the period of cultivation time. $3.0 \cdot 10^6$ ml^{-1} HEK-F cells were transfected, in a total volume of 6 ml, by triple transfection with a molar Ratio of 1:1:1 of pHelper:RepCap:ITR and viable cell density and viability were measured every 24 h. On day 1, 3, 5 11 and 14 after transfection, produced genomic copies were determined by qPCR analysis from combined spent media and from crude cell lysate after three freeze-thaw cycles. (A) For Batch 5.1/5.2, cells were cultivated in HEK-TF medium. Before transfection medium was exchanged to fresh HEK-TF. 4 h after transfection, the cell suspension was filled up with 100 % HEK-TF. 24 h after transfection, 3 ml of FS were added once. (B) For Batch 6.1/6.2, cells were cultivated in HEK-TM medium. Before transfection medium was exchanged to fresh HEK-TF medium. 4 h after transfection, the cell suspension was filled up with 100 % HEK-TF. A daily feed pulse (500 µl) was added, starting 24 h after fill up.

In the next step, the yield of the established protocol for HEK-TF medium was compared with rAAV2 production in F17 medium (Batch 7.1/7.2, Figure 16A). Here, similar productivity was obtained with the alternative medium. The F17 supported a high cell viability for only 3 days which indicates that the F17 medium did not support the initially high cell density, which was also accompanied by an early decline in viability, but this only played a minor role, as with $2.2 \cdot 10^9$ total genomic copies, the highest genomic titer was reached within 24 hours. In Batch 8.1/8.2 (Figure 16B) the F17 medium was used with the transfection protocol optimized for F17 medium from Grieger *et al.*, using 1.5 µg ml^{-1} DNA, a DNA:PEI ratio of 1:2 with a plasmid ratio of pHelper:RepCap:ITR of 1.5:2:1with an initial cell density of $1 \cdot 10^6$ cells ml^{-1}.[149] 24 h after transfection, with $2.9 \cdot 10^9$, almost the same yield was achieved as with the HEK-TF protocol in Batch 7.1/7.2. However, for Batch 8.1/8.2 an increase in total vector yield was observed and by this $1.1 \cdot 10^{10}$ total genomic copies were reached on day 5 (Figure 16B, third column). When comparing those data to the data from Grieger *et al*., a 56 times lower yield per cell was achieved ($3.7 \cdot 10^3$ instead of $2.1 \cdot 10^5$). This may to some extent be related to the determination of the genomic titer. Only in later experiments proteinase K treatment was performed on crude cell extract samples which is used to release endonuclease resistant packaged viral genomes and to digest proteins that inhibit the qPCR reaction.[154] In addition, the reference standard curve should be performed in spent medium in order to

reasonably simulate the qPCR reaction conditions of the sample. Since these steps were not yet established at the time of data acquisition, a comparison with the reference is difficult. Also, not to be disregarded is the aspect that in the work of Grieger *et al.* a cell line optimized for rAAV production was used.

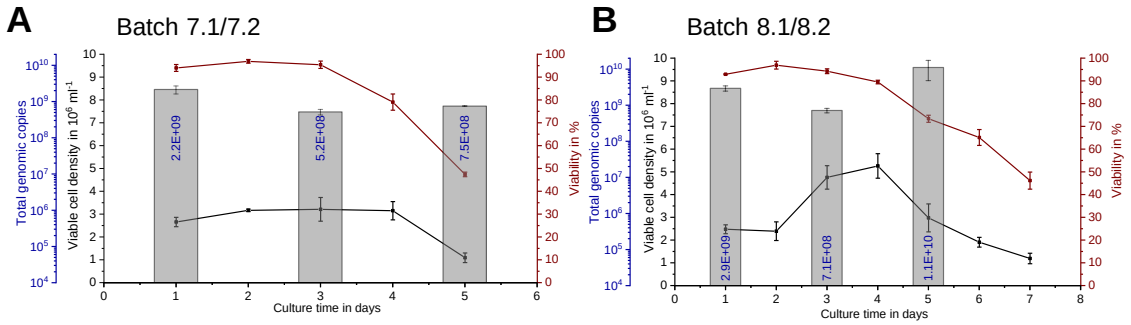

Figure 16: Viability, viable cell density and total genomic copies over the period of cultivation time. (A) For Batch 7.1/7.2, 3.0·10^6 ml^{-1} HEK-F cells were cultivated in F17 medium and before transfection medium was exchanged to fresh F17 medium. Cells were transfected, in a total volume of 6 ml, by triple transfection with a molar ratio of 1:1:1 of pHelper:RepCap:ITR. 4 h after transfection, the cell suspension was filled up with 100 % F17 and viable cell density and viability were measured every 24 h. On day 1, 3 and 5 after transfection, produced genomic copies were determined by qPCR analysis from combined spent media and from crude cell lysate after three freeze-thaw cycles. (B) For Batch 8.1/8.2, 1.0·10^6 ml^{-1} HEK-F cells were cultivated in F17 medium and before transfection medium was exchanged to fresh F17 medium. Cells were transfected in 12 ml F17 medium with 1.5 µg ml^{-1} plasmid DNA and a DNA:PEI ratio of 1:2 with a plasmid ratio of pHelper:RepCap:ITR of 1.5:2:1. Viable cell density and viability were measured every 24 h. On day 1, 3 and 5 after transfection, produced genomic copies were determined by qPCR analysis from combined spent media and from crude cell lysate after three freeze-thaw cycles.

Overall, the different media strategies had only a limited influence on the rAAV2 yield. Within the cultivations, the yield for F17 is comparable with Batch 2.1/2.2, whereby the highest titer was already reached on the third day and not on day 5 (Figure 14B, Figure 16B, respectively. Therefore, the original approach in TF Medium seems to be the most appropriate (Batch 1.1/1.2). Batch 2.1/2.2 is an alternative as it achieved twice the amount of genomic copies. In addition, it offers the possibility to further increase the yield by optimizing the transfection. However, two different media are required here. The use of the F17 medium as an alternative should be carried out with the protocol adapted protocol from Grieger *et al.* as a higher yield is achieved. For later scaling up, this protocol in combination with the F17 medium also offers the advantage that no medium exchange is required at the beginning of the transfection. This not only means a lower amount of required medium, but also a reduction in the risk of contamination, as fewer steps are necessary in the preparation of the transfection.

5.2.3. rAAV2 production in 2 L bioreactor

From the optimized protocol, two 2 L batch processes in bioreactors were started. Here, the main problem regarding the transfection protocol established for HEK-TF came into focus. The medium exchange step by centrifugation before transfection is not easily realized. Therefore, one day before transfection, cells were seeded in HEK-TF medium in half of the transfection volume in a cell

density of $6 \cdot 10^6$ cells ml^{-1}. On day of transfection, they were diluted to the final $3 \cdot 10^6$ cells ml^{-1} and the standard transfection protocol was used. After 4 h, the cell suspension was filled up either with 100 % HEK-TF or with 100 % HEK-GM medium. Transfection efficiency, total cell density and rAAV2 yield were monitored over six days. The transfection efficiency of 49.63 % for HEK-TF and 55.5 % for HEK-GM was slightly lower than for SpinTube bioreactor cultivations ((66.61 %) (Table 4)) possibly due to the modification of the transfection protocol.

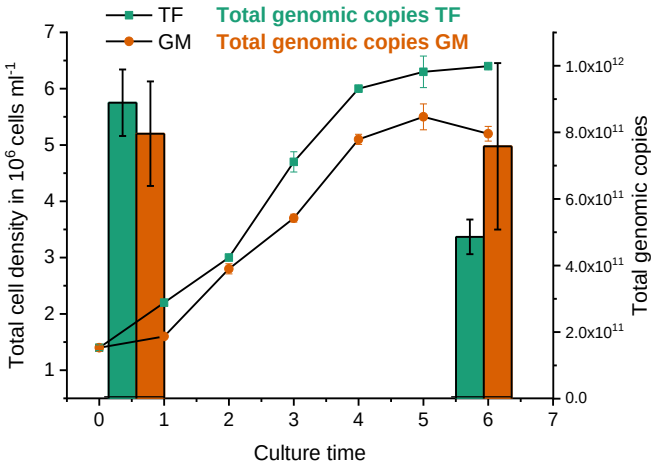

Figure 17: Total cell densities and total genomic copies of a rAAV production in a 2 l bioreactor. $3.0 \cdot 10^6$ ml^{-1} HEK-F cells were transfected, in a total final volume of 800 ml for HEK-TF and 900 ml for HEK-GM bioreactor, by triple transfection with a molar Ratio of 1:1:1 of pHelper:RepCap:ITR. After 4h HEK-TF bioreactor was filled up to a final volume of 1665 ml with HEK-TF and HEK-GM bioreactor was filled up to a final volume of 1833 ml with HEK-GM medium. Viable cell density and viability were measured every 24 h. On day 1 and 6 after transfection, produced genomic copies were determined by qPCR analysis from combined 1ml of combined spent media and from crude cell lysate after three freeze-thaw cycles. Error bars were calculated from the standard deviation of two technical duplicates.

The total cell density (TCD) increased over time regardless of which medium was used for replenishment, with TF Medium even reaching a slightly higher TCD. DNaseI-resistant particles were determined from raw cell lysates by qPCR. Considering the error bars, the rAAV2 yield was the same for both reactors and as seen before, prolonged cultivation times did not yield in higher genomic titers. With about $1 \cdot 10^5$ genomic copies per cell, cell-specific productivity was much higher as seen before for TubeSpin cultivations ($1.4 \cdot 10^3$ for Batch 1.1/1.2). However, a representation of the total vector genomes per cell was deliberately omitted, as the productivity of the individual cell showed significant differences, but the overall process was to be examined for its yield. Although an increased productivity of the individual cell was found for the bioreactor runs, the overall yield of the process was nevertheless low due to low cell numbers, especially at the beginning of the cultivation where most of the rAAVs seem to be produced.

The optimization of rAAV production in HEK-F suspension cells progressed in the master theses of Irina Schierbaum and Thilo Pohle. Until now, downstream processing with standard purification protocols, mainly iodixanol-based ultracentrifugation was not successful implemented which is

possibly related to media components interfering with the viral capsids. For this thesis, required AAVs were therefore mainly produced in adherent HEK-293 cells.

5.3. Establishment of a novel rAAV production cell line

Results for the generation of the rAAV producer cell were summarized in a manuscript with the title 'HEK293-KARE1, a cell line with stably integrated adenovirus helper sequences simplifies rAAV production" and submitted to BMC Biotechnology. The original manuscript is included in the appendix. The data presented in the manuscript are the result of a shared authorship with Rebecca Feiner. Rebecca Feiner performed the experiments to characterize the cell line. Here, only own results about optimization of the rAAV production were summarized.

The standard process for rAAV production relies on the triple transfection of embryonic kidney 293 (HEK-293) cells.[155] These were originally immortalized by exposing the cells to the mechanically sheared DNA of adenovirus type 5 (AD5). During this process, five to six copies of Ad5 early E1 gene were integrated into the genome including the chromosome region 19q 13.2. The 4-kbp adenoviral genome fragment encodes for the E1A/E1B proteins, which interfere with the cell cycle control pathways and counteract apoptosis.[156,157] In the helper-free rAAV production system, the additionally lacking E2A and E4 and the non-coding RNA V need to be provided by a so called 'helper plasmid'. This means the inconvenience of continuous production and co-transfection of invariant adenoviral helper genes of 9279 bp beside the RepCap and ITR plasmid during rAAV production.

5.3.1. Integration of pHelper sequences into HEK-293

In collaboration with Julian Teschner, a cell line was planned with stably integrated pHelper sequences. For selection of positive integration events, the gene of blasticidin deaminase (*bsd*) was cloned into the pHelper plasmid. The HEK-293 cells were transfected with the linearized plasmid and after three days, selective pressure was applied. After two weeks, a limiting dilution in 96 well plates was performed to select single cells. The four clones with the highest growth rate were chosen for further characterization and named HEK-KARE1a-d. Because of decreased viability and transfection efficiency HEK-KARE1d was discarded at a later stage. For all clones, genomic integration of the helper genes was analyzed. Genomic DNA of all clones was isolated using a Chelex100 extraction. The presence of the *bsd* and the E2A gene was verified using PCR with two different sets of primers. The primers Bsd-for and Bsd-rev as well as Ad5-for and Ad5-rev anneal at different regions of the plasmid and, in the case of a successful complete integration, they amplify products with a size of 499 bp for E2A and 524 bp for *bsd*. Experimentally obtained fragments are shown in Figure 18A for all samples, demonstrating that both genes were integrated successfully into the genome of HEK-293. In microscopy analysis of clone KARE1c (Figure 18B) compared to the parental HEK-293 cells, (Figure 18C) no effect on the cell morphology by the integration of such a large fragment was detected.

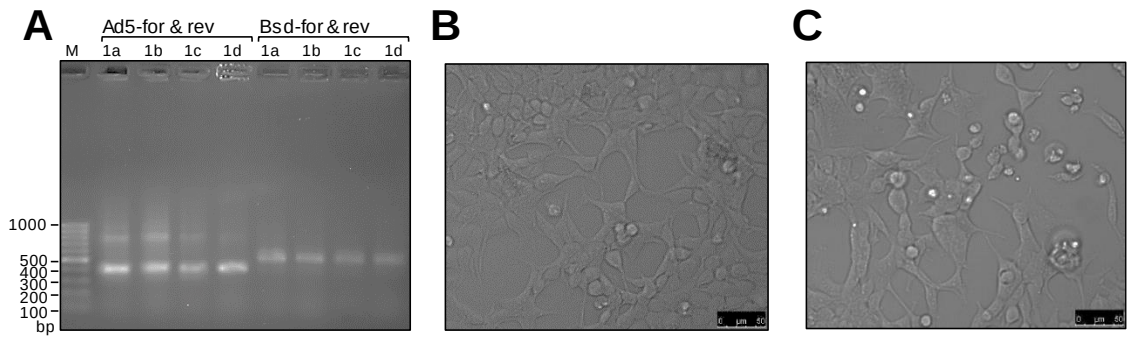

Figure 18: Analysis of genomic DNA integration and cell morphology. (A) Agarose gel of the PCR analysis of pHelper-BSD integration. Genomic DNA of the four clones HEK293-KARE1a to HEK293-KARE1d probed by PCR using the primer pairs given above each lane. (B, C) Comparison of cell morphology in bright field images of (B) HEK293-KARE1c and (C) HEK293. The morphology of HEK293-KARE1c looks similar to the one of the parental HEK293 cell line.

5.3.2. rAAV production in HEK293-KARE1

In order to assess the rAAV production ability and their long-term productivity, three HEK293-KARE1 clones were cultured similar to normal HEK-293 with the only difference of maintaining antibiotic selection at 5 µg BSD. First attempts for rAAV production started with adapting the three-plasmid co-transfection for high titer rAAV production in HEK-293 cells. Here, pHelper plasmid, Rep2Cap2^{587wt}- and ITR-plasmid are transfected in a molar 1:1:1 ratio and a total plasmid DNA amount of 15 µg per 100 mm dish.

First, a double transfection of the Rep2Cap2^{587wt} and ITR plasmid in a ratio of 1:1 was performed, whereby only the pHelper plasmid was omitted, but the total plasmid DNA amount of 15 µg per 100 mm dish was retained. These experiments were carried out with the three cell lines HEK293-KARE1a to 1c after passage 3 and 9 and as a negative control with HEK293 cells and as a positive control with HEK-293 cells and triple plasmid transfection. Genomic titers, or more precisely of DNase I-resistant particles, were determined directly without further purification from the crude cell extract using qPCR with a set of ITR-plasmid specific primers. To get meaningful results, the standard curve used for determination of the genomic titer was set up in equal amounts of crude cell extract from untransfected cells. Resulting genomic titers of this experiment are presented in Figure 19A.

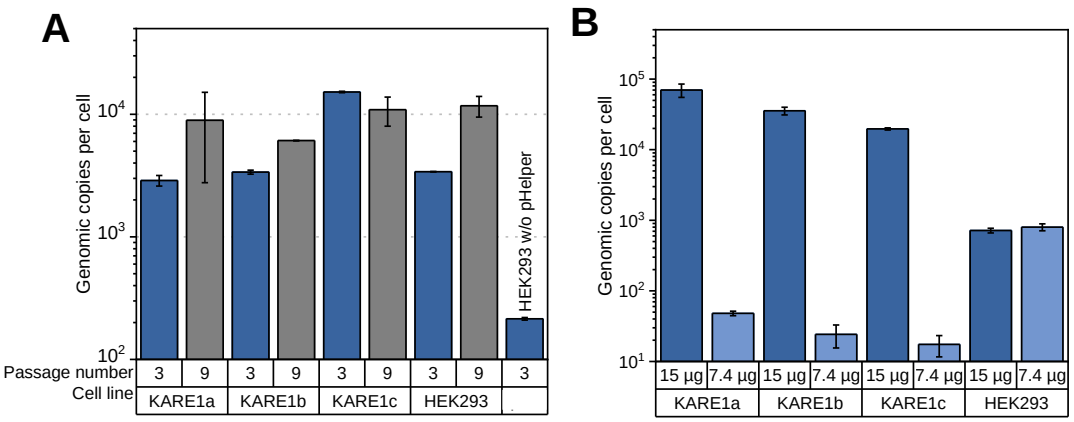

Figure 19: Analysis of rAAV2 production in HEK293-KARE1 and HEK-293 cells (A) HEK293-KARE1 cells (1×100 mm dish) were transfected with ITR-plasmid and RepCap-plasmid, for HEK293 the pHelper was included. Three days after transfection rAAV yield was determined from crude cell lysate after three freeze-thaw cycles by qPCR. A molar ratio of 1:1 of the plasmids RepCap:ITR was used during this experiment with a total of 15 µg plasmid DNA. For HEK2-93 cells experiments were performed also with a plasmid ratio of 1:1:1 for pHelper:RepCap:ITR. (B) HEK293-KARE1 and HEK293 cells (1×100 mm dish) were transfected with ITR-plasmid and RepCap-plasmid excluding the pHelper plasmid. Three days after transfection rAAV yield was determined from crude cell lysate after three freeze-thaw cycles by qPCR. A molar ratio of 1:1 of the plasmids RepCap:ITR was used during this experiment with a total of 15 µg or 7.4 µg plasmid DNA. For each column, standard deviation was calculated from two biological duplicates.

As expected, rAAV production was observed for HEK293-KARE1 clones when omitting the pHelper plasmid. HEK-293 cells transfected without addition of pHelper show a dramatic reduction in production capacity of viral particles. The relative high background may be related to residual plasmid DNA from the transfection. The rAAV yield for HEK293-KARE1 clones was in the range of 3.2×10^4 to 8.4×10^4 GC per cell (Figure 19A). For similar small-scale experiments with HEK-293 cells, albeit in a commercial context, a value of 8.3×10^4 GC per cell has been reported.[158] Other groups determined that the choice of primers and the reference material for qPCR (circular, linear DNA) have a tremendous effect on the genomic titers [159,160].Specifically, ITR primers compared to primers binding the gene of interest yielded up to ten times higher genomic copies when plasmids were used as reference. Here, primers binding the human growth hormone poly adenylation (hGHpA) region where used, whereas in literature primers binding the ITR region have been applied and both experiments used plasmid DNA as reference.[158] After long-time cultivation for nine passages no reduction of rAAV titer was observed and cryopreservation did not alter production capacity as these experiments were conducted from biological duplicates that were independently thawed.

5.3.3. Optimization of rAAV production in HEK293-KARE1c

The high amount of DNA and the addition of the antibiotic during the production process might not be desired. Lowering the required plasmid dose and omitting the antibiotic would reduce production costs and possible sources of product contaminations. Thus, a reduction of the total plasmid DNA amount from 15 µg to 7.4 µg was tested. This value corresponds to the total DNA amount of

Rep2Cap2^{587wt}- and ITR-plasmid in the standard triple-transfection protocol with just omitting the pHelper plasmid DNA. However, the yield decreased dramatically as shown in Figure 19B. Simply reducing the amount of DNA did not lead to a satisfying result. The calcium-phosphate transfection method is based on DNA-calcium phosphate precipitation which is dependent on a specific DNA to calcium ion ratio.[161] During transfection mix preparation a decreased turbidity of the transfection solution was observed, which indicated a deterioration of transfection efficiency and associated lower genomic titer.

For further optimization only clone HEK293-KARE1c was used because the productivity of all clones had a yield in the same order of magnitude. The adaption of the transfection protocol for the reduced amount of DNA resulted in genomic titers comparable to the use of 15 µg total DNA per transfection (Figure 20, first and second bar). In a second optimization step, the need for the selective pressure during the production process was evaluated. As it is known that gene silencing might occur if selective pressure is not maintained, the use of the antibiotic should not be generally omitted. Thus, only during the rAAV production no blasticidin was added. HEK293-KARE1c cells were seeded without addition of blasticidin and transfections was performed the day after. Comparison of genomic titers from crude cell extracts after 72 h proved rAAV production even without the addition of the antibiotic in comparable yields (Figure 20, third and fourth bar). The variations observed between separate biologic experiments (Figure 20, second and third bar) can be attributed to passaging and handling.

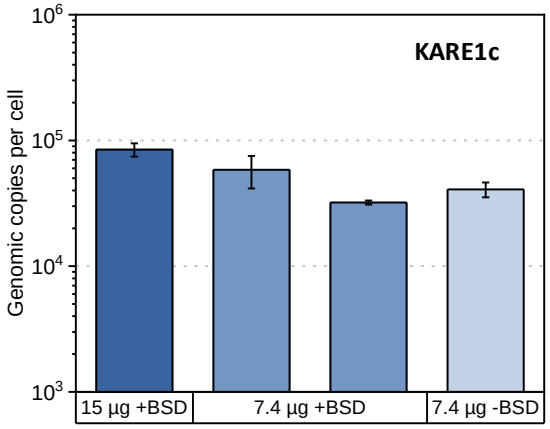

Figure 20: Comparison of rAAV production in HEK293-KARE1c cells depending on 15 µg transfection protocol and the optimized 7.4 µg transfection protocol. rAAV2 yield was quantified in crude lysates by qPCR. In general, RepCap and ITR plasmid were transfected in a molar 1:1 ratio. For each column, standard deviation was calculated from two technical duplicates.

5.3.4. Analysis of rAAV2 produced by HEK293-KARE1c

After reducing the amount of DNA and the concentration of antibiotic, the quality of the produced viral particles was characterized. rAAV2 was produced in the favorite HEK293-KARE1c clone. Cells were seeded on ten 100 mm dishes the day before transfection. Transfections were carried

out using the previously adapted calcium-phosphate transfection protocol with a total plasmid DNA of 7.4 µg (2.5 pg per cell) and 1:1 molar ratio of Rep2Cap2^{587wt} to ITR-plasmid. Viral particles were purified using a standard iodixanol-gradient ultracentrifugation protocol. The transducing titer was determined for a serial dilution of viral particles on HT1080 cells. The ITR-delivered gene of interest coded for the fluorescent protein mVenus under the control of a CMV promoter and thus successful transduction resulted in yellow fluorescent cells, which were analyzed by fluorescence microscopy and flow cytometry.

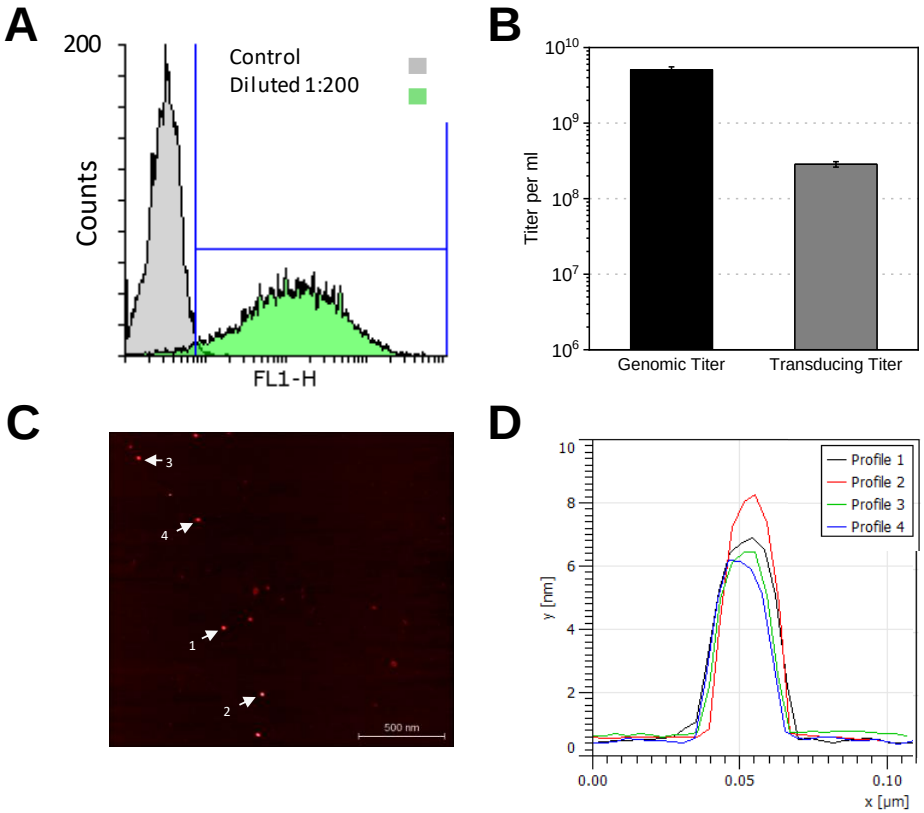

Figure 21: Characterization of rAAV2. Viral particles were produced in the HEK293-KARE1c cell line seeded in ten 100 mm dishes and subsequently purified via iodixanol ultracentrifugation. (A) Determination of transduction ability of rAAV (1:200 diluted sample) on HT-1080 cells using expression of the mVenus gene measured by flow cytometry of 10,000 cells in total. (B) The amount of DNase I-resistant particles was determined by qPCR from a standard curve of the ITR-plasmid. The total volume of the final viral sample was 2.5 ml. The transducing titer was determined based on percent of fluorescent cells as depicted in panel A (see methods). (C, D) rAAV were visualized by atomic force microscopy and resulting particle height profiles were determined. A mean diameter of 21.5 ± 1.8 nm was measured at half maximum height of 8 particles.

To calculate the transducing titer from flow cytometry data, the lowest serial dilution was used (Figure 21A) and the genomic titer was determined via qPCR. Both titers are presented in Figure 21B. The transducing titer is about 10-fold lower compared to the genomic titer which is in agreement with the literature.[162] The sample purified by ultracentrifugation was analyzed by atomic force microscopy (AFM) (Figure 21C). The calculated mean diameter of the marked particles is with 21.5 nm in the expected range of 20 to 24 nm (Figure 21D).[163] Hence, the quality of rAAVs produced using the novel cell line is equivalent.

A first attempt transferring the rAAV2 production platform towards serotypes 6 and 9 was successful with total vector genomes from one 100 mm dish of $1.95 \cdot 10^8$ for rAAV6 and $1.46 \cdot 10^9$ for rAAV9 which represents a 10 to 50 times lower yield compared to rAAV2 ($9.29 \cdot 10^9$ genomic copies per 100 mm dish), but may be associated with observed poor transfection efficiency in this approach.

In summary, by stably integrating the adenoviral helper genes VA RNA, E2A and E4orf6 into HEK-293 cells, the HEK293-KARE1 cell lines offer a simplified production platform for rAAV. The adaption of the transfection procedure towards a lower DNA amount does not only eliminate the time-consuming production and purification of the pHelper plasmid, but also reduces the high costs for the provision of sufficient plasmid DNA. This is even more important in the context of up-scaling. For this reason, an adaption to suspension should be considered in the future.

5.4. Generation and characterization of a HEK-293 AAVR knock-out cell line

After the discovery of the AAV receptor in 2016, the hypothesis arose that the productivity of HEK-293 cells can be improved by a knock out of this receptor, which is known to be essential for transduction.[30] We thereby hoped that rAAVs that were potentially released during production would not reinfect the production cell line and thereby increasing the yield.

A CRISPR/Cas9 (Clustered Regularly Interspaced Short Palindromic Repeats/CRISPR-associated protein 9) approach based on the Pillay *et al.* publication was implemented to induce an indel mutation in the HEK-293 AAVR gene. Two oligonucleotides were designed, hybridized and cloned into pSpCas9(BB)-2A-GFP from Zhang Lab.[164] The target sequence introduced is located in exon 3 of the AAVR receptor, directly adjacent to the protospacer adjacent motif (PAM). For AAVR knock-out, $3 \cdot 10^6$ HEK-293 cells on one 100 mm dish were transfected by calcium-phosphate with 15 µg of CRISPR plasmid DNA. After 2 days, successful transfection was detected by the expression of GFP from the CRISPR plasmid by fluorescence microscopy (Figure 22). Thereafter, cells were trypsinized and GFP-positive cells were sorted by fluorescence activated cell sorting (FACS). For this purpose, 1 ml of DMEM growth medium was added into a FACS vial and 100 of the cells marked as positive were sorted into the vial. From this cell suspension 10 µl each were seeded per well in a 96 well plate and filled up with 140 µl growth medium. Thus, statistically only one cell per well should be found. The sorting strategy is shown in Figure 22B, C. To determine a healthy cell population, only a small amount of cells was chosen based on a plot of sideward-scatter (SSC) against forward scatter (FSC) as marked in Figure 22B as a region of interest (ROI) with a green box. In a second step, only cells of this ROI were analyzed for their green fluorescence. Auto fluorescence of untransfected HEK-293 cells was determined to reach a signal strength of up to 10^1. Therefore, all cells that showed a signal beyond this were assessed as positive transfected. A positive population was determined with about a tenfold increase in signal-strength (Figure 22C, green

bar) and a super positive population with a 100 to 1000 fold increase in signal strength (Figure 22C, yellow bar).

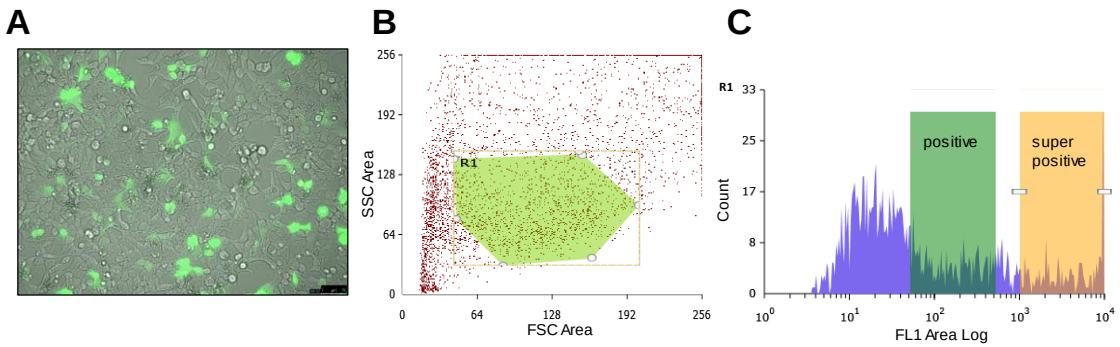

Figure 22: CRISPR-Cas9 knock-out of AAV receptor in adherent HEK-293 cells. $3 \cdot 10^6$ HEK-293 cells were seeded on one 100 mm dish one day before transfection. For transfection by calcium-phosphate precipitation, 15 µg of CRISPR plasmid DNA were used. (A) Detection of GFP expression from the CRISPR-Cas9 plasmid by fluorescence microscopy of transfected HEK-293 cells 48 h after transfection. (B, C) FACS analysis of transfected HEK-293 cells. (B) Plot of sideward scatter against forward scatter to determine living cell population by defining a region of interest (ROI) (R1 in green) (C) Plot of cell count against fluorescence intensity in FL1 channel. Only cell from ROI were plotted. Two regions were defined for GFP positive (green) and GFP super positive (yellow) cells and 100 cells of the respective region were sorted into a FACS vial with 1 ml pre-added DMEM.

After the cells had settled down, each individual well was screened to ensure that it contained only one cell at a time. Cells were cultivated for two weeks until they reached confluence. From the individual clones the genomic DNA was isolated by Chelex genomic DNA extraction and the region around the potential knock-out was amplified in a PCR. Theoretically. the primer pair should amplify a fragment with the size of 668 bp if genomic DNA extraction and PCR were successful (Figure 23A). As can be seen in Figure 23B, for all ten clones a fragment with the expected size was amplified and for all PCR reactions sequencing with Seq-AAVRko-for and Seq-AAVRko-rev was performed.

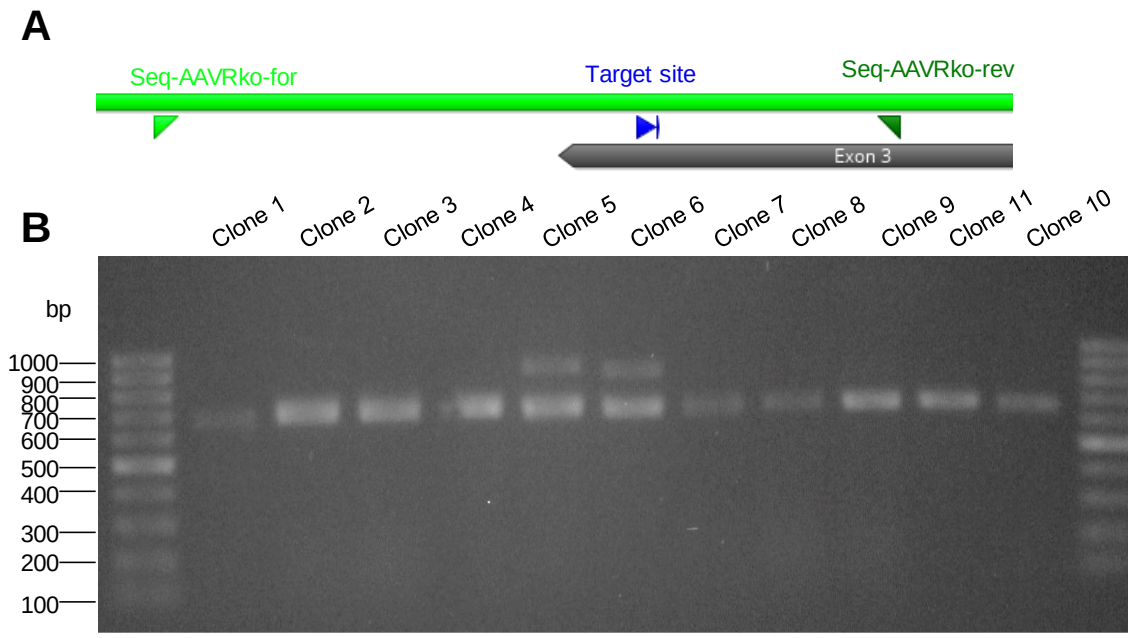

Figure 23: PCR analysis of HEK-293 AAVR knock-out clones. (A) Theoretical approach to amplify the area around the ko in exon 3 of the AAVR gene of 10 clones. A fragment with a size of 668 bp should be amplified if DNA extraction and PCR reaction were successful. (B) Agarose gel of the PCR analysis from amplification of the region surrounding the ko in AAVR gene. Genomic DNA of the ten clones HEK-293-AAVRko1 to HEK-293-AAVRko1 was probed by PCR using the primer pair Seq-AAVRko-for and Seq-AAVRko-rev.

Interestingly, most of the clones from the super positive area did not expanded. Potentially high dose of the CRISPR plasmid led to cellular stress which resulted in increased cell death. The sequencing reactions revealed, that HEK-293 cells were triploid for chromosome 1p34-36 and therefore several sequences overlapped and made an evaluation impossible. In order to avoid this problem, the PCR reactions were cloned into a TOPO TA cloning vector so that all individual sequences could be covered by the delivery of several clones.[165] Most of the clones possessed at least one chromosome where no indel mutation occurred (Figure 24A). These clones were suspected to be heterozygous and still express a certain amount of AAV receptor. For the most promising clone (Figure 24B), two chromosomes showed a deletion of 18 and 5 bp respectively. For the third chromosome, an insertion of 1 bp was detected

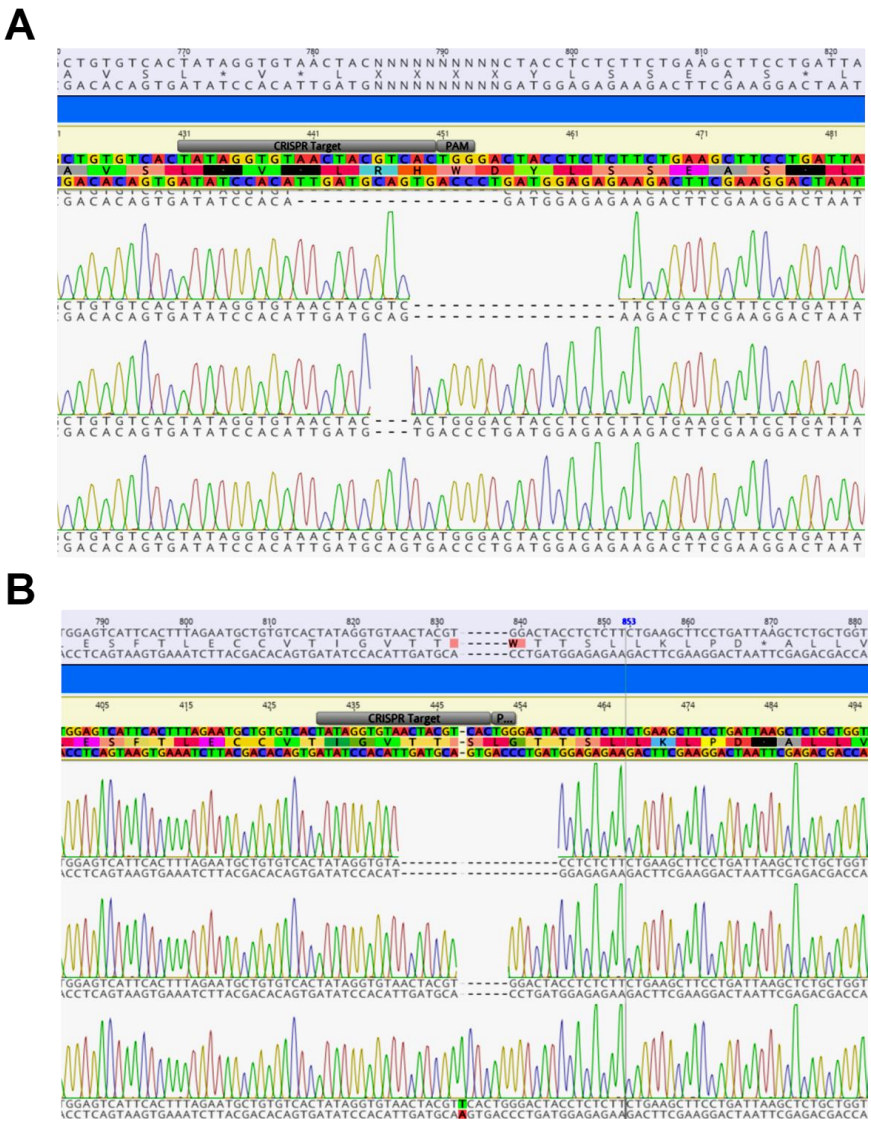

Figure 24: Sequencing results using the primer pair Seq-AAVRko-for and Seq-AAVRko-rev of two clones after cloning of PCR products into TOPO TA cloning vector. (A) Sequencing reaction of a clone with two chromosomes showing a knock-out and one chromosome still possessing the original sequence. (B) Sequencing reaction of a clone with two chromosomes showing a knock-out and one chromosome showing an insertion of one nucleotide.

This clone was further characterized by transduction experiments in a master thesis of Greta Bischof but still transduction by rAAV2 was possible. Since 18 is a multiple of 3, a deletion of 6 amino acids in exon 3 is presumed to have occurred only, and not a shift in the reading frame, so that an AAV receptor can be formed that is still functional. Therefore, in the master thesis of Greta Bischof, this cell line was newly generated which possessed a 2 bp, 4 bp and a 14 bp deletion and by this on all chromosomes a frameshift should occur.[166]

The assumption persisted that produced AAVs that are released from the production cell, for example by cell death, could transduce other production cells thereby reducing the rAAV yield. To resolve this issue, the homozygous AAVR knock-out cell line was utilized for rAAV2 production by triple transfection. In parallel rAAV2 were produced in the standard HEK-293 cells and the

resulting genomic titer was determined. Transfection efficiency was determined by the expression of mVenus gene from the ITR containing plasmid and was comparable for both cell lines with 96 % for HEK-293 and 94 % for HEK-293 AAVR ko and by this no effect of different transfection efficiencies had to be taken into account when comparing total genomic copies. For both cell lines, total genomic copies were determined from crude cell lysate after 3 freeze-thaw cycles. Total genomic copies for HEK-293 was $3.3 \cdot 10^{12}$ and $2.8 \cdot 10^{12}$ for the AAVR knock-out cells. Therefore, no increase in yield was achieved through the AAVR knock-out. Thus, at least for rAAV2 the hypothesis of reinfection and hence a reduction of the yield cannot be confirmed. However, as for rAAV2 the majority of viral vectors were found in the cell pellet,[167] the effect of reinfection is potentially not as pronounced as for other serotypes that are released more into the culture medium which should be studied in the future.

5.5. Establishment of a novel rAAV affinity purification process

Results for the generation of an affinity purification material were summarized in a manuscript with the title 'Generating a quick, easy and low-cost affinity purification method for rAAV based on adeno-associated virus receptor's PKD domain'. Results on this have originated in cooperation with Julian Teschner and Monja Leppin. A summary of my part is presented in the following chapter. The original manuscript is included in the appendix and currently serves as a template for a patent.

Standard processes for the purification of rAAV, relying on a cesium chloride (CsCl) or an iodixanol gradient ultracentrifugation. However, they are restricted in their potential to scale up. Often, several chromatography steps are included into downstream processes like ion exchange, size exclusion and heparin column chromatography. These procedures are not only time intensive but are accompanied by high costs and cumulative loss in yield. In this work a scalable affinity purification strategy, based on the natural AAV receptor AAVR was established. As an affinity ligand, PKD2 was chosen in the first step, as Pillay *et al*. published that AAVR PKD2 is critical for the interaction of AAV2 with AAVR.[32] As a supporting material, cellulose was elected as a cost-effective material with advantageous properties such as low unspecific binding and good physical and chemical resistance under selected process conditions. In order to avoid the clogging of a packed chromatography column by residues of the cell lysate, blotting paper was utilized, so that the incubation of cell lysate containing rAAV was carried out in batch mode and not in the usual flow process of a packed column. An overview of the rAAV purification strategy is given in Figure 25.

In order to avoid time-consuming and elaborate steps in the purification procedure, the method has been designed to be performed directly from the crude cell extract as concentration steps with ammonium sulfate or polyethylene glycol (PEG) precipitation interfere with upscaling due to the need for a centrifugation step.[168] As depicted in Figure 25 section 3, in contrast to a packed column the chosen cellulose material in form of blotting paper allows for a batch process in where the rAAV containing suspension is either stirred or shaken with the PKD functionalized paper. Thereafter, the

column material can be transferred into a spin tube and by this, separation of the column material from the elution can easily be executed. As for commercial POROS CaptureSelect AAVX or AVB Sepharose High Performance, batch processes can also be conducted, but separation of the material from the sample is not easily realized as the small sized particles are sticking to the vessels.

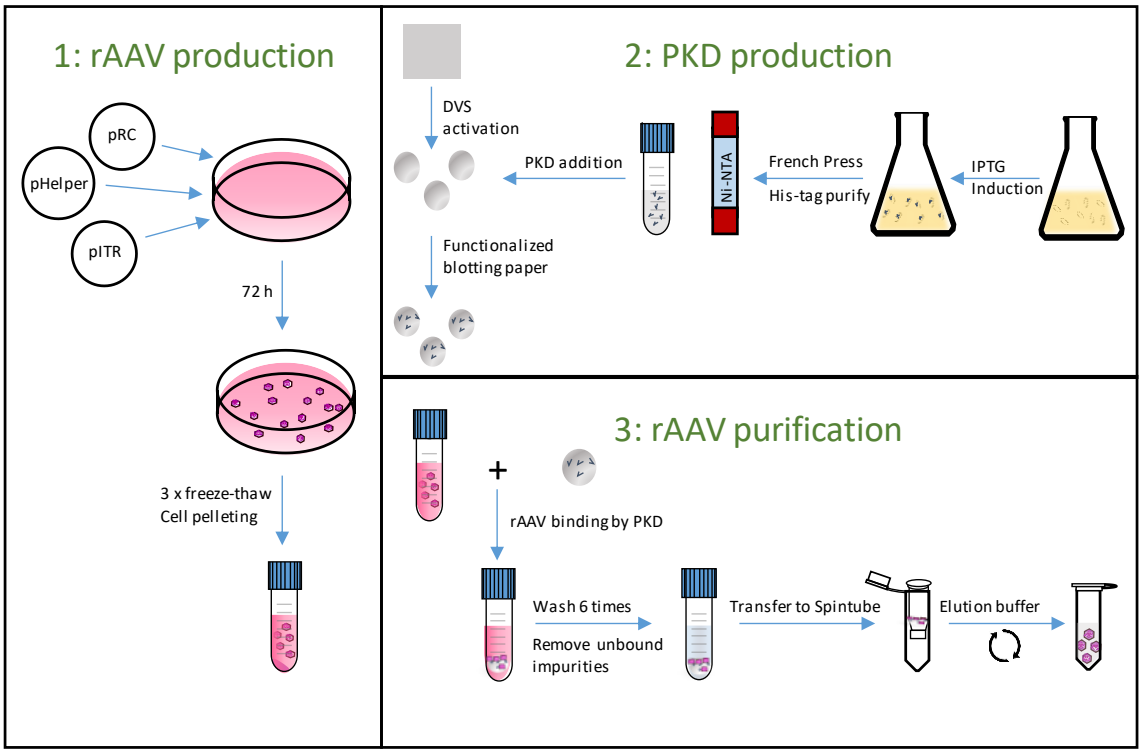

Figure 25: Schematic representation of recombinant adeno-associated virus (rAAV) manufacturing technology. (1) Adherent HEK-293 cells are seeded and transfected with the three-plasmid system and harvested after 72 h. rAAVs were released from the cells by three freeze-thaw cycles and cell debris is pelleted by centrifugation (2) E. coli BL21(DE3) cells expressing PKD-MBP are cultivated in shaker flask for 4 h after induction with IPTG. The cell pellets are resuspended and then lysed using a french press. Lysate is clarified and loaded onto a ÄKTA FPLC and purified using IMAC. Blotting paper (BP) is activated by divinyl sulfone (DVS) and functionalized with purified PKD overnight. (3) rAAV containing clear lysate is incubated with functionalized BP and rAAV are eluted by transferring the BP to a spin tube and covering it with elution buffer. The rAAV containing elution is then dialyzed into the final storage buffer.

5.5.1. Expression and purification of PKD2-MBP in *E. coli*

For the expression of PKD2 as an affinity ligand, it was subcloned into a pET-24b expression vector from KIAA0319L full cDNA clone by PCR amplification of amino acid 405 to 502, which included four amino acids to the left and to the right of the domain as proposed by Pillay *et al*. in order to ensure correct protein folding.[30] To increase solubility the sequence of the maltose-binding protein (MBP) was subjoined separated by a short glycine-serine linker at the 3'-end of PKD2. Here, subsequently a 6× His-tag was introduced to allow purification of the fusion protein from *E. coli* production. A theoretical sequence of the fusion protein is given in Figure 26A. The success of purification after immobilized metal affinity chromatography (IMAC) is shown in Figure 26B. PKD2 can be produced in high concentrations and purity when fused to MBP and thus inexpensive supply of the affinity ligand is possible.

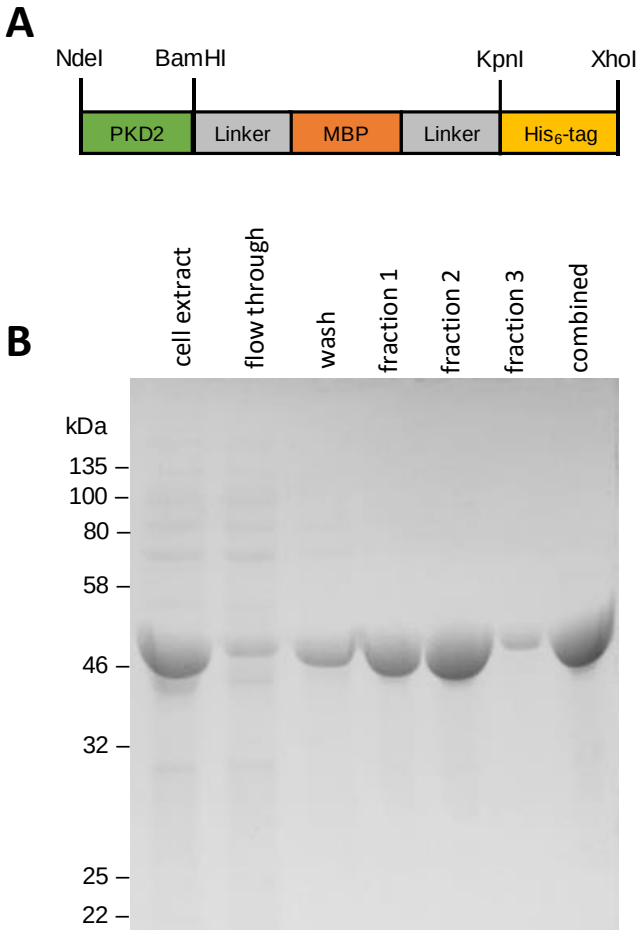

Figure 26: Construction and production of PKD2-MBP fusion protein. (A) Schematic representation of the basic components of the PKD2-MBP-fusion protein with its unique restriction sites for cloning and the position of GGSG linker sequences. (B) Coomassie-stained SDS PAGE protein analysis of PKD2-MBP purification steps. Cell extract, Ni-NTA column flow through and the wash fraction were diluted 1:2 in PBS buffer and elution fractions 1 to3 as well the combined and re buffered elution fraction was diluted 1:10 with PBS before loading.

5.5.2. Proof of binding of rAAV2 to PKD2-cellulose

For covalent binding of PKD, divinyl sulfone (DVS) activation of the cellulose was chosen. Here, one of the vinyl groups reacts with a hydroxyl-group of the cellulose. The remaining vinyl group reacts with nucleophiles and by this covalently attaches biomolecules to the cellulose surface (Figure. 27).[169]

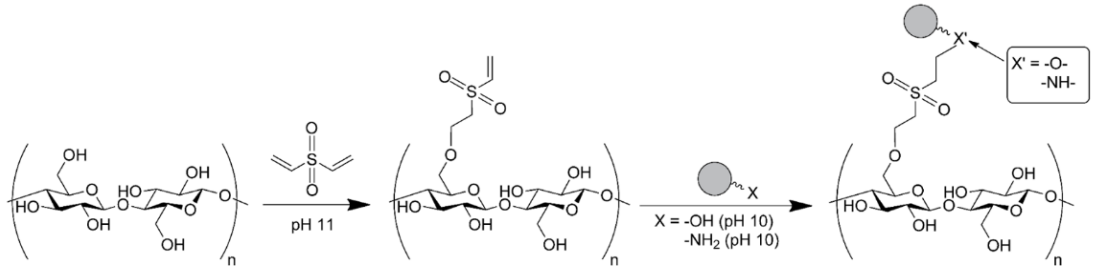

Figure. 27: Activation of cellulose with divinyl sulfone and functionalization with nucleophile-bearing molecules (gray) as published by Yu et al..[169]

The binding of rAAV2 to PKD2 is known, but a negative influence of covalent coupling on PKD2 functionality by steric hindrance or coupling to the cellulose resin with important amino acids could not be excluded. Therefore, the binding of rAAV2 to the PKD2-blotting paper (PKD2-BP) was proven prior to the optimization of the purification strategy. 30 µg PKD2-MBP were coupled to 1 cm^2 DVS activated blotting paper and subsequently incubated with $5.7 \cdot 10^8$ virus genomes (vg) of ultracentrifuge (UC) purified rAAV2 for 20 min, followed by two wash steps. The supernatant, PKD2-BP before (BP-rAAV2) and after the wash step (BP-washed) and the wash fraction where analyzed by western blot analysis. As can be seen in Figure 28A, VP1, VP2 and VP3 were detected in the expected ratio on the PKD2-BP, with the washing procedure (BP-washed) had a low influence on signal strength. In the wash fraction no viral capsids were detected by western blot, which is in good accordance with qPCR data. These data further revealed that 78 % of rAAV2 were bound to the material, suggesting that the resin was saturated Figure 28B.

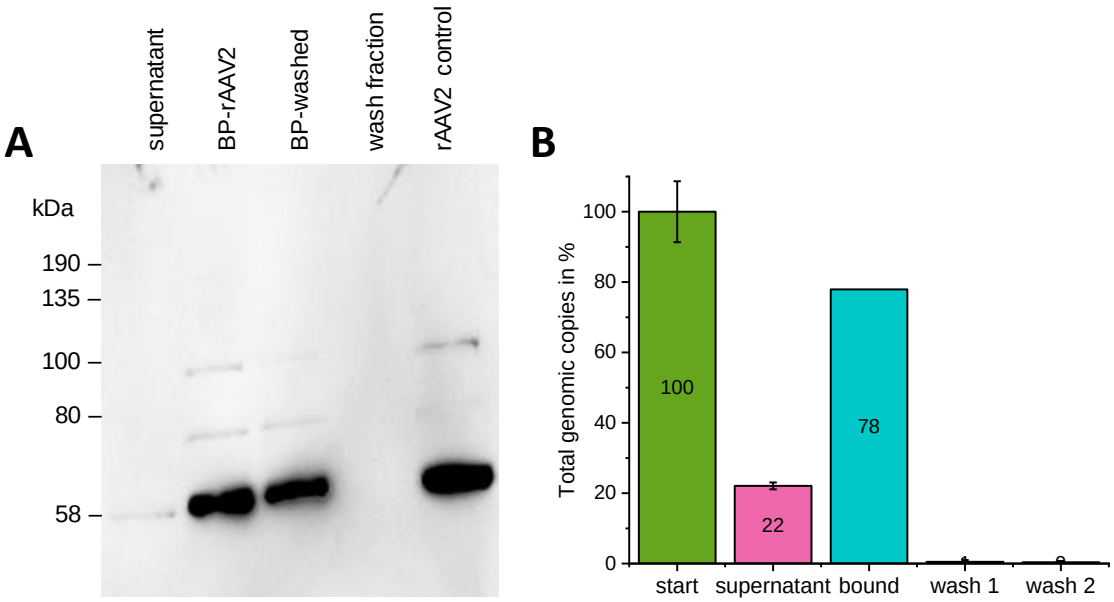

Figure 28: Characterization of rAAV2 binding to the PKD2-BP resin. (A) Western blot analysis of binding of UC purified rAAV2 to the PKD2-BP resin. (B) qPCR analysis of DNase I-resistant particles remaining in the respective fractions. Percentages were calculated by setting the genomic titer of starting material as 100 %. For each column, standard deviation was calculated between two technical replicates.

5.5.3. Optimization of PKD2 amount and elution conditions

Previous western blot analysis confirmed, that covalent binding of the fusion protein to blotting paper by DVS activation did not impair the functionality of PKD2, so that the binding of rAAV2 to the blotting paper was possible.

Even if rAAV binding to the resin was proven, 22 % of the vector genomes were still found in the supernatant. Therefore, the amount of PKD2 applied for covalent coupling was varied in order to optimize the binding conditions. $5.7 \cdot 10^8$ vg of UC purified rAAV2 were applied to 12 µg, 30 µg

and 120 µg PKD2 coupled to BP, and non-bound virus were detected by qPCR in the supernatant. As depicted in Table 5, no correlation between the amount of coupled PKD2 and rAAV2 in the supernatant was seen. Though, taking the excess of PKD2 towards rAAV2 into account no limitation was expected.

Table 5: Relationship between amount of applied PKD2 to the amount of rAAV2 vg in the supernatant and estimated functional PKD2 molecule number.

Amount of PKD2	**rAAV2 vg in supernatant in %**	**PKD2 molecule number**
2 µM (12 µg)	7.8 ± 19.8	$1.2 \cdot 10^{14}$
5 µM (30 µg)	22.1 ± 0.98	$3 \cdot 10^{14}$
20 µM (120 µg)	6.0 ± 26.1	$1.2 \cdot 10^{15}$

The increase in the amount of PKD2 did not decrease the quantity of rAAV2 found in the supernatant. Potentially, even if the amount of PKD2 was raised, no more functional protein was covalently bound, as the method for coupling does not allow for quantification of bound protein as the blotting paper was just soaked with the protein without any protruding solution. After protein coupling SDS-PAGE analysis with subsequent determination of bound protein should be considered in the future. However, as the amount of affinity ligand exceeds applied viral capsids by far it can be speculated, that non bound rAAV2 may be in a structural conformation which does not allow for accurate binding. If this hypothesis could be confirmed, this method would primarily purify biologically relevant viruses and thus would have a substantial advantage over other systems.

As there was no tendency for the most appropriate PKD2 concentration definable, further experiments were carried out with 30 µg PKD2 and elution conditions were evaluated. Lowering the pH or increasing the ionic strength is well known for affinity purification procedures. Therefore, an elution buffer with 100 mM citric acid, pH 2.5 and a 2.5 M magnesium chloride ($MgCl_2$) buffer, pH 7.0 were selected. Starting with UC-purified rAAV2, only 0.2 % of the starting material was found in the pH elution sample, whereas for the $MgCl_2$ elution a 33.5 % yield was reached after buffer exchange. Subsequently, all following attempts were performed with 2.5 M $MgCl_2$ 50 mM Tris pH 7.0. The $MgCl_2$ buffer did not only result in the highest amount of rAAV but also offers the advantage of a neutral pH as other methods relying on elution conditions within a pH range of pH 2.0 - 3.0. AAV undergoes autolytic proteolysis at low pH which results in a decrease in VP1 and VP2 and in an increase in lower-molecular-mass bands.[170] For AAV serotype 8, amino acid side chain conformational rearrangements were observed at low pH values.[171] However, effects on viral preparation potency still need to be investigated.

5.5.4. Description of the purification strategy from crude cell extract

For purification of rAAV2, predetermined conditions were used with crude cell extract of rAAV2 containing HEK-293 cells. rAAV2, which carried the mVenus fluorescent protein as a transgene, were produced in HEK-293 cells by triple plasmid transfection using calcium-phosphate. After

three days, rAAV2-mVenus were released by three cycles of freeze-thaw and the clarified supernatant of one 10 cm dish was incubated for 20 min with PKD2-BP while rotating on a roll-tumble shaker. The resin was then washed rigorously with PBS-Tween until residual phenol red from the spent cell culture medium was undetectable. For elution, the resin was covered with 500 µl elution buffer in a spin tube for 5 min before centrifugation at 1000 × g for 2 min. After three cycles of elution, the fractions were combined and buffer exchange to HBSS was performed by ultra-centrifugal filters units with a cut-off of 100´000 kDa. In qPCR, 41.5 % of vectors genomes were detected in the supernatant which was more than in previous trials with UC purified rAAV2. 24.6 % of total virus genomes were found in the combined elution fraction (Figure 29A). The discrepancy between bound and eluted rAAV2 and the total amount of vector genomes applied shows that not all viruses may have been eluted from the resin. However, it is also conceivable that some viral capsids may be destroyed during elution, creating the gap between the applied and rescued rAAV2 vector genomes. In addition, artefacts of genomic titer determination are possible. On the one hand, the qPCR reaction reacts sensitively to buffer conditions, which differ greatly between the cell extract and the rebuffered elution fraction.[172] On the other hand, the genomic titer is potentially overestimated in the beginning as the DNase I is potentially inhibited during the digestion process of non-encapsulated DNA before genomic titer determination as regularly observed by us.

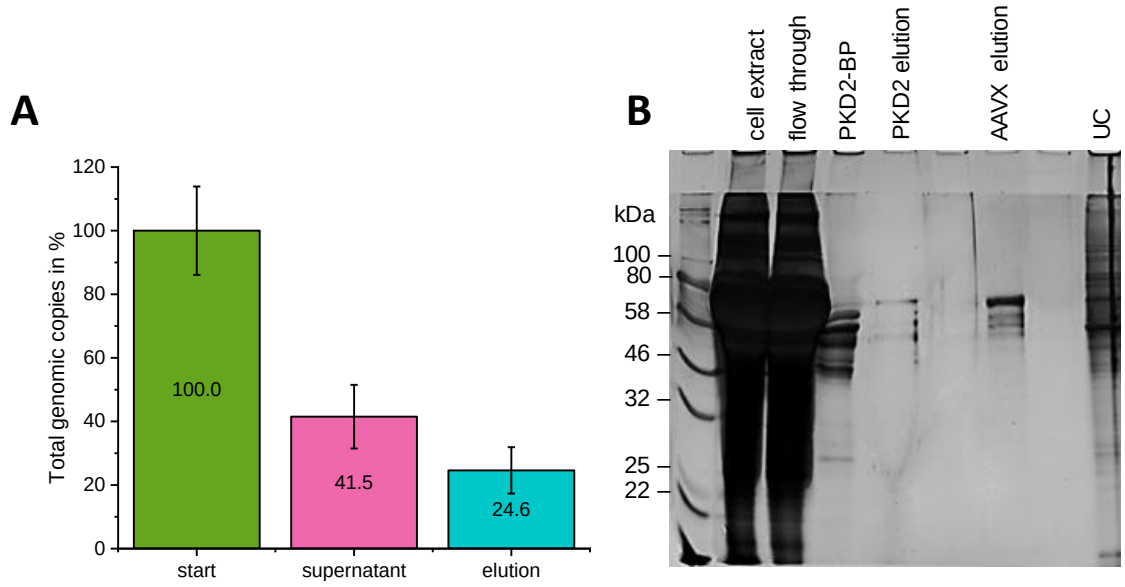

Figure 29: Characterization of rAAV2 binding to PKD2-BP from HEK-293 crude cell extract. (A) Distribution of DNase I resistant particles in the respective fractions. Percentages were calculated by setting the genomic titer of starting material as 100 %. Genomic titer was quantified in crude cell extract after three freeze-thaw cycles for start value and for supernatant value after incubation with PKD2-BP by qPCR. For each column, standard deviation was calculated between two technical replicates. (B) Silver-stained SDS PAGE analysis of rAAV2 sample purity after purification with PKD2-BP, POROS AAVX or UC. Viral particles were produced in HEK-293 cells seeded in two 100 mm dishes for each purification method and subsequently purified via PKD2-BP, POROS AAVX or iodixanol ultracentrifugation.

To compare the conventional UC method with a commercial affinity purification and the new PKD2 resin, two 10 cm dishes were purified either by PKD2, POROS CaptureSelect AAVX affinity resin (POROS AAVX) or UC, and the elution fractions were analyzed by qPCR (Table 6).

Table 6: Comparison of recovery rate for different purification approaches.

	vg loaded in total	**vg recovered total**	**Recovery rate in %**
PKD2	$8.32 \cdot 10^{11}$	$1.46 \cdot 10^{11}$	17.5 %
POROS AAVX	$8.32 \cdot 10^{11}$	$1.12 \cdot 10^{11}$	13.4 %
UC	$8.32 \cdot 10^{11}$	$3.2 \cdot 10^{11}$	38.0 %

For UC-purified rAAV2 the highest recovery rate was reached, whereas for PKD2 and POROS AAVX with 17.5 % and 13.4 %, respectively a similar yield was obtained. In a SDS-PAGE using silver nitrate staining (Figure 29B), many protein contaminants were observed for UC-purified samples and, to a lower extent also for the POROS AAVX column material. Interestingly, the impurities in the POROS AAVX sample showed the same pattern as observed for the PKD2 sample. The most prominent contaminant was detected with a molecular weight of approximately 60 kDa, which may potentially be residual BSA or VP3. For the PKD2-BP resin, some other proteins were bound to the material, indicating that a more rigid wash procedure may be necessary to diminish these.

5.5.5. Biological characteristics of PKD2 purified rAAV2

To analyze the biological activity of PKD2-purified rAAV2, a transducing titer assay on HT1080, as well as a capsid ELISA (enzyme-linked immunosorbent assay) for the determination of empty capsids was performed and compared to UC-purified rAAV2. Additionally, a sample after POROS AAVX purification was used in order to have a comparison to another affinity purification system. Here, 500 µl of slurry were used to purify rAAV2 from the clarified supernatant of a 10 cm dish, analogous to PKD2.

For the determination of the ratio of full to empty capsids, a new capsid ELISA was established. While the standard capsid ELISA from Progen utilizes the A20 monoclonal antibody (mAB) to capture fully assembled AAV capsids, PKD2 was coupled to the surface of a microtiter plate. For detection of captured viral capsids, a recombinant A20 single-chain variant (A20 scFv-Fc) was cloned by Julian Teschner and produced during this work in HEK-F suspension cells.

The conversion of the substrate ABTS (2,2'-azino-bis (3-ethylbenzothiazoline-6-sulphonic acid) by the horseradish peroxidase coupled to the secondary antibody in ELISA was compared to the standard A20 antibody from Progen. The signal strength reached was higher for A20-scFv-Fc as for A20 antibody, and by this has the advantage of giving higher signal to noise ratio in the case of low

signals due to low concentrations (Figure 30A). Whether this is a result of more A20-scFv-Fc molecules bound to the surface of rAAV2 or due to the different secondary antibody (anti-human HRP vs. anti-mouse HRP) does not emerge from this.

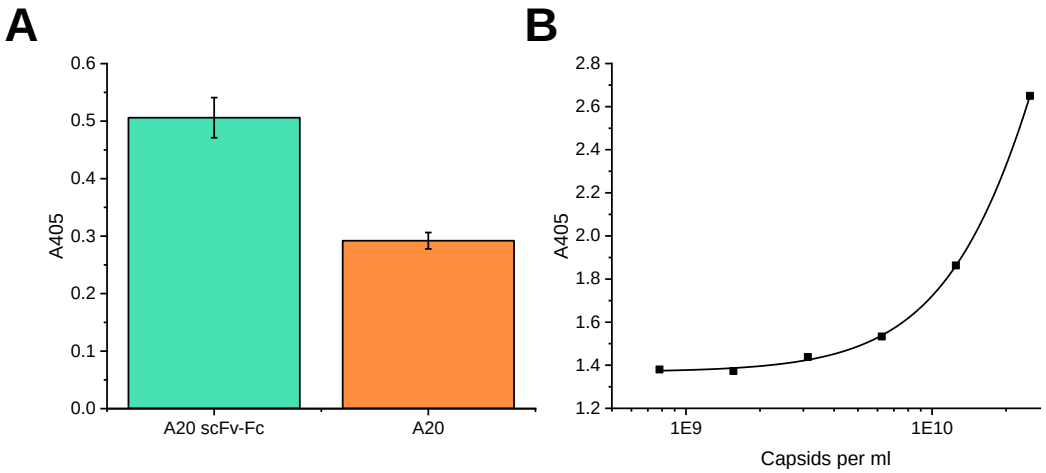

Figure 30: Analysis of A20-scFv-Fc functionality. (A) The AAV capsid ELISA was performed with PKD2 as the primary molecule to bind rAAV2. For detection A20-scFv-Fc or commercial A20 were used with the same final protein concentration (50 µg/ml). These were finally bound either by anti-human HRP or anti-mouse HRP antibody, respectively. Error bars are calculated from the standard deviation of three technical replicates. (B) Standard curve for the determination of capsid titer with PKD2 for capturing and A20-scFv-Fc for detection. The kit control from AAV2 titration ELISA (Progen) was diluted as recommended in the kit instruction. The particle titer was calculated by a 4-parameter logistic fit with OriginPro 2018 software. The equation was: $y = A2 + (A1 - A2)/(1 + \left(\frac{x}{x0}\right))\hat{}p)$ *with A1: 1.368; A2: 6.752; x0: 5.102 and p: 1.631.*

In order to determine the capsid concentration of the individual purified samples, a standard curve based on a known capsid titer was prepared (Figure 30B). This curve showed the expected logarithmic progression as it is also known for the commercially available capsid ELISA. Therefore, results of this newly developed capsid ELISA are to be regarded as reliable. Using this method, the highest ratio of full to empty capsids was determined, for UC-purified rAAV2 with 0.27, whereas for PKD2 and POROS AAVX the ratio is roughly the same.

Table 7: Biological characteristics of PKD2, POROS-AAVX and UC purified rAAV2 samples.

	TU/ml	**Capsids/gc**	**full to empty ratio**
PKD2-BP	$1.6 \cdot 10^8$	7.07	0.14
POROS AAVX	n.D.	5.89	0.17
UC	$1.9 \cdot 10^8$	3.63	0.27

As empty capsids may cause serious side effects in patients, also for UC-purified sample another polishing step is normally applied and by this, UC offers only a slight advantage when used as a one-step purification strategy in the context of research, when the high purity of vector preparation is not needed.

5.5.6. Purification of in suspension produced rAAV2 by PKD2

For an efficient rAAV manufacturing process, a transfer of the purification strategy for the adherent produced rAAV towards serum-free, suspension-based produced rAAVs is desirable. Suspension-based rAAV production in HEK-F cells has already been established in the working group. However, several attempts for the purification of rAAV from the cell extract, using the standard ultracentrifuge protocol, have not yet been successfully completed. Since regular flocculation could be observed during cell disruption, which cannot be eliminated during the subsequent centrifugation step, we assume that medium components react with the viral capsid, thus preventing efficient purification by ultracentrifugation. In order to determine whether purification of rAAV from HEK-F using the PKD affinity resin is possible, HEK-F suspension cells were cultivated in HEK-TF (TF) medium and rAAV2 were produced by PEI-mediated triple transfection. After three days, viral particles were released from the cells by three freeze-thaw cycles and 1 ml of the clarified supernatant was incubated with PKD2-BP (Figure 31A). With 41.5 % a huge amount of rAAV2 vector genomes were found in the supernatant. For the elution fraction a comparable yield of 21.1 % of the initially used vector genomes was achieved as seen before for the rAAV2 purification from adherent HEK-293 cells (Figure 30A). Even though the yield was relatively low, it served as a good starting point for further optimizations.

In order to exclude that the chosen column material has a decisive influence on the yield, a commercial column material was additionally tested for the immobilization of PKD2. The chosen AminoLink™ Plus Coupling Resin (Thermo Scientific) is an aldehyde-activated beaded agarose, where proteins can be covalently attached through primary amines. As recommended by the manufacturer, 300 µg of PKD2 were coupled to 200 µl (400 µL slurry) of the AminoLink (AL) resin.[172] As before, 1 ml of the same clarified cell lysate was incubated with the AL resin, leaving all subsequent steps unchanged. As can be seen in Figure 31B the yield in the elution fraction was comparable to those of the PKD2-BP resin and by this the AL-material showed no advantage over the much cheaper cellulose material. On the contrary, the agarose beads were difficult to handle in the intended batch process and, moreover, the amount of PKD used was disproportionately much higher (300 µg for AL instead of 30 µg for BP).

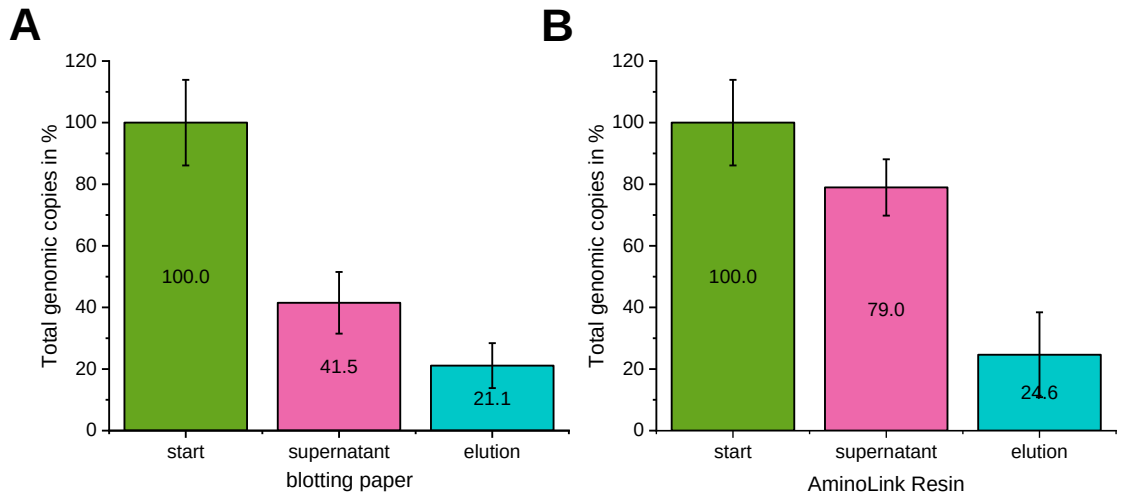

Figure 31: Purification of rAAV2 by PKD2 affinity chromatography from HEK-F suspension cells. (A) Distribution of DNase I resistant particles in the respective fractions after purification with PKD2-BP. (B) Distribution of DNase I resistant particles in the respective fractions after purification with PKD2-AL. Percentages were calculated by setting the genomic titer of starting material as 100 %. Genomic titer was quantified in crude cell extract after three freeze-thaw cycles for start value from 1 ml culture, and for supernatant value after incubation with PKD2-BP by qPCR. For each column, standard deviation was calculated between two technical replicates.

Since no improvement of the yield was achieved by changing the carrier material, variants of the TF medium used were tested in cooperation with Xell AG for the high-titer production of rAAV2 and for the improvement of affinity purification. For this reason, HEK-F cells were adapted for three passages in the respective medium variants and rAAV2 was produced by PEI-mediated triple transfection in a total volume of 10 ml as before. As demonstrated in Figure 32A, the genomic titer, determined by qPCR from the cell lysate after three-freeze thaw cycles, varied between the different media with a factor of about 10 for the worst variant V5 and the two best variants V1 and TF. As the yield was low for variant 3 to 5 no purification was attempted. For variant V1, V2 and TF the POROS-AAVX material was chosen for purification to investigate whether affinity chromatography with PKD2 yields similar results with the selected suspension medium to those obtained with a commercial variant. As presented in Figure 32B, only V2 resulted in a comparable yield with 23.8 % of total vg in the elution fraction. For TF and V3 medium, with 11.6 % and 11.9 %, total vg, respectively in the elution fraction the yield was even lower as with PKD2-based purification.

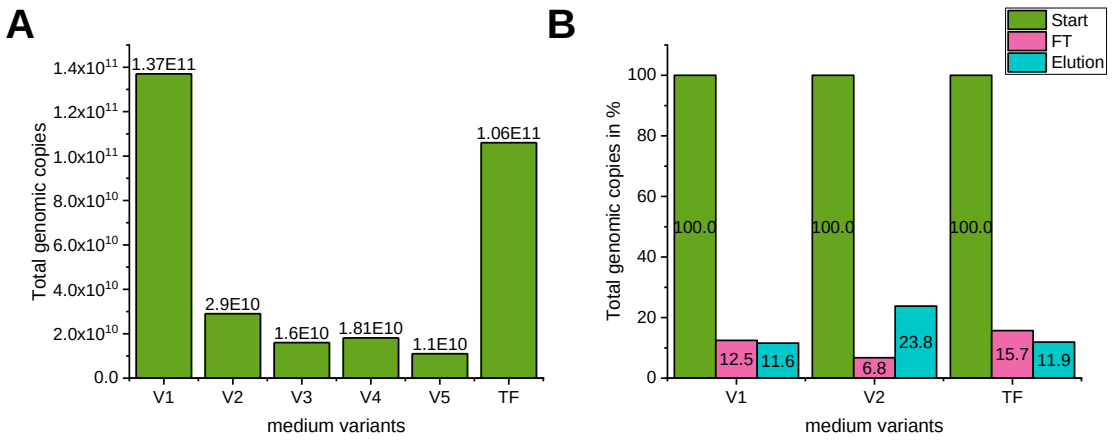

Figure 32: Analysis of different HEK-TF medium variants for rAAV2 production. (A) qPCR analysis of rAAV2 production in HEK-F suspension cells in HEK-TF medium and variant 1 to variant 5 in cleared crude cell extract after three freeze-thaw cycles. rAAV2 was produced by PEI-mediated triple transfection in a total volume of 10 ml. (B) Purification of rAAV2 from HEK-F suspension cell production in HEK-TF medium and the medium variant V1 and V2 from the cell pellet after freeze-thaw of a 10 ml production with POROS AAVX.

Since the yield for rAAV produced in adherent as well as suspension cells is still low, further optimizations need to be made here. However, the results showed that a cellulose-based column material had advantages over an agarose-based material in the planned batch process. The yield achieved is comparable to the commercial POROS AAVX. Further optimization in the field of cell disruption to avoid flocculation and to improve elution conditions must be considered as future steps.

As the affinity chromatography in general was successfully implemented for AAV serotype 2, Monja Leppin transferred the conditions to the other serotypes commonly used in our lab during her master thesis. Combinations of the PKD domains 1 to 5 with AAV serotype 6 and 9 with subsequent elution and qPCR analysis revealed a high affinity of rAAV6 to PKD3 and for rAAV9 towards PKD2 and PKD5. SDS PAGE analysis showed the high purity of the vector preparations. This gives rise to the assumption that a transfer of the method will be possible for other AAV serotypes and needs to be evaluated in the future.

5.6. Extension of the existing plasmid system for the production of mosaic rAAV

Detailed studies on the modifiability of the rAAV2 capsid with regard to its stability and plasticity were carried out in this working group.

Results for this topic were summarized in a manuscript with the title ' rAAV engineering for capsid-protein enzyme insertions and mosaicism reveals resilience to mutational, structural and thermal perturbations ' and submitted to the International Journal of Molecular Sciences. Data presented in the manuscript are the result of a collaborative effort. Only the results generated in this work are summarized here and the original manuscript is included in the appendix.

In this work, rAAV production was primarily conducted by triple transfection of HEK-293 cells with the so-called Helper-free plasmid system. Here, *rep* and *cap* genes are provided in *trans* on a RepCap plasmid whereas the packaged transgene is provided between the ITRs on the ITR plasmid. Required helper functions are delivered by a pHelper plasmid. In the beginning of this thesis, the plasmids used in this work were created during an iGEM competition.[173] In the context of iGEM the BioBrick RFC[10] based cloning strategy was introduced into the plasmids. However, there was the issue that as soon as a part within the plasmid was to be replaced, it had to be reassembled from the individual components from the beginning. The ITR sequences are very prone to mutations during plasmid propagation in *E. coli* and frequent cloning should be avoided. Thus, a new ITR plasmid (pZMB0522_ITR_EXS_CMV_mVenus_hGHpA) was constructed. In this plasmid the ITR sequences were part of a pUC19-based backbone where EcoRI, XbaI as prefix and SpeI as suffix sites were integrated by hybridized oligonucleotides. As before, this plasmid can be modularly assembled using biobricks but without the need for cloning of the ITRs. rAAV2 produced with this ITR plasmid showed the same characteristics regarding rAAV yield and quality as a commercial plasmid (pAAV-RC, GenBank: AF369963.1).

For the RepCap plasmid (pZMB0216_Rep_VP123_453_587wt_ p5tataless) unique restriction sites exist, allowing for easy modification of the loop region 453 and 587. Integration of DNA sequences into these loop regions results in the expression of the corresponding amino acids in all VP proteins which implies a total of 60 modifications on the virus surface. The iGEM plasmid system also allowed for the fusion of proteins to the VP2 N-terminus and by this generation of mosaic viruses.[58] In this approach the start codon of VP2 was mutated in the RepCap plasmid (pZMB0600_Rep_VP13_453_587wt_p5tataless) and a fourth plasmid provides in *trans* modified VP2 and VP3. VP3 is always a part of the VP2 gene since both are encoded by the same mRNA and are differently expressed only by a leaky scanning mechanism at the VP2 start.[174] In N-terminal fusion, the expression of VP3 is unproblematic, since VP3 only has the same C-terminus and not the same N-terminus. In case sequences are to be inserted into the loop regions, the expression of VP3 must be suppressed to ensure the presentation of only five modified VP2 proteins as the loop regions lies within the coding sequence of VP2 and VP3. In order to ensure solely VP2 expression, in a first step the VP3 start codon ATG was mutated towards ATC changing the amino acid methionine to isoleucine as it also contains a hydrophobic side chain. The general cloning procedure is shown in Figure 33. Two PCR reactions were performed on plasmid pZMB0160_CMV_VP2/3_HSPGko to generate two fragments with overlapping ends containing the nucleotide change. In a third PCR, these fragments were combined and amplified with NgoMIV for and SalI rev primer. The resulting fragment was digested with NgoMIV and SalI and religated into the originating pZMB0160 vector which was stored as pZMB0297_CMV_VP2_HSPGko and nucleotide exchange was confirmed by sanger sequencing. Mutating the VP3 start codon was published before,[175] but no western blot was shown, suggesting that a maintained expression of VP3 might have been present.

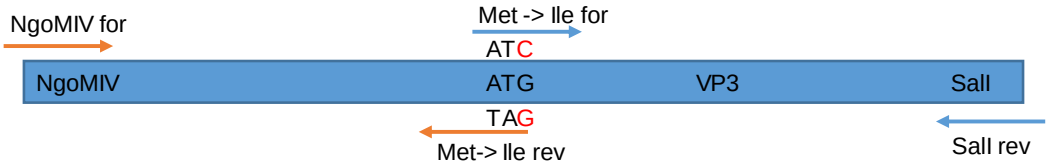

Figure 33: Cloning strategy to introduce a single point mutation into the VP3 coding sequence. Two PCR reactions were conducted with oligonucleotides NgoMIV for and Met-> Ile rev or rather Met->Ile for and Sal1 rev on plasmid pZMB0160_CMV_VP2/3_HSPGko. These fragments were fused by their complementary sequences on the 3' in a subsequent PCR reaction. This PCR product was digested with NgoMIV and SalI and introduced in the likewise opened originating vector, resulting in plasmid pZMB0297_CMV_VP2_HSPGko. Nucleotide exchange was confirmed by sanger sequencing.

To examine if the VP3 protein expression was eliminated by the nucleotide exchange in the VP3 start codon a western blot analysis was performed. 3.5 ml of HEK-F cells with a cell density of $3 \cdot 10^6$ ml^{-1} were transfected with the CMV_VP2/VP3 or the CMV_VP2 plasmid by PEI-mediated transfection. After three days, cells were pelleted, resuspended in lysis buffer and analyzed by SDS PAGE and subsequent Western blot analysis. Expression of VP2 and VP3 was still observed for both approaches (Figure 34A), indicating, that the leaky scanning mechanism is still active. When analyzing the DNA sequence (Figure 34B), it becomes clear that only 24 bp after the first start codon another start codon follows, which is in the correct reading frame and thus a slightly shortened VP3 variant is created (59.39 kDa instead of 60.045 kDa).

.

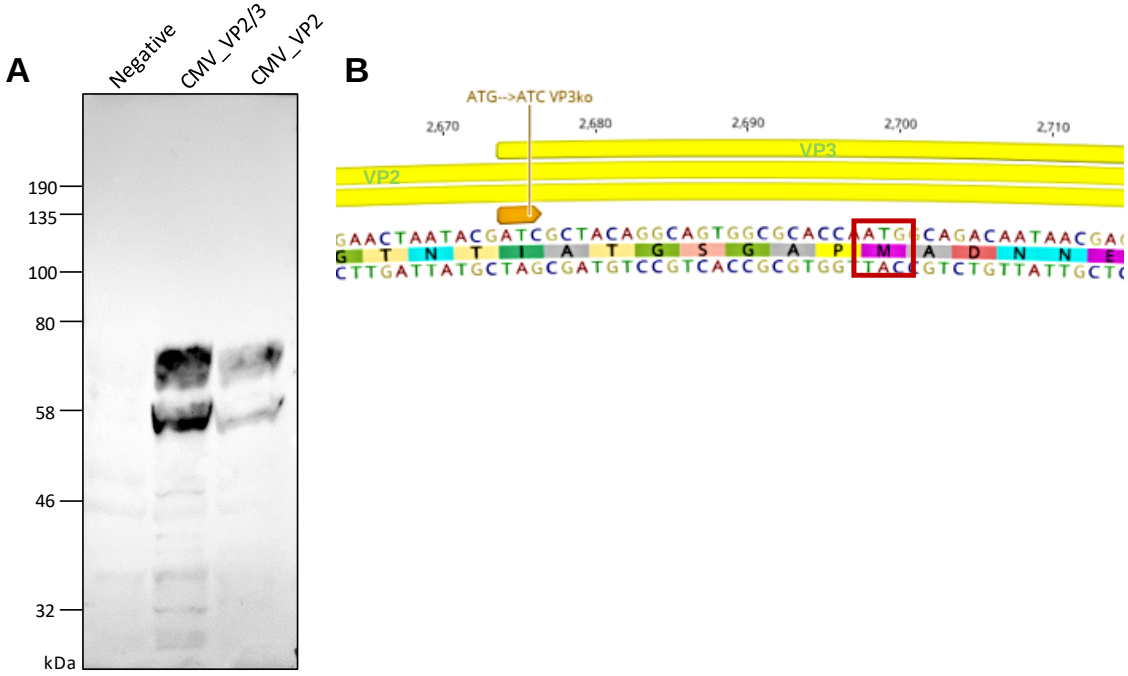

Figure 34: Analysis of VP3 protein expression. (A) Analysis of cap protein expression after transient transfection of HEK-F cells by western blot analysis of crude cell lysates. In lane 1, untransfected HEK-F cell lysate was applied as a control. In lane 2, the VP2/VP3 expression from plasmid CMV_VP23, and in lane 3 the expression from plasmid with VP3 start codon removal CMV_VP2 was applied and VP proteins were detected by B1 antibody. (B) View of the DNA sequence at the beginning of VP3 coding sequence. Expression of VP3 after removal of the start codon can be explained with a second start codon, marked with a red box, 24 bp downstream of the original start codon.

In order to prevent leaky scanning, a strong Kozak consensus sequence (GCC AAC) upstream of the VP2 start codon was introduced. Leaky scanning is based in ribosomes which bypasses the initial start codon because of weak a Kozak sequence and by this continue scanning until the next AUG.[176] For this reason, two oligonucleotides were designed introducing the Kozak sequence in a PCR reaction as an overhang into the amplified fragment, which was then recloned by digestion of the PCR product and the plasmid CMV-VP2 by XbaI and NgoMIV. As before this plasmid was used for expression of VP2 in HEK-F cells, and the cell lysate was analyzed by western blot. Finally, only the expression of VP2 was detected (Figure 35A). A scheme of the final plasmid CMV_Kozak_VP2_453_587(ΔVP3) is given in Figure 35B.

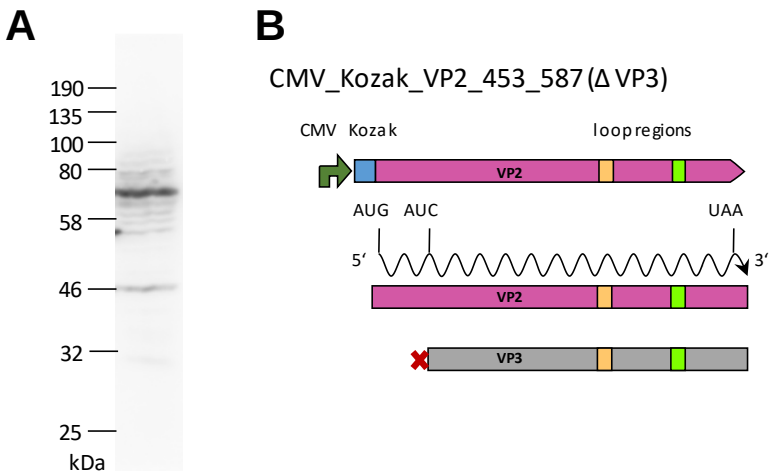

Figure 35: Analysis of VP2/VP3 expression from plasmid CMV_Kozak_VP2_453_587 (ΔVP3). (A) Western Blot analysis of protein expression in HEK F cells after transient transfection. The expected molecular weight for VP2 is 66.6 kDa. Western Blot was performed by Rebecca Feiner (B) Scheme of the final plasmid. From the plasmid DNA a mRNA (meandering line) is transcribed which contains the modified codon AUC instead of AUG. The combination of strong Kozak sequence and mutated VP3 start codon prevents VP3 protein expression.

In the following this plasmid formed the basis for a mosaic virus with the stabilized β-lactamase variant 14FM and Julian Teschner was able to show that rAAV2-VP2_587_bla was produced with comparable titers to those of wild-type preparations. In a nitrocefin enzyme assay the number of active ß-lactamases was calculated to be 5.6 which was in good agreement to the expected number of modified VP2 proteins, as five of the 60 capsid-forming proteins should be VP2.

6. Conclusion and Outlook

AAV cancer gene therapy offers the potential to overcome the lack of specificity of conventional non-invasive therapies. Analyzing the targeting efficiency of rAAV in suicide gene therapy, using tumor specific promoters and miRNA regulated gene expression, was therefore a focus of this work.

In order to achieve high titer rAAV preparations for this project, in the beginning great effort was put in the optimization of the rAAV manufacturing process. To facilitate rAAV production, the HEK-293-KARE1 cell line with stably integrated adenoviral elements was generated which allows for the reduction of plasmid DNA necessary during production and thus offers a significant time and cost advantage. For further optimization, adaptation of this cell line to suspension cultivation would be advisable as it potentially allows for up-scaling in of the production process in the future. In this context, upscaling experiments were performed with the commercial 293-F suspension cell line, and rAAV production was analyzed under varying cultivation conditions in order to optimize the process conditions. A standard suspension-based production protocol was established but cell-specific productivity was still lower compared to the standard adherent cell culture protocol indicating more room for improvement in the future.

Increasing the quality of AAV preparations was a fundamental question of this work, which was answered by a novel affinity chromatography procedure based on the natural cellular receptor AAVR. Covalent coupling of single PKD domains to cellulose allowed for rAAV purification from raw cell extract. Samples showed high purity and comparable potency as vectors purified with the standard ultracentrifugation. Direct capturing of rAAVs from crude cell extract allows for reduced costs and processing times of only few hours instead of more than one day. Nevertheless, a more detailed characterization of storage conditions, the amount of PKD required and the recyclability of the column material is still necessary. Also, an expansion of the PKD affinity chromatography to other AAV serotypes is conceivable for the future.

Next to optimization of the rAAV manufacturing process, analysis of HSV-*tk* gene expression by tumor-specific promoters in four cancerous and two normal cell lines was the focus of this work. As low promoter activities were detected previously, Kozak sequences were introduced in front of the HSV-*tk* start codons and for all promoters, activity was detected by a cytotoxicity assay upon GCV treatment. Overall, non-tumor specific CMV promoter led to the highest decline in cell viability in cancer and non-cancer cell lines. However, by introducing a second layer of tumor specificity by the introduction of the let-7 miRNA target sequences in the 3'-UTR of the CMV- and survivin promoter driven expression cassette, at least for the CMV promoter-driven gene expression a high protective effect on the cell viability was achieved. Therefore, a combination of a strong viral promoter in combination with de-targeting by miRNA, appears to be the preferable strategy to protect healthy cells from damage in suicide gene therapy.

7. Materials

7.1. Technical equipment

Table 8: Technical equipment used during this work.

Device	**Supplier**
Äkta start chromatography system	GE Healthcare Life Science
Analytical camera system Fusion Fx7	Vilber
Atomic force microscope	Bruker
Autoclave FVS 2	Integra Bioscience
Autoclave GE6612	Getinge
Automated cell counter LUNA	Logos Biosystems
BD FACSCalibur	Becton Dickinson
Blue light table	Serva Electrophoresis GmbH
Camera EOS 600D	Canon
Camera system FusionFx7	Vilber
Centrifuge Pico17	Thermo Fisher Scientific
Chemical duty pump WP6122050	Merck Millipore
Clean bench LaminAir HB 2448	Heraeus Instruments
Clean bench LaminAir Model 1.2	Holten
CO_2 Incubator CB E6	Binder GmbH
Fluorescence microscope DMI 6000 SD	Leica Microsystems
Freezer (-150 °C) MDF2156VAN	Panasonic
Freezer (-20 °C)	Liebherr
Freezer (-80 °C) KM-DU 73Y1	Panasonic
French press SLM AMINCO	SLM Instruments
French Pressure Cell (FA-032 (max 40’000 PSI, 35 ml max))	Thermo Fisher Scientific
Fridge (4 °C)	Bosch
Ice machine UBE 50-35	Ziegra Eismaschinen
Incubator B 6120	Heraeus
Light micsoscope Axiovert 25	Zeiss
Magnetic stirrer RCT	Ikamag
Megafuge 1.0	Heraeus Instruments
Microplate Spectrophotometer PowerWave HT	BioTek
Microwave HF 22043	Siemens
Milli-Q water system	Millipore
Mixing Block MB-102 (with orbital shaking function)	BIOER
Orbital shaker ES-X	Kühner
pH electrode InLab Expert Pt1000	Mettler Toledo
pH meter Seven compact S220	Mettler Toledo
Pipette aid Pipetboy Comfort	Integra

Device	Supplier
Pipette Research plus	Eppendorf
Power supply EV231	Consort
Precision scale CP 224 S	Sartorius
Precision scale XA205 DualRange	Mettler Toledo
Real time PCR system Lightcycler 480 II	Roche
Refrigerated centrifuge Multifuge X1R	Thermo Scientific
Refrigerated centrifuge RC5C (SS-34 and GS-3 rotors)	Sorvall Instruments
Refrigerated centrifuge5424R (FA-45-24-11 rotor)	Eppendorf
Rocking shaker Duo Max 1030	Star Lab
Scale BP 2100 S	Sartorius
SDS PAGE chamber SE260	Hoefer
SDS PAGE gel caster	Hoefer
Semi-dry blotter (V20-SDB)	Scie Plas
Shaking incubator SI-600 R (deflection: 40 mm)	Lab. Companion
Shaking platform Sky Line	ELMI
Spectrophotometer NanoDrop 2000c UV/Vis	Thermo Fisher Scientific
Thermoblock TB1	Biometra
Thermocycler Peqstar 96x Universal gradient	Peqlab
Tube Roller N2400-7010	Sartorius
Ultra centrifuge Ultra Pro 80 (T-880 rotor)	Sorvall
Vacuum Manifold QIAvac 24 Plus	Qiagen
Vortex Genie 2	Scientific Instruments
Water bath	GFL
White light table LED, (LP-400N)	Universal Electronics Industries

7.2. Software and web services

Table 9: List of Software and web services.

Software	Developer	Version number
Cell Quest	BD Biosciences	8-1996
Flowing Software	Perttu Terho, Turku Centre for Biotechnology – University of Turku, Finland	2.5.1
FlowJo	BD Biosciences	V10
FUSION-CAPT	Vilber	-
GeneArt online tool	Thermo Fisher Scientific Inc.	-
Geneious	Biomatters Ltd.	9.1.8
Gwyddion	David Nečas and Petr Klapetek	2.48
KC4	BioTek	3.3
LightCycler 480 Software	Roche	1.5

Software	Developer	Version number
Mendeley Desktop	Mendeley Ltd.	1.19.4
NanoDrop 2000/2000c Operating Software	Thermo Fisher Scientific Inc.	1.5
Office 2016	Microsoft	
OriginPro 2019	OriginLab Corporation	9.6.0.172
paint.net	dotPDN LLC	4.2.4
Tm Calculator	New England Biolabs	1.9.13
PyMOL	Schrödinger	2.3
Unicorn start	GE Healthcare Life Science	1.0

7.3. *E. coli* strains

Table 10: E. coli strains used during this work.

Strain	Source
BL21(DE3)	AG Fermentationstechnik
DH5α	AG Fermentationstechnik
TOP10 (DH10β)	Invitrogen

For plasmid production and cloning work, *E. coli* DH5α or *E. coli* TOP10 were used, whereas for recombinant protein expression *E. coli* BL21(DE3) was used.

7.4. Eukaryotic cell lines

Table 11: Eukaryotic cell lines used during this work.

Name	Source
HEK-293	DSMZ
FreeStyle 293-F	Thermo Fisher Scientific
HT-1080	DSMZ
A431	DSMZ
MDA-MB231	DSMZ
MDA-MB453	DSMZ
HDFa	Thermo Fisher Scientific
M1FS	Herz-und Diabeteszentrum NRW

7.5. Reagents

7.5.1. Chemicals

Table 12: Chemicals used during this work.

Name	Supplier
ABTS	AppliChem
Acetic acide	Chemical storage University Bielefeld
Acrylamid-Bisacrylamid 30 % solution (29:1)	AppliChem
Agar-Agar	Sigma Aldrich
Agarose	AppliChem
Ammonium sulphate	Sigma Aldrich
APS	AppliChem
ATP	NEB
Brilliant Blue R-250	Sigma Aldrich
Bromphenol blue	AppliChem
BSA	Sigma Aldrich
$CaCl_2$	Merck
CHAPS	Carl Roth
Citric acid	Carl Roth
Divinyl sulfone	Sigma Aldrich
DMSO	Carl Roth
DTT	Thermo Scientific
EDTA	Carl Roth
Ethanol (absolute)	VWR
Ethanol (denatured)	Chemical storage University Bielefeld
FCS (LOT number: BCBT0730)	Sigma Aldrich
Formaldehyd 37 % (v/v)	Chemical storage University Bielefeld
Glutamine solution (cell culture)	Sigma Aldrich
Glycerol	Carl Roth
Glycine	Carl Roth
H_3PO_4	Chemical storage University Bielefeld
HBSS buffer	Sigma Aldrich
HCl	VWR
HEPES	Carl Roth
HiTrap Protein A HP	GE Healthcare
Imidazole	Sigma Aldrich
IPTG	Carl Roth
KCl	VWR
KH_2PO_4	Fluka
$MgCl_2$	Carl Roth
$MgSO_4$	Fluka
Na_2CO_3	Carl Roth

Name	Supplier
$Na_2S_2O_3 \cdot 5\ H_2O$	Carl Roth
NaCl	VWR
$NaCNBH_3$	Sigma Aldrich
NaH_2PO_4	VWR
NaOH	VWR
Non-fat milk powder	AppliChem
OptiPrep	Progen
PEI_{max}	Polysciences, Inc
Phenolred	Sigma Aldrich
POROS CaptureSelect AAVX Affinity Resin	Thermo Fisher Scientific
Protino Ni-NTA Agarose	Macherey-Nagel
Roti-GelStain	Carl Roth
SDS	Carl Roth
Silica 60 (0.04 – 0.063 mm)	Merck Millipore
Sodium citrate	Carl Roth
Sucrose	Sigma Aldrich
TEMED	Sigma Aldrich
Tris	Carl Roth
Tris-HCl	Carl Roth
Trypan blue solution	Sigma Aldrich
Trypsin/EDTA solution	Sigma Aldrich
Tryptone/Peptone	Carl Roth
Tween 20	Carl Roth
Xylen cyanol FF	Sigma Aldrich
Yeast extract	Carl Roth

7.5.2. Buffers and Solutions

Table 13: List of Buffers and Solutions.

Name	Composition
ABTS buffer with ABTS	3.25 mM BH_2NaO_4, 40 mM citric acid, 60 mM Na_2HPO_4, pH 4.5, 1 $g \cdot l^{-1}$ ABTS (added directly before use)
Agarose gel solution with Roti-GelStain	1 % (w/v) Agarose, 0.005 % (v/v) Roti-GelStain, in TAE buffer
APS solution (1.5 %)	1.5 % (w/v) APS
Blocking buffer (rAAV2 capsid ELISA)	0.8 % (w/v) BSA, in PBS
$CaCl_2$ solution (100 mM)	100 mM $CaCl_2$

Name	Composition
$CaCl_2$ solution (85 mM) with glycerol	85 mM $CaCl_2$, 15 % (v/v) Glycerol
$CaCl_2$ solution (for HEK-293 transfection)	0.3 M $CaCl_2$
CHAPS stock solution	10 % (w/v) CHAPS (make directly before use)
Coomassie staining solution	0.1 % (w/v) Brilliant Blue R-250, 40 % (v/v) Ethanol, 10 % (v/v) Acetic acid
Coupling buffer pH 10	0.1 M Sodium citrate, 0.05 M Sodium carbonate, pH 10
Coupling buffer pH 7.2	0.1 M Sodium phosphate 0.15 M NaCl, pH 7.2
Cyanoborohydride solution	5 M $NaCNBH_3$ in 1M NaOH
Destaining solution (for Coomassie)	10 % (v/v) Acetic acid
DNA loading buffer (10×)	10 mM Tris-HCl, 50 % (v/v) Glycerol, 0.2 % (w/v) Bromphenol blue, 0.2 % (w/v) Xylen cyanol FF, pH 7.5
DNaseI buffer (10×)	100 mM Tris-HCl, 25 mM $MgCl_2$, 5 mM $CaCl_2$, pH 7.6
DVS buffer	10 % (v/v) Divinyl sulfone, 0.1 M Na_2CO_3, pH 11.0
Elution buffer (for POROS)	100 mM Sodium citrate pH 2.5
HBS buffer (2×)	50 mM HEPES, 1.5 mM NaH_2PO_4, 280 mM NaCl, pH 7.05
IMAC elution buffer	50 mM NaH_2PO_4, 300 mM NaCl, 250 mM Imidazole, pH 8.0
IMAC equilibration buffer	50 mM NaH_2PO_4, 300 mM NaCl, 10 mM Imidazole, pH 8.0
IMAC wash buffer	50 mM NaH_2PO_4, 300 mM NaCl, 20 mM Imidazole, pH 8.0
IPTG stock solution	1 M IPTG
Lysis buffer	50 mM Tris, 150 mM NaCl,

Name	**Composition**
	2 mM $MgCl_2$, pH 7.5 – 8.0
$MgCl_2$ solution (100 mM)	100 mM $MgCl_2$
Neutralization buffer (for POROS)	1 M Tris, pH 9.0
PBS buffer (1×)	500 mM NaCl, 100 mM KCl, 10 mM Na_2HPO_4, 10 mM KH_2PO_4, pH 7.5
PBS buffer (10×)	5 M NaCl, 1 M KCl, 100 mM Na_2HPO_4, 100 mM KH_2PO_4, pH 7.5
PBS-MK (10×)	10 mM $MgCl_2$, 25 mM KCl, in 10×PBS
PBS-MK + 2 M NaCl (1×)	2 M NaCl, in PBS-MK
PBST	0.05 % (v/v) Tween-20, in PBS
PEI_{max} stock solution	1 $g \cdot l^{-1}$ PEI_{max}
PKD2 elution buffer	2.5 M $MgCl_2$, 50 mM Tris, pH 7.0
Protein A elution buffer	100 mM Citric acid, pH 3.0
Protein A equilibration buffer	20 mM NaH_2PO_4, pH 7.0
Protein A neutralization buffer	1 M Tris-HCl, pH 9.0
SDS loading buffer (5×)	0.05 % (w/v) Bromophenol blue, 20 % (v/v) Glycerol, 10 % (w/v) SDS, 0.2 M Tris-HCl, 250 mM DTT (DTT is added fresh prior to use)
SDS solution (10 %)	10 % (w/v) SDS
SDS-running buffer (1×)	200 mM Glycerol, 25 mM Tris, 0.1 % (w/v) SDS
Semi-dry transfer buffer	25 mM Tris-HCl, 192 mM Glycine, 20 % (v/v) Ethanol, pH 8.2
Separating gel buffer	1.5 M Tris, pH 8.8
Stacking gel buffer	500 mM Tris,

Name	Composition
	pH 6.8
TAE buffer (1×)	40 mM Tris, 1 mM EDTA, 20 mM Acetic acid, pH 8.0
TBS blocking buffer	10 % (w/v) Non-fat milk powder, in TBS buffer
TBS buffer	50 mM Tris-HCl, 150 mM NaCl pH 7.6
TBST buffer	0.05 % (v/v) Tween 20, in TBS buffer
Wash buffer (rAAV2 capsid ELISA)	0.8 % (w/v) BSA in PBST

7.5.3. Antibiotics

Table 14:Antibiotics used during this work.

Antibiotics	Working concentration	Stock concentration	Supplier
Ampicillin sodium salt	100 µg ml^{-1}	1000×in water	Carl Roth
Blasticidin S hydrochloride	5 µg ml^{-1}	1000×in water	Carl Roth
Chloramphenicol	20 µg ml^{-1}	1000×in absolute ethanol	Carl Roth
Kanamycin	50 µg ml^{-1}	1000×in water	Carl Roth
Penicillin/Streptomycin solution	1 %	100 %	Sigma Aldrich

7.5.4. Media

7.5.4.1. Bacterial cell culture media

Table 15: Bacterial cell culture media used during this work.

Medium	Composition
LB medium (Lennox)	5 g yeast extract 10 g tryptone 5 g NaCl
LB agar plates	LB, 1.5 % agar agar
SOC	5 g yeast extract, 20 g tryptone, 0.6 g NaCl, 0.2 g KCl, 10 mL 1 M $MgCl_2$, 10 mL 1 M $MgSO_4$, 20 ml 1 M Glucose

7.5.4.2. Mammalian cell culture media

Table 16: Mammalian cell culture media used during this work.

Medium	Composition
DMEM	DMEM (Sigma Aldrich), 10 % FCS, 1 % P/S
Freestyle F17 Expression Medium	Freestyle F17 (Thermo Fisher Scientific) 8 mM Glutamine
HEK-TF	HEK-TF (Xell AG) 8 mM Glutamine
HEK-GM	HEK-TF (Xell AG) 8 mM Glutamine
HEK-FS	HEK-TF (Xell AG) 8 mM Glutamine
RPMI 1640	RPMI 1640 (Thermo Fisher Scientific) 10 % FCS, 1 % P/S

7.5.5. Kits

Table 17: Kits used during this work.

Kit	Supplier
GoTaq qPCR Master Mix	Promega
NucleoSpin Gel and PCR Clean-up	Machery-Nagel
NucleoSpin Plasmid	Macherey-Nagel
NucleoBond Xtra Midi	Macherey-Nagel
TOPO-TA cloning kit	Thermo Fisher Scientific

7.5.6. Antibodies

Table 18: Antibodies used during this work.

Antibody	Dilution	Supplier
Tetra-His Antibody, BSA-free, mouse anti-$(H)_4$	1:2000	Qiagen
anti-AAV VP1/VP2/VP3 mouse monoclonal, B1	1:100	Progen
anti-AAV2 (intact particle) mouse monoclonal, A20	1:250	Progen
Goat anti-Mouse IgG (H+L) Secondary Antibody, HRP conjugate	1:5000	Thermo Fisher Scientific
Anti-Human IgG1 (gamma 1 chain specific), mouse antibody, HRP	1:2500	Acris-antibodies

7.5.7. Enzymes

Table 19: Enzymes used during this work.

Enzyme	Supplier
Antarctic Phosphatase	NEB
Benzonase nuclease	Sigma Aldrich

Enzyme	Supplier
DNaseI	NEB
DNaseI	AppliChem
Phusion High-Fidelity DNA Polymerase	NEB
Taq DNA Polymerase	NEB
T4 DNA Ligase	Thermo Fisher Scientific
T4 Polynucleotide Kinase	NEB
Proteinase K	Sigma Aldrich
Restriction enzymes	NEB

7.5.8. Protein and DNA standards

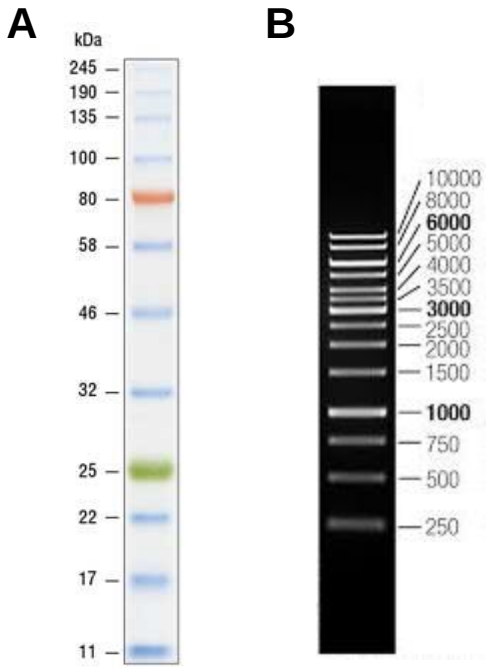

Figure 36: Protein and DNA ladder used during this work. (Color Prestained Protein Standard, Broad Range (11-245 kDa), NEB.[177] *(B) GeneRuler 1 kb DNA-Ladder, Thermo Scientific.*[178]

7.5.9. Oligonucleotides

Oligonucleotides were purchased at Sigma Aldrich and delivered dry in desalt purity. Oligonucleotide names were chosen to represent the name of a vector and if appropriate restriction sites which are in the sequence.

Table 20: List of oligonucleotides used during this work.

Name	Sequence (5'→3')
SEQ-pHelper-1-neu	GTCGCAACCA GGAACAGCTC
SEQ-pHelper-2	GTAGCTGCCT TCCCAAAAAG
SEQ-pHelper-3-neu	GGTACTTGTC CATCAACGCG
SEQ-pHelper-4	GTTTCGCGCT GCTCCTCTTC
SEQ-pHelper-5	ATATCGCCTC GCTCGACGAA

Name	**Sequence (5'→3')**
SEQ-pHelper-6	CGACTGCGTT TACTTATTTC
SEQ-pHelper-7	GTTGAAACTC ACTCCGGG
SEQ-pHelper-8	GCAACATCTC CTTCGCCC
SEQ-pHelper-9	GACTTGCGGC TGGAGCTG
SEQ-pHelper-10	CTGGTAAGGC TGACTGTTAT
SEQ-pHelper-11	TATCGCCGCC CATGCAACAA
SEQ-pHelper-12	TCCCGTGTGT GACTCGCAG
SEQ-pHelper-13	GTCATTGTTC CAGTCCCG
SEQ-pHelper-14	ATCACTGATG AGCGTTTGG
SEQ-pHelper-15	GTCTTGCATG ACGGGGAGG
SEQ-pHelper-16	CATCGGCATA GTATATCGGC
SEQ-pHelper-17	GGCCAGGAA CCGTAAAAAG
SEQ-pHelper-18	GCAAGCAGC AGATTACGC
SEQ-pHelper-19	CAAGGCGAGT TACATGATCC
SEQ-pHelper-20	GCCACCTAAA TTGTAAGCGT
Bsd-for	AAGCCTTTGT CTCAAGAAGA ATCC
Bsd-rev	TTAGCCCTCC CACACATAAC CA
Ad5-for	CAACTCCATG CTTAACAGTC CCCA
Ad5-rev	TCCAGTGCTG CAACCCTGTG TATC
NgoMIV for	GAAATTACTA GATGGCCGGC GC
Met->Ile for	CTAATACGAT CGCTACAGGC AGTGGC
Met->Ile rev	CCTGTAGCGA TCGTATTAGT TCCCAGAC
SalI rev	CGGCCTGAGA AAACTGAAGT CG
AAVRko CRISPR Target for	CACCGTATAG GTGTAACTAC GTCAC
AAVRko CRISPR Target rev	AAACGTGACG TAGTTACACC TATAC
Seq-AAVRko-for	GACACACTCC TCCAATTCCA TG
Seq-AAVRko-rev	GACTGTAACC ACATCAATCA ACTG
XbaI-CMV-for	CTTCTAGAGC GATGTACGGG
CMV_Kozak_NgoMIV-rev	ATAATGCCGG CCATGGTGGC CTAGTAATTT CGATAAGCCA GTAAG
mGMK-TK30_RFC10_for_new	TGGAATTCTT CTAGATGGCC GGCGCAGGAC CTA
mGMK-TK30_2A_rev	CCTCTGCCCT CTCCACTGCC ACCGGTGTTA GCCTCCCCCA T
T2A_eGFP_for_ new	GGCAGTGGAG AGGGCAGAGG AAGTCTGCTA ACATGCGGTG ACGTCGAGGA GAATCCTGGC CCAATGGTGT CCAAGGGCGA GG
eGFP_RFC10_rev_new	GGCATGGACG AGCTGTACAA GTAATACTAG TAGCGGCCGC TGCAGAAA
Pr-for_CMV_MluI	CCAGATATAC GCGTTGACAT TG
Pr-rev_Kozak_CMV	GGTGGCCTAG TAATTTCGAT AAGCCAGTAA GC
Pr-for_CMV_Kozak	GAAATTACTA GGCCACCATG GCCGGCGCAG G
Pr-rev_TK30_SalI	CCTTGTAGGT CGACATCTAG CAC
COX-2-MfeI_Kozak-AvrII_for	AATTGTCATA CTAGAGCCAC CATGGCCGGC GCAGGAC

Name	Sequence (5'→3')
COX-2-MfeI_Kozak-AvrII_rev	CTAGGTCCTG CGCCGGCCAT GGTGGCTCTA GTATGAC
Pr-for_Sur_MluI	CTGCACGCGT TCTTTGAAA
Pr-rev_Sur_Kozak	GGTGGCCTAG TAGCCGCCAC CTCTG
Pr-for_Sur_Kozak	GCGGCTACTA GGCCACCATG GCCGGCGCAGG
Pr-rev_TK30_SalI	CCTTGTAGGT CGACATCTAG CAC
Pr-for_MluI_CXCR-4	CACAGAGAGA CGCGTTCCTA G
Pr-rev_CXCR-4_Kozak	GGTGGCCTAG TAGACAAAGC AGGTTGAAAC TG
Pr-for_CXCR-4_Kozak	CTTTGTCTAC TAGGCCACCA TGGCCGGCGC AGG
Pr-rev_TK30_SalI	CCTTGTAGGT CGACATCTAG CAC
eGFP_ENX_for	AAAGAATTCG CGGCCCTTCT AGATGGTGTC CAAGGGCGAG
eGFP_let-7a_SNP_rev	AAACTGCAGC GGCCGCTACT AGTATGAGGT AGTAGGTTGT ATAGTTTACT TGTACAGCTC GTCCATGCC
NdeI-PKD2-for	AAAAACATAT GAATCGGCCC CCCATTGCTAT TG
BamHI-PKD2-rev	TTTTTGGTAC CACCGCCTGA ACCACCACCA GAGCCACCAC CGGATCCGGG GTAATCCACA GCTTTGTTCA C
BamHI-linker-MBP-for	AAAAAGGATC CGGTGGTGGC TCTGGTGGTG GTTCAGGCGG TAAAATCGAA GAAGGTAAAC TGG
KpnI-linker-MBP-rev	TTTTTGGTAC CACCGCTACC GCCACCTGAA CCACCACCGC TACCAGTCTG CGCGTCTTTC AG
KpnI-His6-tag-XhoI-for	ACCCATCATC ACCATCATCA TTAACTCGA
XhoI-His6-tag-KpnI-rev	GTTAATGATG ATGGTGATGA TGG

7.5.10. Plasmids

Table 21:List of generated and used plasmids.

Number	Name	Source
pzMB0088	pHelper	Agilent
pZMB0135	pSB1C3_hGHpA	iGEM
pZMB0216	pSB1C3_001_Rep_VP123_453_587wt_p5tataless	JTE
pZMB0259	pHelperBsd	MRA
pZMB0300	pSpCas9(BB)-2A-GFP (PX458)	Addgene
pZMB0301	pSpCas9(BB)-2A-GFP-AAVRko Exon3-CRISPR-Target (PX458)	This work
pZMB0307	pSB1C3_001_pCMV_Kozak_VP23_453_587wt	This work
pZMB0382	pcDNA5/FRT IgG-SigP-A20scFv-hFc-His	JTE
pZMB0398	pSB1C3_001_eGFP	GBI
pZMB0442	pSB1C3_CMV_mGMK-TK30_T2A_eGFP_hGHpA	CCU
pZMB0443	pSB1C3_COX-2_mGMK-TK30_T2A_eGFP_hGHpA	CCU
pZMB0444	pSB1C3_Suv_mGMK-TK30_T2A_eGFP_hGHpA	CCU
pZMB0474	pSB1C3_CXCR-4_mGMK-TK30_T2A_eGFP_hGHpA	CCU
pZMB0504	Rep2Cap9	RFE
pZMB0522	pUC19bb_ ITR_EXS_pCMV_mVenus_hGHpolyA	PBO
pZMB0575	pSB1C3_002_RepCap6_VP123_453_587wt_p5tataless	RFE

Number	Name	Source
pZMB0584	pSB1C3_CMV_Kozak_mGMK-TK30_T2A_eGFP_hGHpA	This work
pZMB0585	pSB1C3_COX-2_Kozak_mGMK-TK30_T2A_eGFP_hGHpA	This work
pZMB0586	pSB1C3_Suv_Kozak_mGMK-TK30_T2A_eGFP_hGHpA	This work
pZMB0587	pSB1C3_CXCR-4_Kozak_mGMK-TK30_T2A_eGFP_hGHpA	This work
pZMB0588	pUC19bb_ITR_EXS_CMV_Kozak_mGMK-TK30_T2A_eGFP_hGHpA	This work
pZMB0589	pUC19bb_ITR_EXS_COX-2_Kozak_mGMK-TK30_T2A_eGFP_hGHpA	This work
pZMB0590	pUC19bb_ITR_EXS_Suv_Kozak_mGMK-TK30_T2A_eGFP_hGHpA	This work
pZMB0591	pUC19bb_ITR_EXS_CXCR-4_Kozak_mGMK-TK30_T2A_eGFP_hGHpA	This work
pZMB0616	pet-24b_AAVR_PKD2-MBP-His6	JTE
pZMB0639	pUC19bb_ ITR_EXS_CMV_Kozak_mGMK-TK30_T2A_eGFP1xlet7a_hGHpA	This work
pZMB0640	pUC19bb_ ITR_EXS_Suv_Kozak_mGMK-TK30_T2A_eGFP_1xlet7a_hGHpA	This work

7.6. Consumables

Table 22: List of cunsumables.

Name	Specification	Manufacturer
Adhesive film for real-time PCR-Plates	Ultra-clear (A26979)	GeneOn
Bijou sample containers	7 ml, with screw cap, sterile, PS	Sci Labware Limited
Blotting Paper	Thickness 0.35 mm	Carl Roth
Canula needle	21G, 0.6x80 mm	B. Braun
Cell scraper	25 cm	Sarstedt
Centrifugal filter units	Amicon Ultra-4 100K centrifugal filter units	Merck Millipore
Cryogenic plastic vessel	2.0 ml	Star Lab
Cryogenic plastic vessel (cell culture)	1.8 ml, Internal thread, silicone seal in lid	Star Lab
Empty lab column	5 ml (S10131)	MoBiTec
Lightcycler Plate	96-well, white	Sarstedt
LUNA Cell Counting Slide	Two chamber slides	Logos Biosystems
MaxiSorp plate	96-well, flat-bottom plate	Nunc
Mica for AFM	(50x76 mm, 0.2 mm thick)	PLANO
Multipette Combitips	5 ml	Eppendorf
Multi-well plates	6-, 12-, 96-well, standard TC for adherent cells, flat base, sterile	Sarstedt
Nitrocellulose membrane	0.45 micron	Thermo Scientific
Petri dishes	92x16 mm, with ventilation cams	Sarstedt
Petri dishes (cell culture)	Diameter 100 mm	Sarstedt
pH test strips	MColorpHast, pH 5.0 – 10.0	Merk
Pipette tips	10 µl, 100 µl, 1000 µl, 5000 µl	Star Lab

Name	Specification	Manufacturer
Pipette tips (cell culture)	TipOne Filter Tips (10/20 µl, 200 µl, 1000µl, sterile, graduated)	Star Lab
Reaction tube	15 ml, PP	Sarstedt
Reaction tube	50 ml, PP	Sarstedt
Reaction tube	50 ml, plug style caps, 25k×g	VWR
Reaction vessels	0.5 ml, 1.5 ml, 2.0 ml	Sarstedt
Reaction vessels (for PCR)	0.2 ml, flat cap, thin wall	Star Lab
Scalpel blades	S123	Hartenstein
Shaker flask	250 ml, 500 ml,	Sarsted
Sterile filter	0.2 µm, 0.45 µm, PTFE	Sarstedt/Sartorius
Syringe	1.0 ml, 5 ml, 10 ml, 50 ml	B. Braun
T-flask	25 cm^2, 75 cm^2, 150 cm^2,	Sarstedt
Tube Spin bioreactors	50 ml	TPP
Ultracentrifuge tubes	Open-top, PA, 16x76 mm	Science Service

8. Methods

8.1. Microbiology methods

8.1.1. Cultivation and storage of *E. coli* cells

E. coli cells were cultivated using different liquid or solid media supplemented with the appropriate antibiotic suitable to the resistance mediated by the respective plasmid for the selective growth. Cultures were stored at 4 °C for short-time storage on agar plates and for long-time storage, 1 ml of liquid cultures were mixed with 0.5 ml of a sterile glycerol solution and stored at -80 °C.

8.1.2. Preparation and heat shock transformation of chemical competent *E. coli* cells

Generation of chemical competent *E. coli* cells was performed using a standard $CaCl_2$ protocol.[179] For heat shock transformation, 50 µl aliquots of competent cells were mixed with 5 µl of a ligation mixture or 1 µl of plasmid DNA and stored on ice for 30 min. After a heat shock for 45 s at 42°C and a regeneration for 4 min on ice, 1 ml of SOC medium was added and the cells were cultivated in a 1.5 ml plastic reaction vessel at 37 °C and 200 rpm on a shaking incubator. Cultivation time depended on the plasmid mediated resistance and was 30 min for ampicillin, and 45 min for chloramphenicol and kanamycin resistance. 100 µl of the transformation were plated on LB agar plates supplemented with the respective antibiotic and cultivated at 37 °C overnight.

8.2. Molecular biological methods

8.2.1. Isolation of plasmid DNA

Plasmid-DNA was isolated from *E. coli* cells with the 'NucleoSpin Plasmid' kit from Macherey-Nagel for small scale preparations, primarily in cloning procedures. Here, 4 ml of *E. coli* overnight cultures served as starting material and elution was performed with autoclaved MilliQ water.

For larger amounts of plasmid DNA, e.g. for transient transfections, the 'NucleoBond Xtra Midi' kit from Macherey-Nagel was used. Plasmid DNA was extracted from 200 ml of an overnight grown *E. coli* culture according to the manufacturers protocol and eluted with autoclaved MilliQ water and stored at -20 °C.

8.2.2. Isolation of genomic DNA

For genomic DNA isolation from mammalian cells, Chelex 100 (Bio-Rad) extraction was applied. 2.5×10^6 cells were pelleted in a 1.5 ml plastic reaction tube (1 min 10′000×g) and washed with PBS. The pellet was resuspended in 100 µl Chelex suspension (5 % w/v), incubated for 30 min at 56 °C, vortexed for 10 s and incubated for 8 min at 100 °C. The solution was centrifuged briefly at approx. 15,000×g for 2 min and the genomic DNA containing supernatant was transferred to a new tube. The DNA was stored at -20°C or was directly used for PCR reactions.

8.2.3. Determination of DNA and protein concentrations

The NanoDrop 2000c UV/Vis spectrophotometer from Thermo Fisher Scientific was used for the determination of DNA and protein preparations. For DNA concentration, absorption was measured at 260 nm for protein concentrations a wavelength of 280 nm in combination with the molar extinction coefficient and the molecular weight was used. Calculation of the respective protein concentrations was performed on the basis of the Beer-Lambert law: $c = \frac{A}{\varepsilon \times l}$ with A: absorptivity, ε: molar attenuation coefficient and l: optical path length.

8.2.4. Polymerase chain reaction

The amplification of DNA fragments for cloning procedures was performed with Phusion High fidelity polymerase (NEB). It possesses a 3' → 5' exonuclease activity and by this a lower error rate compared to the *Taq* polymerase (NEB) which was used during this work for detection of DNA fragments in the context of genomic DNA integration.

In the following the optimized composition of the standard protocol for Phusion (Table 23) and Taq Polymerase PCR reaction (Table 24) are given.

Table 23: Composition of a standard Phusion Polymerase PCR reaction.

Components	**Volume in µl**
5× GC buffer	10
10 mM dNTPs	1
Primer for	2.5
Primer rev	2.5
DMSO	1.5
$MgCl_2$	2
Phusion Polymerase	0.5
Plasmid DNA (< 10 ng recommended)	variable
Water	To 50 µl

Table 24: Composition of a standard Taq Polymerase PCR reaction.

Components	**Volume in µl**
10× Thermopol buffer	2
10 mM dNTPs	0.5
Primer for	0.5
Primer rev	0.5
Taq Polymerase	0.15
Genomic DNA	5 (from Chelex DNA extraction)
Water	16.35

The thermocycling conditions were adapted to the annealing temperature of oligonucleotides used, and the length of the final PCR product according to the manufacturer's specifications. In subsequent gel electrophoresis (8.2.5), the success of DNA amplification was confirmed and in case of cloning procedures, the product with the desired size in was excised out and purified from remaining gel by the NucleoSpin® Gel and PCR Clean-up kit (Macherey-Nagel).

8.2.5. Agarose gel electrophoresis

For agarose gel electrophoresis, 1 % w/v agarose gels in TAE buffer were used. For detection of DNA, 0.5 µl of Roti-GelStain per 10 ml gel solution were added and electrophoresis was conducted at 120 V for about 50 min. Visualization of separated DNA fragments was performed by a LED blue light table and a camera with an orange light filter. The size of the fragments was estimated using a DNA length marker (7.5.8).

8.2.6. Restriction endonuclease treatment

Restriction digestion was used to generate DNA fragments with compatible ends for subsequent ligation. In general, type II restriction enzymes from NEB were used. For plasmid DNA approximately 1 µg and for PCR products the total reaction was digested in the following set-up.

Table 25: Composition of a restriction endonuclease digest.

Components	**Volume in µl**
Restriction Endonucleases	0.4 (per enzyme)
DNA	variable
CutSmart Buffer (10×)	2
Water	To 20 µl

Digestion was performed for 1 h at 37 °C and, if possible, enzymes were inactivated by heat inactivation for 20 min at the temperature specified by the manufacturer.

8.2.7. Addition and removal of 5' phosphates

The ligation of DNA fragments requires the presence of 5' phosphate residues, therefore the removal of the 5 'phosphate group is a proven method to avoid religation of a vector opened by restriction endonuclease treatment and thus was performed in parallel by adding Antarctic Phosphatase (NEB) directly to the restriction digest. For this purpose, 1 µl Antarctic Phosphatase and 2 µl 10× Antarctic Phosphatase buffer were added to the restriction digest (8.2.6). Inactivation of the enzyme reaction was performed at 80 °C for 2 min.

In the contrary oligonucleotides do not possess a 5' phosphate residue and in case of oligonucleotide hybridization (8.2.1), where no PCR or restriction digest is performed, leading to the introduction of a 5' phosphate residue, the T4 Polynucleotide Kinase (NEB) treatment in the presence of dATP was performed. The composition for the 5' phosphorylation of oligonucleotides is given in Table 26.

Table 26: Composition of a T4 Polynucleotide Kinase reaction.

Components	Volume in µl
Oligonucleotide 1 (100 mM)	1
Oligonucleotide 2 (100 mM)	1
T4 Ligase Buffer (10×)	1
T4 Polynucleotide Kinase	0.5
Water	6.5

The reaction was performed for 30 min at 37 °C and then the enzyme was heat inactivated at 65 °C for 20 min.

8.2.1. Oligonucleotide hybridization

Complementary oligonucleotides were designed with overlapping ends that, when hybridized, match the overhangs generated during a restriction digest of the target vector. Hybridization was usually performed subsequently after the addition of 5' phosphates residues during T4 Polynucleotide Kinase treatment (8.2.7). In order to ensure correct hybridization of two oligonucleotides a temperature gradient starting from 95 °C, decreasing to 25 °C with 5 °C per min was carried out. The hybridized oligonucleotides were finally used in ligation reactions as 1:200 dilutions in water.

8.2.2. DNA ligation

To form a phosphodiester bond two compatible DNA fragments, the T4 DNA Ligase (NEB) was used. Ligation reactions were usually composed as follows.

Table 27: Composition of a T4 DNA Ligase reaction.

Components	Volume in µl
T4 DNA Ligase Buffer (10×)	2
Linearized Vector DNA	variable (50 ng to 250 ng)
Insert DNA/ hybridized oligonucleotides	variable (5-fold molar ratio of vector DNA)/ 1
T4 DNA Ligase (5 $U \cdot \mu l^{-1}$)	T4 DNA Ligase (5 $U \cdot \mu l^{-1}$)
Water	To 20

Ligation reactions were carried out at RT for at least 1 hour and the mixture could then be used directly for the transformation of competent *E. coli* cells (8.1.2).

8.2.3. DNA sequencing

The success of cloning work was analyzed by sequencing reactions. These were carried out by members of the 'AG für Genomforschung" at the 'Sequencing Core Facility" of the 'CeBiTec" at the University of Bielefeld. Sequencing primers are indicated by the abbreviation SEQ in the name

(Table 20) and 10 µl of primers with a concentration of 10 µM were required per reaction. Sequences were stored as FASTA-, PHERO- and AB1- files and evaluated by local alignments with the Geneious (version 9.1.8) software.

8.3. Protein biochemistry methods

8.3.1. Recombinant protein expression

Recombinant protein expression was either conducted in *E. coli* BL21(DE3) cells using the IPTG inducible T7 expression system based on the pET vector or by mammalian expression using the strong CMV promoter on pcDNA5/FRT vector.

For prokaryotic expression of the PKD-MBP fusion protein, a 50 ml preculture of *E. coli* BL21(DE3) strain carrying the respective pET expression plasmid was grown at 37 °C, 180 rpm overnight to inoculate 500 ml culture with an OD_{600} of 0.1 in LB medium with kanamycin (50µg·ml^{-1}). Cultivation was performed at 37 °C and 180 rpm. Once the OD_{600} reached a value of 0.6, isopropyl-β-D-thiogalactopyranoside (IPTG) with a final concentration of 1 mM was added to induce protein expression and cultivation was continued for another 4 h. Afterwards, cells were harvested by centrifugation (6000×*g*, 15 min, 4 °C) and the cell pellet was stored at -20 °C or directly processed by French Press (8.3.2.1).

For mammalian protein expression of the A20-scFv-Fc, HEK-F cells (Thermo Fisher Scientific) were cultivated in HEK-TF medium (Xell AG). One day before transfection, cells were seeded in a cell density of $1.5 \cdot 10^6$ cells ml^{-1} in a 125 ml Erlenmeyer cell culture flask. Before transient transfection, cells were counted, centrifuged at 150×g for 5 min and resuspended in fresh HEK-TF medium with a cell density of $3 \cdot 10^6$ cells ml^{-1} in a volume of 30 ml. 60 µg DNA (2 µg ml^{-1}, (0.67 pg DNA per cell)) were pre-complexed in 1/8 of the transfection volume in HEK-TF medium (3.75 ml). For polyethylenimine (PEI) Max (Polysciences, Inc). the same procedure was followed with 240 µg (8 µg ml^{-1}) PEI. After 1 min both approaches were combined, rigorously vortexed and incubated for 15 min before the DNA: PEI complex was added to the cells. After 4 h 37.5 ml fresh HEK-TF medium (100 % of the transfection volume) was added and cells were cultivated for 6 days. Cells were pelleted at 2000×g for 5 min and the A20-scFv-Fc containing supernatant was sterile-filtered and stored at -20 °C or directly processed by Protein A chromatography (8.3.2.2).

8.3.2. Protein purification

8.3.2.1. Immobilized metal affinity chromatography

As PKD2-MBP was equipped with a C-terminal His_6-tag (polyhistidine-tag), purification using immobilized metal affinity chromatography (IMAC) on a Ni-NTA resin (Macherey-Nagel) was possible.

In a first step, the *E. coli* cell pellet from protein expression was thawed and resuspended in 30 ml equilibration buffer (50 mM Na_2HPO_4, 300 mM NaCl, 10 mM imidazole pH 8) and the cell membrane of bacteria was disrupted in three repeated French press cycles (SLM AMINCO) at a pressure of 1000 psi. The cell debris was separated from soluble protein by centrifugation at 15.000×g for 30 min at 4 °C. 10× DNase I buffer and 0.1 µl DNase I solution (min 3000 $U \cdot ml^{-1}$) per milliliter were added, and incubated at 37 °C for 20 minutes, before the suspension was sterile filtered and applied to a 1 ml self-packed Ni-NTA column. All chromatography steps were performed on a ÄKTA start chromatography system with a flowrate of 1 ml min^{-1}. The column was equilibrated with a total of 10 CV equilibration buffer before loading of the sample. After washing with 10 CV equilibration buffer containing 20 mM imidazole, the protein was eluted with 5 CV of an elution buffer containing 250 mM imidazole. The elution was collected in 500 µl fractions, and protein concentrations were determined by measuring the absorbance at 280 nm (8.2.3) and the protein containing fractions were combined and buffer was exchanged to PBS using an Amicon Ultra centrifugal filter unit (MWCO 30 kDa). Protein samples were stored at -80 °C as 50 µl aliquots.

8.3.2.2. Protein A column chromatography

The human IgG1-Fc part of the A20-scFv allowed for purification using a Protein A column (HiTrap Protein A HP, GE Healthcare). All chromatography steps were performed on a ÄKTA start chromatography system with a flowrate of 1 ml min^{-1}. The column was equilibrated with a total of 10 column volumes (CV) equilibration buffer before loading of the sample. The sample was mixed with 0.5 volumes of equilibration buffer before it was loaded on the column. After washing with 10 CV of equilibration buffer, elution was performed with 5 CV elution buffer pH 3.5. The elution was collected in 500 µl fractions in 1.5 ml plastic reaction tubes containing 50 µl neutralization buffer each. Protein concentrations were determined by measuring the absorbance at 280 nm (8.2.3). The protein containing fractions were combined and buffer was exchanged to PBS using an Amicon Ultra centrifugal filter unit (MWCO 30 kDa). Protein samples were stored at -80 °C as 20 µl aliquots.

8.3.3. SDS PAGE

SDS PAGE analysis was performed to detect proteins and determine their molecular weight. The composition of the regularly used 10 % separating gel and the 4 % stacking gel is given in Table 28.

Table 28: Composition of 10 % SDS gels (sufficient for 4 gels).

Component	10 % separating gel	4 % stacking gel
Water	16.33 ml	8.17 ml
Separating gel buffer	12.5 ml	-
Stacking gel buffer	-	3.78 ml
10 % SDS solution	0.5 ml	0.15 ml
Acrylamid-Bisacrylamid 30 % solution (29:1)	16.65 ml	3.35 ml

TEMED	0.025 ml	0.015 ml
1.5 % APS solution	4	0.9 ml

Protein samples were mixed with 5× SDS loading buffer and boiled at 95 °C for 5 min before loading. To estimate the size of the proteins, additionally 5 µl of a protein standard were loaded (7.5.8). The Hoefer SE260 chamber was filled with 1× SDS running buffer and gel electrophoresis was performed at 100 V for 30 minutes and was then increased to 200 V for additional 90 min. Polyacrylamide gels were then either stained (8.3.4; 8.3.5) or used for western blot analysis (8.3.6).

8.3.4. Coomassie-staining

For detection of proteins, SDS Gels were rinsed with water and then stained for 1 min in Coomassie staining solution which was warmed up in a microwave (600 W). The gel was washed heated several times with a Coomassie destaining solution before it was covered overnight with the destaining solution.

8.3.5. Silver-staining

If a higher sensitivity was desired SDS gels were silver stained. The protocol was adapted from Blum *et al*. [180]. All steps were performed under constant shaking at 60 rpm on a rocking shaker. At first, the gel was covered for at least 1 h with a fixing solution. For lower background signals, a prolonged incubation time overnight can be chosen. After two wash steps, each 10 min with wash solution and once with water the gel was strongly shaken by hand for exactly 1 min with a thiosulfate (0.02 % (w/v)) solution before it was rinsed three times with water. The gel was the transferred into a new vessel and incubated with a silver nitrate solution for 20 min. After rinsing three times with water, the gel was transferred into the starting vessel, covered with developing solution and was strongly shaken by hand until protein bands were visible. The reaction was stopped by covering the gel with stop solution.

8.3.6. Western Blot

For verification of the presence of proteins as well as for the detection of low concentrated proteins western blot analysis was performed. After separation of proteins by SDS-PAGE (8.3.3), transfer was performed onto a 0.45 µm nitrocellulose membrane (Thermo Fisher Scientific) by a semi-dry electrophoretic transfer. A 35 min transfer time at 4 mA cm^{-2} was chosen and successful transfer was detected by reversible Ponceau S staining of the membrane. Then, the membrane was washed, and remaining protein binding sites were blocked for 1 h or overnight in TBS buffer with 10 % (w/v) non-fat milk (blocking buffer). The following primary antibody (Table 18) was diluted in blocking buffer and incubated for 1 h and was chosen according to the target proteins to be detected. After 2 wash steps, each 10 min, the membrane was incubated with a secondary anti-mouse IgG linked to a horseradish peroxidase for 1 h. After 3 wash steps, each 10 min, proteins were detected by luminescence by mixing equal parts of Detection Reagent 1 and 2 (Pierce ECL Western Blot

Substrate, Thermo Fisher Scientific) with a total volume of 125 µl per cm^2 membrane and a variable exposure time from 30 s to 5 min. Detection was performed with a CCD camera system (Fusion Fx7).

8.4. Cell culture methods

8.4.1. Cultivation of mammalian cells

Generally, cultivation took place in a CO_2 incubator at a humidity of 90 %, 5 % CO_2 and 37 °C. Adherent growing cells were cultivated in T-flasks (Sarstedt), whereas in suspension growing cells were cultivated in tube spin bioreactors (TPP) or Erlenmeyer cell culture flasks on an orbital shaking platform (185 rpm, 5 cm amplitude). Depending on the cell line different medium was needed. For A431, MDA-MB231 and MDA-MB453 RPMI supplemented with 10 %FCS and 1 % penicillin/streptomycin (P/S) and for HEK-293, HT1080, HDFa and M1FS DMEM, high glucose supplemented with 10 %FCS and 1 % penicillin/streptomycin was used. For HEK293-KARE1, blasticidin in a final concentration of 5 µg ml^{-1} was additionally added. Cultivation of HEK-F cells was mainly performed in HEK-TF medium supplemented with 8 mM Glutamine.

8.4.2. Thawing and cryopreservation

For long-term storage, cells were cryopreserved at -150 °C in the respective growth medium (8.4.1) supplemented with 10 % dimethyl sulfoxide (DMSO). Therefore, cells were counted, pelleted (150×g, 5 min) and subsequently resuspended to a final density of $1 \cdot 10^7$ cells ml^{-1}. This suspension was aliquoted in cryogenic vials 1 ml each and cooled down slowly with a cooling rate of 1 °C per min in a freezing container in a -80 °C freezer overnight before transferring to the -150 °C freezer.

For thawing, cryogenic vials were transferred into a 37 °C warm water bath and afterwards spun down (150×g, 5 min) in 20 ml PBS to remove remaining DMSO. For adherent cells, the cell pellet was suspended in 20 ml of the respective growth medium and transferred into a T75 flask. For suspension cells, cells were suspended in 10 ml growth medium and transferred into tube spin bioreactors.

8.4.3. Counting and seeding

To determine the number and viability of mammalian cells, the Luna Automated Cell Counter system (Logos Biosystems) was used. During passaging, 10 µl of the cell suspension was mixed with 10 µl of a trypan blue solution (Sigma Aldrich) and 10ml of this suspension was filled into a counting slide and cell number and viability was determined. These allowed to calculate the required number of cells to be seeded in the respective growth medium and the desired culture vessel.

8.4.4. Alamar Blue Assay

The effect of incorporation of GCV-triphosphate into genomic DNA of transduced cells was measured by determining the cell viability by an Alamar Blue Assay.

10'000 cells with a cell density of 1'000 cells ml^{-1} of HFa, M1Fs, HT1080, MDA-MB231 and MDA-MB453 cells were mixed with rAAV_promoter_mGMK-TK30_T2A_eGFP were the expression is driven by different promoters or rAAV_promoter_mGMK-TK30_T2A_eGFP_let7a where the let-7a miRNA target sequence was included. CMV, COX-2, survivin and CXCR-4 promoters were chosen, and cells were transduced with a MOI of 10,000 in biological duplicates. After careful mixing, 100 µl of the cell suspension was dispensed in 6-fold replicates in a 96-well plate. After 24 h, a final concentration of 1 mM ganciclovir (Sigma Aldrich) from a 20 mM stock solution was added for another 72 h. After the incubation period, 5 µl resazurin of a 1 $g \cdot L^{-1}$ stock solution in PBS was added (final concentration of 0.05 g L^{-1}). The plates were placed in an incubator at 37 °C, 5 % CO_2 and fluorescence intensity were measured at regular intervals in a PowerWave HT (BioTek) plate reader with an excitation wavelength of 545/30 nm and an 590/20 emission filter. Fluorescence data were normalized to the fluorescence signal of cells transduced with rAAV2_mVenus with added ganciclovir. For the analysis of the effect of GCV on non-transduced cells, 1'000 HT1080 cells in 100 µl growth medium were seeded in 6-fold replicates in a 96-well plate and 0, 0.5, 1, 2 and 4 mM GCV was added. After 72 h Alamar Blue Assay was performed. The relative fluorescence of the samples was calculated by setting the fluorescence signal of cells without GCV as 100 % viable. For the other cell lines, only the working concentration of 1 mM GCV was tested as described.

8.5. Virological methods

8.5.1. rAAV production in adherent HEK-293 cells

The production of rAAV was mainly conducted in adherent growing HEK-293 cells using the helper-free plasmid system.[181] Transient transfection was based on calcium phosphate mediated transient transfection.[182] One day before transfection, cells were counted (8.4.3) and a total of $3 \cdot 10^6$ (100 mm) or $9 \cdot 10^6$ (150 mm) cells were seeded in 10 ml or 20 ml complete growth medium, respectively (8.4.1). On the day of transfection, depending on the size of the dish, 15 µg or 45 µg plasmid DNA (5 pg DNA per cell) were mixed in a molar ratio of 1: 1: 1 of pHelper: pRepCap: ITR in 0.5 ml or 1 ml calcium chloride ($CaCl_2$) buffer, respectively. This solution was rigorously vortexed and dropwise added to 0.5 ml or 1 ml 2×HBS buffer, respectively. The reaction mixture was vortexed, and 1 or 2 ml were added to a 100 mm or a 150 mm dish. Transfected cells were cultivated for 72 h and before harvest, the transfection efficiency was estimated by fluorescence microscopy by making use of the gene expression of the fluorescence reporter mVenus delivered by the ITR containing plasmid. Subsequently, cells were detached from the surface using a cell scraper and pelleted (2'000×g, 5 min) and cell pellet and spent medium were stored separately at -80 °C or directly purified by ultracentrifugation (8.5.4) or affinity chromatography (8.5.5).

8.5.2. rAAV production in HEK-F suspension cells

One day before transfection, cells were seeded in a cell density of $1.5 \cdot 10^6$ cells ml^{-1} in a 125 ml Erlenmeyer cell culture flask. Before transient transfection, cells were counted, centrifuged at 150×g for 5 min and resuspended in fresh HEK-TF medium with a cell density of $3 \cdot 10^6$ cells ml^{-1} in a volume of 30 ml. 60 µg DNA (2 µg ml^{-1}) in a molar ratio of 2: 1: 1 of pHelper: pRepCap: ITR were pre-complexed in 1/8 of the transfection volume in HEK-TF medium (3.75 ml). For polyethylenimine (PEI) Max (Polysciences, Inc). the same procedure was followed with 240 µg (8 µg ml^{-1}) PEI. After 1 min both approaches were combined, rigorously vortexed and incubated for 15 min before the DNA: PEI complex was added to the cells. After 4 h, 37.5 ml fresh HEK-TF medium (100 % of the transfection volume) was added and cells were cultivated for 3 days. Cells were pelleted at 2'000×g for 5 min. The rAAV containing cell pellet was then stored at -80 °C or subsequently purified by affinity chromatography (8.5.5; 8.5.6) or genomic titers obtained were determined (8.5.8).

8.5.3. Ammonium sulfate precipitation of rAAV

Viral particles were released from the cell pellet obtained during rAAV production by three freeze-thaw cycles of the pellet resuspended in 2 ml lysis buffer. For degradation of residual DNA and RNA contaminants, 0.8 µl benzonase nuclease (Sigma-Aldrich) were added and incubated at 37 °C for 1 h. Subsequently, 0.5 % (w/v) 3-[(3-cholamidopropyl)dimethylammonio]-1-propanesulfonate hydrate (CHAPS) was added and after an incubation time of 37 °C for 30 min, cell debris was pelleted at 3'000×g for 10 min and the virus containing supernatant was used to resuspend the ammonium sulfate precipitate of the spent medium which was conducted as follows. Per 40 ml spent medium 12.52 g ammonium sulfate were dissolved and incubated for 30 min on ice. The supernatant after centrifugation at 8'300×g for 10 min at 4 °C was discarded and the rAAV-containing pellet was resolved with the supernatant from pellet preparation. This suspension was used for iodixanol density gradient ultracentrifugation (8.5.4) or POROS CaptureSelect AAVX affinity purification (8.5.6).

8.5.4. Discontinuous iodixanol density gradient ultracentrifugation

Iodixanol density gradient ultracentrifugation was used to remove contaminants from production and to enrich full capsids. In a first step, different iodixanol solutions were prepared (Table 29).

Table 29: Composition of solutions for iodixanol ultracentrifugation sufficient for two samples.

Proportion of iodixanol	Volume iodixanol solution	Buffer	Additionally
60 %	Stock solution		Add phenolred
54 %	8 ml of stock solution	0.887 ml 10× PBS-MK	
40 %	4 ml of 54 % solution	1.4 ml 1× PBS-MK	
25 %	2.5 ml of 54 % solution	2.9 ml 1× PBS-MK	Add phenolred
15 %	1.5 ml of 54 % solution	1.2 ml 1× PBS-MK	2.7 ml 1× PBS-MK NaCl

The prepared iodixanol solutions were layered in an open top polyallomer 16 x 76 mm tube (Science Services) with the volumes given in Table 30.

Table 30: Volumes of the respective iodixanol solutions for iodixanol ultracentrifugation for one sample.

Solution	Volume in ml
60 %	1.25
40 %	1.25
25 %	1.5
15 %	2.25

Finally, the sample was applied with a maximal volume of 4 ml. The tubes were sealed with cap assemblies and tared before centrifugation in a T-880 rotor (Sorvall) at 340,000×g for 2 h at 18 °C. To collect the rAAV containing fraction a syringe with a 21G × 1 1/2" injection needle was stabbed into the tube at the interphase between 60 % and 40 % iodixanol layer and a fraction with a size of 500 µl was taken. Finally, the buffer was exchanged to 1× HBSS (Sigma Aldrich) via Amicon Ultra-4 100K centrifugal filter units (Merck pore) and when concentrated to a volume of about 500 µl, 50 µl aliquots were stored at -80 °C. A 10 µl aliquot was stored separately for subsequent determination of the rAAV genomic titer 8.5.8).

8.5.5. PKD affinity purification

In a first step, the PKD affinity resin needs to be prepared. Blotting paper (Rotilabo® Blotting Papers, Thickness 0.35 mm; Carl Roth) was cutted into 1 cm^2 large pieces and incubated in 2 ml DVS buffer (0.1 M Na_2CO_3, pH11) with 10 % DVS (Sigma Aldrich) for 2 h. Then, the blotting paper was washed five times with 10 ml MilliQ and dried for at least 2 h. Each blotting paper was incubated with 100 µl 5 µM PKD in PBS overnight in a water-saturated atmosphere. The remaining surface was blocked with 2 ml of PBS-T for 1 h before it was washed three times with PBS. Afterwards the material could be used for affinity purification or stored in PBS buffer at -20 °C.

For PKD affinity purification from crude cell lysate, one 1 cm^2 of prepared PKD-blotting paper was added to the virus containing lysate for 30 min in a suitable vessel under constant shaking on a roll-tumble shaker. Afterwards the supernatant was removed, and the resin was washed with PBS until no phenol red residues from the medium were seen (usually five to six wash steps with 10 ml PBS). Elution was performed by transferring the PKD-blotting paper into an empty spin column and adding 500 µl of $MgCl_2$ elution buffer. After 2 min incubation, elution was performed by centrifugation (1000×g, 2 min). The elution fractions were combined, and the buffer was exchanged to 1× HBSS (Sigma Aldrich) via Amicon Ultra-4 100K centrifugal filter units (Merck Millipore).

8.5.6. POROS CaptureSelect AAVX affinity purification

For affinity purification with the POROS CaptureSelect AAVX affinity material, a 5 ml empty lab column with Luer-lock connections (MoBiTec S10131) was filled with 500 µl of the slurry and

once the material was settled, equilibrated with 10 column volumes of PBS. The rAAV containing crude cell extract either from adherent or suspension growing cells, was loaded with 1 ml per min with a syringe pump. After washing with 10 CV with PBS-T rAAV2 were eluted three times with 250 µl 100 mM citric acid buffer pH 2.5 and neutralized with Tris-HCl pH 9.0 (80 µl per 250 µl).

8.5.7. PKD-AminoLink Plus affinity purification

At first, PKD was coupled to the AminoLink Plus Coupling Resin, which was mainly performed according to the manufacturer's instructions.[183] 400 µl of the AminoLink slurry were settled in a 2 ml plastic reaction tube at 1'000×g for 1min and equilibrated with 600 µl Coupling buffer pH 10. Afterwards, the settled resin was mixed with 300 µg PKD2 diluted in 300 µl Coupling buffer pH 10 and incubated on a roll-tumble-shaker for 4 h. The resin was washed with 600 µl Coupling buffer pH 7.2 and PKD2 was immobilized by adding 200 µl coupling buffer pH 7.2 and 4 µl cyanoborohydride ($NaCNBH_3$) solution for 4 h at RT or overnight at 4 °C and constant shaking on a roll-tumble shaker. The resin was then washed with 400 µl Quenching buffer and remaining protein binding sites were blocked by adding 200 µl Quenching buffer and 4 µl of $NaCNBH_3$ solution for 30 min under constant shaking. The column was washed with 1 ml wash solution and stored at 4 °C or used directly for affinity purification from HEK-F crude cell lysate. Here, 1 ml of the clarified supernatant, after cell disruption by three freeze-thaw cycles, was incubated for 30 min with the generated affinity resin, washed 6 times with 2 ml PBS-T and viral particles were eluted 3 times with 0.5 ml $MgCl_2$ elution buffer. The elution fractions were combined, and the buffer was exchanged to 1× HBSS (Sigma Aldrich) via Amicon Ultra-4 100K centrifugal filter units (Merck Millipore).

8.5.8. Determination of rAAV genomic titer

To determine the genomic titer of a sample by a qPCR, residual DNA from transfection was removed by a DNaseI digestion. Samples were treated with 10 U DNase I (NEB) in 10× DNaseI buffer in a final volume of 50 µl at 37 °C for 30 min before heat inactivation of the DNase I at 75 °C for 20 min. Crude lysate samples were additionally incubated with 0.8 U Proteinase K (New England Biolabs) for 50 min at 37 °C before heat inactivation at 95 °C for 10 min. A 50-fold dilution with nuclease-free water was used as a template in the following qPCR reaction. 5 µl of the diluted sample was mixed with 2.5 µl of qPCR-hGH-for (5'-CTCCCCAGTG CCTCTCCT-3') and 2.5 µl qPCR-hGH-rev (5´-ACTTGCCCCT TGCTCCATAC-3´) primers, with a stock concentration of 4µM each. Additionally, 10 µl of 2× GoTaq qPCR Mastermix (Promega) was added and the qPCR reaction was carried out as described in Table 31; using a LightCycler 480 II (Roche).

Table 31: Thermocycling conditions for qPCR reactions.

Step	Temperature in °C	Time in s	Cycles
Initial Denaturation	95	600	1
Denaturation	95	15	40
Annealing + Elongation	60	30	

To calculate the genomic titer a standard curve of 10 to 10^6 copies of the ITR plasmid (pZMB0522) was generated with an efficiency between 90-110% and an R value less than 0.1 and saved as a reference. In qPCR reaction a copy number of 10^4 or 10^5 was included as internal control. To determine the genomic titer in crude lysates a standard curve mixed with the same amount of a non-transfected cell lysate was generated. Based on the crossing point (C_p) value of the internal reference, compared to the sample, the genomic titer was calculated by the LightCycler 480 II software. Afterwards, a dilution factor of 50 and a factor of 2, because of the double stranded plasmid DNA, was taken into account.

8.5.9. Determination of transducing titer

Determination of the transducing titer of a rAAV sample was performed on HT1080 cells. 10'000 cells per well were seeded in 500 µl of the corresponding media on a 12-well plate and settled for 1 h before application of dilutions of rAAV preparations in PBS. Based on genomic titers determined by qPCR (8.5.8) a MOI of 10 to 10^5 was chosen. After 12 h incubation 500 µl of fresh medium was added to the cells. Cells were incubated at 37 °C for further 72 h before detaching with 0.25 % Trypsin/EDTA, resuspension in PBS and analysis of 10'000 events using a FACSCalibur. All experiments were performed as biological duplicates. Data sets were analyzed using FlowJo V10. Positive cells were gated above the 99 % interval of the negative control. For calculation of the transducing titer, dilutions with a transduction efficiency less than 30 % were used in order to avoid multiple transduction events per cell and by this leads to an underestimation of the transducing titer. Calculation was based on following formula: $TU = \frac{n \cdot Fp \cdot d}{V}$ with TU: Transducing Units (ml^{-1}); n: number of cells in transduction batch; Fp: Amount of positive fluorescent cells; d: dilution factor of rAAV sample; V: volume of transduction batch (ml).

8.5.10. rAAV2 capsid ELISA

For the determination of viral capsid titer, a 96-well cell culture plate was incubated overnight at 4 °C with purified PKD2 (200 ng in 100 µL per well) in carbonate buffer. Afterwards, the plate was washed three times with PBS-T (wash buffer) and remaining sites were blocked with 200 µl blocking buffer (0.8 % BSA in PBS) per well for 1 h at RT. After three wash steps with wash buffer the A20 scFv was added with 100 ng per well in blocking buffer for 1 h at RT. The wash step was repeated, and the plate was incubated with an anti-human IgG1 HRP antibody (AM08151HR-N, mouse monoclonal, 1:2'000 in wash buffer with 0.8 % BSA, Acris antibodies) for 1 h. The detection was started, after three wash steps with wash buffer, with 150 µl ABTS buffer with 1 g L^{-1} ABTS (2,2'-azino-bis (3-ethylbenzothiazoline-6-sulphonic acid). The absorbance was measured at 405 nm with a microplate spectrophotometer (PowerWave HT, BioTek) after 30 min. Calculation of capsids was performed by a standard curve of a serial dilution of a known capsid concentration (Kit control/Standard, Progen). The particle titer was calculated by a standard curve of a serial dilution

of a known capsid concentration (Kit control/Standard, Progen) by using a 4-parameter logistic fit with OriginPro 2018 software. The equation was: $y = A2 + (A1 - A2)/(1 + \left(\frac{x}{x0}\right))\hat{}p)$.

9. References

(1) Calcedo, R.; Vandenberghe, L. H.; Gao, G.; Lin, J.; Wilson, J. M. Worldwide Epidemiology of Neutralizing Antibodies to Adeno-Associated Viruses. *J. Infect. Dis.* **2009**, *199* (3), 381–390. https://doi.org/10.1086/595830.

(2) Calcedo, R.; Morizono, H.; Wang, L.; McCarter, R.; He, J.; Jones, D.; Batshaw, M. L.; Wilson, J. M. Adeno-Associated Virus Antibody Profiles in Newborns, Children, and Adolescents. *Clin. Vaccine Immunol.* **2011**, *18* (9), 1586–1588. https://doi.org/10.1128/CVI.05107-11.

(3) McLaughlin, S. K.; Collis, P.; Hermonat, P. L.; Muzyczka, N. Adeno-Associated Virus General Transduction Vectors: Analysis of Proviral Structures. *J. Virol.* **1988**, *62* (6), 1963–1973.

(4) King, J. A.; Dubielzig, R.; Grimm, D.; Kleinschmidt, J. A. DNA Helicase-Mediated Packaging of Adeno-Associated Virus Type 2 Genomes into Preformed Capsids. *EMBO J.* **2001**, *20* (12), 3282–3291. https://doi.org/10.1093/emboj/20.12.3282.

(5) Im, D. S.; Muzyczka, N. Partial Purification of Adeno-Associated Virus Rep78, Rep52, and Rep40 and Their Biochemical Characterization. *J. Virol.* **1992**, *66* (2), 1119–1128.

(6) Im, D.-S. S.; Muzyczka, N. The AAV Origin Binding Protein Rep68 Is an ATP-Dependent Site-Specific Endonuclease with DNA Helicase Activity. *Cell* **1990**, *61* (3), 447–457. https://doi.org/10.1016/0092-8674(90)90526-K.

(7) Trempe, J. P.; Carter, B. J. Alternate MRNA Splicing Is Required for Synthesis of Adeno-Associated Virus VP1 Capsid Protein. *J. Virol.* **1988**, *62* (9), 3356–3363.

(8) Sonntag, F.; Schmidt, K.; Kleinschmidt, J. A. A Viral Assembly Factor Promotes AAV2 Capsid Formation in the Nucleolus. *Proc. Natl. Acad. Sci. U. S. A.* **2010**, *107* (22), 10220–10225. https://doi.org/10.1073/pnas.1001673107.

(9) Cao, M.; You, H.; Hermonat, P. L. The X Gene of Adeno-Associated Virus 2 (AAV2) Is Involved in Viral DNA Replication. *PLoS One* **2014**, *9* (8), e104596. https://doi.org/10.1371/journal.pone.0104596.

(10) Samulski, R. J.; Muzyczka, N. AAV-Mediated Gene Therapy for Research and Therapeutic Purposes. *Annu. Rev. Virol.* **2014**, *1* (1), 427–451. https://doi.org/10.1146/annurev-virology-031413-085355.

(11) Weger, S.; Wistuba, A.; Grimm, D.; Kleinschmidt, J. A. Control of Adeno-Associated Virus Type 2 Cap Gene Expression: Relative Influence of Helper Virus, Terminal Repeats, and Rep Proteins. *J. Virol.* **1997**, *71* (11), 8437–8447.

(12) Gonçalves, M. a F. V. Adeno-Associated Virus: From Defective Virus to Effective Vector. *Virol. J.* **2005**, *2*, 43. https://doi.org/10.1186/1743-422X-2-43.

(13) Sonntag, F.; Bleker, S.; Leuchs, B.; Fischer, R.; Kleinschmidt, J. a. Adeno-Associated Virus Type 2 Capsids with Externalized VP1/VP2 Trafficking Domains Are Generated Prior to Passage through the Cytoplasm and Are Maintained until Uncoating Occurs in the Nucleus. *J. Virol.* **2006**, *80* (22), 11040–11054. https://doi.org/10.1128/JVI.01056-06.

(14) Girod, A.; Wobus, C. E.; Zádori, Z.; Ried, M.; Leike, K.; Tijssen, P.; Kleinschmidt, J. A.; Hallek, M. The VP1 Capsid Protein of Adeno-Associated Virus Type 2 Is Carrying a Phospholipase A2 Domain Required for Virus Infectivity. *J. Gen. Virol.* **2002**, *83* (Pt 5), 973–978.

(15) Maurer, A. C.; Pacouret, S.; Cepeda Diaz, A. K.; Blake, J.; Andres-Mateos, E.; Vandenberghe, L. H. The Assembly-Activating Protein Promotes Stability and Interactions between AAV's Viral Proteins to Nucleate Capsid Assembly. *Cell Rep.* **2018**, *23* (6), 1817–1830. https://doi.org/10.1016/j.celrep.2018.04.026.

(16) Myers, M. W.; Carter, B. J. Adeno-Associated Virus Replication. The Effect of L-Canavanine or a Helper Virus Mutation on Accumulation of Viral Capsids and Progeny Single-Stranded DNA. *J. Biol. Chem.* **1981**, *256* (2), 567–570.

(17) Im, D. S.; Muzyczka, N. Factors That Bind to Adeno-Associated Virus Terminal Repeats. *J. Virol.* **1989**, *63* (7), 3095–3104.

(18) Gao, G.; Vandenberghe, L. H.; Alvira, M. R.; Lu, Y.; Calcedo, R.; Zhou, X.; Wilson, J. M. Clades of Adeno-Associated Viruses Are Widely Disseminated in Human Tissues. **2004**, *78* (12), 6381–6388. https://doi.org/10.1128/JVI.78.12.6381.

(19) Summerford, C.; Samulski, R. J. Membrane-Associated Heparan Sulfate Proteoglycan Is a Receptor for Adeno-Associated Virus Type 2 Virions. *J. Virol.* **1998**, *72* (2), 1438–1445.

(20) Zhou, S.; Hansen, J.; Srivastava, A.; Mah, C.; Dwarki, V.; Qing, K. Human Fibroblast Growth Factor Receptor 1 Is a Co-Receptor for Infection by Adeno-Associated Virus 2. *Nat. Med.* **2002**, *5* (1), 71–77. https://doi.org/10.1038/4758.

(21) Iwabuchi, K.; Daida, H.; Matsumoto, K.; Oshimi, K.; Watanabe, M.; Kashiwakura, Y.; Tamayose, K.; Shimada, T.; Nakamura, T.; Hirai, Y. Hepatocyte Growth Factor Receptor Is a Coreceptor for Adeno-Associated Virus Type 2 Infection. *J. Virol.* **2004**, *79* (1), 609–614. https://doi.org/10.1128/jvi.79.1.609-614.2005.

(22) Akache, B.; Grimm, D.; Pandey, K.; Yant, S. R.; Xu, H.; Kay, M. A. The 37/67-Kilodalton Laminin Receptor Is a Receptor for Adeno-Associated Virus Serotypes 8, 2, 3, and 9. *J. Virol.* **2006**, *80* (19), 9831–9836. https://doi.org/10.1128/JVI.00878-06.

(23) Summerford, C.; Bartlett, J. S.; Samulski, R. J. AVβ5 Integrin: A Co-Receptor for Adeno-Associated Virus Type 2 Infection. *Nat. Med.* **1999**, *5* (1), 78–82. https://doi.org/10.1038/4768.

(24) Asokan, A.; Hamra, J. B.; Govindasamy, L.; Agbandje-McKenna, M.; Samulski, R. J. Adeno-Associated Virus Type 2 Contains an Integrin A5β1 Binding Domain Essential for Viral Cell Entry. *J. Virol.* **2006**, *80* (18), 8961–8969. https://doi.org/10.1128/JVI.00843-06.

(25) Opie, S. S. R.; Jr, K. W.; Agbandje-, M.; Warrington, K. H.; Agbandje-McKenna, M.; Zolotukhin, S.; Muzyczka, N.; Muzyczka, N. Identification of Amino Acid Residues in the Capsid Proteins of Adeno-Associated Virus Type 2 That Contribute to Heparan Sulfate Proteoglycan Binding. *J. Virol.* **2003**, *77* (12), 6995–7006. https://doi.org/10.1128/JVI.77.12.6995–7006.2003.

(26) Bartlett, J. S.; Wilcher, R.; Samulski, R. J. Infectious Entry Pathway of Adeno-Associated Virus and Adeno-Associated Virus Vectors. *J. Virol.* **2000**, *74* (6), 2777–2785. https://doi.org/10.1128/jvi.74.6.2777-2785.2000.

(27) Samulski, R.; Zhu, X.; Xiao, X.; Brook, J.; Housman, D.; Epstein, N.; Hunter, L. Targeted Integration of Adeno-Associated Virus (AAV) into Human Chromosome 19. *EMBO J.* **1991**, *10* (12), 3941.

(28) Kotin, R. M.; Linden, R. M.; Berns, K. I. Characterization of a Preferred Site on Human Chromosome 19q for Integration of Adeno-Associated Virus DNA by Non-Homologous Recombination. *EMBO J.* **1992**, *11* (13), 5071–5078.

(29) Richardson, W. D.; Westphal, H. A Cascade of Adenovirus Early Functions Is Required for Expression of Adeno-Associated Virus. *Cell* **1981**, *27* (1 PART 2), 133–141. https://doi.org/10.1016/0092-8674(81)90367-6.

(30) Pillay, S.; Meyer, N. L.; Puschnik, A. S.; Davulcu, O.; Diep, J.; Ishikawa, Y.; Jae, L. T.; Wosen, J. E.; Nagamine, C. M.; Chapman, M. S.; et al. An Essential Receptor for Adeno-Associated Virus Infection. *Nature* **2016**, *530* (7588), 108–112. https://doi.org/10.1038/nature16465.

(31) Poon, M. W.; Tsang, W. H.; Chan, S. O.; Li, H. M.; Ng, H. K.; Waye, M. M. Y. Dyslexia-Associated Kiaa0319-Like Protein Interacts with Axon Guidance Receptor Nogo Receptor 1. *Cell. Mol. Neurobiol.* **2011**, *31* (1), 27–35. https://doi.org/10.1007/s10571-010-9549-1.

(32) Pillay, S.; Zou, W.; Cheng, F.; Puschnik, A. S.; Meyer, N. L.; Ganaie, S. S.; Deng, X.; Wosen, J. E.; Davulcu, O.; Yan, Z.; et al. AAV Serotypes Have Distinctive Interactions with Domains of the Cellular Receptor AAVR. *J. Virol.* **2017**, *91* (18), JVI.00391-17. https://doi.org/10.1128/JVI.00391-17.

(33) Zhang, R.; Cao, L.; Cui, M.; Sun, Z.; Hu, M.; Zhang, R.; Stuart, W.; Zhao, X.; Yang, Z.; Li, X.; et al. Adeno-Associated Virus 2 Bound to Its Cellular Receptor AAVR. *Nat. Microbiol.* **2019**, *4* (4), 675–682. https://doi.org/10.1038/s41564-018-0356-7.

(34) World Health Organization. Latest Global Cancer Data: Cancer Burden Rises to 18.1 Million New Cases and 9.6 Million Deaths in 2018. *Int. Agency Res. cancer* **2018**, No. September, 13–15.

(35) Siegel, R. L.; Miller, K. D.; Jemal, A. Cancer Statistics, 2019. *CA. Cancer J. Clin.* **2019**, *69* (1), 7–34. https://doi.org/10.3322/caac.21551.

(36) Anguela, X. M.; High, K. A. Entering the Modern Era of Gene Therapy. *Annu. Rev. Med.* **2019**, *70* (1), 273–288. https://doi.org/10.1146/annurev-med-012017-043332.

(37) Ginn, S. L.; Amaya, A. K.; Alexander, I. E.; Edelstein, M.; Abedi, M. R. Gene Therapy Clinical Trials Worldwide to 2017: An Update. *J. Gene Med.* **2018**, *20* (5), e3015. https://doi.org/10.1002/jgm.3015.

(38) Yazdani, A.; Alirezaie, Z.; Motamedi, M. J.; Amani, J. Gene Therapy: A New Approach in Modern Medicine. *Int. J. Med. Rev.* **2018**, *5* (3), 106–117. https://doi.org/10.29252/ijmr-050304.

(39) Lambricht, L.; Lopes, A.; Kos, S.; Sersa, G.; Préat, V.; Vandermeulen, G. Clinical Potential of Electroporation for Gene Therapy and DNA Vaccine Delivery. *Expert Opin. Drug Deliv.* **2016**, *13* (2), 295–310. https://doi.org/10.1517/17425247.2016.1121990.

(40) Balazs, D. A.; Godbey, W. Liposomes for Use in Gene Delivery. *J. Drug Deliv.* **2011**, *2011*, 326497. https://doi.org/10.1155/2011/326497.

(41) Clément, N.; Grieger, J. C. Manufacturing of Recombinant Adeno-Associated Viral Vectors for Clinical Trials. *Mol. Ther. - Methods Clin. Dev.* **2016**, *3* (November 2015), 16002. https://doi.org/10.1038/mtm.2016.2.

(42) Grimm, D.; Kay, M. a. From Virus Evolution to Vector Revolution: Use of Naturally Occurring Serotypes of Adeno-Associated Virus (AAV) as Novel Vectors for Human Gene Therapy. *Curr. Gene Ther.* **2003**, *3* (4), 281–304.

(43) Robson, T.; Hirst, D. G. Transcriptional Targeting in Cancer Gene Therapy. *J. Biomed. Biotechnol.* **2003**, *2003* (2), 110–137. https://doi.org/10.1155/S1110724303209074.

(44) Bartel, M.; Schaffer, D.; Büning, H. Enhancing the Clinical Potential of Aav Vectors by Capsid Engineering to Evade Pre-Existing Immunity. *Front. Microbiol.* **2011**, *2* (OCT), 1–10. https://doi.org/10.3389/fmicb.2011.00204.

(45) Kotterman, M. A.; Schaffer, D. V. Engineering Adeno-Associated Viruses for Clinical Gene

Therapy. *Nat. Rev. Genet.* **2014**, *15* (7), 445–451. https://doi.org/10.1038/nrg3742.

(46) Müller, O. J.; Kaul, F.; Weitzman, M. D.; Pasqualini, R.; Arap, W.; Kleinschmidt, J. A.; Trepel, M. Random Peptide Libraries Displayed on Adeno-Associated Virus to Select for Targeted Gene Therapy Vectors. *Nat. Biotechnol.* **2003**, *21* (9), 1040–1046. https://doi.org/10.1038/nbt856.

(47) Koerber, J. T.; Jang, J.-H.; Schaffer, D. V. DNA Shuffling of Adeno-Associated Virus Yields Functionally Diverse Viral Progeny. *Mol. Ther.* **2008**, *16* (10), 1703–1709. https://doi.org/10.1038/mt.2008.167.

(48) Koerber, J. T.; Maheshri, N.; Kaspar, B. K.; Schaffer, D. V. Construction of Diverse Adeno-Associated Viral Libraries for Directed Evolution of Enhanced Gene Delivery Vehicles. *Nat. Protoc.* **2006**, *1* (2), 701–706. https://doi.org/10.1038/nprot.2006.93.

(49) Dalkara, D.; Byrne, L. C.; Klimczak, R. R.; Visel, M.; Yin, L.; Merigan, W. H.; Flannery, J. G.; Schaffer, D. V. In Vivo-Directed Evolution of a New Adeno-Associated Virus for Therapeutic Outer Retinal Gene Delivery from the Vitreous. *Sci. Transl. Med.* **2013**, *5* (189), 189ra76-189ra76. https://doi.org/10.1126/scitranslmed.3005708.

(50) Maheshri, N.; Koerber, J. T.; Kaspar, B. K.; Schaffer, D. V. Directed Evolution of Adeno-Associated Virus Yields Enhanced Gene Delivery Vectors. *Nat. Biotechnol.* **2006**, *24* (2), 198–204. https://doi.org/10.1038/nbt1182.

(51) Novellino, L.; Castelli, C.; Parmiani, G. A Listing of Human Tumor Antigens Recognized by T Cells: March 2004 Update. *Cancer Immunol. Immunother.* **2005**, *54* (3), 187–207. https://doi.org/10.1007/s00262-004-0560-6.

(52) Shin, B. K.; Wang, H.; Yim, A. M.; Le Naour, F.; Brichory, F.; Jang, J. H.; Zhao, R.; Puravs, E.; Tra, J.; Michael, C. W.; et al. Global Profiling of the Cell Surface Proteome of Cancer Cells Uncovers an Abundance of Proteins with Chaperone Function. *J. Biol. Chem.* **2003**, *278* (9), 7607–7616. https://doi.org/10.1074/jbc.M210455200.

(53) Zhong, L.; Li, B.; Mah, C. S.; Govindasamy, L.; Agbandje-McKenna, M.; Cooper, M.; Herzog, R. W.; Zolotukhin, I.; Warrington, K. H.; Weigel-Van Aken, K. A.; et al. Next Generation of Adeno-Associated Virus 2 Vectors: Point Mutations in Tyrosines Lead to High-Efficiency Transduction at Lower Doses. *Proc. Natl. Acad. Sci.* **2008**, *105* (22), 7827–7832. https://doi.org/10.1073/pnas.0802866105.

(54) Gabriel, N.; Hareendran, S.; Sen, D.; Gadkari, R. A.; Sudha, G.; Selot, R.; Hussain, M.; Dhaksnamoorthy, R.; Samuel, R.; Srinivasan, N.; et al. Bioengineering of AAV2 Capsid at Specific Serine, Threonine, or Lysine Residues Improves Its Transduction Efficiency *in Vitro* and *in Vivo*. *Hum. Gene Ther. Methods* **2013**, *24* (2), 80–93.

https://doi.org/10.1089/hgtb.2012.194.

(55) Grifman, M.; Trepel, M.; Speece, P.; Gilbert, L. B.; Arap, W.; Pasqualini, R.; Weitzman, M. D. Incorporation of Tumor-Targeting Peptides into Recombinant Adeno-Associated Virus Capsids. *Mol. Ther.* **2001**, *3* (6), 964–975. https://doi.org/10.1006/MTHE.2001.0345.

(56) Shi, W.; Bartlett, J. S. RGD Inclusion in VP3 Provides Adeno-Associated Virus Type 2 (AAV2)-Based Vectors with a Heparan Sulfate-Independent Cell Entry Mechanism. *Mol. Ther.* **2003**, *7* (4), 515–525. https://doi.org/10.1016/S1525-0016(03)00042-X.

(57) Grieger, J. C.; Johnson, J. S.; Gurda-Whitaker, B.; Agbandje-McKenna, M.; Samulski, R. J. Surface-Exposed Adeno-Associated Virus Vp1-NLS Capsid Fusion Protein Rescues Infectivity of Noninfectious Wild-Type Vp2/Vp3 and Vp3-Only Capsids but Not That of Fivefold Pore Mutant Virions. *J. Virol.* **2007**, *81* (15), 7833–7843. https://doi.org/10.1128/JVI.00580-07.

(58) Hagen, S.; Baumann, T.; Wagner, H. J.; Morath, V.; Kaufmann, B.; Fischer, A.; Bergmann, S.; Schindler, P.; Arndt, K. M.; Müller, K. M. Modular Adeno-Associated Virus (RAAV) Vectors Used for Cellular Virus-Directed Enzyme Prodrug Therapy. *Sci. Rep.* **2014**, *4*, 3759. https://doi.org/10.1038/srep03759.

(59) Chen, C.; Yue, D.; Lei, L.; Wang, H.; Lu, J.; Zhou, Y.; Liu, S.; Ding, T.; Guo, M.; Xu, L. Promoter-Operating Targeted Expression of Gene Therapy in Cancer: Current Stage and Prospect. *Mol. Ther. - Nucleic Acids* **2018**, *11*, 508–514. https://doi.org/10.1016/J.OMTN.2018.04.003.

(60) Perera, D.; Poulos, R. C.; Shah, A.; Beck, D.; Pimanda, J. E.; Wong, J. W. H. Differential DNA Repair Underlies Mutation Hotspots at Active Promoters in Cancer Genomes. *Nature* **2016**, *532* (7598), 259–263. https://doi.org/10.1038/nature17437.

(61) Kagawa, S.; Gu, J.; Swisher, S. G.; Ji, L.; Roth, J. A.; Lai, D.; Stephens, L. C.; Fang, B. Antitumor Effect of Adenovirus-Mediated Bax Gene Transfer on P53-Sensitive and P53-Resistant Cancer Lines. *Cancer Res.* **2000**, *60* (5), 1157–1161.

(62) Ramakrishnan, S.; Eppenberger, U.; Mueller, H.; Shinkai, Y.; Narayanan, R.; Sumiyoshi, H.; Srinivasula, S. M.; Barna, B. P.; Germano, I. M.; Takakura, M.; et al. Expression Profile of the Putative Catalytic Subunit of the Telomerase Gene. *Cancer Res.* **1998**, *58* (4), 622–625.

(63) Modlich, U.; Pugh, C. W.; Bicknell, R. Increasing Endothelial Cell Specific Expression by the Use of Heterologous Hypoxic and Cytokine-Inducible Enhancers. *Gene Ther.* **2000**, *7* (10), 896–902. https://doi.org/10.1038/sj.gt.3301177.

(64) SU, G.-Q.; SU, G.; HUANG, Z.-H. Adenovirus-Mediated Tissue-Targeted Expression of

the CDglyTk Gene for the Treatment of Breast Cancer. *Mol. Med. Rep.* **2012**, *6* (2), 321–329. https://doi.org/10.3892/mmr.2012.925.

(65) Yang, L.; Cao, Z.; Li, F.; Post, D. E.; Van Meir, E. G.; Zhong, H.; Wood, W. C. Tumor-Specific Gene Expression Using the Survivin

Promoter Is Further Increased by Hypoxia. *Gene Ther.* **2004**, *11* (15), 1215–1223. https://doi.org/10.1038/sj.gt.3302280.

(66) Yang, L.; Cao, Z.; Li, F.; Post, D. E.; Van Meir, E. G.; Zhong, H.; Wood, W. C. Tumor-Specific Gene Expression Using the Survivin Promoter Is Further Increased by Hypoxia. *Gene Ther.* **2004**, *11* (15), 1215–1223. https://doi.org/10.1038/sj.gt.3302280.

(67) Konopka, K.; Spain, C.; Yen, A.; Overlid, N.; Gebremedhin, S.; Düzgüneş, N. Correlation between the Levels of Survivin and Survivin Promoter-Driven Gene Expression in Cancer and Non-Cancer Cells. *Cell. Mol. Biol. Lett.* **2009**, *14* (1), 70–89. https://doi.org/10.2478/s11658-008-0034-5.

(68) Maeda, T.; O-Wang, J.; Matsubara, H.; Asano, T.; Ochiai, T.; Sakiyama, S.; Tagawa, M. A Minimum C-ErbB-2 Promoter-Mediated Expression of Herpes Simplex Virus Thymidine Kinase Gene Confers Selective Cytotoxicity of Human Breast Cancer Cells to Ganciclovir. *Cancer Gene Ther.* **2001**, *8* (11), 890–896. https://doi.org/10.1038/sj.cgt.7700389.

(69) Jacob, D.; Schumacher, G.; Bahra, M.; Davis, J.; Zhu, H.-B.; Zhang, L.-D.; Teraishi, F.; Neuhaus, P.; Fang, B.-L. Fiber-Modified Adenoviral Vector Expressing the Tumor Necrosis Factor-Related Apoptosis-Inducing Ligand Gene from the Human Telomerase Reverse Transcriptase Promoter Induces Apoptosis in Human Hepatocellular Carcinoma Cells. *World J. Gastroenterol.* **2005**, *11* (17), 2552–2556. https://doi.org/10.3748/wjg.v11.i17.2552.

(70) Liu, B.; Qu, L.; Yan, S. Cyclooxygenase-2 Promotes Tumor Growth and Suppresses Tumor Immunity. *Cancer Cell Int.* **2015**, *15*, 106. https://doi.org/10.1186/s12935-015-0260-7.

(71) Yamamoto, M.; Alemany, R.; Adachi, Y.; Grizzle, W. E.; Curiel, D. T. Characterization of the Cyclooxygenase-2 Promoter in an Adenoviral Vector and Its Application for the Mitigation of Toxicity in Suicide Gene Therapy of Gastrointestinal Cancers. *Mol. Ther.* **2001**, *3* (3), 385–394. https://doi.org/10.1006/MTHE.2001.0275.

(72) Wang, Z.-X.; Bian, H.-B.; Yang, J.-S.; De, W.; Ji, X.-H. Adenovirus-Mediated Suicide Gene Therapy under the Control of Cox-2 Promoter for Colorectal Cancer. *Cancer Biol. Ther.* **2009**, *8* (15), 1480–1488. https://doi.org/10.4161/cbt.8.15.8940.

(73) Haviv, Y. S.; van Houdt, W. J.; Lu, B.; Curiel, D. T.; Zhu, Z. B. Transcriptional Targeting in Renal Cancer Cell Lines via the Human CXCR-4 Promoter. *Mol. Cancer Ther.* **2004**, *3*

(6), 687–691.

(74) Zhu, Z.; Makhija, S.; Lu, B.; Wang, M.; Kaliberova, L.; Liu, B.; Rivera, A.; Nettelbeck, D.; Mahasreshti, P.; Leath, C.; et al. Transcriptional Targeting of Adenoviral Vector through the CXCR-4 Tumor-Specific Promoter. *Gene Ther.* **2004**, *11* (7), 645–648. https://doi.org/10.1038/sj.gt.3302089.

(75) Xie, X.; Xia, W.; Li, Z.; Kuo, H.-P.; Liu, Y.; Li, Z.; Ding, Q.; Zhang, S.; Spohn, B.; Yang, Y.; et al. Targeted Expression of BikDD Eradicates Pancreatic Tumors in Noninvasive Imaging Models. *Cancer Cell* **2007**, *12* (1), 52–65. https://doi.org/10.1016/j.ccr.2007.05.009.

(76) Li, Z.; Ding, Q.; Li, Y.; Miller, S. A.; Abbruzzese, J. L.; Hung, M. C. Suppression of Pancreatic Tumor Progression by Systemic Delivery of a Pancreatic-Cancer-Specific Promoter Driven Bik Mutant. *Cancer Lett.* **2006**, *236* (1), 58–63. https://doi.org/10.1016/j.canlet.2005.05.001.

(77) Shi, Y.-J.; Gong, J.-P.; Liu, C.-A.; Li, X.-H.; Mei, Y.; Mi, C.; Huo, Y.-Y. Construction of a Targeting Adenoviral Vector Carrying AFP Promoter for Expressing EGFP Gene in AFP-Producing Hepatocarcinoma Cell. *World J. Gastroenterol.* **2004**, *10* (2), 186–189. https://doi.org/10.3748/wjg.v10.i2.186.

(78) JIN, S.; LIN, X.; GUAN, H.; WU, J. Cell-Specific Expression of the Analgesic-Antitumor Peptide Coding Sequence under the Control of the Human α-Fetoprotein Gene Promoter and Enhancer. *Exp. Ther. Med.* **2015**, *9* (3), 863–867. https://doi.org/10.3892/etm.2015.2166.

(79) FANG, H.; KANG, J.; DU, R.; ZHAO, X.; ZHANG, X.; REN, D.; ZHANG, Y.; LU, Z.; WU, S.; ZHENG, W.; et al. Growth Inhibitory Effect of Adenovirus-Mediated Tissue-Targeted Expression of Ribosomal Protein L23 on Human Colorectal Carcinoma Cells. *Oncol. Rep.* **2015**, *34* (2), 763–770. https://doi.org/10.3892/or.2015.4026.

(80) Guo, X.; Evans, T. R. J.; Somanath, S.; Armesilla, A. L.; Darling, J. L.; Schatzlein, A.; Cassidy, J.; Wang, W. In Vitro Evaluation of Cancer-Specific NF-KappaB-CEA Enhancer promoter System for 5-Fluorouracil Prodrug Gene Therapy in Colon Cancer Cell Lines. *Br. J. Cancer* **2007**, *97* (6), 745–754. https://doi.org/10.1038/sj.bjc.6603930.

(81) Kim, N. W.; Prowse, K. R.; Harley, C. B.; West, M. D.; Ho, P. L. C.; Coviello, G. M.; Weinrich, S. L.; Piatyszek, M. A.; Wright, W. E.; Shay, J. W. Specific Association of Human Telomerase Activity with Immortal Cells and Cancer. *Science (80-.).* **1994**, *266* (5193), 2011–2015. https://doi.org/10.1126/science.7605428.

(82) Watanabe, M.; Ueki, H.; Ochiai, K.; Huang, P.; Kobayashi, Y.; Nasu, Y.; Sasaki, K.; Kaku,

H.; Kashiwakura, Y.; Kumon, H. Advanced Two-Step Transcriptional Amplification as a Novel Method for Cancer-Specific Gene Expression and Imaging. *Oncol. Rep.* **2011**, *26* (4), 769–775. https://doi.org/10.3892/or.2011.1371.

(83) Garg, H.; Suri, P.; Gupta, J. C.; Talwar, G. P.; Dubey, S. Survivin: A Unique Target for Tumor Therapy. *Cancer Cell Int.* **2016**, *16*, 49. https://doi.org/10.1186/s12935-016-0326-1.

(84) Rosa, J.; Canovas, P.; Islam, A.; Altieri, D. C.; Doxsey, S. J. Survivin Modulates Microtubule Dynamics and Nucleation throughout the Cell Cycle. *Mol. Biol. Cell* **2006**, *17* (3), 1483–1493. https://doi.org/10.1091/mbc.e05-08-0723.

(85) Chen, J.-S.; Liu, J.-C.; Shen, L.; Rau, K.-M.; Kuo, H.-P.; Li, Y. M.; Shi, D.; Lee, Y.-C.; Chang, K.-J.; Hung, M.-C. Cancer-Specific Activation of the Survivin Promoter and Its Potential Use in Gene Therapy. *Cancer Gene Ther.* **2004**, *11* (11), 740–747. https://doi.org/10.1038/sj.cgt.7700752.

(86) Mita, A. C.; Mita, M. M.; Nawrocki, S. T.; Giles, F. J. Survivin: Key Regulator of Mitosis and Apoptosis and Novel Target for Cancer Therapeutics. *Clin. Cancer Res.* **2008**, *14* (16), 5000–5005. https://doi.org/10.1158/1078-0432.CCR-08-0746.

(87) Garg, H.; Salcedo, R.; Trinchieri, G.; Blumenthal, R. Improved Nonviral Cancer Suicide Gene Therapy Using Survivin Promoter-Driven Mutant Bax. *Cancer Gene Ther.* **2010**, *17* (3), 155–163. https://doi.org/10.1038/cgt.2009.63.

(88) Zhu, Z. B.; Makhija, S. K.; Lu, B.; Wang, M.; Kaliberova, L.; Liu, B.; Rivera, A. A.; Nettelbeck, D. M.; Mahasreshti, P. J.; Leath, C. A.; et al. Transcriptional Targeting of Tumors with a Novel Tumor-Specific Survivin Promoter. *Cancer Gene Ther.* **2004**, *11* (4), 256–262. https://doi.org/10.1038/sj.cgt.7700679.

(89) Sharma, S.; Stolina, M.; Yang, S.-C.; Baratelli, F.; Lin, J. F.; Atianzar, K.; Luo, J.; Zhu, L.; Lin, Y.; Huang, M.; et al. Tumor Cyclooxygenase 2-Dependent Suppression of Dendritic Cell Function. *Clin. Cancer Res.* **2003**, *9* (3), 961–968.

(90) Müller, A.; Homey, B.; Soto, H.; Ge, N.; Catron, D.; Buchanan, M. E.; McClanahan, T.; Murphy, E.; Yuan, W.; Wagner, S. N.; et al. Involvement of Chemokine Receptors in Breast Cancer Metastasis. *Nature* **2001**, *410* (6824), 50–56. https://doi.org/10.1038/35065016.

(91) Kulbe, H.; Levinson, N. R.; Balkwill, F.; Wilson, J. L. The Chemokine Network in Cancer - Much More than Directing Cell Movement. *Int. J. Dev. Biol.* **2004**, *48* (5–6), 489–496. https://doi.org/10.1387/ijdb.041814hk.

(92) Rajendran, S.; Collins, S.; van Pijkeren, J. P.; O'Hanlon, D.; O'Sullivan, G. C.; Tangney, M. Targeting of Breast Metastases Using a Viral Gene Vector with Tumour-Selective Transcription. *Anticancer Res.* **2011**, *31* (5), 1627–1635.

(93) Adinolfi, B.; Pellegrino, M.; Baldini, F. Human Dermal Fibroblasts HDFa Can Be Used as an Appropriate Healthy Control for PMMA Nanoparticles-Survivin Molecular Beacon Cellular Uptake Studies. *Biomed. Pharmacother.* **2015**, *69*, 228–232. https://doi.org/10.1016/j.biopha.2014.12.003.

(94) Geisler, A.; Fechner, H. MicroRNA-Regulated Viral Vectors for Gene Therapy. *World J. Exp. Med.* **2016**, *6* (2), 37–54. https://doi.org/10.5493/wjem.v6.i2.37.

(95) Lee, H.; Han, S.; Kwon, C. S.; Lee, D. Biogenesis and Regulation of the Let-7 MiRNAs and Their Functional Implications. *Protein Cell* **2016**, *7* (2), 100–113. https://doi.org/10.1007/s13238-015-0212-y.

(96) Okada, C.; Yamashita, E.; Lee, S. J.; Shibata, S.; Katahira, J.; Nakagawa, A.; Yoneda, Y.; Tsukihara, T. A High-Resolution Structure of the Pre-MicroRNA Nuclear Export Machinery. *Science* **2009**, *326* (5957), 1275–1279. https://doi.org/10.1126/science.1178705.

(97) Jo, M. H.; Shin, S.; Jung, S.-R.; Kim, E.; Song, J.-J.; Hohng, S. Human Argonaute 2 Has Diverse Reaction Pathways on Target RNAs. *Mol. Cell* **2015**, *59* (1), 117–124. https://doi.org/10.1016/J.MOLCEL.2015.04.027.

(98) Van Rooij, E.; Olson, E. N. MicroRNA Therapeutics for Cardiovascular Disease: Opportunities and Obstacles. *Nat. Rev. Drug Discov.* **2012**, *11* (11), 860–872. https://doi.org/10.1038/nrd3864.

(99) Lu, J.; Getz, G.; Miska, E. A.; Alvarez-Saavedra, E.; Lamb, J.; Peck, D.; Sweet-Cordero, A.; Ebert, B. L.; Mak, R. H.; Ferrando, A. A.; et al. MicroRNA Expression Profiles Classify Human Cancers. *Nature* **2005**, *435* (7043), 834–838. https://doi.org/10.1038/nature03702.

(100) Thomson, J. M.; Newman, M.; Parker, J. S.; Morin-Kensicki, E. M.; Wright, T.; Hammond, S. M. Extensive Post-Transcriptional Regulation of MicroRNAs and Its Implications for Cancer. *Genes Dev.* **2006**, *20* (16), 2202–2207. https://doi.org/10.1101/gad.1444406.

(101) Barh, D.; Malhotra, R.; Ravi, B.; Sindhurani, P. MicroRNA Let-7: An Emerging next-Generation Cancer Therapeutic. *Curr. Oncol.* **2010**, *17* (1), 70–80. https://doi.org/10.3747/co.v17i1.356.

(102) Edge, R. E.; Falls, T. J.; Brown, C. W.; Lichty, B. D.; Atkins, H.; Bell, J. C. A Let-7 MicroRNA-Sensitive Vesicular Stomatitis Virus Demonstrates Tumor-Specific Replication. *Mol. Ther.* **2008**, *16* (8), 1437–1443. https://doi.org/10.1038/MT.2008.130.

(103) Suzuki, T.; Sakurai, F.; Nakamura, S.; Kouyama, E.; Kawabata, K.; Kondoh, M.; Yagi, K.; Mizuguchi, H. MiR-122a-Regulated Expression of a Suicide Gene Prevents Hepatotoxicity Without Altering Antitumor Effects in Suicide Gene Therapy. *Mol. Ther.* **2008**, *16* (10),

1719–1726. https://doi.org/10.1038/MT.2008.159.

(104) Xie, J.; Xie, Q.; Zhang, H.; Ameres, S. L.; Hung, J.-H.; Su, Q.; He, R.; Mu, X.; Seher Ahmed, S.; Park, S.; et al. MicroRNA-Regulated, Systemically Delivered RAAV9: A Step Closer to CNS-Restricted Transgene Expression. *Mol. Ther.* **2011**, *19* (3), 526–535. https://doi.org/10.1038/mt.2010.279.

(105) Moolten, F. L. Tumor Chemosensitivity Conferred by Inserted Herpes Thymidine Kinase Genes: Paradigm for a Prospective Cancer Control Strategy. *Cancer Res.* **1986**, *46* (10), 5276–5281.

(106) McCormick, F. Cancer Gene Therapy: Fringe or Cutting Edge? *Nat. Rev. Cancer* **2001**, *1* (2), 130–141. https://doi.org/10.1038/35101008.

(107) Zarogoulidis, P.; Darwiche, K.; Sakkas, A.; Yarmus, L.; Huang, H.; Li, Q.; Freitag, L.; Zarogoulidis, K.; Malecki, M. Suicide Gene Therapy for Cancer - Current Strategies. *J Genet Syndr Gene Ther* **2013**, *4*. https://doi.org/10.4172/2157-7412.1000139.Suicide.

(108) Rooseboom, M.; Commandeur, J. N. M.; Vermeulen, N. P. E. Enzyme-Catalyzed Activation of Anticancer Prodrugs. *Pharmacol. Rev.* **2004**, *56* (1), 53–102. https://doi.org/10.1124/pr.56.1.3.

(109) Gynther, M.; Kariinen, T. M.; Hakkarainen, J. J.; Jalkanen, A. J.; Petsalo, A.; Lehtonen, M.; Peura, L.; Kurkipuro, J.; Samaranayake, H.; Yla-Herttuala, S.; et al. Brain Pharmacokinetics of Ganciclovir in Rats with Orthotopic BT4C Glioma. *Drug Metab. Dispos.* **2015**, *43* (1), 140–146. https://doi.org/10.1124/dmd.114.059840.

(110) Tomicic, M. T.; Thust, R.; Kaina, B. Ganciclovir-Induced Apoptosis in HSV-1 Thymidine Kinase Expressing Cells: Critical Role of DNA Breaks, Bcl-2 Decline and Caspase-9 Activation. *Oncogene* **2002**, *21* (14), 2141–2153. https://doi.org/10.1038/sj.onc.1205280.

(111) Thust, R.; Schacke, M.; Wutzler, P. Cytogenetic Genotoxicity of Antiherpes Virostatics in Chinese Hamster V79-E Cells. I. Purine Nucleoside Analogues. *Antiviral Res.* **1996**, *31* (1–2), 105–113. https://doi.org/10.1016/0166-3542(96)00961-8.

(112) Beltinger, C.; Fulda, S.; Kammertoens, T.; Meyer, E.; Uckert, W.; Debatin, K. M. Herpes Simplex Virus Thymidine Kinase/Ganciclovir-Induced Apoptosis Involves Ligand-Independent Death Receptor Aggregation and Activation of Caspases. *Proc. Natl. Acad. Sci. U. S. A.* **1999**, *96* (15), 8699–8704. https://doi.org/10.1073/pnas.96.15.8699.

(113) Gamrekelashvili, J.; Krüger, C.; von Wasielewski, R.; Hoffmann, M.; Huster, K. M.; Busch, D. H.; Manns, M. P.; Korangy, F.; Greten, T. F. Necrotic Tumor Cell Death In Vivo Impairs Tumor-Specific Immune Responses. *J. Immunol.* **2007**, *178* (3), 1573–1580. https://doi.org/10.4049/jimmunol.178.3.1573.

(114) Ostermann, N.; Lavie, A.; Padiyar, S.; Brundiers, R.; Veit, T.; Reinstein, J.; Goody, R. S.; Konrad, M.; Schlichting, I. Potentiating AZT Activation: Structures of Wild-Type and Mutant Human Thymidylate Kinase Suggest Reasons for the Mutants' Improved Kinetics with the HIV Prodrug Metabolite AZTMP. *J. Mol. Biol.* **2000**, *304* (1), 43–53. https://doi.org/10.1006/JMBI.2000.4175.

(115) Willmon, C. L.; Krabbenhoft, E.; Black, M. E. A Guanylate Kinase/HSV-1 Thymidine Kinase Fusion Protein Enhances Prodrug-Mediated Cell Killing. *Gene Ther.* **2006**, *13* (17), 1309–1312. https://doi.org/10.1038/sj.gt.3302794.

(116) Ardiani, A.; Sanchez-Bonilla, M.; Black, M. E. Fusion Enzymes Containing HSV-1 Thymidine Kinase Mutants and Guanylate Kinase Enhance Prodrug Sensitivity in Vitro and in Vivo. *Cancer Gene Ther.* **2010**, *17* (2), 86–96. https://doi.org/10.1038/cgt.2009.60.

(117) Black, M. E.; Newcomb, T. G.; Wilson, H. M.; Loeb, L. A. Creation of Drug-Specific Herpes Simplex Virus Type 1 Thymidine Kinase Mutants for Gene Therapy. *Proc. Natl. Acad. Sci. U. S. A.* **1996**, *93* (8), 3525–3529. https://doi.org/10.1073/pnas.93.8.3525.

(118) van Dillen, I.; Mulder, N.; Vaalburg, W.; de Vries, E.; Hospers, G. Influence of the Bystander Effect on HSV-Tk / GCV Gene Therapy. A Review. *Curr. Gene Ther.* **2006**, *2* (3), 307–322. https://doi.org/10.2174/1566523023347733.

(119) Drake, R. R.; Pitlyk, K.; McMasters, R. A.; Mercer, K. E.; Young, H.; Moyer, M. P. Connexin-Independent Ganciclovir-Mediated Killing Conferred on Bystander Effect-Resistant Cell Lines by a Herpes Simplex Virus-Thymidine Kinase-Expressing Colon Cell Line. *Mol. Ther.* **2000**, *2* (5), 515–523. https://doi.org/10.1006/mthe.2000.0192.

(120) Wang, K.; Kievit, F. M.; Zhang, M. Evaluation of Four Tumor-Specific Promoters in Various Cancer Cell Lines. **2016**, *6* (1).

(121) Curdt, C. Transcriptional and Translational Targeting of Human Cancerous Cell Lines as Part of a Virus- Directed Enzyme Prodrug Therapy (VDEPT), 2018.

(122) Grzegorski, S. J.; Chiari, E. F.; Robbins, A.; Kish, P. E.; Kahana, A. Natural Variability of Kozak Sequences Correlates with Function in a Zebrafish Model. *PLoS One* **2014**, *9* (9), e108475. https://doi.org/10.1371/journal.pone.0108475.

(123) Acevedo, J. M.; Hoermann, B.; Schlimbach, T.; Teleman, A. A. Changes in Global Translation Elongation or Initiation Rates Shape the Proteome via the Kozak Sequence. *Sci. Rep.* **2018**, *8* (1), 4018. https://doi.org/10.1038/s41598-018-22330-9.

(124) Gibco. HDFa manual https://assets.thermofisher.com/TFS-Assets/LSG/manuals/HDFa_man.pdf (accessed Oct 11, 2019).

(125) Corriel Institute. GM22143 https://www.coriell.org/0/Sections/Search/Sample_Detail.aspx?Ref=GM22143 (accessed Oct 11, 2019).

(126) Gong, Y.; Li, Y.; Abdolmaleky, H. M.; Li, L.; Zhou, J. R. Tanshinones Inhibit the Growth of Breast Cancer Cells through Epigenetic Modification of Aurora a Expression and Function. *PLoS One* **2012**, *7* (4). https://doi.org/10.1371/journal.pone.0033656.

(127) Yang, L.; Cao, Z.; Li, F.; Post, D. E.; Van Meir, E. G.; Zhong, H.; Wood, W. C. Tumor-Specific Gene Expression Using the Survivin Promoter Is Further Increased by Hypoxia. *Gene Ther.* **2004**, *11* (15), 1215–1223. https://doi.org/10.1038/sj.gt.3302280.

(128) Zhang, F.; Wang, S.; Yin, L.; Yang, Y.; Guan, Y.; Wang, W.; Xu, H.; Tao, N. Quantification of Epidermal Growth Factor Receptor Expression Level and Binding Kinetics on Cell Surfaces by Surface Plasmon Resonance Imaging. *Anal. Chem.* **2015**, *87* (19), 9960–9965. https://doi.org/10.1021/acs.analchem.5b02572.

(129) Subik, K.; Lee, J.-F.; Baxter, L.; Strzepek, T.; Costello, D.; Crowley, P.; Xing, L.; Hung, M.-C.; Bonfiglio, T.; Hicks, D. G.; et al. The Expression Patterns of ER, PR, HER2, CK5/6, EGFR, Ki-67 and AR by Immunohistochemical Analysis in Breast Cancer Cell Lines. *Breast Cancer (Auckl).* **2010**, *4*, 35–41. https://doi.org/10.1177/117822341000400004.

(130) Feiner, R. C.; Pennè, I.; Müller, B.; Müller, K. M. EGF-MCherry Fusion Protein Expressed in *E. Coli* Shows Product Heterogeneity but a High Biological Activity. *Biochemistry* **2019**, *58* (8), 1043–1047. https://doi.org/10.1021/acs.biochem.9b00021.

(131) Szymczak, A. L.; Vignali, D. A. Development of 2A Peptide-Based Strategies in the Design of Multicistronic Vectors. *Expert Opin. Biol. Ther.* **2005**, *5* (5), 627–638. https://doi.org/10.1517/14712598.5.5.627.

(132) Liu, Z.; Chen, O.; Wall, J. B. J.; Zheng, M.; Zhou, Y.; Wang, L.; Ruth Vaseghi, H.; Qian, L.; Liu, J. Systematic Comparison of 2A Peptides for Cloning Multi-Genes in a Polycistronic Vector. *Sci. Rep.* **2017**, *7* (1), 2193. https://doi.org/10.1038/s41598-017-02460-2.

(133) Kim, J. H.; Lee, S.-R.; Li, L.-H.; Park, H.-J.; Park, J.-H.; Lee, K. Y.; Kim, M.-K.; Shin, B. A.; Choi, S.-Y. High Cleavage Efficiency of a 2A Peptide Derived from Porcine-1 in Human Cell Lines, Zebrafish and Mice. *PLoS One* **2011**, *6* (4), e18556. https://doi.org/10.1371/JOURNAL.PONE.0018556.

(134) iGem_Freiburg. Virus Construction Kit for Therapy http://2010.igem.org/Team:Freiburg_Bioware.

(135) Nociari, M. M.; Shalev, A.; Benias, P.; Russo, C. A Novel One-Step, Highly Sensitive

Fluorometric Assay to Evaluate Cell-Mediated Cytotoxicity. *J. Immunol. Methods* **1998**, *213* (2), 157–167. https://doi.org/10.1016/S0022-1759(98)00028-3.

(136) Li Bi, W.; Parysek, L. M.; Warnick, R.; Stambrook, P. J. In Vitro Evidence That Metabolic Cooperation Is Responsible for the Bystander Effect Observed with HSV Tk Retroviral Gene Therapy. *Hum. Gene Ther.* **1993**, *4* (6), 725–731. https://doi.org/10.1089/hum.1993.4.6-725.

(137) Kuriyama, S.; Nakatani, T.; Masui, K.; Sakamoto, T.; Tominaga, K.; Yoshikawa, M.; Fukui, H.; Ikenaka, K.; Tsujii, T. Bystander Effect Caused by Suicide Gene Expression Indicates the Feasibility of Gene Therapy for Hepatocellular Carcinoma. *Hepatology* **1995**, *22* (6), 1838–1846. https://doi.org/10.1016/0270-9139(95)90213-9.

(138) Guo, J.; He, K.; Zeng, H.; Shi, Y.; Ye, P.; Zhou, Q.; Pan, Z.; Long, X. Differential MicroRNA Expression Profiles Determined by Next-Generation Sequencing in Three Fulvestrant-Resistant Human Breast Cancer Cell Lines. *Oncol. Lett.* **2019**, *17* (4), 3765–3776. https://doi.org/10.3892/ol.2019.10061.

(139) Riaz, M.; van Jaarsveld, M. T.; Hollestelle, A.; Prager-van der Smissen, W. J.; Heine, A. A.; Boersma, A. W.; Liu, J.; Helmijr, J.; Ozturk, B.; Smid, M.; et al. MiRNA Expression Profiling of 51 Human Breast Cancer Cell Lines Reveals Subtype and Driver Mutation-Specific MiRNAs. *Breast Cancer Res.* **2013**, *15* (2), R33. https://doi.org/10.1186/bcr3415.

(140) Rabiau, N.; Trraf, H.-K.; Adjakly, M.; Bosviel, R.; Guy, L.; Fontana, L.; Bignon, Y.-J.; Bernard-Gallon, D. J. MiRNAs Differentially Expressed in Prostate Cancer Cell Lines after Soy Treatment. *In Vivo* **2011**, *25* (6), 917–921.

(141) Nam, S.; Kim, B.; Shin, S.; Lee, S. MiRGator: An Integrated System for Functional Annotation of MicroRNAs. *Nucleic Acids Res.* **2008**, *36* (Database issue), D159. https://doi.org/10.1093/NAR/GKM829.

(142) Grimm, D.; Kern, A.; Rittner, K.; Kleinschmidt, J. A. Novel Tools for Production and Purification of Recombinant Adenoassociated Virus Vectors. *Hum. Gene Ther.* **1998**, *9* (18), 2745–2760. https://doi.org/10.1089/hum.1998.9.18-2745.

(143) Janakiraman, V.; Kwiatkowski, C.; Kshirsagar, R.; Ryll, T.; Huang, Y.-M. Application of High-Throughput Mini-Bioreactor System for Systematic Scale-down Modeling, Process Characterization, and Control Strategy Development. *Biotechnol. Prog.* **2015**, *31* (6), 1623–1632. https://doi.org/10.1002/btpr.2162.

(144) Nass, S. A.; Mattingly, M. A.; Woodcock, D. A.; Burnham, B. L.; Ardinger, J. A.; Osmond, S. E.; Frederick, A. M.; Scaria, A.; Cheng, S. H.; O'Riordan, C. R. Universal Method for the Purification of Recombinant AAV Vectors of Differing Serotypes. *Mol. Ther. - Methods*

Clin. Dev. **2018**, *9*, 33–46. https://doi.org/10.1016/J.OMTM.2017.12.004.

(145) Hildinger, M.; Baldi, L.; Stettler, M.; Wurm, F. M. High-Titer, Serum-Free Production of Adeno-Associated Virus Vectors by Polyethyleneimine-Mediated Plasmid Transfection in Mammalian Suspension Cells. *Biotechnol. Lett.* **2007**, *29* (11), 1713–1721. https://doi.org/10.1007/s10529-007-9441-3.

(146) Lock, M.; Alvira, M.; Vandenberghe, L. H.; Samanta, A.; Toelen, J.; Debyser, Z.; Wilson, J. M. Rapid, Simple, and Versatile Manufacturing of Recombinant Adeno-Associated Viral Vectors at Scale. *Hum. Gene Ther.* **2010**, *21* (10), 1259–1271. https://doi.org/10.1089/hum.2010.055.

(147) Rossmiller, B. P. AAV vector production and purification https://www.researchgate.net/publication/319623927_Adeno-associated_virus_AAV_vector_production_and_purification_protocol (accessed Sep 19, 2019). https://doi.org/10.13140/RG.2.2.26538.93127.

(148) Guo, P.; El-Gohary, Y.; Prasadan, K.; Shiota, C.; Xiao, X.; Wiersch, J.; Paredes, J.; Tulachan, S.; Gittes, G. K. Rapid and Simplified Purification of Recombinant Adeno-Associated Virus. *J. Virol. Methods* **2012**, *183* (2), 139–146. https://doi.org/10.1016/j.jviromet.2012.04.004.

(149) Grieger, J. C.; Soltys, S. M.; Samulski, R. J. Production of Recombinant Adeno-Associated Virus Vectors Using Suspension HEK293 Cells and Continuous Harvest of Vector From the Culture Media for GMP FIX and FLT1 Clinical Vector. *Mol. Ther.* **2016**, *24* (2), 287–297. https://doi.org/10.1038/mt.2015.187.

(150) Xell AG. Protocol for use HEK-GM https://www.xell.ag/shop/media/pdf/6d/63/ca/Protocol-for-use_HEK-GM_851.pdf (accessed Sep 23, 2019).

(151) Xell AG. Protocol for use HEK-TF https://www.xell.ag/shop/media/pdf/71/5e/60/Protocol-for-use_HEK-TF_861.pdf (accessed Sep 23, 2019).

(152) Xell AG. Protocol for use HEK-FS https://www.xell.ag/shop/media/pdf/22/c7/c3/Protocol-for-use_HEK-FS_871.pdf (accessed Sep 23, 2019).

(153) McKee, T. J.; Komarova, S. V. Is It Time to Reinvent Basic Cell Culture Medium? *Am. J. Physiol. - Cell Physiol.* **2017**, *312* (5), C624–C626. https://doi.org/10.1152/ajpcell.00336.2016.

(154) Wang, Y.; Cooper, R.; Kiladjian, A.; Bergelson, S.; Feschenko, M. A Digestion-Free Method for Quantification of Residual Host Cell DNA in RAAV Gene Therapy Products. *Mol. Ther. - Methods Clin. Dev.* **2019**, *13*, 526–531.

https://doi.org/10.1016/J.OMTM.2019.05.005.

(155) Miyake, K.; Miyake, N.; Yamazaki, Y.; Shimada, T.; Hirai, Y. Serotype-Independent Method of Recombinant Adeno-Associated Virus (AAV) Vector Production and Purification. *J. Nippon Med. Sch.* **2012**, *79* (6), 394–402. https://doi.org/10.1017/CBO9781107415324.004.

(156) Berk, A. J. Recent Lessons in Gene Expression, Cell Cycle Control, and Cell Biology from Adenovirus. *Oncogene* **2005**, *24* (52), 7673–7685. https://doi.org/10.1038/sj.onc.1209040.

(157) Sha, J.; Ghosh, M. K.; Zhang, K.; Harter, M. L. E1A Interacts with Two Opposing Transcriptional Pathways to Induce Quiescent Cells into S Phase. *J. Virol.* **2010**, *84* (8), 4050–4059. https://doi.org/10.1128/JVI.02131-09.

(158) Rego, M.; Hanley, L. M.; Ersing, I.; Guerin, K.; Tasissa, M.; Haery, L.; Mueller, I.; Sanders, E.; Fan, M. Improved Yield of AAV2 and RAAV2-Retro Serotypes Following Sugar Supplementation during the Viral Production Phase. *bioRxiv* **2018**, 488585. https://doi.org/10.1101/488585.

(159) Furuta-Hanawa, B.; Yamaguchi, T.; Uchida, E. 2D Droplet Digital PCR as a Tool for Titration and Integrity Evaluation of Recombinant Adeno-Associated Viral Vectors. *Hum. Gene Ther. Methods* **2019**, hgtb.2019.031. https://doi.org/10.1089/hgtb.2019.031.

(160) Wang, F.; Cui, X.; Wang, M.; Xiao, W.; Xu, R. A Reliable and Feasible QPCR Strategy for Titrating AAV Vectors. *Med. Sci. Monit. Basic Res.* **2013**, *19*, 187–193. https://doi.org/10.12659/MSMBR.883968.

(161) Jordan, M.; Wurm, F. Transfection of Adherent and Suspended Cells by Calcium Phosphate. *Methods* **2004**, *33* (2), 136–143. https://doi.org/10.1016/j.ymeth.2003.11.011.

(162) Zeltner, N.; Kohlbrenner, E.; Clément, N.; Weber, T.; Linden, R. M. Near-Perfect Infectivity of Wild-Type AAV as Benchmark for Infectivity of Recombinant AAV Vectors. *Gene Ther.* **2010**, *17* (7), 872–879. https://doi.org/10.1038/gt.2010.27.

(163) Chen, H. Comparative Observation of the Recombinant Adeno-Associated Virus 2 Using Transmission Electron Microscopy and Atomic Force Microscopy. *Microsc. Microanal.* **2007**, *13* (5), 384–389. https://doi.org/10.1017/S1431927607070808.

(164) Ran, F. A.; Hsu, P. D.; Wright, J.; Agarwala, V.; Scott, D. A.; Zhang, F. Genome Engineering Using the CRISPR-Cas9 System. *Nat. Protoc.* **2013**, *8* (11), 2281–2308. https://doi.org/10.1038/nprot.2013.143.

(165) Thermo Fisher Scientific. TOPO TA cloning kit https://assets.thermofisher.com/TFS-Assets/LSG/manuals/topota_man.pdf (accessed Sep 25, 2019).

(166) Bischof, G. Analyse Der Extrazellulären Domäne Des AAV-Rezeptors Im Kontext Der Transduktion Mit Rekombinanten Adeno- Assoziierten Viren, University of Bielefeld, 2018.

(167) Vandenberghe, L. H.; Xiao, R.; Lock, M.; Lin, J.; Korn, M.; Wilson, J. M. Efficient Serotype-Dependent Release of Functional Vector into the Culture Medium during Adeno-Associated Virus Manufacturing. *Hum. Gene Ther.* **2010**, *21* (10), 1251–1257. https://doi.org/10.1089/hum.2010.107.

(168) Vandenberghe, L. H.; Xiao, R.; Lock, M.; Lin, J.; Korn, M.; Wilson, J. M. Efficient Serotype-Dependent Release of Functional Vector into the Culture Medium during Adeno-Associated Virus Manufacturing. *Hum. Gene Ther.* **2010**, *21* (10), 1251–1257. https://doi.org/10.1089/hum.2010.107.

(169) Yu, A.; Shang, J.; Cheng, F.; Paik, B. A.; Kaplan, J. M.; Andrade, R. B.; Ratner, D. M. Biofunctional Paper via the Covalent Modification of Cellulose. *Langmuir* **2012**, *28* (30), 11265–11273. https://doi.org/10.1021/la301661x.

(170) Salganik, M.; Venkatakrishnan, B.; Bennett, A.; Lins, B.; Yarbrough, J.; Muzyczka, N.; Agbandje-McKenna, M.; McKenna, R. Evidence for PH-Dependent Protease Activity in the Adeno-Associated Virus Capsid. *J. Virol.* **2012**, *86* (21), 11877–11885. https://doi.org/10.1128/JVI.01717-12.

(171) Nam, H.; Gurda, B. L.; Mckenna, R.; Potter, M.; Byrne, B.; Salganik, M.; Muzyczka, N.; Agbandje-mckenna, M. Structural Studies of Adeno-Associated Virus Serotype 8 Capsid Transitions Associated with Endosomal Trafficking □. **2011**, *85* (22), 11791–11799. https://doi.org/10.1128/JVI.05305-11.

(172) Schrader, C.; Schielke, A.; Ellerbroek, L.; Johne, R. PCR Inhibitors - Occurrence, Properties and Removal. *J. Appl. Microbiol.* **2012**, *113* (5), 1014–1026. https://doi.org/10.1111/j.1365-2672.2012.05384.x.

(173) Freiburg iGEM Team. Virus Construction Kit For Therapy http://2010.igem.org/Team:Freiburg_Bioware (accessed Jan 24, 2019).

(174) Stutika, C.; Gogol-Döring, A.; Botschen, L.; Mietzsch, M.; Weger, S.; Feldkamp, M.; Chen, W.; Heilbronn, R. A Comprehensive RNA Sequencing Analysis of the Adeno-Associated Virus (AAV) Type 2 Transcriptome Reveals Novel AAV Transcripts, Splice Variants, and Derived Proteins. *J. Virol.* **2016**, *90* (3), 1278–1289. https://doi.org/10.1128/JVI.02750-15.

(175) Zhang, H.; Xie, J.; Dmitriev, I.; Kashentseva, E.; Curiel, D. T.; Hsu, H.; Mountz, J. D. Addition of Six-His-Tagged Peptide to the C Terminus of Adeno-Associated Virus VP3 Does Not Affect Viral Tropism or Production. *J. Virol.* **2002**, *76* (23), 12023–12031.

https://doi.org/10.1128/JVI.76.23.12023.

(176) Stacey, S. N.; Jordan, D.; Williamson, A. J.; Brown, M.; Coote, J. H.; Arrand, J. R. Leaky Scanning Is the Predominant Mechanism for Translation of Human Papillomavirus Type 16 E7 Oncoprotein from E6/E7 Bicistronic MRNA. *J. Virol.* **2000**, *74* (16), 7284–7297. https://doi.org/10.1128/jvi.74.16.7284-7297.2000.

(177) NEB. Color Protein Standard, Broad Range https://international.neb.com/products/p7712-color-prestained-protein-standard-broad-range-11-245-kda#Protocols, Manuals & Usage (accessed Oct 2, 2019).

(178) Scientific, F. Thermo Scientific GeneRuler 1kb DNA-Leiter https://www.fishersci.de/shop/products/fermentas-generuler-1kb-dna-ladder/11823963 (accessed Oct 2, 2019).

(179) Chang, A. Y.; Chau, V. W.; Landas, J. A.; Yvonne. Preparation of Calcium Competent Escherichia Coli and Heat-Shock Transformation. *JEMI methods* **2017**, *1* (June), 22–25.

(180) Blum, H.; Beier, H.; Gross, H. J. Improved Silver Staining of Plant Proteins, RNA and DNA in Polyacrylamide Gels. *Electrophoresis* **1987**, *8* (2), 93–99. https://doi.org/10.1002/elps.1150080203.

(181) Agilent. AAV Helper-Free System https://www.agilent.com/en/product/protein-expression/protein-expression-vectors-kits/viral-mediated-delivery-systems/aav-helper-free-system-232989 (accessed Feb 12, 2019).

(182) Kingston RE, Chen CA, R. J. Transfection of DNA into Eukaryotic Cells. *Curr. Protoc. Mol. Biol.* **2003**, No. 1996, 1–11. https://doi.org/10.1002/0471142727.mb0901s63.

(183) Scientific, T. AminoLink Plus Coupling Resin https://assets.thermofisher.com/TFS-Assets/LSG/manuals/MAN0011262_AminoLnk_Plus_Coupling_Resin_UG.pdf (accessed Sep 16, 2019).

10. Appendix: Publications

Article

rAAV engineering for capsid-protein enzyme insertions and mosaicism reveals resilience to mutational, structural and thermal perturbations

Rebecca C. Feiner[1,†], Julian Teschner[1, †], Kathrin E. Teschner[1], Marco T. Radukic[1], Tobias Baumann[2], Sven Hagen[3], Yvonne Hannappel[4], Niklas Biere[5], Dario Anselmetti[5], Katja M. Arndt[6], Kristian M. Müller[1,*]

[1] Cellular and Molecular Biotechnology, Faculty of Technology, Bielefeld University, Bielefeld, Germany; rebecca.feiner@uni-bielefeld.de (R.C.F.); julian.teschner@uni-bielefeld.de (J.T.); kathrin.schlicht@uni-bielefeld.de (K.E.T.); marco.radukic@uni-bielefeld.de (M.T.R.)
[2] present address: Biocatalysis group, Department of Chemistry, Technische Universität Berlin, Berlin, Germany; tobias.baumann@tu-berlin.de (T.B.)
[3] present address: CO.DON AG, Berlin, Germany; sven.hagen@outlook.com (S.H.)
[4] Physical and Biophysical Chemistry (PCIII), Department of Chemistry, Bielefeld University, Germany; yvonne.hannappel@uni-bielefeld.de (Y.H.)
[5] Experimental Biophysics and Applied Nanoscience, Physics Department, Bielefeld University, Germany; nbiere@physik.uni-bielefeld.de (N.B.); dario.anselmetti@physik.uni-bielefeld.de (D.A.)
[6] Molecular Biotechnology, Institute for Biochemistry and Biology, University of Potsdam, 14476 Potsdam, Germany; arndtk@uni-potsdam.de (K.M.A.)

† Both authors contributed equally.
* Correspondence: kristian@syntbio.net; Tel.:+49-521-106-6323

Received: date; Accepted: date; Published: date

Abstract: Recombinant adeno-associated viruses (rAAV) provide outstanding options for customization and superior capabilities for gene therapy. To access their full potential, facile genetic manipulation is pivotal, including capsid loop modifications. Therefore, we assessed capsid tolerance to modifications of the VP proteins in terms of stability and plasticity. Flexible glycine-serine linkers of increasing sizes were, at the genetic level, introduced into the 587 loop region of the VP proteins of serotype 2, the best studied AAV representative. Analyses of biological function and thermal stability with respect to genome release of viral particles revealed structural plasticity. In addition, insertion of the 29 kDa enzyme β-lactamase into the loop region was tested with a complete or a mosaic modification setting. For the mosaic approach, investigation of VP2 trans expression revealed that a Kozak sequence was required to prevent leaky scanning. Surprisingly, even the full capsid modification with β-lactamase allowed for the assembly of capsids with a concomitant increase in size. Enzyme activity assays revealed lactamase functionality for both rAAV variants, which demonstrates the structural robustness of this platform technology.

Keywords: Adeno-associated-virus; β-lactamase; inverted terminal repeat (ITR); loop modification; capsid stability

---

Introduction

Recombinant adeno-associated viruses (rAAV) are frequently used as a basic research tool and are emerging as therapeutic agents. For example, the US FDA recently approved voretigene

neparvovec (Luxturna), which is based on rAAV serotype 2 (rAAV2) and delivers a gene to supplement biallelic RPE65 mutation-associated retinal dystrophy [237]. In addition, products based on AAV1 (Alipogene tiparvovec / Glybera) and very recently AAV9 (Onasemnogene abeparvovec / Zolgensma) obtained approval in Europe or the United States. The increasing impact of rAAV on gene therapy relies on a high safety profile resulting from the inability to replicate autonomously and on long-term target gene expression [118]. Wild-type AAVs have a non-enveloped, icosahedral capsid formed by 60 subunits of VP1, VP2 and VP3 proteins in an approximate molar ratio of 1:1:10 [7, 238]. In the AAV wild-type setting, the single-stranded DNA genome of about 4.7 kb includes two main reading frames (Rep and Cap) and is flanked by inverted terminal-repeat (ITR) sequences, which provide the encapsidation signal. Genetic engineering enables decoupling of the capsid coding genes from the encapsidated DNA. In the recombinant setting, *rep* and *cap* genes are provided *in trans* on a RepCap plasmid whereas a transgene expression cassette, frequently named gene of interest (GOI), is provided between the ITRs on the ITR plasmid. AAV needs additional 'helper' functionality from other viruses for production, which is provided on a separate pHelper plasmid [239, 240]. For this reason, a three-plasmid system is often used, wherein the pHelper delivers the essential adenoviral elements E2A, E4 and the non-coding RNA VA. As host, HEK293 cells provide further adenoviral elements (E1A, E1B) and allow for high-titer production[239, 240]. Alternative versions are also used such as a two-plasmid system combining the genetic information of the adenoviral helper sequences with AAV serotype specific *rep* and *cap* genes [113].

For diverse applications, e.g. virus-directed enzyme prodrug therapy (VDEPT) [241], viral targeting of specific cells is desired. AAV serotypes differ in their tropism and thus provide a first choice to achieve target specificity [242]. Deeper control over the target tropism requires genetic intervention. For this purpose, directed randomization and selection or rational engineering have been applied. Chimeric rAAV capsids are composed of proteins, which originate from different serotypes, and are often identified by evolutionary methods [243]. On the rational side, N-terminal fusions to e.g. the VP2 protein in rAAV2 have been studied [76, 107, 244]. In these cases, the addition of larger proteins, e.g. GFP and DARPins was compatible with capsid assembly and targeting.

A further and early adopted rational approach, which is extended in this publication, is the integration of motifs in previously identified loop positions of the VP proteins. Two groups demonstrated that capsid formation and gene packaging are only slightly influenced by integration of peptide sequences in VP proteins at various residue positions [245, 246]. Insertions in these positions has also been used for biorthogonal labelling of capsids [247, 248]. Capsid accommodation capacity was shown for the integration of larger moieties such as the minimal F_c-binding motif Z34C (34 amino acids) into the 587 loop region [249]. Production of such a Z34C rAAV2 with subsequent binding of an antibody was shown and transduction of target cells was observed. For vaccination via viral particle display, peptides up to 35 or 31 amino acids were integrated in the 453 or 587 position, respectively [250]. To our knowledge, the largest reported insertion to date is the fluorescent protein mCherry, which was functionally included in variable region IV at the 453 position of VP1, and allowed for the production of mosaic particles [251].

Our aim was to expand the loop modification strategy in combination with a systematic analysis of the engineering capacity of rAAV. For the construction of viruses, we extended an existing plasmid toolbox for rAAV2 manipulation and production [76, 252]. Insertion of peptides in capsid proteins was studied with regard to rAAV productivity and transduction capability. The impact of capsid protein modifications on thermal stability has, to our knowledge, not been investigated. Thus, we first tested rAAV stability with glycine-serine insertions of varying length at residue position 587. These experiments confirmed that larger insertions are tolerated and we opted to insert the enzyme β-lactamase. As the introduction of an entire protein could interfere with capsid assembly, we tested partial insertions only in VP2 proteins. This required adaptation of the plasmid system for the production of mosaic rAAVs exclusively bearing VP2 loop modifications. Resulting mosaic particles were found to tolerate the insertion of a full-length β-lactamase in VP2 proteins. Finally, we set up a complete β-lactamase modification of all VP proteins. Production of these fully decorated rAAVs was possible and allowed for further characterization. In summary, our analyses demonstrated resilience of the virus to modifications at the genetic and protein level. We believe

that the plasmid system combines facile genetic manipulation with a broad range of rAAV capsid engineering options.

Results

Modifications of ITR and RepCap plasmids are compatible with rAAV production.

Despite the availability of different ITR and RepCap plasmids for rAAV2 production, options for facile loop capsid modification are sparse. In this work, previously modularized versions of the RepCap and ITR plasmids were used, which are largely compatible with the BioBrick RFC[10] cloning strategy (SI Figure 1) [252]. The RepCap plasmid (pZMB0216_Rep_VP123_453_587wt_ p5tataless) was retained but the ITR plasmid was redesigned to reduce cloning steps and serve user expectations outside the synthetic biology community. The new ITR plasmid (pZMB0522_ITR_EXS_ CMV_mVenus_hGHpA) contains the viral ITRs as part of a pUC19-based backbone, provides restriction sites for insertions based on BioBrick RFC[10] flanking the fluorescent reporter mVenus, and serves as a final destination plasmid. Plasmid generations are described in SI Method 1, final constructs used during this work are given in Table 1 and selected plasmids of the plasmid toolbox are given in SI table 1.

For sequence analysis of the ITRs, which commonly defy Sanger cycle sequencing, we cleaved the ITR DNA with BsaHI, generating two halves that are amenable to standard sequencing protocols (SI Figure 2, SI Method 2). Our plasmid pZMB0522 carries one complete ITR (in this plasmid notation referred to as 5′-ITR) and an ITR shortened by 11 bp (Figure 1).

Table 1. Overview of plasmids submitted to Addgene including a short description of their features. Information on the cloning of the plasmids is available in the supplementary information.

Plasmid name with description	Length	Backbone
pZMB0522_ITR_EXS_CMV_mVenus_hGHpA AAV2 ITR flanking a CMV promoter expressing the fluorescent protein mVenus	4014 bp	pUC19
pZMB0216_Rep_VP123_453_587wt_p5tataless expression of VP1/2/3 of AAV2 with cloning ready 453 and 587 loop regions, arginines in 587 loop region are intact, p5 promoter at end of expression cassette	5455 bp	pSB1C3_001
pZMB0600_Rep_VP13_453_587wt_p5tataless expression of VP1 and VP3 with cloning ready 453 and 587 loop regions Arg in 587 loop region are intact	6455 bp	pSB1C3_001
pZMB0315_CMV_Kozak_VP2_453_587wtHis expression of VP2 with Kozak sequence to prevent leaky scanning and VP3 start knock out, cloning ready 453 and 587 loop regions, Arg in 587 intact, His-tag in 587 loop	4705 bp	pSB1C3_001

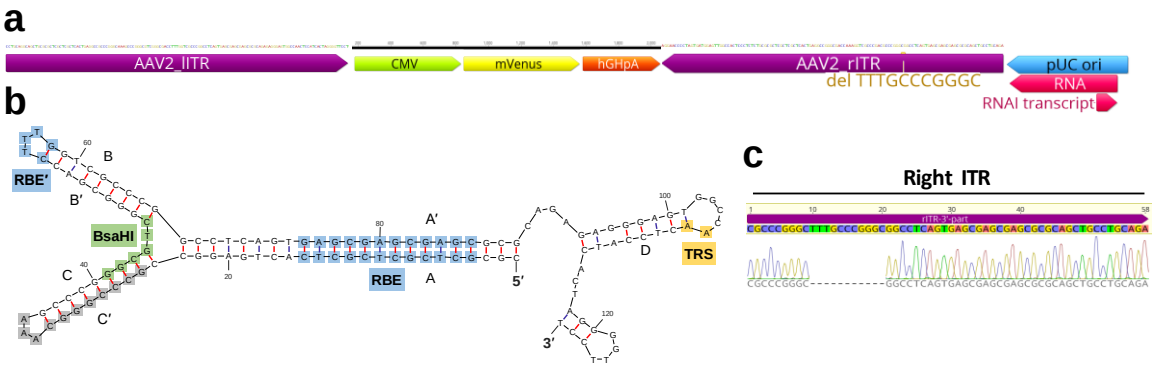

Figure 1. Overview of the ITR sequences of rAAV2. (a) Scheme of ITR plasmid components. The ITRs are enlarged compared to the interchangeable GOI (CMV promoter, mVenus fluorescent protein gene and hGHpolyA sequence). The deleted 11 bp sequence is highlighted in the right ITR adjacent to the pUC ori. (b) Structure of one ITR computed by Mfold webserver (150 mM NaCl, 5 mM $MaCl_2$, 37°C) [253]. Standard Sanger DNA-sequencing of ITRs was enabled by digestion with BsaHI whose recognition site is highlighted. (c) Results of Sanger-DNA sequencing aligned to original ITR sequences. Fragments were sequenced with oligonucleotides given in SI Method 2. The 3'-part of rITR shows a deletion of 11 bp (5'-TTTGCCCGGGC-3'). Sequencing results of the remaining ITR fragments are shown in SI Figure 2 c, d.

Production of DNaseI-resistant particles and thus functionality of the ITR plasmid (pZMB0522) in combination with either the RepCap plasmid (pZMB0216) or a commercially available counterpart (pAAV-RC, GenBank: AF369963.1) was assayed using small-scale transfections and quantitative real-time PCR (qPCR). Genomic titers in crude lysates with both plasmids showed no significant differences (Figure 2a). A larger preparation (pZMB0522, pZMB0216) was purified by precipitation [254] and imaged by transmission electron microscopy. Capsid diameter measurements resulted in an average of 23.7 ± 1.2 nm (SI Figure 3), which is in good agreement with the expected value of 25 nm [255]. Manually counting over 500 particles yielded a fraction of filled capsid between 60% and 80% (Figure 2b, SI Figure 3).

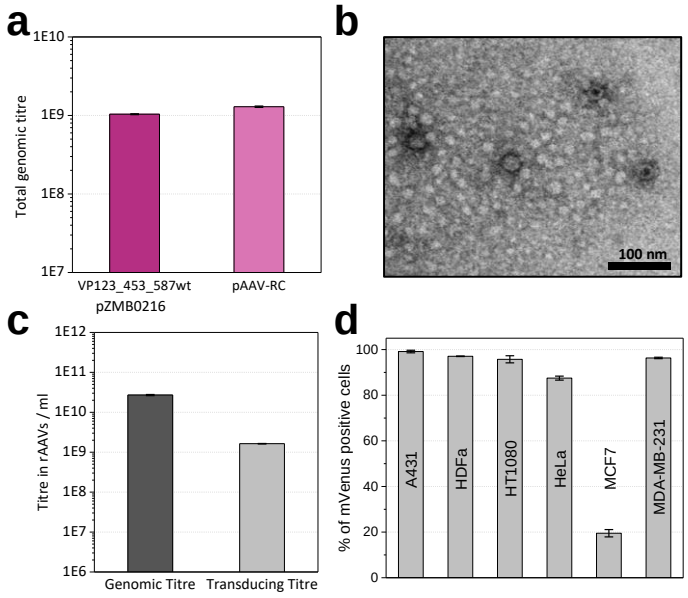

Figure 2. Production of rAAVs packaging the fluorescent reporter mVenus gene with plasmids pZMB0522 and pZMB0216. (a) Production yields of rAAV samples determined by qPCR from crude cell lysate from one 100 mm cell culture dish. Comparable values were obtained either using the new RepCap plasmid (left bar) or the commercial pAAV-RC plasmid (right bar). Standard deviations of three biological and two technical replicates were calculated for each sample type. (b) Transmission electron microscopy image analysis of precipitation-purified viral samples at 39,000-fold magnification revealed viral particles with a size of about 24 nm. (c) Comparison of viral genomic and transducing titers. Genomic titers were determined via qPCR from three technical replicates of ultracentrifugation-purified viral samples. Transducing titers were analyzed by mVenus expression from biological and technical duplicates after flow cytometry analysis of HT1080 cells. (d) Transduction of different cell lines. Cells were incubated with a MOI of 10,000. Biological duplicates at two time points were analyzed by flow cytometry, measuring mVenus fluorescence and counting 10,000 events. Histograms of flow cytometry analysis can be found in SI Figure 4.

To obtain higher purity samples, all further preparations were purified by iodixanol gradient ultracentrifugation. For unmodified rAAV2 wt (pZMB0522, pZMB0216) genomic titers were determined by qPCR (Figure 2c). Using a comparable setup but depending on culture conditions and transfection efficiencies, titers between 1×10^{10} to 1×10^{12} vg/ml have been obtained.

Functionality of gene delivery was investigated with transduction assays. As common for AAV2, HT1080 cells were used, which express high levels of the rAAV2 primary receptor heparan sulfate proteoglycane (HSPG). Successful transduction was detected by the expression of the delivered transgene mVenus using flow cytometry. Based on a dilution series, the transducing titer was calculated. Genomes to infectious units yielded a specific infectivity of 16:1 (Figure 2c). This is in agreement with previous values, since for wild-type AAV2 a ratio of 1:1 and for rAAV2 ratios between 55:1 and 124:1 have been observed [256]. In addition, also transduction of the cancer cell lines A431, HeLa, MCF7, MDA-MB-231 and normal adult human dermal fibroblasts (HDFa) was tested with a multiplicity of infection (MOI) of 10,000. Flow cytometry analysis (Figure 2d) revealed that the rAAV2 wt preparation was able to transduce a variety of different cells with high efficiencies. In agreement with previous reports, only the breast cancer cell line MCF7 showed low transduction [257]. These results demonstrated production and function of the rAAV plasmid system and provided the basis for further investigations regarding the tolerance of the viral capsid to insertions in the 587 loop region.

Systematic variation of loop modifications shows a complex pattern of stability and transduction efficiency.

Previous experiments showed that, VP proteins tolerate peptide insertions at residue positions 453 and 587 [245, 246]. We aimed at systematically analyzing the impact of increasing insertion length on rAAV thermal stability and biological function. Since a protein had already been inserted in the 453 loop region [251] and the 587 loop region is even more frequently used for modification, we opted to integrate linkers with increasing size at residue position 587 and investigated production and function of the resulting rAAVs. Glycine-serine linkers were chosen because of their flexibility and solubility, resulting in incremental changes correlating with length. Specifically, amino-acid linkers with the sequences GG, GGSG, $(GGSG)_2$ and $(GGSG)_4$ were integrated at the genetic level in all VP proteins to yield homogeneously decorated viral particles as presented in a schematic overview in Figure 3a.

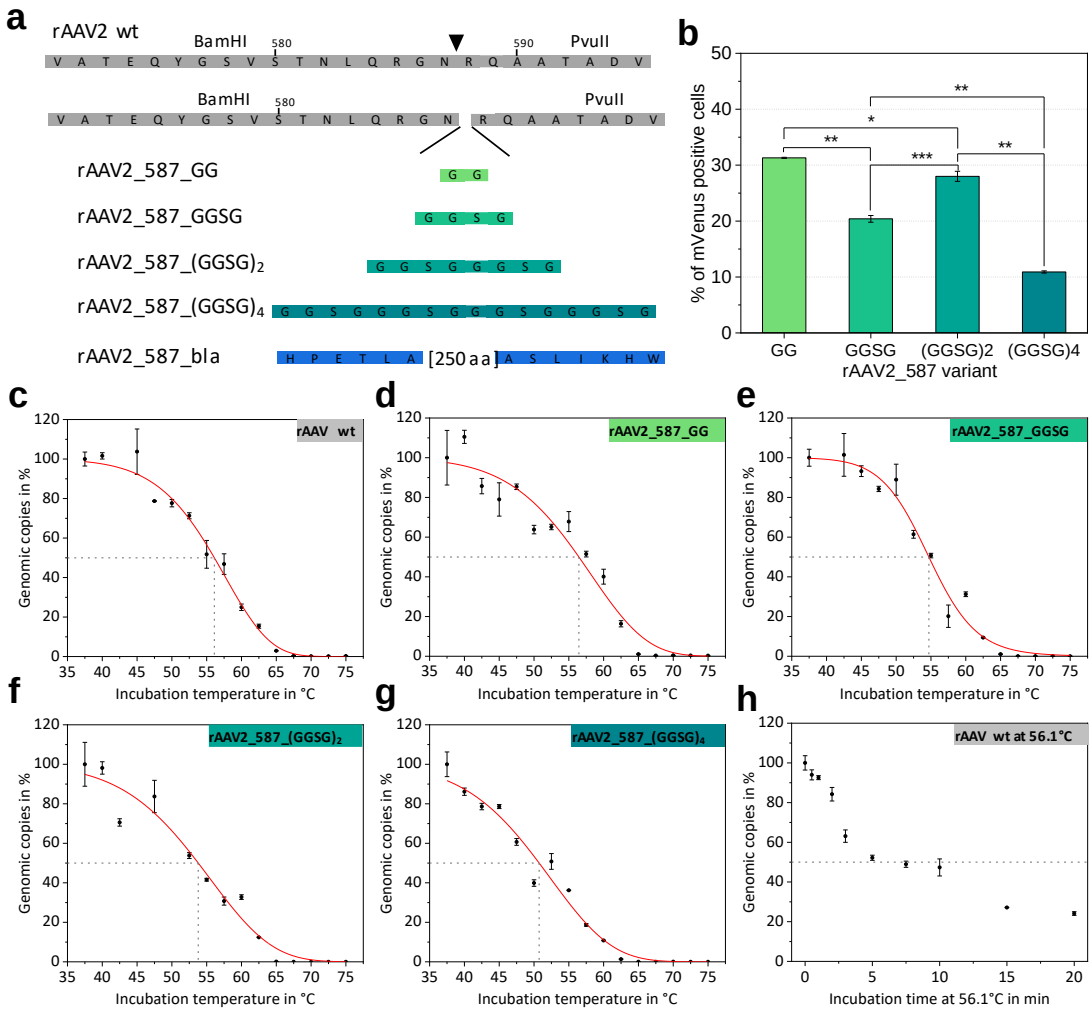

Figure 3. Comparison of different 587 loop variants and results of thermal stability assays. (a) Schematic overview on the coding sequence of the rAAV wt VP sequence. Restrictions site positions enabling the introduction of motifs flanking the 587 position (triangle) are indicated and amino-acid sequences of inserted linkers are shown. For β-lactamase only the first and the last amino acids are given. (b) Transduction efficiencies of different serine-glycine linker rAAV variants. Histograms of flow cytometry analysis can be found in SI Figure 7. Statistical analysis was performed as described in the Material and Methods section. (c-g) Thermal stability assays of rAAV particles measured in PBS. The percentage of qPCR detected genomic copies is plotted against the incubation temperature. Each point represents a technical duplicate with the standard deviation. Fitted curves (red) were calculated using a logistic function to determine the disintegration temperature for all rAAV variants. Table 2 lists the T_d values. (h) Disintegration kinetics of rAAV2 wt samples incubated at T_d = 56.1°C for different time periods. A dashed line indicates the point where 50% of genomic copies were released from the capsid.

Cloning was facilitated by the unique restriction sites of RepCap plasmid pZMB0216 flanking the loop region (SI Figure 1). Genomic titers of iodixanol-purified preparations demonstrated that all genetic constructs lead to rAAV production and that integration of flexible linkers only affected the titer for large integrations (Table 2). rAAV transduction ability was determined based on mVenus expression in HT1080 cells incubated with a MOI of 50,000 viral genomes. Increasing linker length impeded transduction (Table 2), but not in a linear fashion. The integration of only two amino acids resulted in a decrease of transduction ability from 97% (rAAV2 wt) to 31% (rAAV_587_GG) in the given experiment. Interestingly, increasing the linker length to four amino acids (GGSG) resulted in a further decrease of transduction to 20%, but rAAV with an insertion of eight amino acids ((GGSG)$_2$) showed a relatively improved transduction of 28% followed by a further drop in transduction to 11% for 16 amino acids (Figure 3b).

Table 2. Overview of plasmids submitted to Addgene including a short description of their features. Information on the cloning of the plasmids is available in the supplementary information.

Sample	Titer in vg ml^{-1} [a]	Transduction ability in % [b]	$T_{d, 5\ min}$ in °C[c]
rAAV2 wt	3.1×10^{10}	96.7 ± 0.1	56.1 ± 0.5
rAAV2_587_GG	7.1×10^{9}	31.3 ± 0.1	56.4 ± 0.8
rAAV2_587_GGSG	4.0×10^{10}	20.4 ± 0.6	54.7 ± 0.5
rAAV2_587_(GGSG)2	2.4×10^{10}	28.0 ± 0.9	53.8 ± 0.8
rAAV2_587_(GGSG)4	4.7×10^{9}	10.9 ± 0.2	50.7 ± 0.7
rAAV2_587_bla	1.3×10^{10}	1.2 ± 0.1	55.6 ± 0.4
rAAV2_VP2_587_bla	6.3×10^{10}	57.0 ± 2	n.d.

[a] Genomic titers are given in viral genomes (vg) per ml as determined by qPCR. Each value corresponds to a production with 10× 10 cm cell culture dishes and a final purified volume of 0.5 ml.

[b] Transduction ability was assayed with flow cytometry of HT1080 cells using a MOI of 50,000 and is given as percentage of mVenus expressing cells. The error is based on biological triplicates from one viral preparation.

[c] Disintegration temperatures T_d were determined in the qPCR-based stability assay.

Thermal stability of AAV capsids is an interesting biological and biophysical parameter and various methods to assess capsid stability have been described, such as differential scanning calorimetry (DSC), differential scanning fluorimetry (DSF) and electron microscopy[198], all of which monitor capsid breakdown but do not detect DNA release. We propose that the point of DNA release during heat treatment is a biological relevant event to describe capsid stability and that rAAV capsid integrity can be monitored by the DNase accessibility of the encapsidated DNA. Consequently, we repurposed the standard assay for genomic copy number determination and incubated rAAV samples at different temperatures before the treatment with DNase I. Subsequent analysis via qPCR yielded genomic copies of the rAAV sample plotted against the incubation temperature (Figure 3c-g). The disintegration temperature after a five-minute incubation ($T_{d, 5\ min}$) was determined as the temperature at which 50% of rAAVs have released their DNA. The term disintegration temperature T_d was chosen to distinguish the value from the melting temperature (T_m) reported by other methods (e.g. DSF, DSC). The results for all glycine-serine linker variants are listed in Table 2. With an increase in linker size T_d decreases slightly, showing that the capsid is destabilized by large insertions, but also that despite significant structural intervention, stability is maintained at physiological temperatures.

To estimate the influence of the incubation time and the decay kinetics in our thermal release assay, rAAV2 wt was isothermally incubated at the previously determined T_d (56.1 °C) for different time points. The percentage of intact genomic copies decreased in a hyperbolic fashion albeit displaying different phases (Figure 3h).

Mosaic rAAVs with a 29 kDa β-lactamase at position 578 in VP2 require a Kozak consensus sequence.

To illuminate the possibly even larger insertion capacity of rAAV capsids, we chose the well-studied TEM β-lactamase [206] as a protein with a small distance between the N- and C-terminus, which approximately matches the distance of the β-hairpin residues in the variable region of the VP protein. The protein was inserted at the genetic level at residue position 587 of the VP proteins. Lactamase offers the possibility to easily measure enzyme activity. In order to avoid maximum interference with capsid assembly, β-lactamase was in this experiment incorporated only into the 587 loop of solely VP2.

The modular rAAV plasmid system, which we used as a starting point, had been deployed to produce N-terminal VP2 protein fusions and the respective modified rAAV particles [76]. A mutation in the RepCap plasmid eliminated the VP2 start codon (pZMB0600_Rep_VP13_453_587wt_p5tataless) and a fourth plasmid expressing VP2 and VP3 (here named shortly CMV_VP23 plasmid) was provided *in trans*. The regulatory mechanisms for expression of the three VP proteins is complex [12, 258]. Briefly, splicing results in two mRNA transcripts

that code for VP1 or for VP2/3, respectively. VP2 and VP3 are coded by the same mRNA and expression is controlled by a leaky-scanning mechanism at the VP2 start, thus the VP3 sequence is always part of a VP2 gene. For the previous modifications leaky scanning did not pose a problem, because they were located at the unique N-terminus (SI Figure 1c). However, since the 587 loop region lies within the coding sequence of both VP2 and VP3 proteins, loop modifications desired for VP2 only require suppression of concomitant expression of a likewise modified VP3.
In order to understand and insure the sole expression of VP2, we conducted an expression and mutation analysis starting with the RepCap and the CMV_VP23 plasmid. Transient transfection of HEK293 cells with this plasmid and subsequent Western blot analysis of VP expression was performed. Expression of all three VP proteins after transfection with the unmodified RepCap plasmid showed approximately the expected molar ratio between the three VP proteins (1:1:10) (Figure 4a, lane 1). A strong expression of both VP2 and VP3 proteins was observed for the CMV_VP23 plasmid (Figure 4a, lane 2). Apparently the leaky scanning mechanism is still active in the context of the CMV promoter and the cloning context (iGEM RFC[10]). To prevent undesired VP3 expression, a new plasmid abbreviated as CMV_VP2 was constructed, in which the VP3 start codon was removed by an exchange from ATG to ATC (Ile) (Figure 4b). As seen in the third lane of Figure 4a, expression of VP3 is unexpectedly still observed, which might be due to a second start codon located 24 bp downstream. To suppress leaky scanning, a strong Kozak sequence (GCC ACC) was introduced upstream of the VP2 start codon resulting in plasmid CMV_Kozak_VP2 (pZMB0315). Finally, solely the expression of VP2 (Figure 4a, lane 4) was detected with an expected increase in chemiluminescence intensity, indicating a higher level of expression.

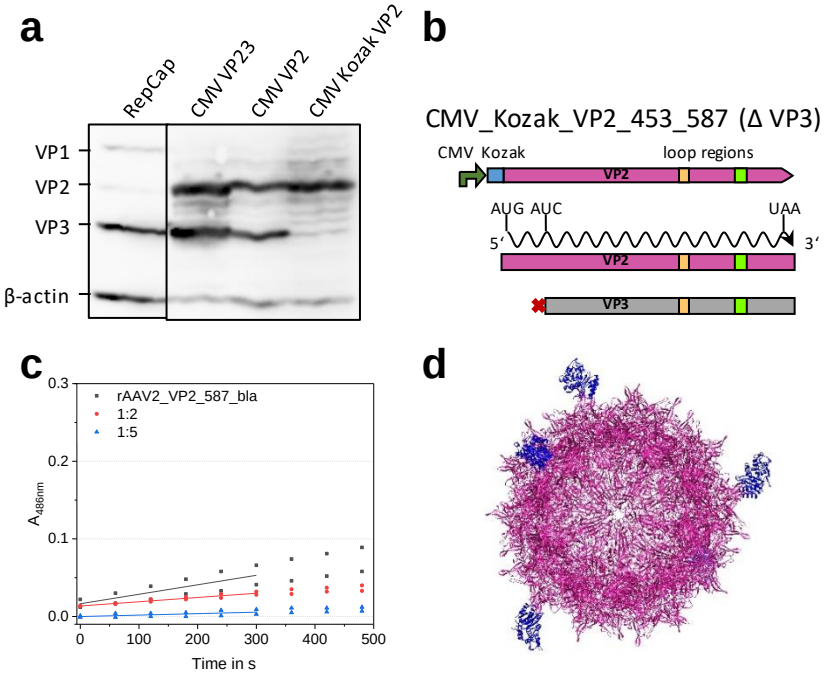

Figure 4. Establishment of mosaic 587 rAAV production using a modified four-plasmid system. (a) Analysis of *cap* protein expression after transient transfection in Western blots of crude cell lysates. Transfection of pZM0216_RepCap showed the expected ratio of 1:1:10 for VP1, VP2 and VP3 (lane 1). Three plasmid versions for VP2 expression were analyzed containing i) the VP2 and VP3 cassette (lane 2, CMV_VP23, pZMB0160), ii) the cassette with VP3 start codon removal (lane 3, CMV_VP2, pZMB0298), and iii) the cassette with an upstream Kozak sequence and VP3 start knock out (lane 4, CMV_Kozak_VP2 (pZMB0315). Expression of VP3 after removal of the start codon can be explained with a second start codon 24 bp downstream and persistent leaky scanning. SI Figure 5 shows full length images. (b) Scheme of the final expression construct. (c) Nitrocefin assay probing rAAV2_VP2_587_bla mosaic viral particles in different concentrations for lactamase activity. Slopes of linear regressions of the first 300 s were used to calculate the concentration of active β-lactamases.

(d) Theoretical structure of the mosaic particle (UCSF Chimera [259]) composed of the AAV2 wt structure (purple, PDB: 1LP3) and five copies of β-lactamase (blue, PDB: 3DTM).

The gene of the stabilized β-lactamase variant 14FM was cloned into plasmid CMV_Kozak_VP2. The resulting plasmid (pZMB0577_pSB1C3_001_CMV_Kozak_VP2 _453_587wtbla) was used for rAAV production in combination with Rep_VP13 plasmid (pZMB0600), the mVenus bearing ITR plasmid (pZMB0522) and pHelper. The molar ratio of these plasmids, particularly of the VP expressing plasmids, needed to be controlled in order to provide the right amounts of each VP protein (1:1:10 for VP1:VP2:VP3) for desired capsid assembly and relative amount of modified VP protein. The AAV promoter p40 is weaker compared to CMV and the Kozak sequence additionally enhances expression. Two molar plasmid ratios of 5:5:1:4 and 5:5:4:1 (pHelper : ITR : Rep_VP13 : CMV_VP2_587_bla) were tested for protein expression and production. The ratio of 5:5:1:4 (higher amount of modified plasmid) was associated with a high proportion of VP2 protein (SI Figure 6), which potentially leads to a higher portion of modified VP2 in the assembled capsid compared to the wild-type ratio. Next to Western blot, crude cell lysate samples from one 100 mm cell culture dish were analyzed regarding their genomic titers. The sample with the lower plasmid dose of the modified VP2_587_bla protein resulted in roughly three times higher amounts of viral particles (2.48×10^{10} vg/ml for a 1:4 VP13 : VP2_587_bla ratio compared to 7.98×10^{10} vg/ml for a 4:1 VP13 : VP2_587_bla (pZMB0600:pZMB0577)).

Based on the higher particle yield, mosaic rAAV2-VP2_587_bla particles were subsequently produced using the 5:5:4:1 ratio. A genomic titer of iodixanol-purified particles of 6.3×10^{9} vg was obtained per 100 mm dish. Thus, production using the four-plasmid system yielded rAAVs in the same range as the triple transfection production (Table 2). Incubation of HT1080 cells with a MOI of 50,000 resulted in about 57 ± 2% mVenus-positive cells (Table 2, SI Figure 7h). Comparison with transduction values of rAAV2 wt shows a reduction of transduction ability for the enzyme-bearing particles (SI Figure 7b). However, it should be noted that fully modified glycine-serine linker variants showed a much stronger reduction of the transduction ability.

We were interested if the enzymes presented on the capsid surface retained activity and thus, a colorimetric nitrocefin assay was performed. Enzymatic activity was evaluated from the linear correlation of absorbance against incubation time (Figure 4c). From this data we were able to estimate the number of active β-lactamases on the capsid surface. The β-lactamase variant 14FM which we used is a semi-rational combination of mutations described in literature (Hecky, Baumann unpublished data)[211]. Characteristics of this enzyme are presented in SI Table 2. Combining the genomic copy number and the known turnover number of the free lactamase k_{cat} allows for the estimation of the total number of active lactamases in the sample. In this experiment a β-lactamase concentration of 1.73×10^{-11} mol l^{-1} was calculated. This value is equivalent to 5.6 enzymes per DNaseI-resistant particle. Such particles with five β-lactamases might look as illustrated in Figure 4d. In conclusion, mosaic rAAV2s (rAAV2-VP2_587_bla) with an incorporated full-length protein were produced with unaltered efficiency - thus capsid assembly was not posing a problem. Functionality for β-lactamase was proven for enzymes presented on the viral particle surface.

Fully-lactamase decorated rAAV capsids can be produced and show enzyme activity.

As a limit for the integration of motives into the capsid was not found in the mosaic experiment, we aimed at the production of rAAV with all VP proteins modified with a lactamase named rAAV2_587_bla. The β-lactamase gene was thus cloned in the RepCap plasmid (pZMB0216) at the 587 position (yielding pZMB0221_Rep_VP123_453_587bla_p5tataless). A fully modified capsid model is depicted in Figure 5a. The genomic titer after ultracentrifugation was comparable to those of glycine-serine linker insertions (Table 2). To our surprise, the insertion with the size of approximately 29 kDa in every VP protein did not abrogate capsid assembly.

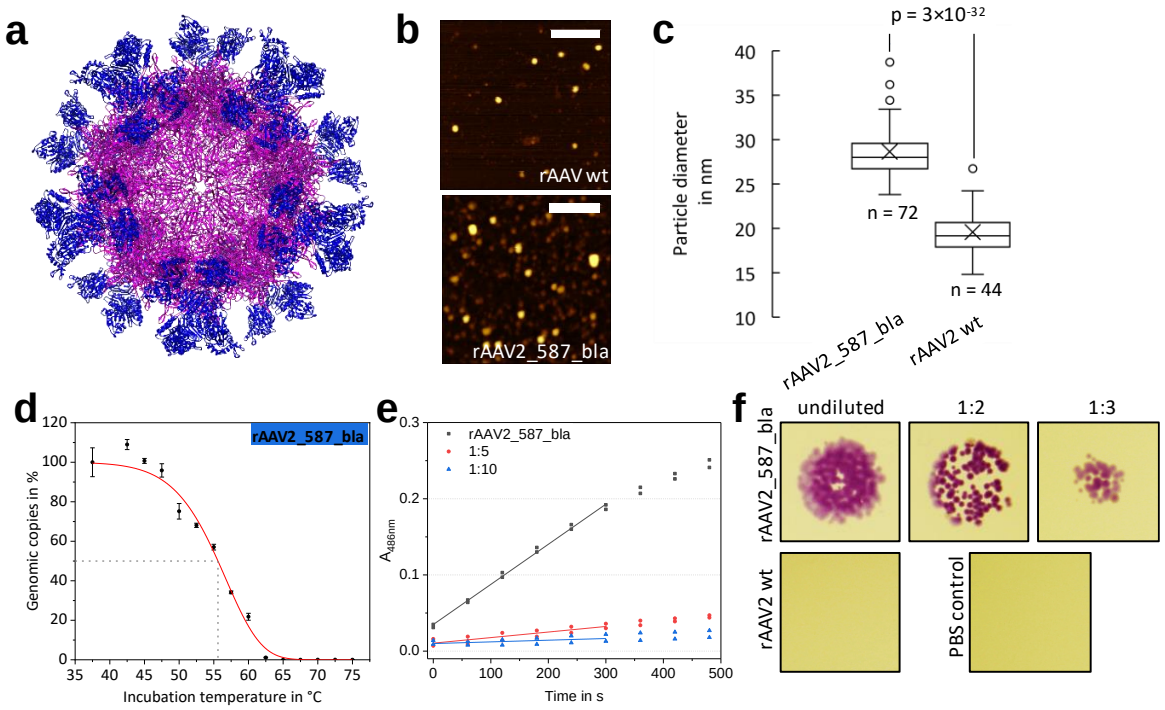

Figure 5. Comparison of rAAV2 wt and rAAV2_587_bla with respect to structure and β-lactamase activity. (a) Theoretical structure of rAAV2_587_bla constructed from the AAV2 wt structure (purple, PDB: 1LP3) and 60 copies of β-lactamase (blue, PDB: 3DTM). (b, c) AFM micrographs and particle size analysis of rAAV2 wt and rAAV2_587_bla. The calculated mean diameter of rAAV2 wt is 20 nm and 29 nm for rAAV_587_bla. SI Figure 8 gives AFM raw data. (d) Results of thermal stability assay based on qPCR data for rAAV_587_bla. Each point represents the standard deviation of a technical duplicate. $T_{d,5\ min}$ was calculated with 55.6 ± 0.4 °C. (**e)** Nitrocefin assay, probing the β-lactamase activity of rAAV2_587_bla in different dilutions. (f) Images of a bacterial growth assay on LB Agar plates for β-lactamase activity. Samples with rAAV2_587_bla show a β-lactamase activity up to 1:3 dilutions, whereas for rAAV2 wt and PBS no colony growth was observed.

We were interested to see how the 60 insertions would affect the overall size of the capsid. Measuring the particle width by atomic force microscopy (Figure 5b) a diameter of approx. 20 nm for rAAV2 wt was found. Note that the 5 nm deviation in particle size compared to the TEM measurements can be attributed to the type of method used and sample preparation. In contrast, a significantly higher viral particle diameter of approx. 29 nm was found for rAAV2_587_bla (Figure 5d). From the capsid model in Figure 5a a diameter of 35 nm was estimated for a fully enzyme-modified rAAV and estimations for the wild-type capsid resulted in an average of 25 nm, which agrees with the observation.

When rAAV2_587_bla samples were assayed for transduction ability on HT1080 cells, almost no transduction was measurable (Table 2). The thermal stability assay revealed a disintegration temperature Td for rAAV2_587_bla of 55.6 °C. Surprisingly, this value corresponds approximately to that of rAAV2 wt. (Figure 5d, Table 2).

Besides testing the effect of the enzyme decoration on capsid integrity, functionality of the integrated β-lactamases was evaluated. From the nitrocefin assay a β-lactamase concentration of 1.65×10-10 mol l^{-1} was calculated, equivalent to 26.9 lactamases per DNaseI-resistant particle (Figure 5e). Looking from a different angle and assuming all 60 β-lactamase are active, yields a catalytic rate of 20,056.2 s^{-1} per capsid and a k_{cat} value of 334.3 s^{-1} for each β-lactamase. The presence of active enzyme was furthermore studied in a simplistic bacterial growth assay. *E. coli* cells lacking the corresponding resistance gene are not able to survive on agar plates supplemented with ampicillin. The presence of functional β-lactamase, however, leads to degradation of the antibiotic and thus bacterial growth is possible. Mixing samples of rAAV2 wt with *E. coli* does not allow for bacterial

growth, whereas for samples of rAAV2_587_bla growth of bacterial colonies was observed (Figure 5f) - again indicating the presence of active enzyme in the viral particle preparation.

3. Discussion

At the outset of the project, which relies on modular RepCap and ITR plasmids that are largely compatible with the BioBrick cloning standard, we first constructed an ITR plasmid. In this context we reconsidered the very old problem, that the ITR sequences in plasmids are not stable during plasmid propagation in *E. coli* and that specifically one ITR is prone to deletions despite the symmetry of their sequences [202]. To our knowledge no explanation has been put forward. We hypothesize that the mechanism of plasmid replication of the prevalently used pMB1-derived origin of replication, which works unidirectional with respect to RNA II elongation and result in a switch between PolI and PolIII about 200 bp downstream of the replication start contributes to this genetic instability (SI Figure 2) [204]. In several ITR plasmids including our version, the distance between ori-start (end of RNAII) and the ITR with the more frequent deletion is about 74 bp. PolI and the polymerase switch, which might take place around the observed deletion site, might be more prone to induce deletions compared to the PolIII mediated replication. Since the most often observed deletion of 11 bp is also present in commercial and Addgene plasmids (e.g. pAAV_MCS [203]) and since it has been reported that even larger ITR deletions reduce production but increase transgene expression [205], we maintained the deletion in one ITR and placed it strategically next to the ori. Due to the pUC numbering scheme and expected GOI orientation of our plasmid, the deletion is located in the right or 3´ ITR, respectively (Figure 2e). Future experiments with various ITR to ori distances with high throughput ITR sequencing will test our hypothesis.

We were pleased to see that production of rAAV2 wt with the modified RepCap plasmid and the ITR plasmid (Table 2) enabled production in useful quantity and quality. Previous work has shown that insertion of motifs at various sites of VP proteins is possible [260, 261]. We investigated glycine-serine linkers incorporated at residue position 587 by assaying capsid assembly, functionality and thermal stability. Production yields equal to that of rAAV wt showed compatibility with capsid assembly. Regarding transduction, we observed a significant impact of increasing insertion size with a non-linear decrease. The insertion of eight amino acids $(GGSG)_2$ showed a significantly higher transduction compared to four amino acids (GGSG). Variable region VIII harbors residues R585 and R588, which mediate the primary interaction of AAV2 with the cell via HSPG [20, 21]. Spatial separation of the two arginines is known to interfere with cell binding and internalization [22]. The insertion of small motifs presumably increases the tension within the β-hairpin and hence the distance between the arginines (Figure 6). Larger flexible insertions probably are compatible with the correct arginine positioning but with increasing size a shielding effect becomes more and more prevalent.

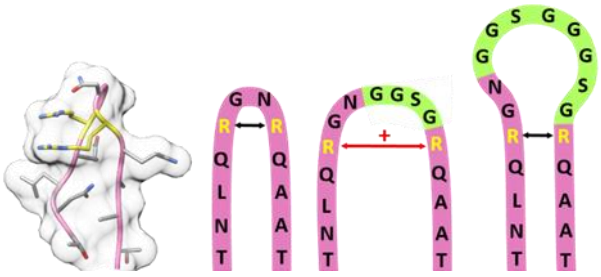

Figure 6. Model of the 587 loop region, from left to right: Structural model of the wild-type 587 loop with residue R585 and R588 highlighted in yellow (PDB: 1LP3); schematic model of 587 wild-type loop region (pink), 587 loop region with GGSG linker (light green) insertion leading to an increased arginine-arginine-distance; 587 loop region with $(GGSG)_2$ linker (light green) insertion leading to a regular arginine-arginine-distance but steric shielding of HSPG binding motif.

Next, we analyzed thermal stability using a qPCR-based method. We propose that the temperature of viral DNA release given by a disintegration temperature named T_d is a physical value

that is on a par or even better corresponding to the biological activity of rAAV as values obtained by DSF or DSC experiments. It was hypothesized that viral particles transfer to a *metastable* state upon heating, which is defined by ejection of the encapsulated ssDNA [208, 209]. Further temperature increases then completely rupture the capsid. DSC and DSF are more likely to capture the complete disassembly of the capsid, and thus are expected to result in higher T_m values compared to the T_d values. This is in agreement with our data which yielded disintegration temperatures about 15 °C lower than the melting temperatures published so far [198, 210].

As seen in the time course of isothermal disintegration (Figure 3h), the particles are not in thermal equilibrium at elevated temperatures discouraging thermodynamic interpretations. Thus, the T_d values obtained are sensitive to the incubation time, which is expected for the megadalton complex. Interestingly, Figure 2h reveals a multi-phase behavior, which could be either interpreted by different composition or structural states of the initial capsid ensemble or by two unfolding pathways. Longer incubation times (> 5 min) most likely result in even lower T_d values. Since most experimentally determined thermal stability changes within variants are minor, one can conclude that the capsid proteins form a stable framework highly resilient to sequence insertions.

Since peptide insertions of up to 16 amino acids were well tolerated, a β-lactamase was integrated at residue position 587. In one experiment β-lactamase was to be integrated only within the VP2 protein and not the VP3, which results from the same reading frame. An expression analysis of our existing CMV_VP2 plasmid revealed VP3 expression despite the CMV promoter for VP2 and even after deletion of the VP3 start codon. This can be explained by persistent leaky scanning and by a second AUG codon present 24 bp downstream of the mutated VP3 start. Mutating the first AUG of the VP3 protein was described before [262], but no Western blot was provided suggesting that a retained expression of VP3 could have occurred. That the VP2/3 gene retains expression of two proteins even if taken out of context and after a start codon removal indicates a deeply engrailed resilience to mutations and points to high robustness of the complex viral genome. We found that an additional strong Kozak sequence in front of VP3 resulted in the expression of solely modified VP2 [263].

Initial experiments of the mosaic lactamase approach indicated that the molar ratio (i.e. gene dose) of the transfected plasmids plays a crucial role for the amount of modified VP2 proteins in the final capsid. Optimizing the quadruple setting, mosaic viral particles displaying lactamases were obtained with titers only slightly lower than those of wild-type preparations. Transduction efficiency of mosaic β-lactamase particles was reduced, but not as dramatically as in case of the 16 amino acids insertion into the homogenously modified rAAV_587_$(GGSG)_4$. Most likely the lactamases pose a steric hindrance to the interaction with the cell, but the wild-type capsid proteins can still engage with HSPG. To our knowledge, this presents the first example of a successful enzyme incorporation at position 587 in the AAV capsid.

From a nitrocefin enzyme assay the number of active β-lactamases on the mosaic rAAV2_VP2_587bla capsid was estimated to be 5.6. Our calculations are based on the genomic titer and the proportion of empty capsids has not been taken into account. An alternative analysis of the full capsid titer using ELISA techniques is probably equally misleading as the modification of the capsid surface might interfere with antibody binding. Another uncertainty for the exact determination of the lactamase concentration lies within the assumption of a constant k_{cat} value, which was experimentally determined for the enzyme in solution. Due to immobilization on the capsids surface, the enzymes possess less degrees of freedom and substrate access is hindered, which might result in lower turnover numbers. Taken together, the true number of capsids is higher than estimated by genomic titer, because of empty capsids, but the true k_{cat} on the surface is lower than the one taken from solution measurements. It is conceivable that a heterogeneous mixture of active, partially active and inactive enzymes is presented, but due to the highly cooperative unfolding of lactamase this is less likely. Therefore, the deduced enzyme concentration should only be taken as an estimate. Still, the calculated number of 5.6 enzymes per viral capsid is very close to the expected number of modified VP2 proteins in the wild-type setting where five of the 60 capsid-forming proteins would be VP2. In combination, the data for a rAAV2 mCherry modification in the VP1 453

position [251] and for a lactamase modification in the VP2 587 position support the conclusion of a high structural plasticity of the AAV2 capsid.

In order to further explore the robustness of AAV assembly, the integration of β-lactamase was expanded to all VP proteins. We were intrigued to see that introduction of the enzyme into position 587 is possible while viral integrity and thermal stability are maintained. AFM measurements showed an increase in capsid diameter of 10 nm, which corresponds well to our estimations. Genomic titers were in the same range compared to the one of rAAV2 wt, which is remarkable considering the size of the β-lactamase. This suggests that VP folding, core capsid assembly and DNA encapsidation are not significantly affected by bulky insertions. Like the originating β-lactamase variants [211], the enzyme variant used herein is known to fold well and to possess high thermodynamic stability (Hecky, Baumann unpublished data), which might contribute to the robustness of the modified VP protein and the corresponding capsid assembly. The high thermal stability of the inserted enzyme might even protect the VP proteins from unfolding. In contrast, glycine-serine linkers are intrinsically disordered. As expected, they were found to destabilize the VP proteins and the overall capsid. Enzyme activity of the sterically confined β-lactamases was measured. Calculations on the basis of the genomic titer and the turnover number show that approximately the equivalent of 26.9 active enzymes are presented. As discussed above, enzyme activity could be reduced and deduced numbers of active enzymes per intact capsid present only an estimation.

In summary we provide plasmids for facile genetic manipulation of AAV2 capsids and illuminate the intriguing resilience of AAV2 to a breadth of genetic and structural modifications.

Materials and Methods

Construction of plasmids.

All constructs were made by standard cloning techniques mainly using idempotent cloning strategies according to RFC[10] or RFC[25], respectively [264, 265]. AAV plasmids listed in Table 1 and SI Table 1 were cloned as described in SI Method 1. ITR sequencing is described in SI Method 2. The CMV and hGHpA containing plasmids are from the iGEM parts registry (parts.igem.org). Resulting vectors were analyzed for their correctness by Sanger DNA-sequencing (Sequencing Core Facility, CeBiTec, Bielefeld, Germany).

Cell Culture.

HDFa (Thermo Fisher Scientific), HEK293, HeLa, HT1080 (DSMZ) cells were cultured in Dulbecco's Modified Eagle Medium supplemented 10% (v/v) fetal calf serum and 1% (v/v) penicillin/streptomycin (Sigma Aldrich). MCF7, A431 and MDA-MB-231 (DSMZ) were cultured in RPMI supplemented 10% (v/v) fetal calf serum and 1% (v/v) penicillin/streptomycin. Cells were maintained at 37 °C and 5% CO_2.

Viral particle production.

HEK293 cells were seeded at a density of 3×10^6 cells per 100 mm dish the day before transfection. A total amount of 15 μg DNA per 100 mm dish was transfected using calcium phosphate. RepCap plasmid, ITR-containing plasmid and pHelper plasmid were used in a 1:1:1 molar ratio [266]. For mosaic viral particles four plasmids were used in a 5:5:4:1 molar ratio of pHelper:ITR:RepCap_VP13:CMV_VP2. After 72 h of incubation at 37 °C, cells were harvested and pelleted by centrifugation (2000×g, 5 min).

Purification of viral particles.

Cells were resuspended in lysis buffer (50 mM Tris, 150 mM NaCl, 2 mM $MgCl_2$, pH 7.5) and viral particles were released from cells with three freeze-thaw cycles. Remaining DNA contamination was degraded by incubation with benzonase nuclease (final 100 U/ml, Sigma Aldrich) at 37 °C prior to addition of CHAPS (3-[(3-cholamidopropyl)dimethylammonio]-1-propane sulfonate, 0.5% w/v final). The crude lysate was cleared from cell debris by centrifugation (3,000×g, 10 min). This crude viral stock was further purified with a discontinuous iodixanol gradient[134]. Briefly, the

lysate was transferred onto a gradient of 60%, 40%, 25% and 15% iodixanol in an open top polyallomer 16 x 76 mm tube (Science Services). Tubes were sealed and centrifuged in a T-880 rotor (Sorvall) at 340,000×g for 2 h at 18 °C. The rAAV containing fraction was collected with a 21G x 1 1/2″ injection needle and the buffer was exchanged to 1× PBS (137 mM NaCl, 2.6 mM KCl, 10 mM Na_2HPO_4, 1.8 mM KH_2PO_4, pH 7.2) via Amicon Ultra-4 100K centrifugal filter units (Merck Millipore).

SDS-PAGE and Western blot analysis.

Cell pellets from rAAV production (1× 100 mm dish) were resuspended in 100 µl PBS and 5× SDS loading buffer. Samples were incubated at 95 °C for 10 min, centrifuged and 20 µl per lane were loaded on a 10% SDS-polyacrylamide gel (Hoefer SE260). Samples were blotted onto a 0.45 µm nitrocellulose membrane (Thermo Fisher Scientific) using semi-dry electrophoretic transfer (V20-SDB, Sci Plas). After blocking the membrane with 10% (w/v) non-fat milk in TBS, the membrane was incubated simultaneously for 1.5 h with the B1 antibody (mouse monoclonal, supernatant, 1:100, Progen) and an anti β-Actin antibody (8H10D10, mouse monoclonal, 1:1000, Cell Signaling Technology). After incubation with an anti-mouse IgG, HRP-linked antibody (1:5000, Cell Signaling Technology), blots were imaged by luminescence detection (Pierce ECL Western Blot Substrate, Thermo Fisher Scientific).

Determination of genomic titers.

Before determination of genomic titers via qPCR, samples were treated with 10 U DNase I (New England Biolabs) in 10× DNaseI buffer in a final volume of 50 µl at 37 °C for 30 min before heat inactivation of the DNase I (75 °C, 20 min). Crude lysate samples were additionally incubated with 0.8 U Proteinase K (New England Biolabs) for 50 min at 37 °C before heat inactivation (95 °C, 10 min). Dilutions of the DNase I digest were used as template in the qPCR reaction. The sample was mixed with 2.5 µl primer qPCR-hGH-for (5'-CTCCCCAGTG CCTCTCCT-3') and 2.5 µl primer qPCR-hGH-rev (5′-ACTTGCCCCT TGCTCCATAC-3′), each at a stock concentration of 4 µM, and 10 µl of 2× GoTaq qPCR Mastermix (Promega). The qPCR reaction was carried out as described in the manual (TM318 6/14, Promega) with an increased time interval for the first denaturation step (95 °C, 10 min) using a LightCycler 480 II (Roche). The genomic titer was calculated from a standard curve of 10^2 to 10^7 copies of the ITR plasmid (pZMB0522) with an efficiency between 90-110% and an R value less than 0.1. Genomic titers in crude lysates were estimated from a standard curve mixed with the same amount of a non-transfected cell lysate.

Transducing titer assay.

10,000 cells per well were seeded in 500 µl of the corresponding media on a 12-well plate, settled for 1 h at 37 °C and then ultracentrifugation-purified rAAV samples were added. After 12 h incubation, 500 µl fresh medium was added. After further 72 h incubation, cells were detached with 0.25% Trypsin/EDTA, resuspended in PBS and analyzed using a FACSCalibur and counting 10,000 events. All experiments were performed as biological duplicates from two independent rAAV preparations.

Transmission electron microscopy.

Carbon-coated copper grids, 200 mesh (Electron Microscopy Science) were treated with oxygen plasma (Zepto, Diener electronic GmbH). After this, 3 µl of precipitation-purified rAAV sample [254] was applied to the grid and incubated for 2 min. Excess liquid was drained off, the grid was dried at room temperature and washed with three drops of distilled water. Negative staining was performed using 3 µl 2% (v/v) uranyl acetate replacement stain (Electron Microscopy Sciences) for 30 s. Excess liquid was drained off and grids were dried before channeling the sample into the microscope. rAAVs were visualized with a Philips CM100 (PW6021) instrument with an acceleration voltage of 80 kV. Images were analyzed using the Soft Imaging Viewer (Olympus) and ImageJ [267].

Atomic force microscopy.

AFM measurements of rAAV2 wt and rAAV2_587_bla were performed on a Multimode 8 AFM (Bruker) with Tap300Al-G cantilevers (BudgetSensors) in tapping mode in air. 2 µl of sample

in PBS were spotted onto freshly cleaved mica and incubated for one minute. The mica was then briefly rinsed with water and dried under a gentle nitrogen flow. Data analysis was performed with Gwyddion 2.48. Obtained images were treated with offset and plane correction algorithms and the size of visualized particles was measured at half maximum particle height. Statistical analysis of size measurements was performed using Excel 2016.

AAV stability assay.

Thermal stability was analyzed using iodixanol-purified rAAV2 variants in two technical replicates. rAAV2 samples were diluted to 1.5×10^9 vg ml^{-1} with PBS. 10 µL aliquots of rAAV2 samples were incubated at temperatures ranging from 37.5 °C to 75.0 °C in 2.5 °C steps for 5 min in a thermocycler (peqSTAR 96 Universal Gradient, peqlab). To determine the disintegration time kinetics rAAV2 wt samples were incubated at 56.1 °C for different time points. Immediately after incubation, samples were stored on ice. Genomic titers of each sample (10 µl) were determined by qPCR as described above. Due to the conceptual identity to the qPCR titration method, sensitivity and reliability are from this point on well established. A complete digest of the not encapsidated DNA was assured by additional tests. We evaluated the minimum titer of the starting material for a successful evaluation of vector particle stability. This needed to be higher than 1×10^9 genomic copies per ml in order to result in a data set that covers the sigmoidal-shaped disintegration curve. Our qPCR standard curve shows a linear correlation between 10^2 and 10^7 genomic copies per sample which represents the dynamic range. Note that our qPCR primers hybridize in the hGHpolyA region and that we detect completeness of this region. Probing of different parts or the whole genome is possible. Data analysis was performed using Origin2018. The total rAAV amount per reaction was normalized to 100% and a logistic regression $y = A_{min} + \frac{(A_{max}-A_{\min})}{\left(1+\left(\frac{x_0}{x}\right)^h\right)^s}$ was performed with A_{min} = 0, A_{max} = 100, no weighting). The disintegration temperature (T_d) was determined as the temperature at which 50% of rAAVs released its DNA.

β-lactamase activity assays.

Activity of β-lactamase presented on the rAAV capsid was determined using a nitrocefin and a bacterial assay. For the spectrophotometric nitrocefin assay 91 µl of rAAV sample containing either rAAV2_587_bla or rAAV2_VP2_587_bla (each 3.7×10^8 vg total) or PBS (negative control) were mixed with 9 µl of nitrocefin buffer (2 mM nitrocefin, 500 mM KH_2PO_4 and 5% (v/v) DMSO at pH 7.0) in a 96-well plate. Absorption at 486 nm was measured with a microplate spectrophotometer (PowerWave HT, BioTek) in 1 min intervals for 40 min at room temperature. Calculations are based on Lambert-Beer' rule as given in the formula: $\frac{\Delta A}{\Delta t} = \Delta\varepsilon_{486} \cdot c_{bla} \cdot k_{cat_{bla}}$ with $\frac{\Delta A}{\Delta t}$ = slope of linear regression from nitrocefin assay; $\Delta\varepsilon_{486}$ = molar extinction coefficient of nitrocefin shift (here 16000 l mol^{-1} cm^{-1}); c_{bla} = concentration of β-lactamase; $k_{cat_{bla}}$ = catalytic constant of β-lactamase; d = distance (here 0.267 cm). Either the turnover number (here 746 s^{-1}) or the concentration of active lactamases was assumed to be known.

In the bacterial assay an aliquot of about 200 µl of an *E. coli* DH5α culture transfected with plasmid pSB1C3_BBa_J04450 harboring a constitutively expressed chloramphenicol acetyltransferase and a red fluorescent protein was plated on LB agar supplemented with ampicillin (100 µg ml^{-1} final) and chloramphenicol (20 µg ml^{-1} final). rAAV samples (3 µl) were spotted (rAAV2_587_bla undiluted, 1:2, 1:3 and rAAV2 wt undiluted). The dish was incubated at 37 °C overnight. Due to lacking ampicillin resistance, growth and colony formation of *E. coli* cells only occur, when ampicillin is hydrolyzed by active β-lactamase of the rAAV sample. Growing *E. coli* colonies could be easily detected by eye via their red appearance.

Statistical analysis and reproducibility.

Standard deviation was calculated for all biological and technical replicates. To test whether differences were statistically significant based on a 0.05 significance level, data were checked for a normal distribution by a Shapiro-Wilk-test, then an independent Student's t-test was performed and p-values are given according to: * $p \leq 0.05$; ** $p \leq 0.01$; *** $p \leq 0.001$. Variation of transduction

efficiency determination was exemplarily tested in fully independent experiments with independent viral rAAV2 wt preparations by two authors. These data agree nicely with 95.7% (Figure 2d, SI Figure 4a) and 96.7% (Table 2, SI Figure 7b). Variation in the qPCR stability assay was tested with two independent viral preparations in two settings as shown in Figure 3c and 3h. In both assays 50% of genomic copies are detected after 5 min incubation.

Supplementary Materials: Supplementary materials can be found at www.mdpi.com/xxx/s1.

Author Contributions: RCF, JT and KET contributed to the design and generation of the plasmids. RCF, JT, KET and KMM conceived and designed the experiments. RCF and JT prepared the figures, wrote and edited the manuscript. KMM helped with writing and edited the manuscript. YH performed electron microscopy sample preparation and data acquisition. MTR generated the AFM images and performed data analysis. NB and DA contributed to AFM measurements. TB characterized and provided the β-lactamase for integration into the viral capsid. SH, TB, KMA and KMM were former members of the iGEM team and provided information on design and generation of the plasmid system. KMM secured funding and supervised all experiments. All authors critically read and approved the final manuscript.

Funding: We acknowledge the financial support of the German Research Foundation (DFG) and the Open Access Publication Fund of Bielefeld University for the article processing charge.

Acknowledgments: We thank Philipp Borchert for experimental assistance. We acknowledge the iGEM team Freiburg 2010 for making their plasmid system available for further research and analysis. The team designed and cloned the plasmids, which form the basis of the presented work.

Conflicts of Interest: The authors declare no conflict of interest.

Abbreviations

rAAV	Recombinant Aden-associated virus
TEM	Transmission electron Microscopy
AFM	Atomic force microscopy
bla	β-lactamase

References

1. FDA Advisory Committee. *Spark Therapeutics Briefing Document*. (2017).
2. Clément, N. & Grieger, J. C. Manufacturing of recombinant adeno-associated viral vectors for clinical trials. *Mol. Ther. - Methods Clin. Dev.* **3**, 16002 (2016).
3. Xie, Q. *et al.* The atomic structure of adeno-associated virus (AAV-2), a vector for human gene therapy. *Proc. Natl. Acad. Sci. U. S. A.* **99**, 10405–10 (2002).
4. Rose, J. A., Maizel, J. V, Inman, J. K. & Shatkin, A. J. Structural proteins of adenovirus-associated viruses. *J. Virol.* **8**, 766–770 (1971).
5. Matsushita, T. *et al.* Adeno-associated virus vectors can be efficiently produced without helper virus. *Gene Ther.* **5**, 938–45 (1998).
6. Xiao, X., Li, J. & Samulski, R. J. Production of high-titer recombinant adeno-associated virus vectors in the absence of helper adenovirus. *J. Virol.* **72**, 2224–32 (1998).
7. Grimm, D., Kay, M. A. & Kleinschmidt, J. A. Helper virus-free, optically controllable, and two-plasmid-based production of adeno-associated virus vectors of serotypes 1 to 6. *Mol. Ther.* **7**, 839–50 (2003).
8. Feiner, R. C. & Müller, K. M. Recent progress in protein-protein interaction study for EGFR-targeted therapeutics. *Expert Rev. Proteomics* **13**, 817–32 (2016).
9. Grimm, D. & Kay, M. a. From virus evolution to vector revolution: use of naturally occurring

serotypes of adeno-associated virus (AAV) as novel vectors for human gene therapy. *Curr. Gene Ther.* **3**, 281–304 (2003).

10. Wu, Z., Asokan, A. & Samulski, R. J. Adeno-associated virus serotypes: vector toolkit for human gene therapy. *Mol. Ther.* **14**, 316–27 (2006).

11. Lux, K. *et al.* Green Fluorescent Protein-Tagged Adeno-Associated Virus Particles Allow the Study of Cytosolic and Nuclear Trafficking. *J. Virol.* **79**, 11776–11787 (2005).

12. Münch, R. C. *et al.* Displaying high-affinity ligands on adeno-associated viral vectors enables tumor cell-specific and safe gene transfer. *Mol. Ther.* **21**, 109–18 (2013).

13. Hagen, S. *et al.* Modular adeno-associated virus (rAAV) vectors used for cellular virus-directed enzyme prodrug therapy. *Sci. Rep.* **4**, 3759 (2014).

14. Girod *et al.* Genetic capsid modifications allow efficient re-targeting of adeno-associated virus type 2. *Nat. Med.* **5**, 1438 (1999).

15. Shi, W. & Bartlett, J. S. RGD inclusion in VP3 provides adeno-associated virus type 2 (AAV2)-based vectors with a heparan sulfate-independent cell entry mechanism. *Mol. Ther.* **7**, 515–25 (2003).

16. Liu, Y. *et al.* Site-specific modification of adeno-associated viruses via a genetically engineered aldehyde tag. *Small* **9**, 421–9 (2013).

17. Falck, G. & Müller, K. M. Enzyme-Based Labeling Strategies for Antibody–Drug Conjugates and Antibody Mimetics. *Antibodies* **7**, 4 (2018).

18. Ried, M. U., Girod, A., Leike, K., Büning, H. & Hallek, M. Adeno-associated virus capsids displaying immunoglobulin-binding domains permit antibody-mediated vector retargeting to specific cell surface receptors. *J. Virol.* **76**, 4559–66 (2002).

19. Nieto, K. *et al.* Development of AAVLP(HPV16/31L2) particles as broadly protective HPV vaccine candidate. *PLoS One* **7**, e39741 (2012).

20. Judd, J. *et al.* Random Insertion of mCherry Into VP3 Domain of Adeno-associated Virus Yields Fluorescent Capsids With no Loss of Infectivity. *Mol. Ther. Nucleic Acids* **1**, e54 (2012).

21. Freiburg iGEM Team. Virus Construction Kit For Therapy. Available at: http://2010.igem.org/Team:Freiburg_Bioware. (Accessed: 24th January 2019)

22. Guo, P. *et al.* Rapid and simplified purification of recombinant adeno-associated virus. *J. Virol. Methods* **183**, 139–146 (2012).

23. Horowitz, E. D. *et al.* Biophysical and ultrastructural characterization of adeno-associated virus capsid uncoating and genome release. *J. Virol.* **87**, 2994–3002 (2013).

24. Zeltner, N., Kohlbrenner, E., Clément, N., Weber, T. & Linden, R. M. Near-perfect infectivity of wild-type AAV as benchmark for infectivity of recombinant AAV vectors. *Gene Ther.* **17**, 872–9 (2010).

25. Ellis, B. L. *et al.* A survey of ex vivo/in vitro transduction efficiency of mammalian primary cells and cell lines with Nine natural adeno-associated virus (AAV1-9) and one engineered adeno-associated virus serotype. *Virol. J.* **10**, 74 (2013).

26. Judd, J. *et al.* Random Insertion of mCherry Into VP3 Domain of Adeno-associated Virus Yields Fluorescent Capsids With no Loss of Infectivity. *Mol. Ther. Nucleic Acids* **1**, e54 (2012).

27. Rayaprolu, V. *et al.* Comparative Analysis of Adeno Associated Virus Capsid Stability and

Dynamics. *J. Virol.* **87**, 13150–13160 (2013).

28. Speck, J. *et al.* Exploring the molecular linkage of protein stability traits for enzyme optimization by iterative truncation and evolution. *Biochemistry* **51**, 4850–4867 (2012).

29. Trempe, J. P. & Carter, B. J. Alternate mRNA splicing is required for synthesis of adeno-associated virus VP1 capsid protein. *J. Virol.* **62**, 3356–63 (1988).

30. Stutika, C. *et al.* A Comprehensive RNA Sequencing Analysis of the Adeno-Associated Virus (AAV) Type 2 Transcriptome Reveals Novel AAV Transcripts, Splice Variants, and Derived Proteins. *J. Virol.* **90**, 1278–89 (2016).

31. Hecky, J. & Müller, K. M. Structural perturbation and compensation by directed evolution at physiological temperature leads to thermostabilization of β-lactamase. *Biochemistry* **44**, 12640–12654 (2005).

32. Samulski, R. J., Srivastava, A., Berns, K. I. & Muzyczka, N. Rescue of adeno-associated virus from recombinant plasmids: gene correction within the terminal repeats of AAV. *Cell* **33**, 135–43 (1983).

33. Troll, C. *et al.* The mutagenic footprint of low-fidelity Pol I ColE1 plasmid replication in E. coli reveals an extensive interplay between Pol I and Pol III. *Curr. Genet.* **60**, 123–34 (2014).

34. CellBiolabs. *pAAV-MCS expression vector VPK-410*. *Product Data Page* (2016).

35. Xie, J. *et al.* Short DNA Hairpins Compromise Recombinant Adeno-Associated Virus Genome Homogeneity. *Mol. Ther.* **25**, 1–12 (2017).

36. Warrington, K. H. *et al.* Adeno-associated virus type 2 VP2 capsid protein is nonessential and can tolerate large peptide insertions at its N terminus. *J. Virol.* **78**, 6595–609 (2004).

37. Shi, W., Arnold, G. S. & Bartlett, J. S. Insertional mutagenesis of the adeno-associated virus type 2 (AAV2) capsid gene and generation of AAV2 vectors targeted to alternative cell-surface receptors. *Hum. Gene Ther.* **12**, 1697–1711 (2001).

38. Kern, A. *et al.* Identification of a heparin-binding motif on adeno-associated virus type 2 capsids. *J. Virol.* **77**, 11072–81 (2003).

39. Opie, S., Jr, K. W. & Agbandje-, M. Identification of amino acid residues in the capsid proteins of adeno-associated virus type 2 that contribute to heparan sulfate proteoglycan binding. *J. Virol.* **77**, 6995–7006 (2003).

40. Perabo, L. *et al.* Heparan sulfate proteoglycan binding properties of adeno-associated virus retargeting mutants and consequences for their in vivo tropism. *J. Virol.* **80**, 7265–9 (2006).

41. Ros, C., Baltzer, C., Mani, B. & Kempf, C. Parvovirus uncoating in vitro reveals a mechanism of DNA release without capsid disassembly and striking differences in encapsidated DNA stability. *Virology* **345**, 137–147 (2006).

42. Bernaud, J. *et al.* Characterization of AAV vector particle stability at the single-capsid level. *J. Biol. Phys.* **44**, 181–194 (2018).

43. Bennett, A. *et al.* Thermal Stability as a Determinant of AAV Serotype Identity. *Mol. Ther. - Methods Clin. Dev.* **6**, 171–182 (2017).

44. Zhang, H. *et al.* Addition of six-His-tagged peptide to the C terminus of adeno-associated virus VP3 does not affect viral tropism or production. *J. Virol.* **76**, 12023–12031 (2002).

45. Kozak, M. Initiation of translation in prokaryotes and eukaryotes. *Gene* **234**, 187–208 (1999).

46. Knight, T. Idempotent Vector Design for Standard Assembly of Biobricks Standard Biobrick Sequence Interface. *BBF RFC* (2007). Available at: http://hdl.handle.net/1721.1/45138. (Accessed: 24th January 2019)

47. Müller, K. M., Arndt, K. M., IGEM_Freiburg & Grünberg, R. Fusion Protein (Freiburg) Biobrick assembly standard. Available at: http://hdl.handle.net/1721.1/45140. (Accessed: 24th January 2019)

48. Agilent Technologies. AAV Helper-Free System Instruction Manual. Available at: https://www.agilent.com/cs/library/usermanuals/Public/240071.pdf. (Accessed: 24th January 2019)

49. Zolotukhin, S. *et al.* Recombinant adeno-associated virus purification using novel methods improves infectious titer and yield. *Gene Ther.* **6**, 973–85 (1999).

50. Schneider, C. A., Rasband, W. S. & Eliceiri, K. W. NIH Image to ImageJ: 25 years of image analysis. *Nat. Methods* **9**, 671–5 (2012).

51. Zuker, M. Mfold web server for nucleic acid folding and hybridization prediction. *Nucleic Acids Res.* **31**, 3406–15 (2003).

Author 1, A.B. Title of Thesis. Level of Thesis, Degree-Granting University, Location of University, Date of Completion.

1. Title of Site. Available online: URL (accessed on Day Month Year).

Supplementary information

rAAV engineering for capsid-protein enzyme insertions and mosaicism reveals resilience to mutational, structural and thermal perturbations

Rebecca C. Feiner[1†], Julian Teschner[1†], Kathrin E. Teschner[1], Marco T. Radukic[1], Tobias Baumann[2], Sven Hagen[3], Yvonne Hannappel[4], Niklas Biere[5], Dario Anselmetti[5], Katja M. Arndt[6], Kristian M. Müller[1*]

1 Methods

1.1 SI Method 1. Plasmid construction

1.1.1 Plasmids constructed in this work

pZMB0522_ITR_EXS_CMV_mVenus_hGHpA. This is the streamlined version of the rAAV ITR plasmid. To allow BioBrick compatible integration of expression casettes into the ITR plasmid, the region in-between the ITRs of vector pGolden-AAV (Addgene plasmid # 51424 was a gift from Yonglun Luo [47]) was changed and EcoRI, XbaI as prefix and SpeI as suffix sites were integrated by hybridized oligonucleotides through the unique BsmFI and AgeI sites. The backbone of this new generated RFC[10]-compatible ITR plasmid was digested with PstI and ligated with PCR-amplified pUC19 backbone (pUC19_PstI_for 5´-CTGCAGAAAA GGCCAGCAAA AGGC and pUC19_PstI_rev 5´-CTGCAGGCAC TTTTCGGGGA AATG) yielding pUC19_ITR_EXS. In the last step, the previously assembled BioBrick CMV_mVenus_hGHpA was cloned via EcoRI and SpeI into pUC19_ITR_EXS to generate pZMB0522_ITR_EXS_CMV_mVenus_hGHpA. This plasmid can be used to test GOI expression and at the same time allows integration of other genes. Note that XbaI and SpeI generate compatible cohesive ends. Facilitating new assemblies, a BioBrick CMV promoter (pZMB0143-CMV) and BioBrick hGHpA (pZMB0135_hGHpA) are also available.

pZMB0315_CMV_Kozak_VP2_453_587wtHis. This vector was constructed in two steps starting from pZMB0156_VP23_453_587wt. After RFC[10] integration of the CMV promoter, the VP3 initiation codon was mutated from ATG (Met) to ATC (Ile) using site-directed mutagenesis primers SDM_VP3ko_for 5´-CTAATACGAT CGCTACAGGC AGTGGC and SDM_VP3ko_rev 5´-CCTGTAGCGA TCGTATTAGT TCCCAGAC. In the second step, a strong Kozak sequence was introduced via PCR primers XbaI_CMV-for 5´-CTTCTAGAGC GATGTACGGG and CMV_Kozak_NgoMIV-rev 5´-ATAATGCCGG CCATGGTGGC CTAGTAATTT CGATAAGCCA GTAAG and recloning of the fragment. The HisTag in 587 position was integrated by hybridization of oligonucleotide as described in **SI Figure 11**.

Rep_VP123_453_587wtGG_p5tataless. This plasmid was constructed based on pZMB0216_Rep_VP123_453_587wt_p5tataless. A sequence coding for a Gly-Gly linker was integrated in position 587 by hybridization of oligonucleotides as described in **SI Figure 11** upon digestion with BamHI and PvuII. The cloning strategy for other GGSG linker constructs is similar to this one.

Rep_VP123_453_587wtbla_p5tataless. This plasmid was constructed based on iGEM plasmid BBa_K404250. Amongst others BBa_K404250 codes for a thermostabilised variant of β-lactamase which was amplified by PCR using BamHI_wt_bla-for 5´- AAAGGATCCG TATCTACCAA CCTCCAGAGA GGCAACCACC CAGAAACGCT GGCGAAAG and PvuII_wt_bla-rev 5´- AAACAGCTGT AGCTGCTTGT CTCCAATGCT TAATCAGTGA GGCACC primers. The BamHI and PvuII digested PCR product was inserted in 587 position of pZMB0216_Rep_VP123_453_587wt_p5tataless by standard cloning techniques.

1.1.2 Plasmids previously generated and deposited

pZMB0216_Rep_VP123_453_587wt_p5tataless. Base pair numbering given here refers to the start codon of the RepCap coding region. Starting with the pAAV-RC plasmid (GenBank: AF369963.1) silent mutations of two PstI restriction sites (nucleotide substitutions G177C and G3940C) in the Rep coding region were introduced by site-directed mutagenesis (QuikChange II Site-Directed Mutagenesis Kit, Agilent Technologies). Two EcoRI sites (substitutions A1449G and T1668C) and a PstI site (substitution C1641T) were removed by cloning a synthesized DNA fragment (GeneArt, Darmstadt, Germany) into rep via BstEII/SwaI. To enable restriction-based modification of the 453 or 587 loop coding sequences, the unique restriction sites SspI/SalI (G3202A, C3205T, C3206T; T3254A, C3255G, A3256T, A3257C, G3259A) and BamHI/PvuII (T3613A, T3616C; C3658A, A3661T) were introduced adjacent to the 453 and 587 loop of the viral capsid protein (VP), respectively. This was achieved by cloning a second synthesized DNA fragment (GeneArt) into the respective region via XcmI and BsiWI. BamHI (C729T) and SalI (C1110G) within the Rep coding region were removed by silent site-directed mutagenesis. The final RepCap construct was cloned in pSB1C3_001 via PCR using the primer Prefix_Rep68_78-ex (5´-GGAATTCGCG GCCGCTTCTA GATGGCGGGG TTTTACGAGA TTGTGATTAA G) and Suffix VP123ex RFC_25 5´-GCTACTAGTA TTAACCGGTG

TAGTTAATGA TTAACCCGCC ATGCTACTTA TC) yielding pSB1C3_001_Rep_VP123_453_ 587wt. The promoter p5 TATA-less was converted into a BioBrick using p5_primer_for 5´-GCTCTAGAGG GAGGGGTGGA GTCGTGACGT G and p5_primer_rev 5´-TTCTGCAGCGG CCGCTACTAG TAG-TTCAAAC CTCCCGCTTC AAAATGG and was cloned into pSB1C3_001_Rep_VP123_453_587wt via RFC[10] to generate the final construct pZMB0216_Rep_VP123_453_587wt_p5tataless.

pZMB0600_Rep_VP13_453_587ko_p5tataless. This plasmid was obtained by silent site-directed mutagenesis of the ACG initiation codon of VP2 in pZMB0216_Rep_VP123_453_587wt_p5tataless with the primers: VP2-ko_for 5´-GGTTGAGGAACCTGTTAAGACCGCTCCGGGAAAAAAGAGG and VP2-ko_rev 5´-CCTCTTTTTTCCCGGAGCGGTCTTAACAGGTTCCTCAACC to ACC.

pZMB0091_CMV_DARPinE01_mli_VP23 _453_587koHis. This vector is the product of two BioBrick cloning steps. First DARPinE01 with a GGSGGGSG linker sequence was cloned via RFC[25] into pZMB0156_VP23_453_587wt and then the CMV promoter from pZMB0143_CMV was added via RFC[10]. The HSPGko and the His-tag were integrated into the 587 loop region via hybridization of oligonucleotides as described in **SI Figure 11**.

pZMB0246_CMV_VP1up_NLS_mVenus_VP23_453_587koHis. This plasmid was generated by integrating the mVenus gene in pZMB0156_VP23_453_587wt fusing the VP1up_NLS part from pZMB0503_VP1up_NLS using the RFC[25] standard and adding the CMV promoter of pZMB0143_CMV. Finally, the 587 loop region was modified by hybridization of oligonucleotide coding for a His-Tag and the HSPGko as described in **SI Figure 11**.

pZMB0156_VP23_453_587wt. This vector is a BioBrick plasmid for subcloning purposes and was constructed by PCR amplification of the cap part from pZMB0216_Rep_VP123_453_587wt_p5tataless with the primers Prefix_VP2ex 5‘-ATGGCCGGCG CTCCGGGAAA AAAGAGGCCG and Suf-fix_VP123ex_RFC_25 5´-GCTACTAGT ATTAACCGGT GTAGTTAATG ATTAACCCGC CATGC-TACTT ATC followed by cloning the product into pSB1C3_001 via RFC[10] to generate pZMB0156_VP23_453_587wt. This plasmid serves for further N-terminal modifications. Thus, the VP3 initiation codon was not mutated. R585 and R588 (587ko) was introduced by hybridization of oligonucleotide as described in **SI Figure 11**.

pZMB0503_VP1up_NLS. A fragment of VP1 named VP1up was converted to a RFC[25] Biobrick by PCR amplification from pAAV-RC using the primers Prefix_VP1ex 5´-ATGGCCGGCG CTGCCGATGG TTATCTTCCA G and VP1up_Suffix_rev 5´-GGACTAGTA TTAACCGGTC GCCTTAACAG GTTCCTCAAC CAGG and cloning into pSB1C3. The NLS was generated in RFC[25] standard with the oligonucleotides NLS_for 5´-AATTCGCGGC CGCTTCTAGA TGGCCGGCCC TGCAAGAAAA AGATTGAATA CCGGTTAATA CTAGTAGCGG CCGCTGCA and NLS_rev 5´-GCGGCCGCT ACTAGTATTA ACCGGTATTC AATCTTTTTC TTGCAGGGCC GGCCATCTAG AAGCGGCCGC G and cloned downstream of the VP1up sequence.

pZMB0143_CMV. The CMV promoter was kindly provided by the iGEM team Ljubljana 2007 (BBa_I712004). A sequence alignment of this BioBrick with the CMV promoter used in pAAV-MCS shows slight differences.

pZMB0135_hGHpA. The human growth hormone polyadenylation signal (hGHpA) was converted into RFC[10] by PCR using pAAV-MCS as template and hGH_primer_for 5´-GCTCTAGACG GGTGGCATCC CTGTGAC and hGH_primer_rev 5´-GAACTGCAGC GGCCGCTACT AGTAAGGACAG GGAAGGGAGC AG and cloning the fragment in a pSB1C3 backbone.

1.2 SI Method 2. Determination of ITR sequences using Sanger sequencing

About 60 µg of ITR plasmid pZMB0522 were digested with 120 U MlyI in a total volume of 240 µl at 37 °C for 1.5 h and separated on an agarose gel. lITR and rITR fragments were isolated using NucleoSpin Gel and PCR Clean-up kit (MACHEREY-NAGEL). About 18 µg of each fragments were digested with 60 U BsaHI in a total volume of 120 µl at 37 °C for 2 h to split the sequence forming the major stem loop of the ITR sequence in half. Resulting fragments were separated on an agarose gel and 5´- and 3´-parts of the lITR and rITR were isolated. Sufficient material for several sequencing reactions was recovered. The obtained four DNA fragments were analysed by Sanger DNA-sequencing (Sequencing Core Facility, CeBiTec, Bielefeld, Germany). The sequencing primers were SEQ-lITR-5: 5´-GAAATGTTGA ATACTCATAC TCTTCC, SEQ-lITR-3: 5´-ATGAACTAAT GACCCCGTAA TTG, SEQ-rITR-5: 5´-CCTAATCTCA GGTGATCTACC and SEQ-rITR-3: 5´-AACGCCTGGT ATCTTTATAG TCC. Results are shown in **SI Figure 2.**

2 Supplementary Information Figures

2.1 SI Figure 1

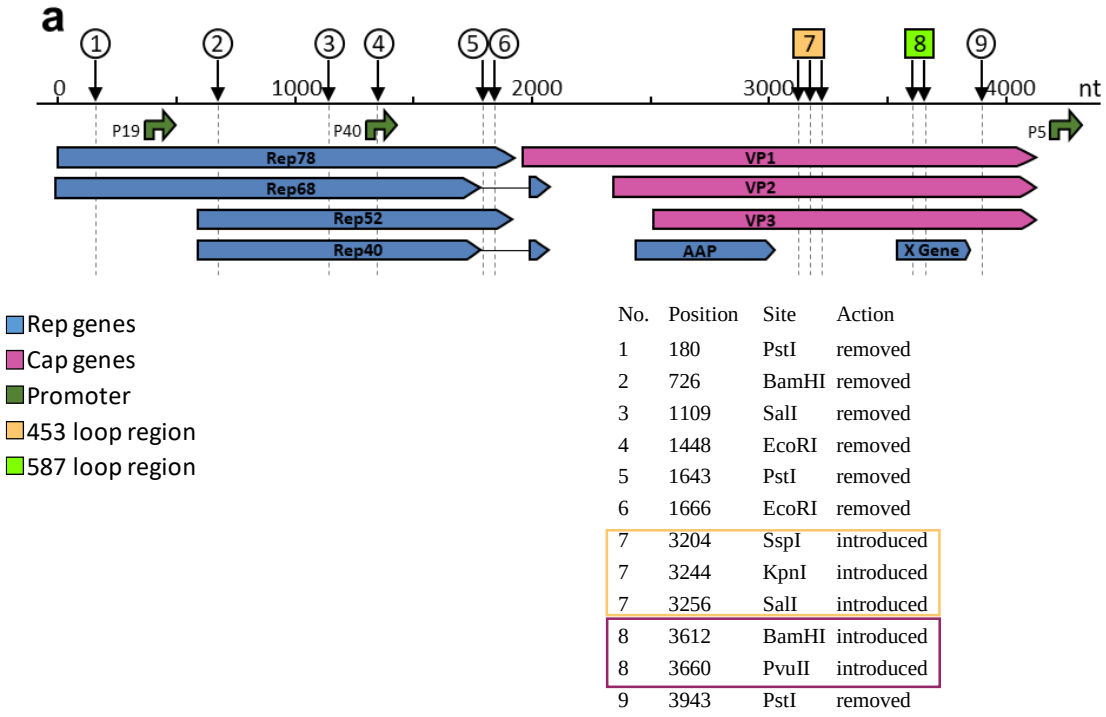

No.	Position	Site	Action
1	180	PstI	removed
2	726	BamHI	removed
3	1109	SalI	removed
4	1448	EcoRI	removed
5	1643	PstI	removed
6	1666	EcoRI	removed
7	3204	SspI	introduced
7	3244	KpnI	introduced
7	3256	SalI	introduced
8	3612	BamHI	introduced
8	3660	PvuII	introduced
9	3943	PstI	removed

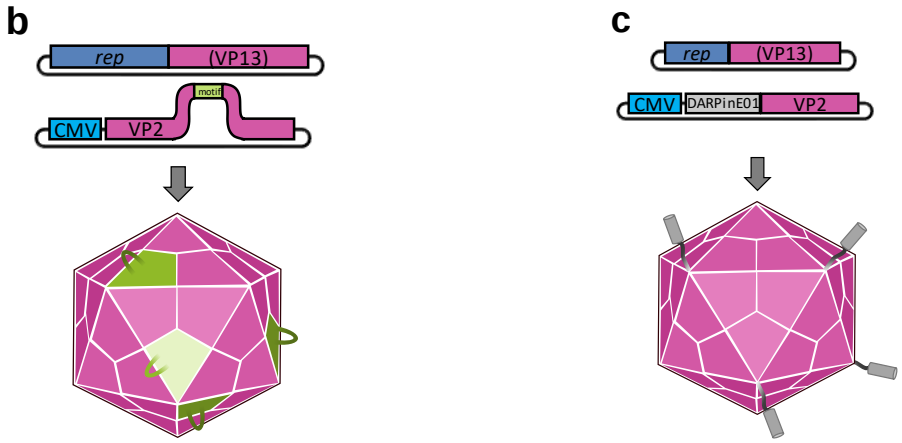

SI Figure 1. Construction of the AAV2 RepCap plasmid (pZMB0216_Rep_VP123_453_587wt_p5tataless) and schematic overview of the rAAV plasmid production system. **a)** *Rep* and *cap* genes were integrated into the pSB1C3_001 backbone. Restriction sites not compatible with the RFC[10] standard were eliminated. Removal of restriction sites is marked with numbers and explained in the inset. For easy modification of 453 and 587 loop regions, the recognition sequences of SspI and SalI, as well as BamHI and PvuII were introduced. These allow for easy modification of the loop regions. Promoters are marked as green arrows. **b)** A forth plasmid allows for the production of mosaic rAAVs with e.g. modified 453 or 587 loop regions (green, e.g. His-tag) of the virion. Expressing a modified VP2 from a separate plasmid reduces the number of motifs on the capsid surface. **c)** Displaying proteins (grey, e.g. DARPinE01) on the capsid surface is also possible using a N-terminal fusion to VP2. **d)** Assembly of fusion proteins is carried out using the RFC[25] standard. The RFC[25] compatible multiple cloning site is visualized here.

2.2 SI Figure 2

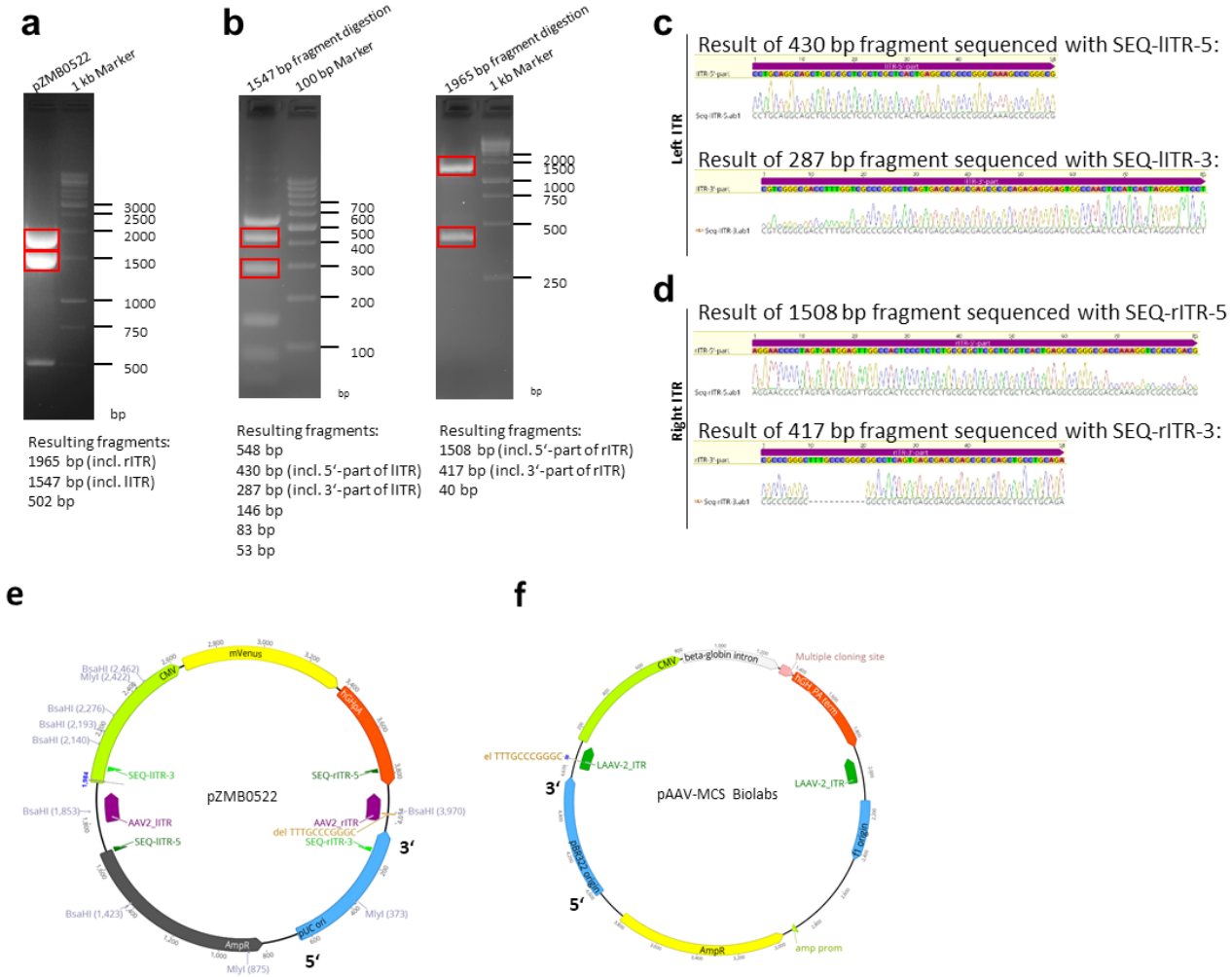

SI Figure 2: Preparation of fragments suitable for sequencing of ITRs**. a, b)** Agarose gel electrophoresis using a 1 % gel at a voltage of 120 V for 90 min. **a)** The restriction digest of pZMB0522 with MlyI results in three fragments and both ITRs are separated on an agarose gel as highlighted in red. **b)** The larger fragments are further digested with BsaHI to break up the T-shaped stem loop and to enable Sanger DNA-sequencing. **c, d)** Results of Sanger-DNA sequencing aligned to original ITR sequences. Fragments were sequenced with oligonucleotides given in the methods. **c)** The left ITR is completely intact. **d)** The 3'-part of rITR shows a deletion of 11 bp (5'-TTTGCCCGGGC-3'). **e)** Schematic overview of the ITR plasmid with used restriction sites. The 3' end of the ori is orientated towards the right ITR. **f)** Overview of the commercially available pAAV-MCS from Cell Biolabs with highlighted left and right ITR. The 3' end of the ori is oriented towards the left ITR which shows the 11 bp deletion. The distance between 3' end of the ori and the ITR with deletions is 74bp and 85 bp, respectively.

We hypothesize that the distance of an ITR to the plasmid origin, the type of origin and the occurrence of Okazaki fragment processing sites may affect genetic ITR stability. In particular we assume that the *E. coli* PolI itself and the switch to PolII, which takes place shortly downstream of pMB1 type ori, contribute to the genetic instability.

Note that the original modular ITR plasmid was numbered and presented as most ITR plasmids (panel f) and the deletion carrying ITR was the left or 5´ ITR. In the new ITR plasmid (pZMB0522) we kept the classical pUC numbering and thus the deletion is formally now in the right or 3´ ITR.

2.3 SI Figure 3

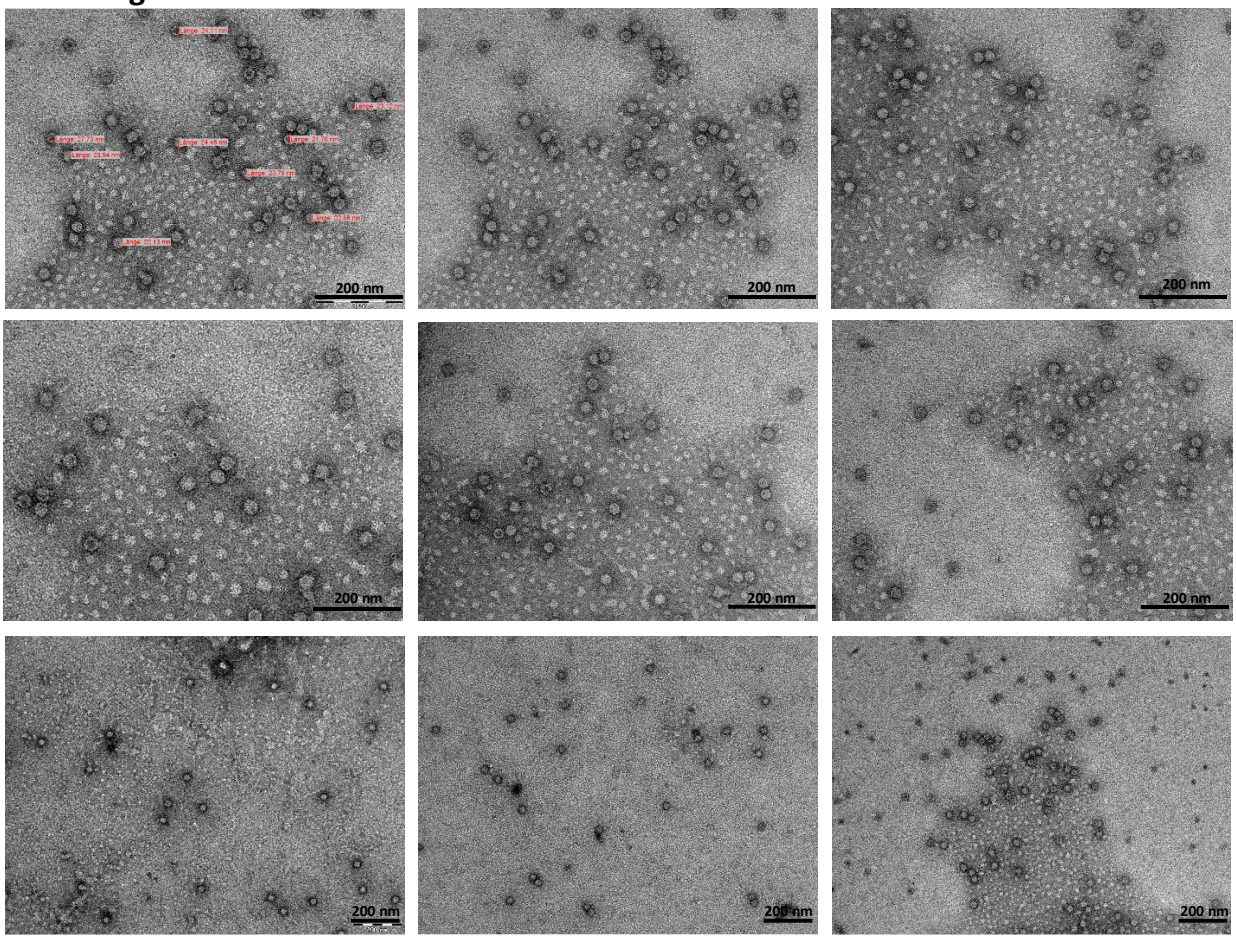

SI Figure 3. Transmission electron microscopy micrographs to calculate the full to empty capsid ratio of rAAV particles. An overview of images used for calculations is shown. Samples were applied to carbon-coated copper grids and stained with 2% uranyl acetate replacement stain (Science Services). rAAVs were visualized with a Philips CM100 (PW6021) with an acceleration voltage of 80 kV. Image analysis was performed using Soft Imaging viewer (Olympus). Scale bars indicate 200 nm. The first image shows diameter measurements to verify the diameter of rAAV particles.

2.4 SI Figure 4

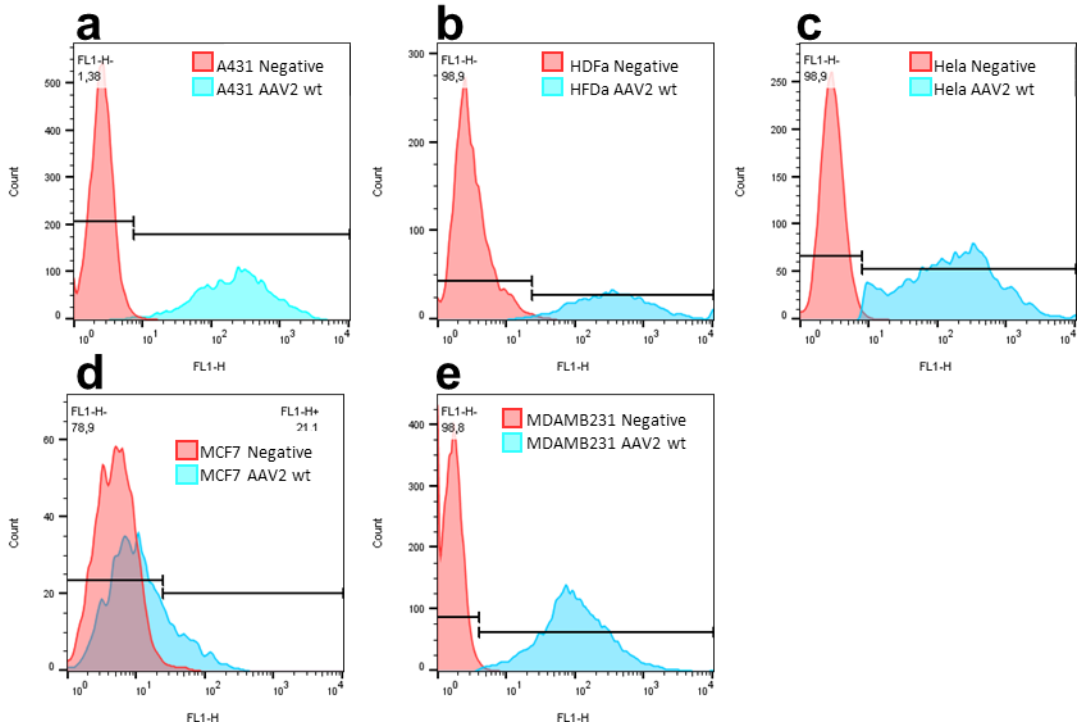

SI Figure 4. Flow cytometry data for rAAV variants in comparison to the negative buffer control. Cells were transduced with rAAVs at a MOI of 10,000 and analyzed via flow cytometry after incubation. Data analysis was performed using FlowJo. In a first step a population of live cells was gated. In a second step a gate of 1% false positive cells was selected in the sample of the negative control. This gate is visualized in each diagram.

2.5 SI Figure 5

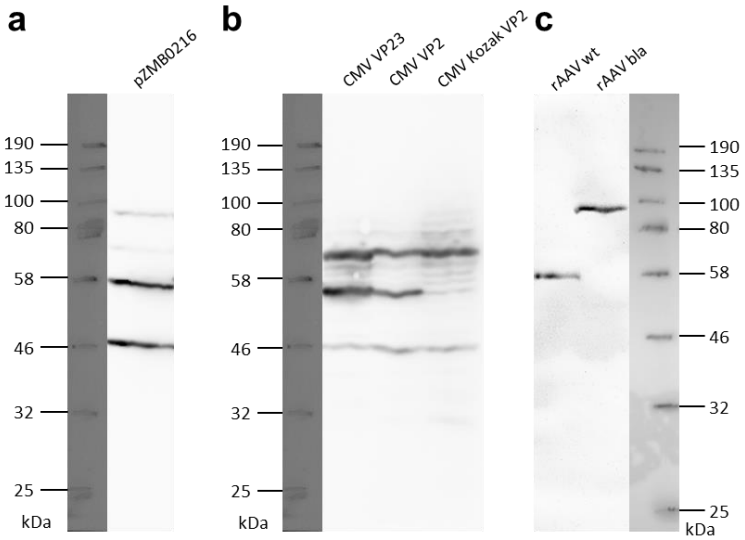

SI Figure 5. Full length western blot images. **a)** Western blot of crude cell lysate after HEK293 triple-transfection with pZMB0216, pZMB0522 and the pHelper plasmid. VP proteins were detected with the B1 antibody (Progen), a secondary HRP-coupled antibody and subsequent chemiluminescence imaging for 270 s. **b)** Western blot of crude cell lysate after transfection with the above mentioned plasmids. VP proteins were detected with the B1 antibody (Progen), a secondary HRP-coupled antibody and subsequent chemiluminescence imaging for 200 s. **c)** Western blot of a rAAV wt and rAAV bla from purified viral stocks. VP proteins were detected with the B1 antibody (Progen), a secondary HRP-coupled antibody and subsequent chemiluminescence imaging for 600 s.

2.6 SI Figure 6

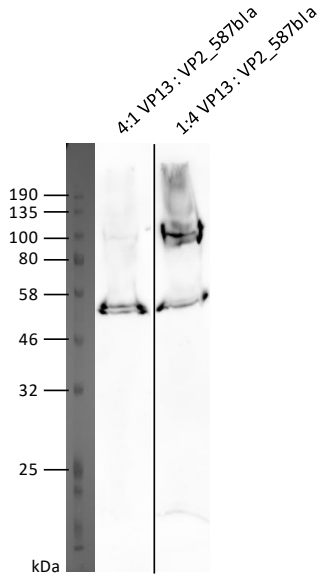

SI Figure 6. Western Blot analysis for rAAV2_mosaicVP2_587bla with respect to the gene dose of each plasmid. Crude cell lysate was applied to a 10 % SDS PAGE gel for electrophoresis. After semi-dry blotting onto a nitrocellulose membrane the VP proteins were detected with the B1 antibody (Progen). The plasmid ratio of the quadruple transfection was based on the ratio of the triple transfection. ITR, RC and pHelper plasmid have been used in a molar ratio of 1:1:1. To create a mosaic virus, CMV_Kozak_VP2_587bla and Rep2Cap2_VP13 have been transfected. The ratio of these plasmids was varied between 4:1 and 1:4.

2.7 SI Figure 7

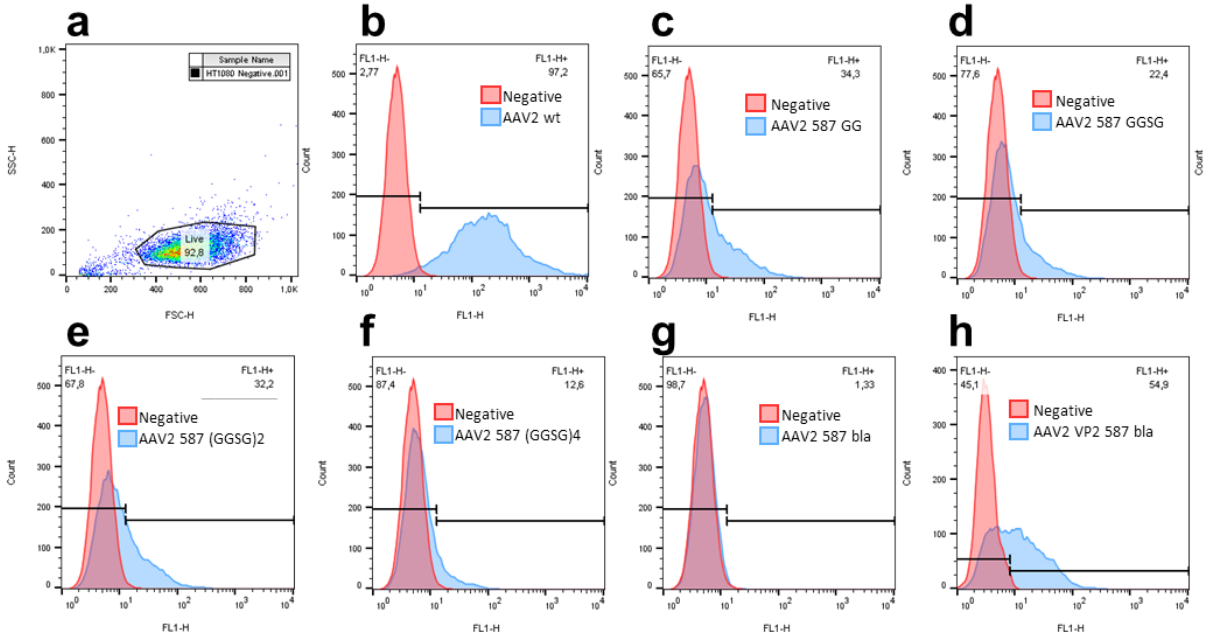

SI Figure 7. Flow cytometry data for rAAV variants in comparison the negative buffer control. HT1080 cells were transduced with rAAVs at a MOI of 50,000 and analyzed via flow cytometry after incubation. Data analysis was performed using FlowJo. In a first step a population of live cells was gated (**a**). In a second step a gate of 1% false positive cells was selected in the sample of the negative control. This gate is visualized in each diagram. Overlay histograms for the wild-type rAAV2 **b**), all glycine-serine linker variants **c**-**f**) and both bla variants **g**-**h**) are shown.

2.8 SI Figure 8

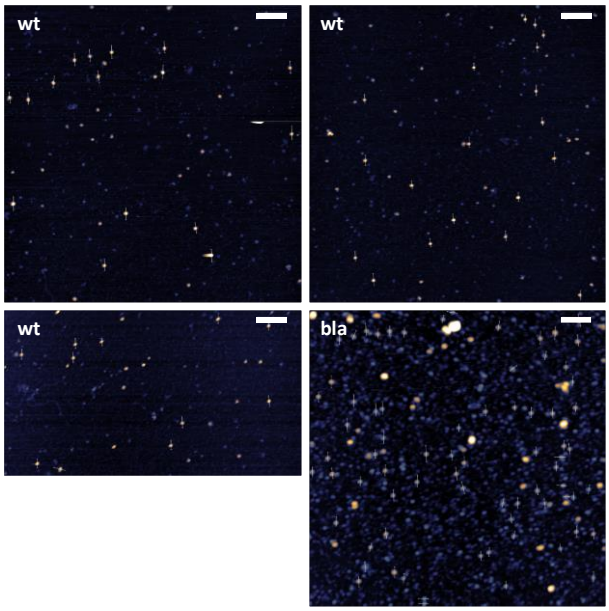

SI Figure 8. Atomic force micrographs of wild-type (wt) and fully β-lactamase modified rAAV (bla). The scale bars indicate 200 nm. Thin white lines with ticks show height profiles that were extracted to measure the individual particle diameter for particles that met a height threshold of 5 nm (wild-type capsids) and 6 nm respectively. Particle width was determined at half maximum height.

2.9 SI Figure 9

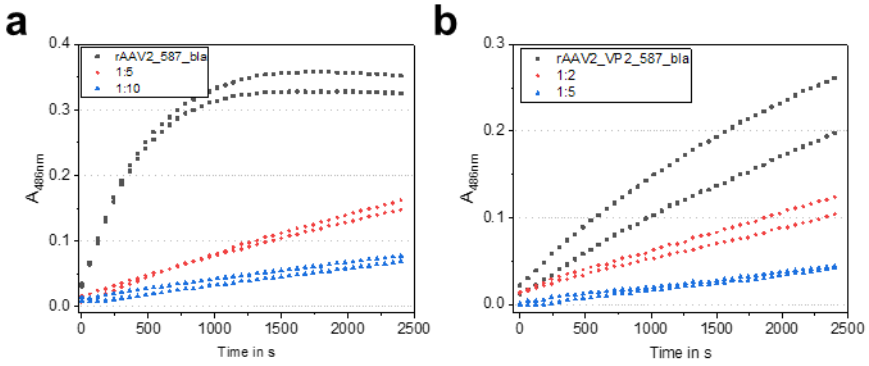

c

$$\frac{\Delta A}{\Delta t} = \Delta\varepsilon_{486} \cdot c_{bla} \cdot k_{cat_{bla}} \cdot d$$

Sample	Slope in s^{-1}	c(bla) in mol/L	c(rAAV) in mol/L	k_{Cat} in s^{-1}
AAV bla full	5.26×10^{-4}	1.65×10^{-10}	6.14×10^{-12}	334.3
AAV bla full 1:5	7.31×10^{-5}	2.29×10^{-11}	1.23×10^{-12}	232.1
AAV bla full 1:10	2.21×10^{-5}	6.95×10^{-12}	6.14×10^{-13}	140.6
AAV bla mosaic	1.22×10^{-4}	3.83×10^{-11}	6.14×10^{-12}	930.7
AAV bla mosaic 1:2	5.50×10^{-5}	1.73×10^{-11}	3.07×10^{-12}	838.2
AAV bla mosaic 1:5	1.88×10^{-5}	5.90×10^{-12}	1.23×10^{-12}	716.6

SI Figure 9. Nitrocefin assay for determination of β-lactamase activity. **a, b)** Absorption measurements of rAAV2_587_bla and rAAV2_VP2_587_bla in different concentrations at 486 nm. Data points were measured in 1 min intervals. **c)** The first six data point were included in linear regression calculations. Resulting values are given in the table and correlate with dilution. Since very low concentrations were used, there are variations which can be explained in the pipetting the dilutions.

3 SI Tables

3.1 SI Table 1

SI Table 1. Overview of plasmids provided by the iGEM competition in 2010 including a short description of their features.

Plasmid name with description	Length	Backbone
pZMB0246_CMV_VP1up_NLS_mVenus_VP23_453_587koHis expression of VP1 with N-terminal mVenus as well as VP2 and VP3, R585 and R588 in 587 loop regions are changed to Ala (HSPGko), His-tag in 587 loop	5863 bp	pSB1C3_001
pZMB0091_CMV_DARPinE01_mli_VP23 _453_587koHis expression of VP2 with N-terminal DARPin E01 fusion, Arg in 587 loop changed to Ala (HSPGko)	5191 bp	pSB1C3_001
pZMB0156_VP23_453_587wt construct for cloning, encodes VP2/3 with cloning ready loop regions, allows for the construction of a N-terminal VP2 fusion	4004 bp	pSB1C3_001 RFC[25]
pZMB0503_VP1up_NLS construct for cloning, encodes the unique upstream region of VP1 (VP1up) and a nuclear localization sequence (NLS), precursor for assembly of surface exposed VP1 integrations	2525 bp	pSB1C3_001 RFC[25]
pZMB0143_CMV CMV promoter in RFC[10] for construction of N-terminal VP2 fusion vectors or ITR plasmid assembly	2725 bp	pSB1C3 RFC[10]
pZMB0135_hGHpA hGH polyadenylation signal in RFC[10] for assembling of the ITR plasmid.	2550 bp	pSB1C3 RFC[10]

3.2 SI Table 2

SI Table 2. Characteristics of TEM β-lactamase variant 14FM.

	β-lactamase 14FM
Mutations compared to wild-type TEM-116 β-lactamase (GenBank ID: AY425988)	V31A, A36L, L51I, R120G, E147G, H153R, V159T, M182T, L201P, I208M, E212K, A224V, A249V, T264M
Melting temperature T_M determined using far-UV circular dichroism in phosphate buffer	71.6 °C (2 µM) 72.7 °C (20 µM)
Catalytic constant k_{cat} for nitrocefin conversion in s^{-1}	746 ± 76 s^{-1}

Source: T. Baumann, 2013, PhD thesis, University of Potsdam, Germany, "Stability and interconnected protein properties studied with TEM β-lactamase"

4 Cloning strategy

4.1 Cloning of loop modifications in pZMB0216

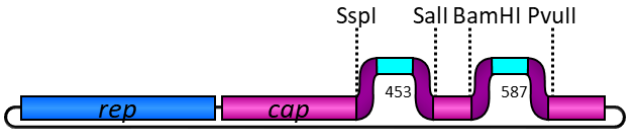


```
Residue 453 (position determined via Uniprot #P03135)
For 5´-ATTTGTATTACTTGAGCAGAACAAACACTCCAAGTGGTNNN…NNNACCACCACGCAGAG-3´
Rev 5´-TAAACATAATGAACTCGTCTTGTTTGTGAGGTTCACCANNN…NNNTGGTGGTGCGTCTCAGCT-3´

Residue 587 WT
For 5´-GATCCGTATCTACCAACCTCCAGAGAGGCAACNNN…NNNAGACAAGCAGCTACAG-3´
Rev 5´-GCATAGATGGTTGGAGGTCTCTCCGTTGNNN…NNNTCTGTTCGTCGATGTC-3´

Residue 587 KO
For 5´-GATCCGTATCTACCAACCTCCAGGCTGGCAACNNN…NNNGCCCAAGCAGCTACAG-3´
Rev 5´-GCATAGATGGTTGGAGGTCCGACCGTTGNNN…NNNCGGGTTCGTCGATGTC-3´

Viral Brick 587ko-empty
For 5´-GATCCGTATCTACCAACCTCCAGGCTGGCAACGCCCAAGCAGCTACAG-3´
Rev 5´-CTGTAGCTGCTTGGGCGTTGCCAGCCTGGAGGTTGGTAGATACG-3´

Viral Brick 587-GG
For 5´-GATCCGTATCTACCAACCTCCAGAGAGGCAACGGAGGCAGACAAGCAGCTACAG-3´
Rev 5´-CTGTAGCTGCTTGTCTGCCTCCGTTGCCTCTCTGGAGGTTGGTAGATACG-3´

Viral Brick 587-GGSG
For 5´-GATCCGTATCTACCAACCTCCAGAGAGGCAACGGAGGCTCTGGTAGACAAGCAGCTACAG-3´
Rev 5´-CTGTAGCTGCTTGTCTACCAGAGCCTCCGTTGCCTCTCTGGAGGTTGGTAGATACG-3´

Viral Brick 587-2x(GGSG)
For 5´-GATCCGTATCTACCAACCTCCAGAGAGGCAACGGAGGCTCTGGTGGCGGTTCAGGAAGACAAGCAGCTACAG-3´
Rev 5´-CTGTAGCTGCTTGTCTTCCTGAACCGCCACCAGAGCCTCCGTTGCCTCTCTGGAGGTTGGTAGATACG-3´

Viral Brick 587-4x(GGSG)
For 5´-GATCCGTATCTACCAACCTCCAGAGAGGCAACGGAGGCTCTGGTGGCGGTTCAGGAGGTG-
GAAGCGGCGGAGGTAGTGGCAGACAAGCAGCTACAG-3´
Rev 5´-CTGTAGCTGCTTGTCTGCCACTACCTCCGCCGCTTCCACCTCCTGAACCGCCACCAGAGCCTCCGTTGCCTCTCTGGAGGTTGGTAGATACG-3´
```

SI Figure 11: Cloning strategy for 453 and 587 loop regions. Sequences of oligonucleotides used for the generation of different loop modifications by hybridization are shown. The given oligonucleotides have been cloned via the above mentioned restriction enzymes.

4.2 Cloning of N-terminal VP2 modifications in rAAV2

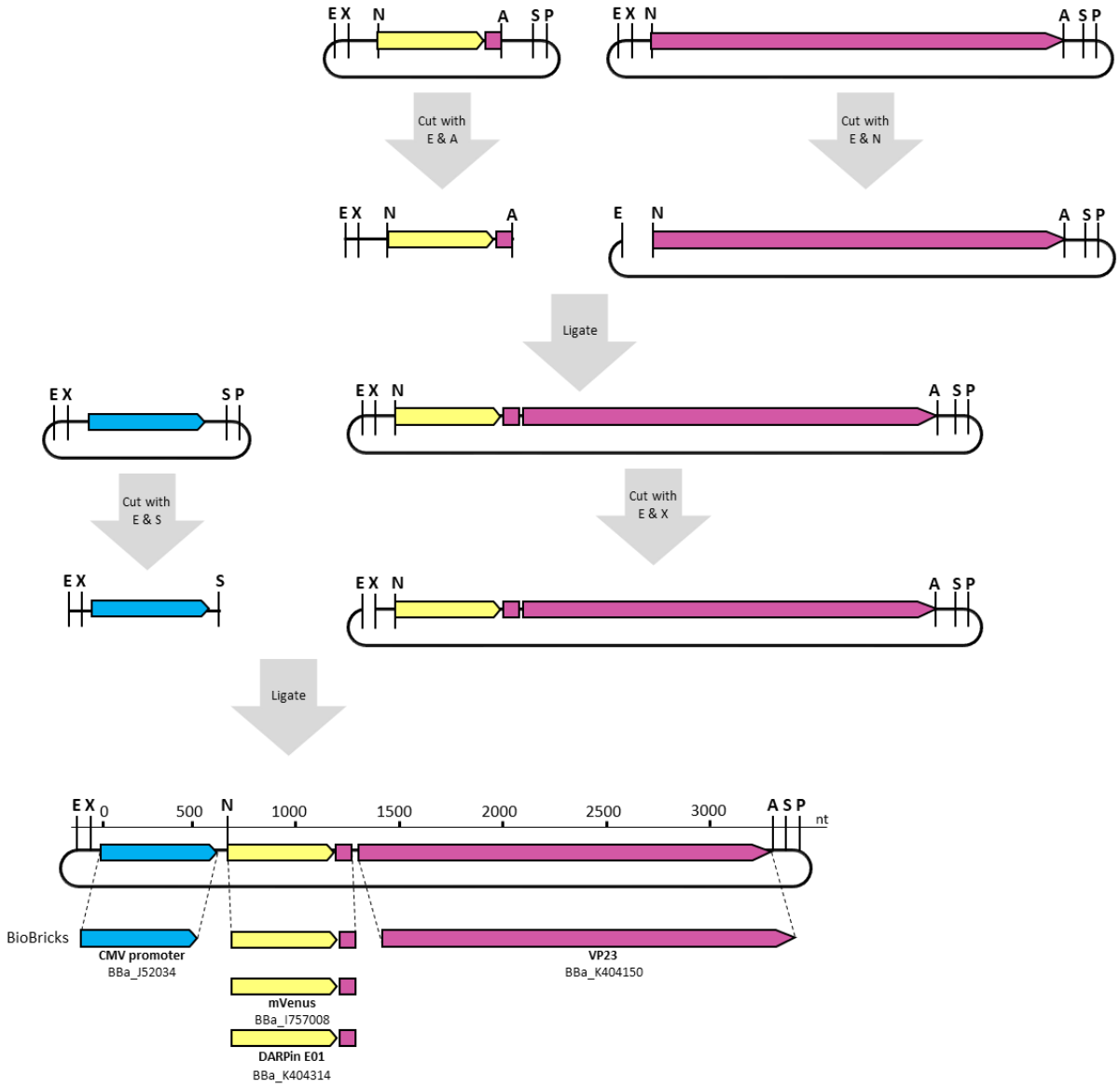

SI Figure 12: Cloning strategy for pZMB0091_CMV_GOI_mli_VP23 _453_587koHis. This plasmid was not used during this work but shows the potential assembly of N-terminal fusion proteins. Assembly of Bio-Bricks can be performed as shown. The following abbreviations are used for the restriction enzymes and their recognition sites, respectively: E= EcoRI, X= XbaI, N= NgoMIV, A= AgeI, S= SpeI, P= PstI.

HEK293-KARE1, a cell line with stably integrated adenovirus helper sequences simplifies rAAV production

Rebecca C. Feiner[1,†], rebecca.feiner@uni-bielefeld.de

Kathrin E. Teschner[1,†,], kathrin.schlicht@uni-bielefeld.de

Julian Teschner[1], jteschner@uni-bielefeld.de

Kristian M. Müller[1,*], kristian@syntbio.net

† Both authors contributed equally to this work.

[1] Cellular and Molecular Biotechnology, Faculty of Technology, Bielefeld University, Bielefeld, Germany

[*]Corresponding author information (Address; Email; Phone)

Kristian M. Müller, Cellular and Molecular Biotechnology, Faculty of Technology, Bielefeld University, Universitätsstraße 25, 33615 Bielefeld, Germany; Email: kristian@syntbio.net; Tel. +49-521-106-6323

Abstract

Background: Recombinant adeno-associated viruses (rAAV) bear great potential for gene therapy and their production with helper-free plasmid systems in HEK293 cells is well established. However, current approaches require the tedious preparation and co-transfection of the invariant adenoviral helper genes for each production cycle. Genomic integration of essential elements can simplify the manufacturing process.

Results: We engineered a HEK293 cell line by stably integrating adenoviral elements E2A, E4 and the non-coding VA RNA. After selection, single cell colonies were analyzed for sequence integration. Insert stability was maintained over more than four months of continuous culture. The novel HEK293-KARE1 cell line was characterized with regard to growth and cell cycle state demonstrating a very small influence of adenoviral genes. RNA Expression of E2A and E4 was verified using RT-PCR at a low level compared to already present E1A. Transduction and rAAV2 production in the new cell line by solely providing a RepCap and a ITR/vector plasmid was established with yields comparable to those obtained with the well-established three-plasmid system in the original HEK293 cells.

Conclusions: The results show that HEK293-Ad-helper cell lines have the potential to reduce upstream time and cost while ensuring consistent and safe rAAV manufacturability.

Keywords: AAV2, adenovirus, virus-like particle

Background

Recombinant adeno-associated virus (rAAV) approaches gained an outstanding reputation in gene therapy due to their beneficial characteristics. Among the numerous advantages over other virus-based gene therapy approaches is the attainable long-term gene expression and the high safety profile resulting from the inability to autonomously replicate without additional genes from a wild type and a helper virus. AAVs target dividing and non-dividing cells, possess low immunogenicity and are produced at larger scale for clinical applications [1]. The AAV toolbox for gene therapy is large: currently 13 different serotypes are characterized and over 100 AAV variants are known [2]. Serotype 2 was studied intensively and was the first serotype to be produced in mammalian cells [3, 4]. Mammalian cells and insect cells are well established as host systems. The best studied and most widely used system relies on the human embryonic kidney cell line 293 (HEK293) [5]. Formerly, a helper virus (e.g. adenovirus (Ad)) was used to facilitate production, but nowadays the biologically safer use of a plasmid system is the standard, in which the genes coding for supporting adenoviral proteins are encoded *in trans* [6]. The latter is named the helper-free plasmid system and handling is in many countries regarded as biosafety level 1 work. The helper-free production was independently published by two research groups in 1998, demonstrating that the presence of the Ad genes E1A, E1B, E2A and E4 and the non-coding RNA VA are required for replication of AAV [7, 8]. The production cell line HEK293 cell line was generated by transfection with fragments of mechanically sheared adenovirus 5 DNA and the presence of adenoviral E1A and E1B in chromosome 19 (19q13.2) was confirmed indicating random integration [9–11]. Besides their biological function for immortalization, transcripts from both genes were identified. The gene of E1A (early E1A protein) promotes host DNA synthesis and stabilizes the tumor suppressor p53 inducing apoptosis [12]. Two gene products generated from E1B (E1B19K and E1B55K) are able to protect cells from the cytotoxic effects of E1A [12]. In the helper-free system the remaining genes E2A and E4 and the non-coding RNA VA are provided by plasmids called pVAE2AE4-5 or pXX6 [7, 8], which are collectively referred to as ‘helper plasmids’. More specifically, pHelper GenBank AF369965.1 contains the VA RNAs, the E2A part coding for the 72 kDa single stranded DNA binding protein, and the coding region of E4orf6 [13]. Undesired adenovirus late genes were omitted from those helper plasmids eliminating the possibility of a wild-type adenovirus contamination. Expression of E1A and E1B induces expression of E2A and E4. E1A also acts on the AAV P5 promoter and induces expression of AAV Rep and Cap genes *in trans* [14]. E2A codes mainly for the Ad single-stranded DNA binding protein (DBP), which is besides several other functions involved in augmentation of rAAV circular intermediate formations [15]. The gene E4 codes for several proteins but during rAAV production mainly E4orf6 is of importance. E4orf6 is able to associate to E1B55K and regulates p53 stability promoting apoptosis [16, 17]. The last important feature required for helper-free rAAV production is VA I RNA. VA I RNA generates a small RNA transcript, that regulates gene expression at the level of translation in transfected cells [18]. In presence of DBP it enhances AAV cytosolic mRNA by stabilization [19].

For rAAV production, the two commonly used helper-free plasmid systems either employ a two- or a three-plasmid system [20, 21]. By distributing the genetic information of rAAV on different plasmids the likelihood

of the emergence of a replicative competent virus becomes extremely low. The three-plasmid system consists of the pHelper plasmid coding for the required Ad5 genes, a RepCap plasmid and an ITR-containing plasmid often named vector plasmid. The RepCap plasmid provides the information for the four nonstructural proteins Rep 78, 68, 52, 40 and the three proteins VP1, VP2, VP3 forming the icosahedral capsid structure. Furthermore, the Cap open reading cassette codes, in an alternative reading frame, for the assembly activating protein (AAP) as well the X protein, which influences replication and vision production [22–25]. The third plasmid needed is the ITR-containing plasmid, which harbors the gene of interest flanked on both sites by an inverted terminal repeat (ITR) sequence. ITRs mediate DNA replication and function as packaging signal for the single-stranded DNA into the capsid shell [26]. The two-plasmid system, which was devised by Grimm *et al.* in 2003, combines the genetic information of the adenoviral helper sequences E2A, E4 and VA with AAV serotype specific *rep* and *cap* genes on the pDG plasmid [20]. This approach has been further optimized by the use of minicircle DNA [27].

The widely adopted helper-free plasmid systems are reliable, but pose the inconvenience of the continuous production and co-transfection of the invariant adenoviral helper genes of 9279 bp. So far, even in cellular optimized processes for clinical rAAV production developed by leading research groups, the three-plasmid system is deployed [1].

Several groups have tried to establish production cell lines harboring either single parts of the adenoviral elements or combinations of different elements. First trials to create a production cell line started with genomic integration of rAAV RepCap and ITR parts into HeLa cells [28]. rAAV production starts upon infection with adenovirus and, thus does not need DNA transfection. Next, groups started with integration of RepCap and ITR parts into a E1A and E1B inducible cell line and went on by further introducing adenoviral elements E2, E4 and VA [29]. Nonetheless, integration of all necessary elements resulted in less stable cell lines with decreasing yields of viral particles. Other attempts to create AAV production cell lines relied on genomic integration of adenoviral elements or RepCap parts but also resulted in cell lines where either transfection of invariant plasmids or the use of the adenovirus are required [30, 31].

In order to ease and improve rAAV production, we generated a HEK293-Ad-helper cell line, that stably provides the Ad5 genes necessary for rAAV formation. As known from previous work, high levels of early adenoviral gene products can have toxic effects to cells [32]. Until now, the most effective gene dose for high-titer rAAV production is not known, which provides the opportunity that cells producing a non-toxic level of proteins are able to produce viral particles without addition of a helper plasmid. Such an engineered cell line was generated and named HEK293-KARE1. The integration of helper genes was verified in three clones. rAAV2 virus-particle production was monitored and the transfection protocol was optimized with regard to the amount of required DNA and the potential need for selection pressure for genomic integration. Furthermore, genomic and transducing titers were determined and compared to the common three-plasmid production system. The presented methodology simplifies the well-established AAV production process and reduces the risks of undesired DNA packaging of pHelper DNA [33].

Results

Integration of pHelper sequences into HEK293

As introduced above, pHelper plasmid (GenBank Accession number: AF369965.1) harbors the three adenoviral elements E2A, E4 and VA and a BLAST comparison confirms 100 % sequence coverage with the corresponding parts of the genome of adenovirus 2 (GenBank: J01917.1). Integration of the entire pHelper plasmid into the genome of HEK293 was facilitated by introduction of a selectable marker into the pHelper plasmid. The gene for blasticidin S deaminase from *Aspergillus terreus* was amplified and cloned into pHelper via two unique restriction sites (NdeI, SalI) yielding pHelper-BSD (**Figure 1**). This plasmid was linearized, dephosphorylated and transfected in HEK293 cells. Three days post transfection selective pressure was applied and cell death of putatively non-transfected cells was observed after further incubation for two days. Medium was exchanged every second day and after two weeks dividing cells were observable, that potentially carried the desired construct. Consequently, a limiting dilution in 96-well plates was used to select single cells for further cultivation and characterization. Cells growing as monoclonal colonies were identified by microscopy and, after reaching confluence, four monoclonal cultures were transferred in a 6-well plate and named HEK293-KARE1a to HEK293-KARE1d. These clones were chosen, because they showed the highest growth rates. The growth of all clones was comparable to that of the parental HEK293 cell line, while maintaining the blasticidin concentration. Cells were passaged regularly, and since HEK293-KARE1d showed decreased viability and transfection efficiency this clone was discarded. For cell lines HEK293-KARE1a to 1c characteristic HEK293-like growth in monolayers, adherence and viability were confirmed beyond 30 passages. During subculturing no changes in morphology were seen in bright field microscopy at 40-fold magnification as exemplified by HEK293-KARE1c after 20 passages (**Figure 2A**) in comparison to the parental HEK293 (**Figure 2B**). Growth behavior of HEK293 and HEK293-KARE1a to 1c was analyzed for 72 h after passage three and is depicted in **Figure 2C**. Experimental results were fitted with an exponential function to determine the population doubling times. Clones HEK293-KARE1a and 1c showed a doubling time comparable to that of HEK293 cells. For HEK293-KARE1b a slower growth rate was calculated.

Verifying genomic integration of pHelper sequences

After isolation of monoclonal cultures and detection of normal cell growth, genomic integration of the helper genes was analyzed. Genomic DNA of the three clones was isolated using a Chelex100 extraction. The presence of the *bsd* and the E2A gene was verified using PCR with two different sets of primers. As seen in **Figure 1** primers Bsd-for and Bsd-rev as well as Ad5-for and Ad5-rev anneal at different regions of the plasmid and, in the case of a successful complete integration, amplification products with a size of 499 bp and 524 bp respectively for E2A and *bsd* should emerge. Experimentally obtained fragments are shown in **Figure 2D** for all samples, demonstrating that both genes were integrated successfully into the genome of HEK293. Genetic integration of the plasmid sequence might not automatically result in successful gene expression. In a next step, the presence of the gene products was verified.

Gene expression of adenoviral E2A and E4 does not interfere with cell growth and cell cycle progression

The resistance of monoclonal cells to blasticidin indicated that integrated genes are not silenced and gene expression is likely. To verify the presence and expression of the integrated elements E2A and E4 the mRNA level was determined. RNA from HEK293 and HEK293-KARE1 cells was extracted and subsequently cDNA was generated. A qPCR was carried out with three different sets of primers for E1A, E2A and E4. Oligonucleotide sequences to amplify E2A were selected to bind in the coding sequences for the DNA-binding protein of human adenovirus type 2 (GenBank: AAA92217.1). The primer pair used to amplify E4 was selected to anneal at open reading frame 6 coding for E4 34k, mainly involved in the AAV production process [34]. Calculation of ΔΔCt values showed an elevated relative expression level of both adenoviral early genes in HEK293-KARE1 clones compared to HEK293 (**Figure 3A**). These calculations were based on E1A as a normalizing gene which is present in the parental and the novel HEK293 cell line. Since expression of E2A and E4 might influence the expression of E1A, we evaluated three independent RNA isolations and qRT-PCR reaction to show that cycle thresholds for E1A were constant during the experiments and E1A expression is not altered (SI Table 1). The expression level of E2A was higher compared to the E4 expression. Analysis of the PCR products on an agarose gel (**Figure 3B**) revealed the correct sizes with 68 bp, 65 bp and 143 bp for E1A, E2A and E4 respectively. Previously published work showed that expression of adenoviral parts in HEK293 cells can have a strong impact on cell growth and cell cycle. Integration of E4 in an inducible system showed that the progression through the cell cycle can be altered [35]. Furthermore, it is known that high levels of E2A and E4 in the presence of E1 gene products are toxic to cells [32]. To gain a deeper insight in the newly developed cell line, cell cycle progression was determined.

In literature, it was proposed that expression of the E4 ORF6 protein leads to an accumulation of the cells in the S-phase of the cell cycle [35]. To this end, we investigated the effect of adenoviral elements on the cell cycle under general AAV production conditions. A delay in the S-phase was not observed as seen in **Figure 3C** and **D**. Cells were seeded at the same high density as typically done for AAV production (3×10^6 per 100 mm dish), and thus, cell growth was limited. The observed distribution of cell cycle states over the typical production time of 72 h of the cultivation is expected. There is no significant difference between the HEK293 cell lines and the newly developed HEK293-KARE1 cell lines. As a control for adenoviral element expression, a rAAV producing HEK293 sample was used. This showed a high accumulation in G1 phase right after the transfection, which was reversed as the cells adapted to the conditions of the transfection. These experiments suggest that production of rAAVs in HEK293-KARE1 cells is possible, because necessary proteins are expressed and cell proliferation is largely unaltered upon genetic intervention.

rAAV production was confirmed for HEK293-KARE1

In order to assess the rAAV production ability and their long-term productivity, three HEK293-KARE1 clones were cultured similar to normal HEK293 with the only difference of maintaining antibiotic selection. First attempts for rAAV production started with adapting the three-plasmid co-transfection for high titer rAAV production in HEK293 cells. Here, pHelper plasmid, Rep2Cap2^{587wt}- and ITR-plasmid are transfected in a

molar 1:1:1 ratio and a total plasmid DNA amount of 15 µg per 100 mm dish. We started with a double-transfection of the Rep2Cap2^{587wt} - and ITR-plasmid in a 1:1 ratio omitting the pHelper plasmid but keeping the total plasmid DNA amount of 15 µg per 100 mm dish. These experiments were carried out with the three cell lines HEK293-KARE1a to 1c after passage 3 and 9 and as a negative control with HEK293 cells and as a positive control with HEK293 cells and triple plasmid transfection. Genomic titers, or more precisely of DNase I-resistant particles, were determined directly without further purification from the crude cell extract using qPCR with a set of ITR-plasmid specific primers. To get meaningful results, the standard curve used for determination of the genomic titer was set up in equal amounts of crude cell extract from untransfected cells. Resulting genomic titers of this experiment are presented in **Figure 4A**. As expected, rAAV production was observed for HEK293-KARE1 clones when omitting the pHelper plasmid. HEK293 cells transfected without addition of pHelper show a dramatic reduction in production capacity of viral particles. Note that this background may be related to small impurities of transfected plasmid. Productivity of all clones is comparable to the parental HEK293 cell line after the well-known triple transfection. Optimization of the rAAV production process was performed only with clone HEK293-KARE1c which yielded in the highest genomic titer ($4.6x10^{10}$ vg per ml) in crude cell extract. Furthermore, no reduction of rAAV titer was observed when cells were cultivated for nine passages. Cryopreservation did not alter production capacity as these experiments were conducted from biological duplicates that were independently thawed. We additionally optimized the production process as the high DNA amount and addition of the antibiotic might not be desired during the production process. Lowering the required plasmid dose and omitting the antibiotic would reduce production costs and possible sources of product contaminations. We hypothesized that reduction of the total DNA amount is compatible with rAAV production. Thus, a reduction of the total plasmid DNA amount from 15 µg to 7.4 µg was tested. This value corresponds to the total DNA amount of Rep2Cap2^{587wt}- and ITR-plasmid in the standard triple-transfection protocol with just omitting the pHelper plasmid DNA. Previous attempts using the standard calcium-phosphate transfection protocol indicated a deterioration of transfection efficiency and associated lower genomic titer (data not shown). The calcium-phosphate transfection method is based on DNA-calcium phosphate precipitation which is dependent on a specific DNA to calcium ion ratio [36]. Simply reducing the DNA amount did not lead to satisfying precipitation, which was observed by a decreased turbidity of the transfection solution. We adapted the transfection protocol for a reduced amount of DNA which resulted in genomic titers comparable to the use of 15 µg total DNA per transfection (**Figure 4B,** first and second bar). In a second optimization step we evaluated the need for the selective pressure during the production process. We did not want to generally omit the use of the antibiotic as it is known that gene silencing might occur if the selective pressure is not maintained. We seeded cells for rAAV production without addition of blasticidin and performed transfections the day after. Comparison of genomic titers from crude cell extracts after 72 h proved rAAV production even without the addition of the antibiotic in comparable yields (**Figure 4B,** third and fourth bar). The variations observed between separate biologic experiments (**Figure 4B**, second and third bar) can be attributed to passaging and handling. These differences might seem high but it should be considered that experiments were conducted in the course of cell line characterization.

rAAV2 was successfully produced in HEK293-KARE1c, purified and characterized

After reducing the amount of DNA and the concentration of antibiotic, the quality of the produced viral particles was characterized. We produced rAAV2 in the favorite HEK293-KARE1c clone. Cells were seeded on ten 100 mm dishes the day before transfection. Transfections were carried out using the previously adapted calcium-phosphate transfection protocol with a total plasmid DNA of 7.4 µg (2.5 pg per cell) and 1:1 molar ratio of Rep2Cap2^{587wt} to ITR-plasmid. Viral particles were purified using a standard iodixanol-gradient ultracentrifugation protocol. The transducing titer was determined for a serial dilution of viral particles on HT 1080 cells. The ITR-delivered gene of interest coded for the fluorescent protein mVenus under the control of a CMV promoter and thus successful transduction resulted in yellow fluorescent cells, which were analyzed by fluorescence microscopy and flow cytometry. To calculate the transducing titer from flow cytometry data, the lowest serial dilution was used **(Figure 5A)** and the genomic titer was determined via qPCR. Both titers are presented in **Figure 5B**. The transducing titer is about 10-fold lower compared to the genomic titer which is in agreement with the literature [37]. The sample purified by ultracentrifugation was analyzed by atomic force microscopy (AFM) (**Figure 5C**). The calculated mean diameter of the marked particles is with 21.5 nm in the expected range of 20 to 24 nm **(Figure 5D**) [38].

Discussion

The demand for an effective, safe rAAV production system is high. A well-known DNA contaminant in rAAV preparations is, beside others, DNA from the Helper plasmid. Depending on the rAAV purification method, 0.01 % to 0.07 % contaminating Helper DNA has been found [33]. This can reduce vector potency and is therefore undesirable in rAAV preparations. Staying with the well-established production system in HEK293 cells, we describe the generation and characterization of a new mammalian cell line providing all necessary adenoviral elements. By eliminating the need of transfecting the Helper plasmid and simultaneously reducing the DNA amount for successful rAAV production, this cell line offers a significant time and cost advantage compared to the use of the parental HEK293 cell line.

rAAV production in HEK293 is classified as biosafety level 1 work in many countries. We assume that a stable HEK293-Ad-helper cell line does not change this assessment. The risk of the generation of a replicative adenovirus or a replicative AAV is not altered whether the adenoviral helper genes are maintained on plasmids or within the genome. Late adenoviral genes required for adenovirus capsid assembly are nonexistent in either system and the risk of unintended recombination or contamination of the culture with other viruses remains at the same level. One could even speculate that recombination events are rarer due to the genomic fixation. Furthermore, the remaining two plasmid system is unchanged disallowing production of replication competent wtAAV, because ITRs and RepCap genes are separated.

The HEK293-KARE1 cell line described here was generated using linear, dephosphorylated DNA. This allowed for a random integration of the construct into the genome. Integration can cause dysregulation or impede the expression of endogenous genes leading to cell death. Surviving cells can show different levels

of the transgene product as the expression is strongly influenced by the surrounding genomic structure. A cell line that highly expresses adenoviral genes could show an inhibited cell growth or high mortality as seen for HEK293-KARE1d. These potential problems might also explain why a directed integration via CRISPR/Cas9 that we previously attempted at a predetermined locus did fail.

Integration of adenoviral elements was proven by PCR for all clones. Analysis of cell growth and cell cycle progression revealed, that for all isolated clones the effect of transgene expression was not significant. The slower growth rate seen for HEK293-KARE1b in Figure 2C might be explained by the initial higher cell density limiting growth after 72 h or indeed by impeded growth. In comparison with the parental HEK293 cell line, growth characteristics of the other KARE clones were nearly equivalent suggesting that an adaptation to suspension and subsequent culturing without serum is possible. This would open new chances for a large-scale production of rAAVs, e.g. in a bioreactor.

The mRNA expression level of E2A and E4 was shown to be elevated compared to the parental HEK293 cell line. To our knowledge, the helper-gene dose required for highly efficient AAV production is not known. Expression of early adenoviral genes is controlled by several promoters starting from the E1A promoter. Upon E1A expression the promoters of E1B, E2, E3 and E4 become active [39]. The strength of the promoter and thus the transcription of mRNA can differ between adenoviral elements, even when all parts are integrated at the same genomic site. The observed relative expression levels were expected, as high E2A expression would compromise cell growth. Previous work showed that a high level of E2A in presence of E1 proteins can have toxic effects on cells [32].

All HEK293-KARE1 clones were analyzed for their ability to produce virus in a two-plasmid system. Transfecting a RepCap plasmid offers the opportunity to change parts of the capsid and the packaged DNA and thus provides the user with maximum flexibility. In comparison to the parental HEK293 cell line, all clones show a high capacity to produce rAAV. We observed during our experiments that the HEK293-KARE1 cell lines require more time to adapt to growth conditions after cryopreservation. For this reason, we believe that at later passages cells were better adapted and yielded in higher titer. To a lower extent we observed the influence on cell adaptation also for HEK293 cells. Adjusting transfection conditions and DNA ratios for HEK293-KARE1c increased the overall titer. These results demonstrate that the low mRNA levels of E2A and E4 support rAAV manufacturing. HEK293-KARE1c was chosen for a larger scale production with subsequent rAAV purification using a well-established purification protocol. These rAAV2 particles showed the expected ratio between genomic and transducing titer as it was known from the three-plasmid system [37]. The rAAV yield was in the range of 3.2×10^4 to 8.4×10^4 GC per cell (Fig. 4B). For similar small-scale experiments with HEK293 cells, albeit in a commercial context, a value of 8.3×10^4 GC per cell has been reported [40]. Other groups determined that the choice of primers and the reference material for qPCR (circular, linear DNA) have a tremendous effect on the genomic titers [41, 42].Specifically, ITR primers compared to primers binding the gene of interest yielded up to ten times higher genomic copies when plasmids were used as reference. We would like to mention that we used primers binding the hGHpA region whereas in literature primers binding the ITR region have been applied and both experiments used plasmid DNA as reference [40].

Also size and shape of the produced viral particles, as detected by AFM, are in good agreement with traditionally produced rAAV. Hence, the quality of rAAVs produced using the novel cell line is equivalent.

This cell line also opens up the new possibility for experiments that require a wild-type intermediate step, e.g. directed evolution of rAAV. Directed evolution requires the presence of either a wild-type rAAV or the helper genes to allow for amplification of the viral particles. The HEK293-KARE cell line facilitates this method, since neither wild type virus nor transfections have to be used.

Conclusions

For efficient AAV vector production a self-sufficient packaging cell line was created. Based on previous work by others the adenoviral genes VA RNA, E2A and E4orf6 were stably integrated in HEK293 cells in addition to the already present genes E1A and E1B19K. We demonstrated that the resulting HEK293-KARE1c cell line provides a cost-efficient production platform for rAAV2, because a helper plasmid is no longer required. This means not only higher safety, but also the necessity of their time-consuming production and purification. It also offers a streamlined method for the directed evolution approaches.

. The simplified production and the final quality of the preparations show the potential of stably transfected cell lines. We assume that our approach can be combined with other stable transfection strategies such as the integration of the ITR plasmid or the RepCap plasmid open up avenues for inexpensive and safe large scale rAAV production. An adaption to suspension will allow large scale production of rAAVs, e.g. in a bioreactor

Methods

Plasmids. The gene for blasticidin S deaminase of *Aspergillus terreus* was amplified from pcDNA6/myc-His (Thermo Fisher Scientific, Cat. No. V22120; sequence available from the vendor's website), without designated promoter and poly(A) signal, using the primers bsd-SalI (5'-AAAAAAGTCG ACGTTTAAA*C GGATCTGATC AGCACGTGTT*-3') and bsd-NdeI (5'-AAAAAACATA TG*ATCTCGTA GCACGTGTCA GT*-3'), which introduced the underlined SalI and NdeI restriction sites. For better comprehensibility the hydrizinding area is italicized. The digested insert was ligated to the likewise opened pHelper plasmid (GenBank: AF369965.1) resulting in pHelper-BSD (see Additional File). Successful cloning was confirmed by Sanger DNA sequencing (Sequencing Core Facility, CeBiTec, Bielefeld, Germany).

Plasmids for viral particle production were based on a pSB1C3 backbone and were assembled using the iGEM RFC10 BioBrick assembly standard [43]. pZMB0216_Rep_VP123_453_587wt_p5tataless contains a genetically modified *rep/cap* similar to one encoded in pAAV-RC (Genbank Accession number: AF369963.1). In the ITR containing plasmid pZMB0522_ITR_EXS_CMV_mVenus_hGHpA, a CMV promoter expresses the fluorescent protein mVenus. Plasmids are described in detail by Feiner et. al [submitted 2019].

Cell Culture. HEK293 (ACC-305, DSMZ) and HT-1080 (ACC-315, DSMZ) were cultured in DMEM (Sigma Aldrich) supplemented with 10 % fetal calf serum (v/v) (FCS, Sigma Aldrich) and 1 % penicillin/streptomycin (v/v) (P/S, Sigma Aldrich) further called DMEM growth medium. The genomic profile of these cells was frequently verified using STR analysis.

HEK293-Ad-helper cell line generation. The pHelper-BSD plasmid was linearized with SalI and dephosphorylated. 9×10^6 HEK293 cells were seeded on a 150 mm^2 T-flask one day before transfection. A total of 45 µg plasmid DNA of pHelper-BSD was transfected using calcium phosphate. Three days after transfection 10 µg/ml of the antibiotic blasticidin (BSD, Sigma Aldrich) was added for selective pressure. Culture medium (DMEM, 10 % FCS, 1% P/S, 10 µg/ml BSD) was changed every second day until cell growth was observable (approximately two weeks). Cells were trypsinized and subjected to limiting dilution on a 96-well plate. From this point on, cells were cultured in DMEM growth medium with 5 µg/ml BSD. Growth of single cell colonies was observed after about two additional weeks. Single cell colonies were subcultured and characterized for the integration of the adenoviral elements.

Analysis of genomic integration. Genomic DNA from subcultured monoclonal cell clones was isolated by Chelex 100 (Bio-Rad) extraction. 2.5×10^6 cells were centrifuged (1 min 10000×g) and washed with PBS. The pellet was resuspended in 100 µl Chelex suspension (5 % w/v), incubated for 30 min at 56 °C, vortexed for 10 s and incubated for 8 min at 100 °C. The solution was centrifuged briefly at approx. 17,000×g and the supernatant was transferred to a new tube. The primer pairs Ad5-for (5'-CAACTCCATG CTTAACAGTC CCCA-3')/Ad5-rev (5'-TCCAGTGCTG CAACCCTGTG TATC-3') and Bsd-for (5'-GGATCTGATC AGCACGTGTT-3')/Bsd-rev (5'-ATCTCGTAGC ACGTGTCAGT-3') are binding on E2A- and bsd-gene, respectively (Figure 1 A) and were used for the PCR reaction. After successful detection of integration four clones were selected and name HEK293-KARE1a to HEK293-KARE1d.

Growth curves. 1×10^5 cells of each clone were seeded in a 12-well plate and incubated under standard conditions. Cells were harvested by trypsinization and resuspended in 1 ml cell culture medium. Samples for viable cell density and viabilities were taken daily and analyzed using an automated cell counting system (CEDEX, Roche Diagnostics). Growth curves were analyzed by exponential fitting with Origin (OriginLab 2018) and population doubling times were calculated.

Cell cycle analysis. 2×10^6 cells were harvested by trypsinization and washed with ice-cold PBS. Briefly, cells were resuspended in 500 µl ice-cold PBS before 500 µl 2 % (w/v) paraformaldehyde was added to the solution. The mixture was stored 1 h on ice before washing with ice-cold PBS and resuspension in 1 ml ice-cold 70 % ethanol. Samples were taken daily and stored at -20 °C for 5-7 days. After permeabilization cells to be analyzed by flow cytometry were washed with PBS before treatment with 1 ml staining solution (100 µg/ml RNase A (AppliChem) and 30 µg/ml propidium iodide (AppliChem)) in PBS at 37 °C for 30 min in the dark. Measurements of samples were performed on a Becton-Dickenson FACSCalibur. 10,000 counted events were analyzed with the software ModFit LT (Verity House Software).

RNA isolation and quantitative RT-PCR. Total cellular RNA from HEK293 and HEK293-KARE1 clones was isolated using Trizol reagent (Invitrogen) according to the instructions by the manufacturer. 1 µg of RNA

was subsequently digested by 1 U DNase I (ThermoFisher Scientific) for 30 min at 37 °C. cDNA was synthesized by oligo(dT)$_{18}$ and Revert Aid M-MuLV reverse transcriptase (ThermoFisher Scientific). Quantitative real-time PCR using GoTaq® qPCR Master Mix (Promega) was performed with a LightCycler 480 II detection system (Roche) according to the manufacturer's protocol. The following primer pairs were used at a 4 µM concentration to detect E1A (forward primer: 5'-AACCAGTTGC CGTGAGAGTTG-3'; reverse primer: 5'-CTCGTTAAGC AAGTCCTCGA TACAT-3'), E2A (forward primer: 5'-TCAGGCACAA CCATCCGCGG-3'; reverse primer 5'-GGTCGGGCGC CGATATCTTGA-3') and E4 (forward primer: 5'-GAACCCTAGT ATTCAACCTG CCAC-CTCCC-3'; reverse primer: 5'- CCACACGGTT TCCTGTCGAGCC-3'). All samples were run in triplicate. Ct values of technical replicates were averaged and averages were used for further calculations. The relative expression ΔΔCt of E2A and E4 in HEK293-KARE1 cells was calculated from the differences in HEK293 and HEK293-KARE1a to HEK293-KARE1c after normalizing to E1A gene expression (ΔΔCt=Ct(Gene$^{HEK293\text{-}KARE}$)-Ct(E1A$^{HEK293\text{-}KARE}$)-[Ct(Gene^{HEK293})-Ct(E1A^{HEK293})]).

Viral particles production and purification. HEK293-KARE1 cells were seeded at a density of 3×10^6 cells per 100 mm dish the day before transfection. On the day of transfection, a total amount of 15 µg DNA per 100 mm dish of pSB1C3_001-RepCap^{587WT} (pZMB0216) and pUC19bb-CMV_mVenus_hGH-pA (pZMB0522) was transfected using the calcium-phosphate method. The DNA was added to 0.5 ml 0.3 M $CaCl_2$ and added dropwise to 0.5 ml of 2× HBS buffer (50 mM HEPES pH 7.05, 1.5 mM Na_2HPO_4, 280 mM NaCl). The transfection solution was mixed well and added immediately to the cells. After 72 h incubation at 37 °C the cells were harvested and separated from the medium by centrifugation (900×g, 5 min). The cell pellet was subjected to three freeze-thaw cycles by alternating between liquid nitrogen and a 37 °C water bath. After Benzonase (50 U/ml, Sigma Aldrich) treatment at 37 °C for 30 min, the lysate was clarified via centrifugation at 3,000×g, 10 min. The crude lysate was added to a discontinuous iodixanol gradient (Progen Biotechnik GmbH) of 60 %, 40 %, 25 % and 15 % iodixanol in an open top polyallomer 16 × 76 mm tube (Science Services) using a syringe equipped with a 23G x 3 1/8" injection needle as described in literature [44]. Tubes were sealed with cap assemblies and centrifuged in a T-880 rotor (Sorvall) at 340,000×g for 4 h at 18 °C. The fraction containing viral particles was collected with a 21G x 1 1/2" injection needle from the bottom of the tube and the buffer was exchanged to 1× HBSS (Sigma Aldrich) via an Amicon Ultra-4 100K ultrafiltration unit.

Optimized viral particles production. HEK293-KARE1c cells were seeded as described before in DMEM without BSD. On the day of transfection, a total amount of 7.4 µg DNA per 100 mm dish of pSB1C3_001-RepCap^{587WT} (pZMB0216) and pUC19bb-CMV_mVenus_hGH-pA (pZMB0522) in a molar ratio of 1:1 was used. The DNA was added to 0.25 ml 0.3 M $CaCl_2$ and added dropwise to 0.25 ml of 2× HBS buffer. The transfection solution was mixed well and added immediately to the cells. After a 72 h incubation at 37 °C cells were harvested and processed as described in viral particles production and purification.

Determination of genomic titers. Genomic titers of viral particles were determined via quantitative real-time PCR (qPCR). An aliquot of rAAV containing sample (5 µl) was incubated with 4 U DNase I (NEB) at 37 °C for 30 min followed by a 20 min heat inactivation at 75 °C. In the qPCR reaction 5 µl of a fivefold dilution of the DNase I digest was mixed with 5 µl primer-mix at a final concentration of 4 µM (qPCR-hGH-for: 5'-

CTCCCCAGTG CCTCTCCT-3' / qPCR-hGH-rev: 5'-ACTTGCCCCT TGCTCCATAC-3') and 2x GoTaq qPCR Mastermix (Promega) to a final volume of 20 µl. The reaction was carried out as described by the manufacturers protocol using a LightCycler 480 II system (Roche Life Science). The genomic titer was calculated from a standard curve of 10 to 10^6 copies of the ITR plasmid (pZMB0522) with an efficiency between 90-110 % and an R value less than 0.1 (mean squared error of the single data points fit to the regression line). Genomic titers in crude lysates were estimated from a standard curve mixed with the same amount of a non-transfected cell lysate. Since DNase I is partially inhibited in the presence of cell debris a small plasmid background can remain. All samples were processed identically in technical triplicates.

Transduction assay. Functionality of purified rAAV2 preparations was analyzed by transduction of HT-1080 cells with a vector plasmid coding for the fluorescence reporter mVenus (pZMB0522). 10,000 cells were seeded on a 12-well plate and after cells had settled a serial dilution of viral particles was applied to each well. Cells were detached by trypsinization for flow cytometry analysis. 10,000 events were counted using a Becton-Dickenson FACSCalibur instrument. Data sets were analyzed using Flowing Software 2.5.1. Positive cells were gated above the 99 % interval of the negative control.

Atomic force microscopy. AFM measurements were performed on a Multimode 8 AFM (Bruker, Santa Barbara, CA, USA) with Tap300Al-G cantilevers (BudgetSensors, Sofia, Bulgaria) in tapping mode in air. 2 µl sample of UC purified rAAV2 from HEK293-KARE1c was spotted onto freshly cleaved mica for 1 min before it was rinsed three times with distilled water and dried under a gentle nitrogen flow. Data analysis was performed with Gwyddion 2.48. Obtained images were treated with offset and plane correction algorithms and the size of visualized particles was measured at half maximum particle height.

List of abbreviations

rAAV: recombinant Adeno-associated virus

Ad5: Adenovirus type 5

qPCR: quantitative polymerase chain reaction

hGH: human Growth hormone

BSD: blasticidin

ORF: Open reading frame

ITR: Inverted terminal repeat

Declarations

Ethics approval and consent to participate

Not applicable

Consent for publication

Not applicable

Availability of data and material

All data generated or analyzed during this study are included in this published article.

Competing interests

The authors declare that they have no competing interests.

Funding

We acknowledge support of the publication fee by Deutsche Forschungsgemeinschaft and the Open Access Publication Funds of Bielefeld University. This work was supported by Bielefeld University.

Authors' contributions

All authors were involved in the design of this study. JT and KT generated the cell line. RF performed the experiments to characterize the cell line. KT analyzed and optimized rAAV production. RF, KT and KM wrote the manuscript. All authors read and approved the final manuscript.

Acknowledgements

We thank Marco Radukic for cloning of pHelper-BSD and Philipp Borchert for experimental assistance.

References

1. Grieger JC, Soltys SM, Samulski RJ. Production of Recombinant Adeno-associated Virus Vectors Using Suspension HEK293 Cells and Continuous Harvest of Vector From the Culture Media for GMP FIX and FLT1 Clinical Vector. Mol Ther. 2016;24:287–97.

2. Wu Z, Asokan A, Samulski RJ. Adeno-associated virus serotypes: vector toolkit for human gene therapy. Mol Ther. 2006;14:316–27.

3. Hagen S, Baumann T, Wagner HJ, Morath V, Kaufmann B, Fischer A, et al. Modular adeno-associated virus (rAAV) vectors used for cellular virus-directed enzyme prodrug therapy. Sci Rep. 2014;4:3759.

4. Srivastava A. In vivo tissue-tropism of adeno-associated viral vectors. Curr Opin Virol. 2016;21:75–80.

5. Miyake K, Miyake N, Yamazaki Y, Shimada T, Hirai Y. Serotype-independent method of recombinant adeno-associated virus (AAV) vector production and purification. J Nippon Med Sch. 2012;79:394–402.

6. Richardson WD, Westphal H. A cascade of adenovirus early functions is required for expression of adeno-associated virus. Cell. 1981;27 1 PART 2:133–41.

7. Matsushita T, Elliger S, Elliger C, Podsakoff G, Villarreal L, Kurtzman GJ, et al. Adeno-associated virus vectors can be efficiently produced without helper virus. Gene Ther. 1998;5:938–45.

8. Xiao X, Li J, Samulski RJ. Production of high-titer recombinant adeno-associated virus vectors in the absence of helper adenovirus. J Virol. 1998;72:2224–32.

9. Louis N, Evelegh C, Graham FL. Cloning and sequencing of the cellular-viral junctions from the human adenovirus type 5 transformed 293 cell line. Virology. 1997;233:423–9.

10. Lin Y-C, Boone M, Meuris L, Lemmens I, Van Roy N, Soete A, et al. Genome dynamics of the human embryonic kidney 293 lineage in response to cell biology manipulations. Nat Commun. 2014;5:4767.

11. Graham FL, Smiley J, Russell WC, Nairn R. Characteristics of a human cell line transformed by DNA from human adenovirus type 5. J Gen Virol. 1977;36:59–74.

12. Lowe SW, Ruley HE. Stabilization of the p53 tumor suppressor is induced by adenovirus-5 E1A and accompanies apoptosis. Genes Dev. 1993;7:535–45.

13. Colosi P. Patent US 6,004,797 Adenovirus helper-free recombinant AAV Virion production. 1999.

14. Chang LS, Shi Y, Shenk T. Adeno-associated virus P5 promoter contains an adenovirus E1A-inducible element and a binding site for the major late transcription factor. J Virol. 1989;63:3479–88.

15. Duan D, Sharma P, Dudus L, Zhang Y, Sanlioglu S, Yan Z, et al. Formation of adeno-associated virus circular genomes is differentially regulated by adenovirus E4 ORF6 and E2a gene expression. J Virol. 1999;73:161–9.

16. Sarnow P, Hearing P, Anderson CW, Halbert DN, Shenk T, Levine AJ. Adenovirus early region 1B 58,000-dalton tumor antigen is physically associated with an early region 4 25,000-dalton protein in productively infected cells. J Virol. 1984;49:692–700.

17. Querido E, Marcellus RC, Lai A, Charbonneau R, Teodoro JG, Ketner G, et al. Regulation of p53 levels by the E1B 55-kilodalton protein and E4orf6 in adenovirus-infected cells. J Virol. 1997;71:3788–98.

18. Akusjärvi G, Svensson C, Nygård O. A mechanism by which adenovirus virus-associated RNAI controls translation in a transient expression assay. Mol Cell Biol. 1987;7:549–51.

19. Janik JE, Huston MM, Cho K, Rose JA. Efficient synthesis of adeno-associated virus structural proteins requires both adenovirus DNA binding protein and VA I RNA. Virology. 1989;168:320–9.

20. Grimm D, Kay MA, Kleinschmidt JA. Helper virus-free, optically controllable, and two-plasmid-based production of adeno-associated virus vectors of serotypes 1 to 6. Mol Ther. 2003;7:839–50.

21. Grieger JC, Choi VW, Samulski RJ. Production and characterization of adeno-associated viral vectors. Nat Protoc. 2006;1:1412–28.

22. Sonntag F, Schmidt K, Kleinschmidt JA. A viral assembly factor promotes AAV2 capsid formation in the nucleolus. Proc Natl Acad Sci U S A. 2010;107:10220–5.

23. Sonntag F, Köther K, Schmidt K, Weghofer M, Raupp C, Nieto K, et al. The assembly-activating protein promotes capsid assembly of different adeno-associated virus serotypes. J Virol. 2011;85:12686–97.

24. Cao M, Chiriva-Internati M, Hermonat PL. AAV2 X increases AAV6 rep/cap-driven rAAV production. Virology. 2015;482:84–8.

25. Cao M, You H, Hermonat PL. The X gene of adeno-associated virus 2 (AAV2) is involved in viral DNA replication. PLoS One. 2014;9:e104596.

26. Yan Z, Zak R, Zhang Y, Engelhardt JF. Inverted terminal repeat sequences are important for intermolecular recombination and circularization of adeno-associated virus genomes. J Virol. 2005;79:364–79.

27. Schnödt M, Schmeer M, Kracher B, Krüsemann C, Espinosa LE, Grünert A, et al. DNA Minicircle Technology Improves Purity of Adeno-associated Viral Vector Preparations. Mol Ther Acids. 2016;5:e355.

28. Clark KR, Voulgaropoulou F, Fraley DM, Johnson PR. Cell lines for the production of recombinant adeno-associated virus. Hum Gene Ther. 1995;6:1329–41.

29. Qiao C, Li J, Skold A, Zhang X, Xiao X. Feasibility of generating adeno-associated virus packaging cell lines containing inducible adenovirus helper genes. J Virol. 2002;76:1904–13.

30. Nakamura S, Nakamura R, Shibata K, Kobayashi M, Sahara N, Shigeno K, et al. Development of packaging cell lines for generation of adeno-associated virus vectors by lentiviral gene transfer of trans-complementary components. Eur J Haematol. 2004;73:285–94.

31. Yuan Z, Qiao C, Hu P, Li J, Xiao X. A versatile adeno-associated virus vector producer cell line method for scalable vector production of different serotypes. Hum Gene Ther. 2011;22:613–24.

32. Klessig DF, Grodzicker T, Cleghon V. Construction of human cell lines which contain and express the adenovirus DNA binding protein gene by cotransformation with the HSV-1 tk gene. Virus Res. 1984;1:169–88.

33. Lecomte E, Tournaire B, Cogné B, Dupont JB, Lindenbaum P, Martin-Fontaine M, et al. Advanced characterization of DNA molecules in rAAV vector preparations by single-stranded virus next-generation sequencing. Mol Ther - Nucleic Acids. 2015;4:e260.

34. Mohammadi ES, Ketner EA, Johns DC, Ketner G. Expression of the adenovirus E4 34k oncoprotein inhibits repair of double strand breaks in the cellular genome of a 293-based inducible cell line. Nucleic Acids Res. 2004;32:2652–9.

35. Grifman M, Chen NN, Gao G p, Cathomen T, Wilson JM, Weitzman MD. Overexpression of cyclin A inhibits augmentation of recombinant adeno-associated virus transduction by the adenovirus E4orf6 protein. J Virol. 1999;73:10010–9.

36. Jordan M, Wurm F. Transfection of adherent and suspended cells by calcium phosphate. Methods. 2004;33:136–43.

37. Zeltner N, Kohlbrenner E, Clément N, Weber T, Linden RM. Near-perfect infectivity of wild-type AAV as benchmark for infectivity of recombinant AAV vectors. Gene Ther. 2010;17:872–9.

38. Chen H. Comparative observation of the recombinant adeno-associated virus 2 using transmission electron microscopy and atomic force microscopy. Microsc Microanal. 2007;13:384–9.

39. Berk AJ. Adenovirus promoters and E1A transactivation. Annu Rev Genet. 1986;20:45–79.

40. Rego M, Hanley LM, Ersing I, Guerin K, Tasissa M, Haery L, et al. Improved yield of AAV2 and rAAV2-retro serotypes following sugar supplementation during the viral production phase. bioRxiv. 2018;:488585.

41. Furuta-Hanawa B, Yamaguchi T, Uchida E. 2D droplet digital PCR as a tool for titration and integrity evaluation of recombinant adeno-associated viral vectors. Hum Gene Ther Methods. 2019;:hgtb.2019.031.

42. Wang F, Cui X, Wang M, Xiao W, Xu R. A reliable and feasible qPCR strategy for titrating AAV vectors. Med Sci Monit Basic Res. 2013;19:187–93.

43. Shetty RP, Endy D, Knight TF. Engineering BioBrick vectors from BioBrick parts. J Biol Eng. 2008;2:5.

44. Zolotukhin S, Byrne BJ, Mason E, Zolotukhin I, Potter M, Chesnut K, et al. Recombinant adeno-associated virus purification using novel methods improves infectious titer and yield. Gene Ther. 1999;6:973–85.

Figures/Figure Legends

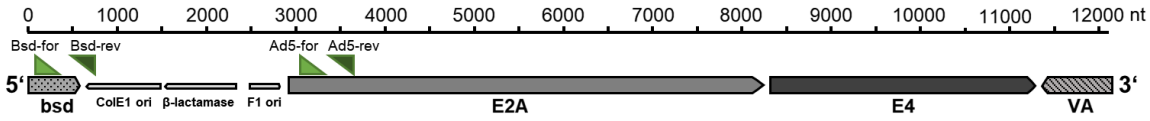

Figure 1: Integration of adenoviral elements into HEK293. Scheme of the linearized helper plasmid after restriction digest with SalI. The blasticidin resistance gene *bsd* is located at the 5'-end. PCR primer positions are marked with green triangles.

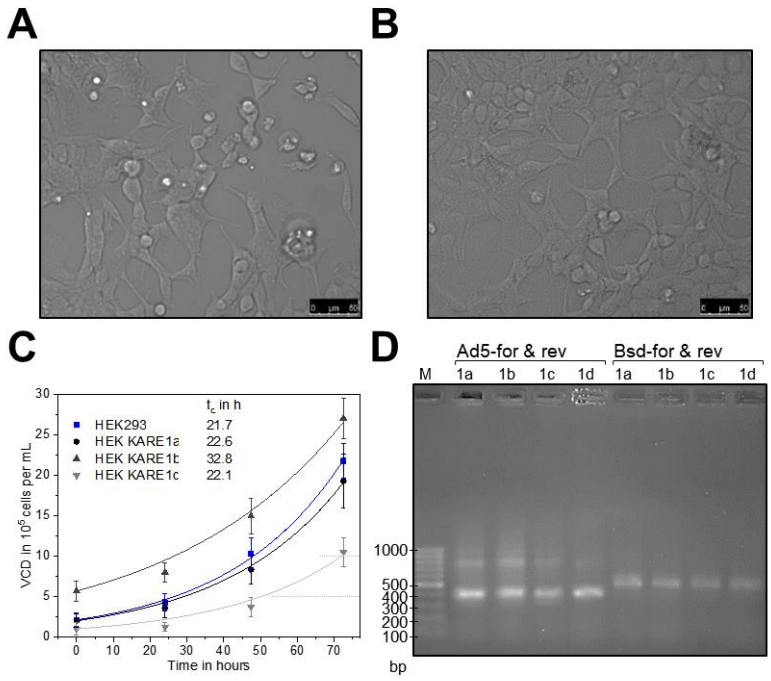

Figure 2: Analysis of cell morphology and growth. (A, B) Comparison of cell morphology in bright field images of (A) HEK293-KARE1c and (B) HEK293. The morphology of HEK293-KARE1c looks similar to the one of the parental HEK293 cell line. (C) Growth curves of HEK293-KARE1 clones and HEK293 were recorded. Cells were seeded on a 12-well plate and harvested after the indicated incubation time. Viable cell density and viabilities were analyzed using an automated cell counting system (CEDEX, Roche Diagnostics). Doubling times t_d were calculated from an exponential fit with Origin 2018 (OriginLab) and are given in the inset of the graph. (D) Agarose gel of the PCR analysis of pHelper-BSD integration. Genomic DNA of the four clones HEK293-KARE1a to HEK293-KARE1d probed by PCR using the primer pairs given above each lane.

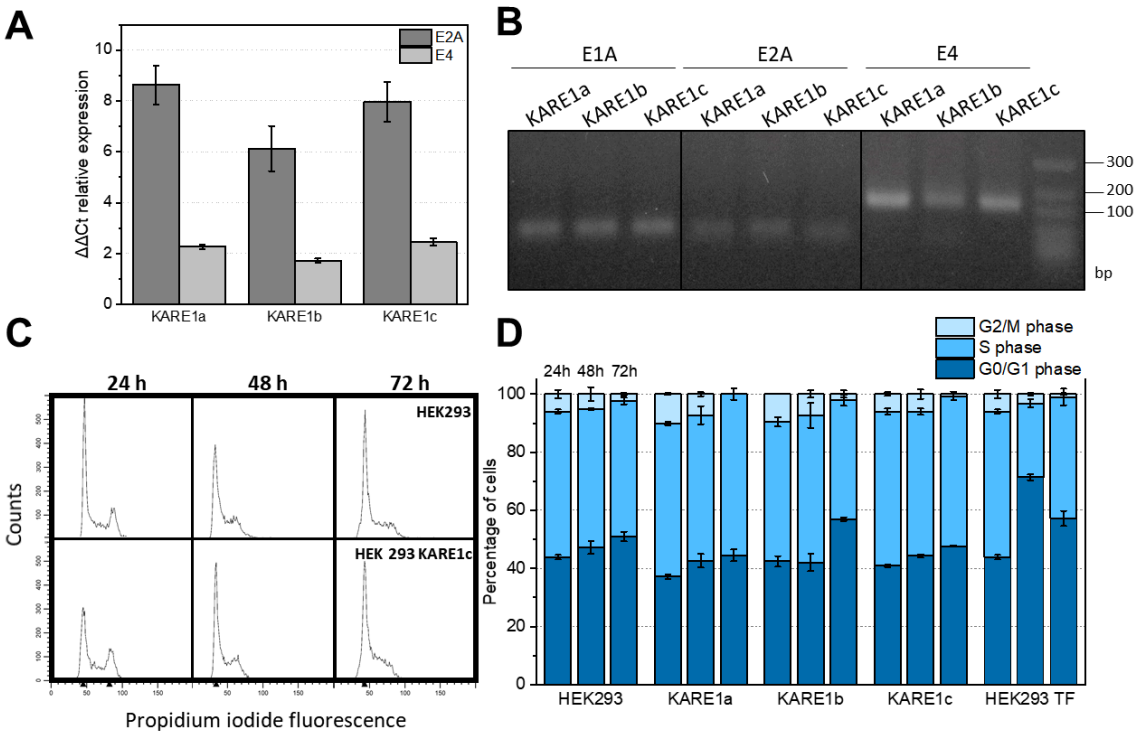

Figure 3: Analysis of adenoviral elements expression and their effect on the cell cycle of HEK293-KARE cell lines. (A) RNA was isolated from HEK293 and HEK293-KARE1 cells. The mRNA levels of E2A and E4 were determined by RT-qPCR, the error bars represent the standard deviation from three technical replicates. ΔΔCt values were calculated from the difference between expression in HEK293 and HEK293-KARE1 cells after normalizing to E1A gene expression. (B) Agarose gel from qPCR products for HEK293-KARE1-clones. (C, D) Effects of adenoviral early genes on cell cycle progression. (C) The DNA content of cells (exemplary for HEK293, HEK293-KARE1c) was measured after propidium iodide staining by flow cytometry at defined time points (24 h, 48 h, 72 h). In total 10,000 events were counted. (D) Percentage of cells in different cell cycle phases are presented for each cell line. HEK293 TF represent triple-transfected HEK293 cells for AAV production. Transfection was carried out 24 hours after seeding. This latter analysis was done based on cells gated for mVenus production present on the ITR plasmid. The flow cytometry data were analyzed with ModFit LT (Verity Software House).

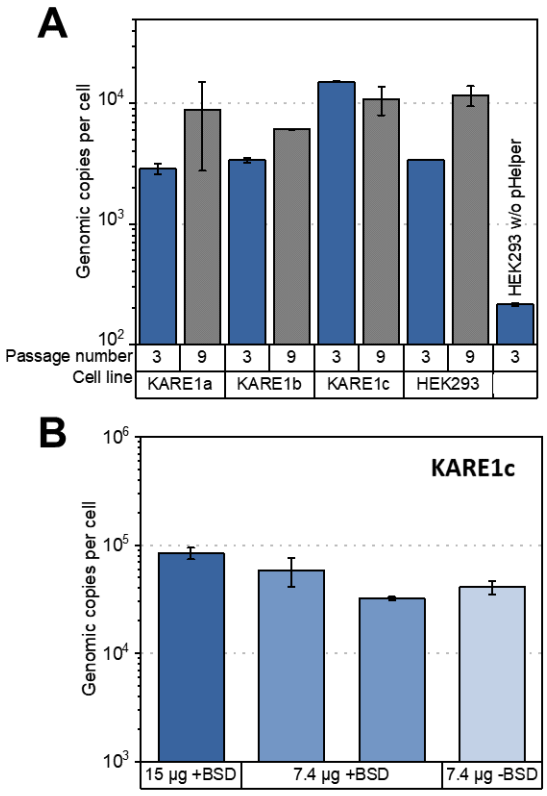

Figure 4: Analysis of rAAV2 production in HEK293-KARE1 and HEK293 cells at passage three and nine after cryopreservation. (A) HEK293-KARE1 cells (1×100 mm dish) were transfected with ITR-plasmid and RepCap-plasmid, for HEK293 the pHelper was included. Three days after transfection rAAV yield was determined from crude cell lysate after three freeze-thaw cycles by qPCR. A molar ratio of 1:1 of the plasmids Rep-Cap:ITR was used during this experiment. For HEK293 cells experiments were performed also with a plasmid ratio of 1:1:1 for pHelper:RepCap:ITR. (B) Comparison of rAAV production in HEK293-KARE1c cells depending on15 µg transfection protocol and the optimized 7.4 µg transfection protocol. rAAV2 yield was quantified in crude lysates by qPCR. In general, RepCap and ITR plasmid were transfected in a molar 1:1 ratio.

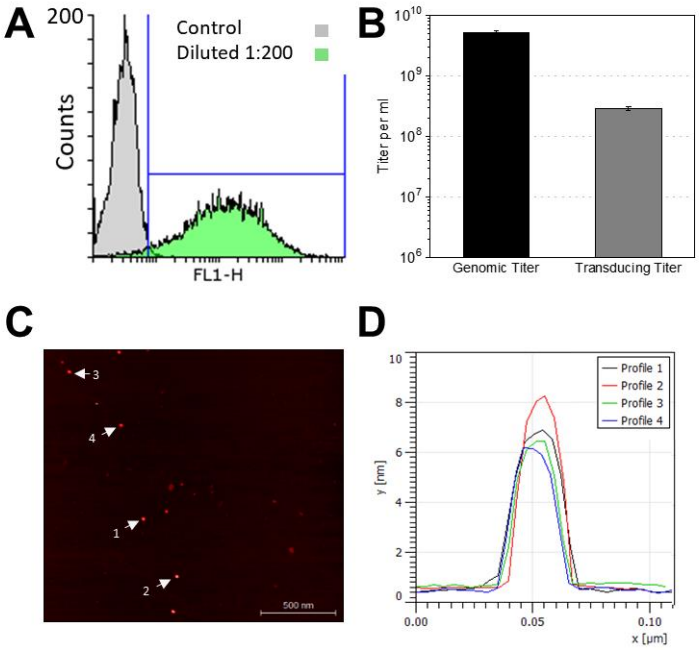

Figure 5: Characterization of rAAV2. Viral particles were produced in the HEK293-KARE1c cell line seeded in ten 100 mm dishes and subsequently purified via iodixanol ultracentrifugation. (A) Determination of transduction ability of rAAV (1:200 diluted sample) on HT-1080 cells using expression of the mVenus gene measured by flow cytometry of 10,000 cells in total. (B) The amount of DNase I-resistant particles was determined by qPCR from a standard curve of the ITR-plasmid. The total volume of the final viral sample was 2.5 ml. The transducing titer was determined based on percent of fluorescent cells as depicted in panel A (see methods). (C, D) rAAV were visualized by atomic force microscopy and resulting particle height profiles were determined. A mean diameter of 21.5 ± 1.8 nm was measured at half maximum height of 8 particles.

Additional File

HEK293-KARE1, a cell line with stably integrated adenovirus helper sequences simplifies rAAV production

Rebecca C. Feiner[1,†], Kathrin E. Teschner[1,†], Julian Teschner[1],Kristian M. Müller[1,*],

† Both authors contributed equally to this work.

[1] Cellular and Molecular Biotechnology, Faculty of Technology, Bielefeld University, Bielefeld, Germany

[*]Corresponding author information (Address; Email; Phone)

Kristian M. Müller, Cellular and Molecular Biotechnology, Faculty of Technology, Bielefeld University, Universitätsstraße 25, 33615 Bielefeld, Germany; Email: kristian@syntbio.net; Tel. +49-521-106-6323

SI Table 1: Raw data of E1A mRNA analysis from three independent qRT-PCR experiments. mRNA samples were isolated from cells directly before the experiment.

	Ct (1)	Ct (2)	Ct (3)
Kare1a	19.22	15.01	15.78
Kare1b	18.98	14.55	15.80
Kare1c	19.70	14.95	15.76
HEK293	19.22	15.89	15.77

Sequence information for pHelper-BSD

```
   1 ggtacccaac tccatgctta acagtcccca ggtacagccc accctgcgtc gcaaccagga
  61 acagctctac agcttcctgg agcgccactc gccctacttc cgcagccaca gtgcgcagat
 121 taggagcgcc acttcttttt gtcacttgaa aaacatgtaa aaataatgta ctaggagaca
 181 ctttcaataa aggcaaatgt ttttatttgt acactctcgg gtgattattt acccccccacc
 241 cttgccgtct gcgccgttta aaaatcaaag gggttctgcc gcgcatcgct atgcgccact
 301 ggcagggaca cgttgcgata ctggtgttta gtgctccact taaactcagg cacaaccatc
 361 cgcggcagct cggtgaagtt ttcactccac aggctgcgca ccatcaccaa cgcgtttagc
 421 aggtcgggcg ccgatatctt gaagtcgcag ttggggcctc cgccctgcgc gcgcgagttg
 481 cgatacacag ggttgcagca ctggaacact atcagcgccg ggtggtgcac gctggccagc
 541 acgctcttgt cggagatcag atccgcgtcc aggtcctccg cgttgctcag ggcgaacgga
 601 gtcaactttg gtagctgcct tcccaaaaag ggtgcatgcc caggctttga gttgcactcg
 661 caccgtagtg gcatcagaag gtgaccgtgc ccggtctggg cgttaggata cagcgcctgc
```

```
 721 atgaaagcct tgatctgctt aaaagccacc tgagcctttg cgccttcaga gaagaacatg
 781 ccgcaagact tgccggaaaa ctgattggcc ggacaggccg cgtcatgcac gcagcacctt
 841 gcgtcggtgt tggagatctg caccacattt cggccccacc ggttcttcac gatcttggcc
 901 ttgctagact gctccttcag cgcgcgctgc ccgttttcgc tcgtcacatc catttcaatc
 961 acgtgctcct tatttatcat aatgctcccg tgtagacact taagctcgcc ttcgatctca
1021 gcgcagcggt gcagccacaa cgcgcagccc gtgggctcgt ggtgcttgta ggttacctct
1081 gcaaacgact gcaggtacgc ctgcaggaat cgccccatca tcgtcacaaa ggtcttgttg
1141 ctggtgaagg tcagctgcaa cccgcggtgc tcctcgttta gccaggtctt gcatacggcc
1201 gccagagctt ccacttggtc aggcagtagc ttgaagtttg cctttagatc gttatccacg
1261 tggtacttgt ccatcaacgc gcgcgcagcc tccatgccct tctcccacgc agacacgatc
1321 ggcaggctca gcgggtttat caccgtgctt tcactttccg cttcactgga ctcttccttt
1381 tcctcttgcg tccgcatacc ccgcgccact gggtcgtctt cattcagccg ccgcaccgtg
1441 cgcttacctc ccttgccgtg cttgattagc accggtgggt tgctgaaacc caccatttgt
1501 agcgccacat cttctctttc ttcctcgctg tccacgatca cctctgggga tggcgggcgc
1561 tcgggcttgg gagaggggcg cttctttttc ttttggacg caatggccaa atccgccgtc
1621 gaggtcgatg gccgcgggct gggtgtgcgc ggcaccagcg catcttgtga cgagtcttct
1681 tcgtcctcgg actcgagacg ccgcctcagc cgcttttttg ggggcgcgcg gggaggcggc
1741 ggcgacggcg acggggacga cacgtcctcc atggttggtg gacgtcgcgc cgcaccgcgt
1801 ccgcgctcgg gggtggtttc gcgctgctcc tcttcccgac tggccatttc cttctcctat
1861 aggcagaaaa agatcatgga gtcagtcgag aaggaggaca gcctaaccgc ccccttgag
1921 ttcgccacca ccgcctccac cgatgccgcc aacgcgccta ccaccttccc cgtcgaggca
1981 cccccgcttg aggaggagga agtgattatc gagcaggacc caggttttgt aagcgaagac
2041 gacgaggatc gctcagtacc aacagaggat aaaaagcaag accaggacga cgcagaggca
2101 aacgaggaac aagtcgggcg gggggaccaa aggcatggcg actacctaga tgtgggagac
2161 gacgtgctgt tgaagcatct gcagcgccag tgcgccatta tctgcgacgc gttgcaagag
2221 cgcagcgatg tgcccctcgc catagcggat gtcagccttg cctacgaacg ccacctgttc
2281 tcaccgcgcg taccccccaa acgccaagaa aacggcacat gcgagcccaa cccgcgcctc
2341 aacttctacc ccgtatttgc cgtgccagag gtgcttgcca cctatcacat ctttttccaa
2401 aactgcaaga taccctatc ctgccgtgcc aaccgcagcc gagcggacaa gcagctggcc
2461 ttgcggcagg gcgctgtcat acctgatatc gcctcgctcg acgaagtgcc aaaaatcttt
2521 gagggtcttg gacgcgacga gaaacgcgcg gcaaacgctc tgcaacaaga aaacagcgaa
2581 aatgaaagtc actgtggagt gctggtggaa cttgagggtg acaacgcgcg cctagccgtg
2641 ctgaaacgca gcatcgaggt cacccacttt gcctacccgg cacttaacct acccccaag
2701 gttatgagca cagtcatgag cgagctgatc gtgcgccgtg cacgacccct ggagagggat
2761 gcaaacttgc aagaacaaac cgaggagggc ctacccgcag ttggcgatga gcagctggcg
2821 cgctggcttg agacgcgcga gcctgccgac ttggaggagc gacgcaagct aatgatggcc
2881 gcagtgcttg ttaccgtgga gcttgagtgc atgcagcggt tctttgctga cccggagatg
2941 cagcgcaagc tagaggaaac gttgcactac acctttcgcc agggctacgt gcgccaggcc
3001 tgcaaaattt ccaacgtgga gctctgcaac ctggtctcct accttggaat tttgcacgaa
3061 aaccgcctcg ggcaaaacgt gcttcattcc acgctcaagg gcgaggcgcg ccgcgactac
3121 gtccgcgact gcgtttactt atttctgtgc tacacctggc aaacggccat gggcgtgtgg
3181 cagcaatgcc tggaggagcg caacctaaag gagctgcaga agctgctaaa gcaaaacttg
3241 aaggacctat ggacggcctt caacgagcgc tccgtggccg cgcacctggc ggacattatc
3301 ttccccgaac gcctgcttaa aaccctgcaa cagggtctgc cagacttcac cagtcaaagc
3361 atgttgcaaa actttaggaa ctttatccta gagcgttcag gaattctgcc cgccacctgc
3421 tgtgcgcttc ctagcgactt tgtgcccatt aagtaccgtg aatgccctcc gccgctttgg
3481 ggtcactgct accttctgca gctagccaac taccttgcct accactccga catcatggaa
3541 gacgtgagcg gtgacggcct actggagtgt cactgtcgct gcaacctatg caccccgcac
3601 cgctccctgg tctgcaattc gcaactgctt agcgaaagtc aaattatcgg taccttgag
3661 ctgcagggtc cctcgcctga cgaaaagtcc gcggctccgg ggttgaaact cactccgggg
3721 ctgtggacgt cggcttacct tcgcaaattt gtacctgagg actaccacgc ccacgagatt
3781 aggttctacg aagaccaatc ccgcccgcca aatgcggagc ttaccgcctg cgtcattacc
3841 cagggccaca tccttggcca attgcaagcc atcaacaaag cccgccaaga gtttctgcta
3901 cgaaagggac gggggggttta cctggacccc cagtccggcg aggagctcaa cccaatcccc
3961 ccgccgccgc agccctatca gcagccgcgg gcccttgctt cccaggatgg cacccaaaaa
4021 gaagctgcag ctgccgccgc cgccacccac ggacgaggag gaatactggg acagtcaggc
4081 agaggaggtt ttggacgagg aggaggagat gatggaagac tgggacagcc tagacgaagc
4141 ttccgaggcc gaagaggtgt cagacgaaac accgtcaccc tcggtcgcat tcccctcgcc
4201 ggcgccccag aaattggcaa ccgttcccag catcgctaca acctccgctc ctcaggcgcc
4261 gccggcactg cctgttcgcc gacccaaccg tagatgggac accactggaa ccagggccgg
4321 taagtctaag cagccgccgc cgttagccca agagcaacaa cagcgccaag gctaccgctc
4381 gtggcgcggg cacaagaacg ccatagttgc ttgcttgcaa gactgtgggg gcaacatctc
4441 cttcgcccgc cgctttcttc tctaccatca cggcgtggcc ttcccccgta acatcctgca
4501 ttactaccgt catctctaca gcccctactg caccggcggc agcggcagcg gcagcaacag
4561 cagcggtcac acagaagcaa aggcgaccgg atagcaagac tctgacaaag cccaagaaat
4621 ccacagcggc ggcagcagca ggaggaggag cgctgcgtct ggcgcccaac gaacccgtat
4681 cgacccgcga gcttagaaat aggatttttc ccactctgta tgctatattt caacaaagca
4741 ggggccaaga acaagagctg aaaataaaaa acaggtctct gcgctccctc acccgcagct
4801 gcctgtatca caaaagcgaa gatcagcttc ggcgcacgct ggaagacgcg gaggctctct
4861 tcagcaaata ctgcgcgctg actcttaagg actagtttcg cgccctttct caaatttaag
4921 cgcgaaaact acgtcatctc cagcggccac acccggcgcc agcacctgtc gtcagcgcca
```

```
4981 ttatgagcaa ggaaattccc acgccctaca tgtggagtta ccagccacaa atgggacttg
5041 cggctggagc tgcccaagac tactcaaccc gaataaacta catgagcgcg ggaccccaca
5101 tgatatcccg ggtcaacgga atccgcgccc accgaaaccg aattctcctc gaacaggcgg
5161 ctattaccac cacacctcgt aataacctta atccccgtag ttggcccgct gccctggtgt
5221 accaggaaag tcccgctccc accactgtgg tacttcccag agacgcccag gccgaagttc
5281 agatgactaa ctcaggggcg cagcttgcgg gcggctttcg tcacagggtg cggtcgcccg
5341 ggcgttttag ggcggagtaa cttgcatgta ttgggaattg tagtttttt aaaatgggaa
5401 gtgacgtatc gtgggaaaac ggaagtgaag atttgaggaa gttgtgggtt ttttggcttt
5461 cgtttctggg cgtaggttcg cgtgcggttt tctgggtgtt ttttgtggac tttaaccgtt
5521 acgtcatttt ttagtcctat atatactcgc tctgtacttg gccctttta cactgtgact
5581 gattgagctg gtgccgtgtc gagtggtgtt ttttaatagg tttttttact ggtaaggctg
5641 actgttatgg ctgccgctgt ggaagcgctg tatgttgttc tggagcggga gggtgctatt
5701 ttgcctaggc aggagggttt ttcaggtgtt tatgtgtttt tctctcctat taattttgtt
5761 atacctccta tgggggctgt aatgttgtct ctacgcctgc gggtatgtat tcccccgggc
5821 tatttcggtc gctttttagc actgaccgat gttaaccaac ctgatgtgtt taccgagtct
5881 tacattatga ctccggacat gaccgaggaa ctgtcggtgg tgctttttaa tcacggtgac
5941 cagtttttt acggtcacgc cggcatggcc gtagtccgtc ttatgcttat aagggttgtt
6001 tttcctgttg taagacaggc ttctaatgtt taaatgtttt tttttttgtt attttatttt
6061 gtgtttaatg caggaacccg cagacatgtt tgagagaaaa atggtgtctt tttctgtggt
6121 ggttccggaa cttacctgcc tttatctgca tgagcatgac tacgatgtgc ttgctttttt
6181 gcgcgaggct ttgcctgatt ttttgagcag caccttgcat tttatatcgc cgcccatgca
6241 acaagcttac ataggggcta cgctggttag catagctccg agtatgcgtg tcataatcag
6301 tgtgggttct tttgtcatgg ttcctggcgg ggaagtggcc gcgctggtcc gtgcagacct
6361 gcacgattat gttcagctgg ccctgcgaag ggacctacgg gatcgcggta tttttgttaa
6421 tgttccgctt ttgaatctta tacaggtctg tgaggaacct gaatttttgc aatcatgatt
6481 cgctgcttga ggctgaaggt ggagggcgct ctggagcaga tttttacaat ggccggactt
6541 aatattcggg atttgcttag agacatattg ataaggtggc gagatgaaaa ttatttgggc
6601 atggttgaag gtgctggaat gtttatagag gagattcacc ctgaagggtt tagcctttac
6661 gtccacttgg acgtgagggc agtttgcctt ttggaagcca ttgtgcaaca tcttacaaat
6721 gccattatct gttctttggc tgtagagttt gaccacgcca ccggagggga gcgcgttcac
6781 ttaatagatc ttcattttga ggttttggat aatcttttgg aataaaaaaa aaaaaacatg
6841 gttcttccag ctcttcccgc tcctcccgtg tgtgactcgc agaacgaatg tgtaggttgg
6901 ctgggtgtgg cttattctgc ggtggtggat gttatcaggg cagcggcgca tgaaggagtt
6961 tacatagaac ccgaagccag ggggcgcctg gatgctttga gagagtggat atactacaac
7021 tactacacag agcgagctaa gcgacgagac cggagacgca gatctgtttg tcacgcccgc
7081 acctggtttt gcttcaggaa atatgactac gtccggcgtt ccatttggca tgacactacg
7141 accaacacga tctcggttgt ctcggcgcac tccgtacagt agggatcgcc tacctccttt
7201 tgagacagag acccgcgcta ccatactgga ggatcatccg ctgctgcccg aatgtaacac
7261 tttgacaatg cacaacgtga gttacgtgcg aggtcttccc tgcagtgtgg gatttacgct
7321 gattcaggaa tgggttgttc cctgggatat ggttctgacg cgggaggagc ttgtaatcct
7381 gaggaagtgt atgcacgtgt gcctgtgttg tgccaacatt gatatcatga cgagcatgat
7441 gatccatggt tacgagtcct gggctctcca ctgtcattgt tccagtcccg gttccctgca
7501 gtgcatagcc ggcgggcagg ttttggccag ctggtttagg atggtggtgg atggcgccat
7561 gtttaatcag aggtttatat ggtaccggga ggtggtgaat tacaacatgc caaaagaggt
7621 aatgtttatg tccagcgtgt ttatgagggg tcgccactta atctacctgc gcttgtggta
7681 tgatggccac gtgggttctg tggtccccgc catgagcttt ggatacagcg ccttgcactg
7741 tgggattttg aacaatattg tggtgctgtg ctgcagttac tgtgctgatt taagtgagat
7801 cagggtgcgc tgctgtgccc ggaggacaag gcgtctcatg ctgcgggcgg tgcgaatcat
7861 cgctgaggag accactgcca tgttgtattc ctgcaggacg gagcggcggc ggcagcagtt
7921 tattcgcgcg ctgctgcagc accaccgccc tatcctgatg cacgattatg actctacccc
7981 catgtaggcg tggacttccc cttcgccgcc cgttgagcaa ccgcaagttg gacagcagcc
8041 tgtggctcag cagctggaca gcgacatgaa cttaagcgag ctgcccgggg agtttattaa
8101 tatcactgat gagcgtttgg ctcgacagga aaccgtgtgg aatataacac ctaagaatat
8161 gtctgttacc catgatatga tgctttttaa ggccagccgg ggagaaagga ctgtgtactc
8221 tgtgtgttgg gagggaggtg gcaggttgaa tactagggtt ctgtgagttt gattaaggta
8281 cggtgatcaa tataagctat gtggtggtgg ggctatacta ctgaatgaaa aatgacttga
8341 aattttctgc aattgaaaaa taaacacgtt gaaacataac atgcaacagg ttcacgattc
8401 tttattcctg ggcaatgtag gagaaggtgt aagagttggt agcaaaagtt tcagtggtgt
8461 attttccact ttcccaggac catgtaaaag acatagagta agtgcttacc tcgctagttt
8521 ctgtggattc actagaatcg atgtaggatg ttgcccctcc tgacgcggta ggagaagggg
8581 agggtgccct gcatgtctgc cgctgctctt gctcttgccg ctgctgagga ggggggcgca
8641 tctgccgcag caccggatgc atctgggaaa agcaaaaaag gggctcgtcc ctgtttccgg
8701 aggaatttgc aagcggggtc ttgcatgacg gggaggcaaa cccccgttcg ccgcagtccg
8761 gccggcccga gactcgaacc gggggtcctg cgactcaacc cttggaaaat aaccctccgg
8821 ctacagggag cgagccactt aatgctttcg ctttccagcc taaccgctta cgccgcgcgc
8881 ggccagtggc caaaaaagct agcgcagcag ccgccgcgcc tggaaggaag ccaaaaggag
8941 cgctcccccg ttgtctgacg tcgcacacct gggttcgaca cgcgggcggt aaccgcatgg
9001 atcacggcgg acggccggat ccggggttcg aaccccggtc gtccgccatg atacccttgc
9061 gaatttatcc accagaccac ggaagagtgc ccgcttacag gctctccttt tgcacggtct
9121 agagcgtcaa cgactgcgca cgcctcaccg gccagagcgt cccgaccatg gagcactttt
9181 tgccgctgcg caacatctgg aaccgcgtcc gcgactttcc gcgcgcctcc accaccgccg
```

```
     9241 ccggcatcac ctggatgtcc aggtacatct acggattacg tcgacgttta aacggatctg
     9301 atcagcacgt gttgacaatt aatcatcggc atagtatatc ggcatagtat aatacgacaa
     9361 ggtgaggaac taaaccatgg ccaagccttt gtctcaagaa gaatccaccc tcattgaaag
     9421 agcaacggct acaatcaaca gcatccccat ctctgaagac tacagcgtcg ccagcgcagc
     9481 tctctctagc gacggccgca tcttcactgg tgtcaatgta tatcatttta ctgggggacc
     9541 ttgtgcagaa ctcgtggtgc tgggcactgc tgctgctgcg gcagctggca acctgacttg
     9601 tatcgtcgcg atcggaaatg agaacagggg catcttgagc ccctgcggac ggtgccgaca
     9661 ggtgcttctc gatctgcatc ctgggatcaa agccatagtg aaggacagtg atggacagcc
     9721 gacggcagtt gggattcgtg aattgctgcc ctctggttat gtgtgggagg gctaagcact
     9781 tcgtggccga ggagcaggac tgacacgtgc tacgagatca tatgatcagc tcactcaaag
     9841 gcggtaatac ggttatccac agaatcaggg gataacgcag gaaagaacat gtgagcaaaa
     9901 ggccagcaaa aggccaggaa ccgtaaaaag gccgcgttgc tggcgttttt ccataggctc
     9961 cgccccccctg acgagcatca caaaaatcga cgctcaagtc agaggtggcg aaacccgaca
    10021 ggactataaa gataccaggc gtttccccct ggaagctccc tcgtgcgctc tcctgttccg
    10081 accctgccgc ttaccggata cctgtccgcc tttctccctt cgggaagcgt ggcgctttct
    10141 catagctcac gctgtaggta tctcagttcg gtgtaggtcg ttcgctccaa gctgggctgt
    10201 gtgcacgaac cccccgttca gcccgaccgc tgcgccttat ccggtaacta tcgtcttgag
    10261 tccaacccgg taagacacga cttatcgcca ctggcagcag ccactggtaa caggattagc
    10321 agagcgaggt atgtaggcgg tgctacagag ttcttgaagt ggtggcctaa ctacggctac
    10381 actagaagaa cagtatttgg tatctgcgct ctgctgaagc cagttacctt cggaaaaaga
    10441 gttggtagct cttgatccgg caaacaaacc accgctggta gcggtggttt ttttgtttgc
    10501 aagcagcaga ttacgcgcag aaaaaaagga tctcaagaag atcctttgat cttttctacg
    10561 gggtctgacg ctcagtggaa cgaaaactca cgttaaggga ttttggtcat gagattatca
    10621 aaaaggatct tcacctagat ccttttaaat taaaaatgaa gttttaaatc aatctaaagt
    10681 atatatgagt aaacttggtc tgacagttac caatgcttaa tcagtgaggc acctatctca
    10741 gcgatctgtc tatttcgttc atccatagtt gcctgactcc ccgtcgtgta gataactacg
    10801 atacgggagg gcttaccatc tggccccagt gctgcaatga taccgcgaga cccacgctca
    10861 ccggctccag atttatcagc aataaaccag ccagccggaa gggccgagcg cagaagtggt
    10921 cctgcaactt tatccgcctc catccagtct attaattgtt gccgggaagc tagagtaagt
    10981 agttcgccag ttaatagttt gcgcaacgtt gttgccattg ctacaggcat cgtggtgtca
    11041 cgctcgtcgt ttggtatggc ttcattcagc tccggttccc aacgatcaag gcgagttaca
    11101 tgatccccca tgttgtgcaa aaaagcggtt agctccttcg gtcctccgat cgttgtcaga
    11161 agtaagttgg ccgcagtgtt atcactcatg gttatggcag cactgcataa ttctcttact
    11221 gtcatgccat ccgtaagatg cttttctgtg actggtgagt actcaaccaa gtcattctga
    11281 gaatagtgta tgcggcgacc gagttgctct tgcccggcgt caatacggga taataccgcg
    11341 ccacatagca gaactttaaa agtgctcatc attggaaaac gttcttcggg gcgaaaactc
    11401 tcaaggatct taccgctgtt gagatccagt tcgatgtaac ccactcgtgc acccaactga
    11461 tcttcagcat cttttacttt caccagcgtt tctgggtgag caaaaacagg aaggcaaaat
    11521 gccgcaaaaa agggaataag ggcgacacgg aaatgttgaa tactcatact cttccttttt
    11581 caatattatt gaagcattta tcagggttat tgtctcatga gcggatacat atttgaatgt
    11641 atttagaaaa ataaacaaat aggggttccg cgcacatttc cccgaaaagt gccacctaaa
    11701 ttgtaagcgt taatattttg ttaaaattcg cgttaaattt ttgttaaatc agctcatttt
    11761 ttaaccaata ggccgaaatc ggcaaaatcc cttataaatc aaaagaatag accgagatag
    11821 ggttgagtgt tgttccagtt tggaacaaga gtccactatt aaagaacgtg gactccaacg
    11881 tcaaagggcg aaaaaccgtc tatcagggcg atggcccact acgtgaacca tcaccctaat
    11941 caagtttttt ggggtcgagg tgccgtaaag cactaaatcg gaaccctaaa gggagccccc
    12001 gatttagagc ttgacgggga aagccggcga acgtggcgag aaaggaaggg aagaaagcga
    12061 aaggagcggg cgctagggcg ctggcaagtg tagcggtcac gctgcgcgta accaccacac
    12121 ccgccgcgct taatgcgccg ctacagggcg cgatggatcc
//
```

Generating a quick, easy and low-cost affinity purification method for rAAV based on adeno-associated virus receptor's PKD domain

Kathrin E. Teschner[a], kathrin.schlicht@uni-bielefeld.de

Monja Leppin[a], monja.jochmann@uni-bielefeld.de

Julian Teschner[a], julian.teschner@uni-bielefeld.de

Kristian M. Müller[a], kristian@syntbio.net

[a] Cellular and Molecular Biotechnology, Faculty of Technology, Bielefeld University, Bielefeld, Germany

Corresponding author information (Address; Email; Phone)

Kristian M. Müller, Cellular and Molecular Biotechnology, Faculty of Technology, Bielefeld University, Universitätsstraße 25, 33615 Bielefeld, Germany; Email: kristian@syntbio.net; Tel. +49-521-106-6323

Abstract

Background: Recombinant adeno associated virus (rAAV) gained an outstanding reputation in gene therapy. However, the prospective success of rAAV relies on efficient and cost-effective purification strategies which must be suitable for future up-scale requirements. Affinity chromatography based on a relevant biological interaction allows for sufficient purity in one step and allows to simplify downstream processing of rAAV.

Results: We generated an affinity chromatography resin based on the natural AAV receptor AAVR. Single polycystic kidney disease (PKD) domains were easily produced in *E. coli* as fusion proteins to maltose-binding protein (MBP). Cellulose was chosen as a suitable chromatography resin with advantageous properties such as low unspecific binding, low costs and ease of availability. Covalent coupling of PKD2 to divinyl sulfone activated cellulose allowed for affinity purification of rAAV2 from crude cell extract. Purified samples showed superior purity and recovery rates comparable to other affinity purification strategies. Based on the established protocol for rAAV2 the process was successfully transferred to rAAV6 and rAAV9 purification and by this showed the universality of the novel affinity chromatography material.

Conclusions: The results show that individual AAVR domains have the potential to reduce downstream costs while ensuring high purity rAAV manufacturing.

Keywords: AAVR, recombinant adeno-associated virus, downstream processing, Gene therapy

Background

Recombinant Adeno-associated viruses (rAAV) are a rapidly expanding class of biologics for research and therapy. They combine efficient gene delivery to dividing and non-dividing cells, long-term gene expression and a high safety profile due to their inability to replicate autonomously without a helper virus [1,2]. This market pull requires efficient and cost effective purification meth-

ods, which is met with limited options. Despite several publications on the use of ultracentrifugation methods, classical chromatography methods such as ion-exchange [3] or semi specific materials such as heparin, affinity purification for AAV is very popular. Affinity chromatography materials are available from GE Healthcare, namely AVB Sepharose [4] based on an immobilized nanobody (cameloid V_HH heavy chain only fragment)[5] and from Thermo, namely AAV Capture select AAVX, AAV8, and AAV9 [6], which are also based on nanobodies. The wide dependence of laboratories on the AVB sepharose material even prompted recent considerations to modify AAV capsids for improved compatibility with the immobilized nanobody [7] as well as protein sequencing and reengineering efforts of the immobilized nanobody [8]. In a research publication, the monoclonal antibody A20 has been used for a purification test [9], but this route has not been followed and no commercial product has been developed.

AAV typically engage a primary receptor for cell adhesion and then enter the cell while interacting with additional cellular components, of which some are described as secondary receptors. For many AAV serotypes the primary receptors are known. In the case of AAV2, the primary receptor is heparin sulfate proteoglycan (HSPG). According to a review by Srivastava [10], AAV1 interacts with α2-3 and α2-6 N-linked sialic acid (SIA); AAV2, AAV2, and AAV13 interact with HSPG, AAV4 and AAV5 interact with α2-3 O-linked and α2-3 N-linked SIAs; AAV6 interacts with HSPG and α2-3 and α2-6 N-linked SIA; AAV9 interacts with terminal N-linked galactose (GAL) of SIA; and the primary cellular receptors for AAV7, AAV8, AAV9, AAVrh10, AAV11, AAV12, and AAV13 remain unknown. The glycans are abundant on the cell surface of several cell types and they do also interact with other (i.e. non AAV) proteins. Hence, these molecules were not chosen for affinity purification.

Next to the primary receptors several co-receptors have been identified. For AAV 2 these are αVβ5/α5β1 integrin, human fibroblast growth factor receptor 1 (FGFR1), hepatocyte growth factor receptor (HGFR) and laminin receptor (LamR) [11]. These are potentially interesting candidates to derive an affinity ligand, yet according to the literature they merely support infection but are

expendable. Using one of these molecules for purification would pose an unnecessary limitation for the options for capsid modifications.

In contrast, a protein named AAV-Receptor (AAVR) was recently described in detail based on a genetic screen as a protein with so far unknown function but high significance for the transduction ability of several AAV serotypes [12]. This protein has a predicted molecular weight of 108 kDA and is the same as a previously described 150 kDa glycoprotein, which was discovered in a membrane assay.[13] Even if in the absence of AAVR some basal transduction can occur [14], an interaction with this receptor seems important for clinical relevant transduction efficiencies for most AAV serotypes. The extracellular part of AAVR is composed of a N-terminal MANEC domain followed by five PKD (polycystic kidney disease) domains named PKD1 to PKD5. Dominant interactions of certain domains with specific serotypes have been described and in general the most distal PKD domains play the most prominent roles [15]. Glycosylation is not required for interaction.

PKD2 is important for AAV2 transduction and we chose this domain to demonstrate the generation of an affinity material based on a relevant biological interaction. In this study we could show that it is possible to bind rAAV2 particles very efficiently from HEK293 total cell extract. The protocol was then adopted for AAV6 and AAV9 purification. For AAV6, PKD3 and for AAV9 PKD5 was identified as promising interaction partners for affinity purification as so far the main interaction domains for these serotypes were not known. So generated AAV vectors show a higher purity, which was verified by SDS-PAGE using silver nitrate staining and Western blot. All in all, the costs for the purification could be reduced by a factor of more than ten with a reduced processing time from about two working days to about two to three hours.

Results

Development of a PKD-based affinity chromatography material

The aim of this study was to generate a scalable and low cost manufacturing process for the purification of rAAV from HEK293 crude cell lysate. In contrast to ultracentrifugation, affinity chromatography offers the great advantage for scaling up. As an affinity ligand, PKD2 was chosen in the first step, as Pillay *et al*. published that AAVR PKD2 is critical for the interaction of AAV2 with AAVR.[15] As a supporting material, cellulose was elected as a cost-effective material with advantageous properties such as low unspecific binding and good physical and chemical resistance under selected process conditions. In order to avoid the clogging of a packed chromatography column by residues of the cell lysate, blotting paper was utilized, so that the incubation of cell lysate containing rAAV was carried out in batch mode and not in the usual flow process of a packed column. An overview of the rAAV purification strategy is given in **Figure 1**.

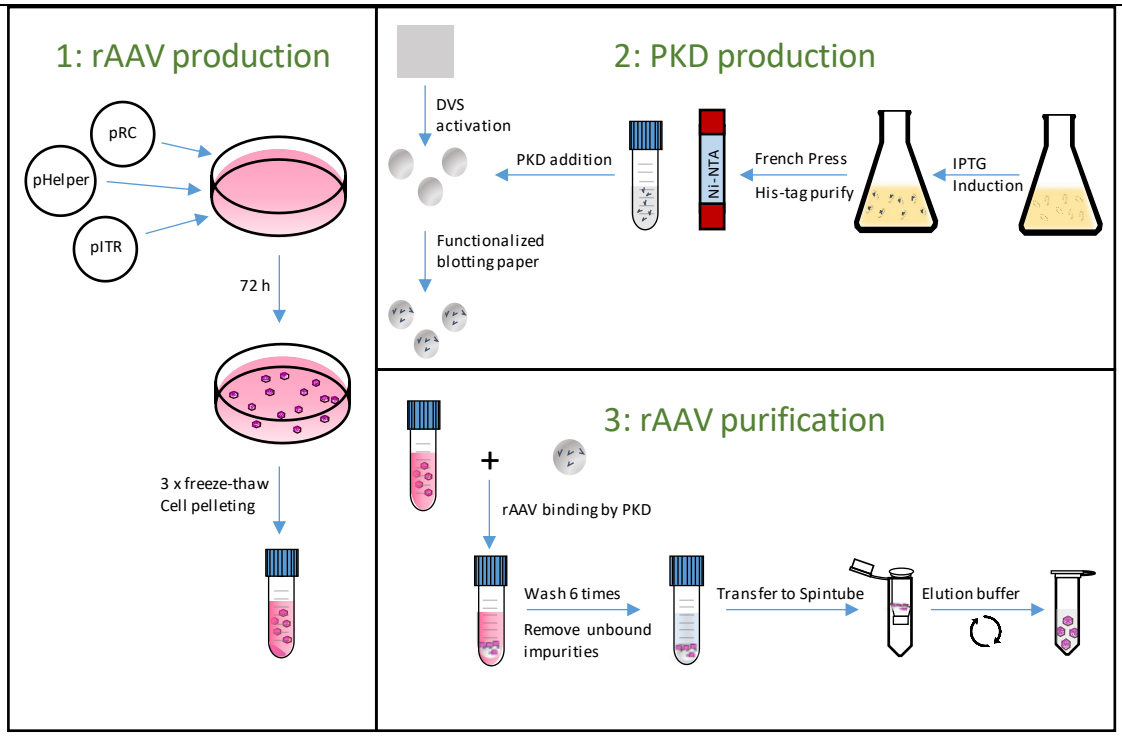

Figure 1 Schematic representation of recombinant adeno-associated virus (rAAV) manufacturing technology. (1) Adherent HEK293 cells are seeded and transfected with the three-plasmid system and harvested after 72 h. rAAVs were released from the cells by three freeze-thaw cycles and cell debris is pelleted by centrifugation (2) E. coli BL21(DE3) cells expressing PKD-MBP are cultivated in shaker flask for 4 h after induction with IPTG. The cell pellets are resuspended and then lysed using a french press. Lysate is clarified and loaded onto a AKTA FPLCand purified using IMAC. Blotting paper (BP) is activated by divinyl sulfone (DVS) and functionalized with purified PKD overnight. (3) rAAV containing clear lysate is incubated with functionalized BP and rAAV are eluted by transferring the BP to a spin tube and covering it with elution buffer. The rAAV containing elution is then dialyzed into the final storage buffer.

Production and purification of PKD2

For the expression of PKD2 as an affinity ligand, it was subcloned into a pET-24b expression vector from KIAA0319L full cDNA clone by PCR amplification of amino acid 405 to 502, which included 4 amino acids to the left and to the right of the domain as proposed by Pillay *et al.* in order to ensure correct protein folding.[12] To increase solubility the sequence of the maltose-binding protein was subjoined separated by a short glycine-serine linker at the 3'-end of PKD2. Here, subsequently a 6x His-tag was introduced to allow purification of the fusion protein from *E. coli* production. A

theoretical sequence of the fusion protein is given in **Figure 2A**. The success of purification after Immobilized metal affinity chromatography (IMAC) is shown in **Figure 2B**.

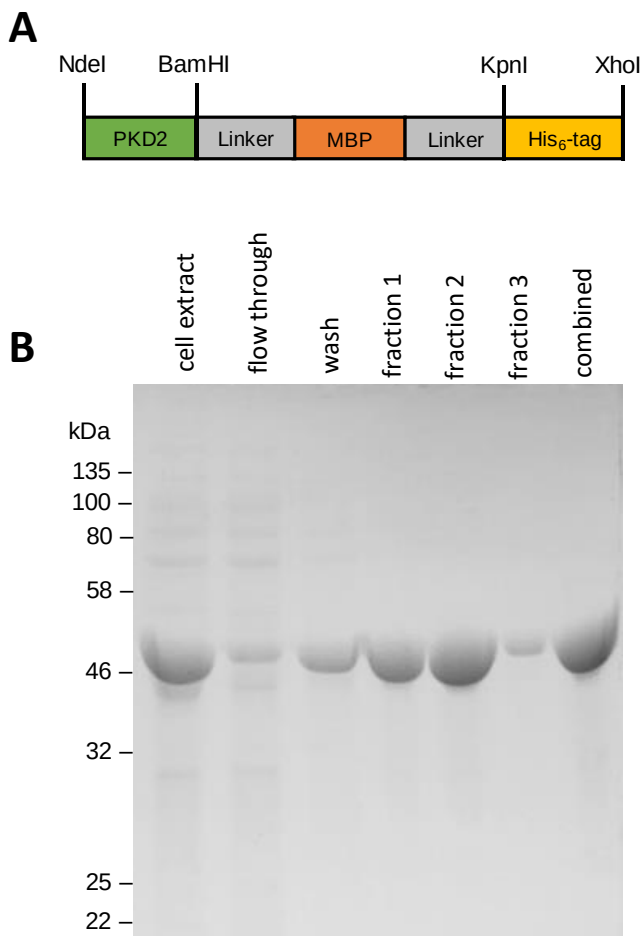

Figure 2: Construction and production of PKD2-MBP fusion protein. (A) Schematic representation of the basic components of the PKD2-MBP-fusion protein with its unique restriction sites for cloning and the position of GGSG linker sequences. (B) Coomassie-stained SDS PAGE protein analysis of PKD2-MBP purification steps. Cell extract, Ni-NTA column flow through and the wash fraction were diluted 1:2 in PBS buffer and elution fractions 1 to3 as well the combined and re buffered elution fraction was diluted 1:10 with PBS before loading.

Proof of binding of rAAV2 to PKD2-cellulose

For covalent binding of PKD, divinyl sulfone (DVS) activation of the cellulose was chosen. Here, one of the vinyl groups reacts with a hydroxyl-group of the cellulose. The remaining vinyl group reacts with nucleophiles and by this covalently attaches biomolecules to the cellulose surface.[16] The binding of rAAV2 to PKD2 is known, but a negative influence of covalent coupling on PKD2

functionality by steric hindrance or coupling to the cellulose resin with important amino acids could not be excluded. Therefore, the binding of rAAV2 to the PKD2-blotting paper (PKD2-BP) was proven prior to the optimization of the purification strategy. 30 µg PKD2-MBP were coupled to 1 cm^2 DVS activated blotting paper and subsequently incubated with $5.7 \cdot 10^8$ virus genomes (vg) of ultracentrifuge (UC) purified rAAV2 for 20 min, followed by two wash steps. The supernatant, PKD2-BP before and after the wash step and the wash fraction where analyzed by western blot analysis. As can be seen in **Figure 3A**, VP1, VP2 and VP3 were detected in the expected ratio on the PKD2-BP, with the washing procedure (BP-washed) had a low influence on signal strength. In the wash fraction no viral capsids were detected by western blot. The qPCR data where in accordance with observed western blot data and calculated 78 % of rAAV2 were bound to the material, suggesting that the resin was saturated **(Figure 3B)**.

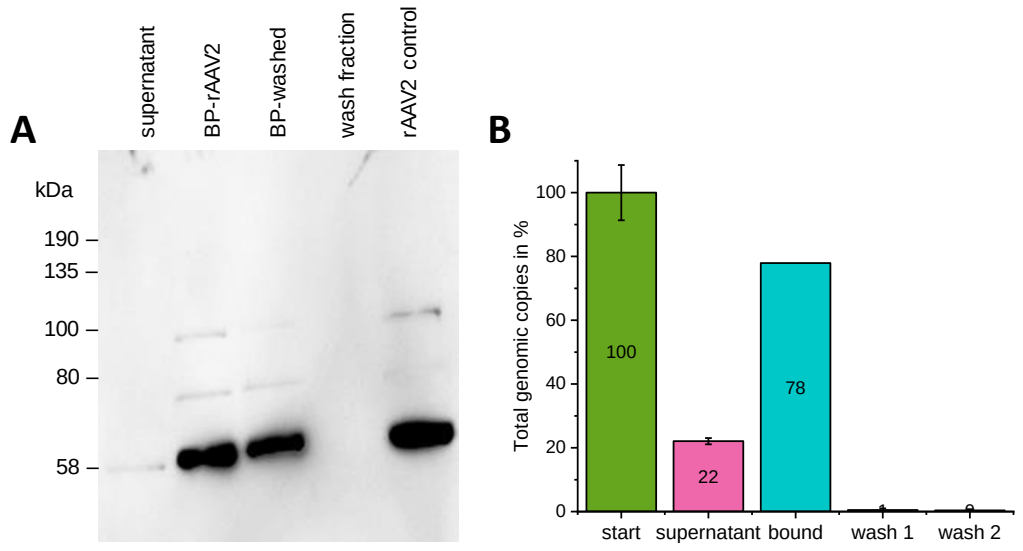

Figure 3: Characterization of rAAV2 binding to the PKD2-BP resin. (A) Western blot analysis of binding of UC purified rAAV2 to the PKD2-BP resin. (B) qPCR analysis of rAAV remaining in the respective fractions. Percentages were calculated by setting the genomic titer of starting material as 100 %. For each column, standard deviation was calculated between two technical replicates.

Optimization of PKD2 amount and elution conditions

Since a huge amount of virus genomes of 22 % were still found in the supernatant after incubation of rAAV2 with PKD2-BP, varying amounts of coupled PKD2 where tested with $5.7 \cdot 10^8$ vg, and non-bound virus were detected by qPCR in the supernatant. As depicted in **Table 1**, no correlation between the amount of coupled PKD2 and rAAV2 in the supernatant was seen. Though, taking the excess of PKD2 towards rAAV2 into account no limitation was expected.

Table 32: Relationship between amount of applied PKD2 to the amount of rAAV2 vg in the supernatant.

Amount of PKD2	**rAAV2 vg in supernatant in %**	**PKD2 molecule number**
2 µM (12 µg)	7.8 ± 19.8	$1.2 \cdot 10^{14}$
5 µM (30 µg)	22.1 ± 0.98	$3 \cdot 10^{14}$
20 µM (120 µg)	6.0 ± 26.1	$1.2 \cdot 10^{15}$

Further experiments were carried out with 30 µg PKD2 and elution conditions were evaluated. Lowering the pH or increasing the ionic strength is well known for affinity purification procedures. Therefore, an elution buffer with 100 mM citric acid pH 2.5 and a 2.5 M magnesium chloride ($MgCl_2$) buffer pH 7.0 were selected. Starting with UC purified rAAV2, only 0.2 % of the starting material were found in the pH elution sample, whereas for the $MgCl_2$ elution a 33.5 % yield was reached. Subsequently, all following attempts were performed with 2.5 M $MgCl_2$ 50 mM Tris pH 7.0.

Description of the purification strategy from crude cell extract

For purification of rAAV2, predetermined conditions were used with crude cell extract of rAAV2 containing HEK293 cells. rAAV2, which carried the mVenus fluorescent protein as a transgene, were produced in HEK293 cells by triple plasmid transfection using calcium-phosphate. After three days, rAAV2-mVenus were released by three cycles of freeze-thaw and the clarified super-natant of one 10 cm dish was incubated for 20 min with PKD2-BP while rotating on a roll-tumble

shaker. The resin was then washed rigorously with PBS-Tween until residual phenol red was undetectable. For elution, the resin was covered with 500 µl elution buffer in a spin tube for 5 min before it was centrifuged at 1000 × g for 2 min. After three cycles of elution, the fractions were combined and buffer exchange to HBSS was performed by ultra-centrifugal filters with a cut-off of 100´000 kDa. In qPCR, 41.5 % of vectors genomes were detected in the supernatant which was more than in previous trials with UC purified rAAV2. 24.6 % of total virus genomes were found in the combined elution fraction **(Figure 4A)**.

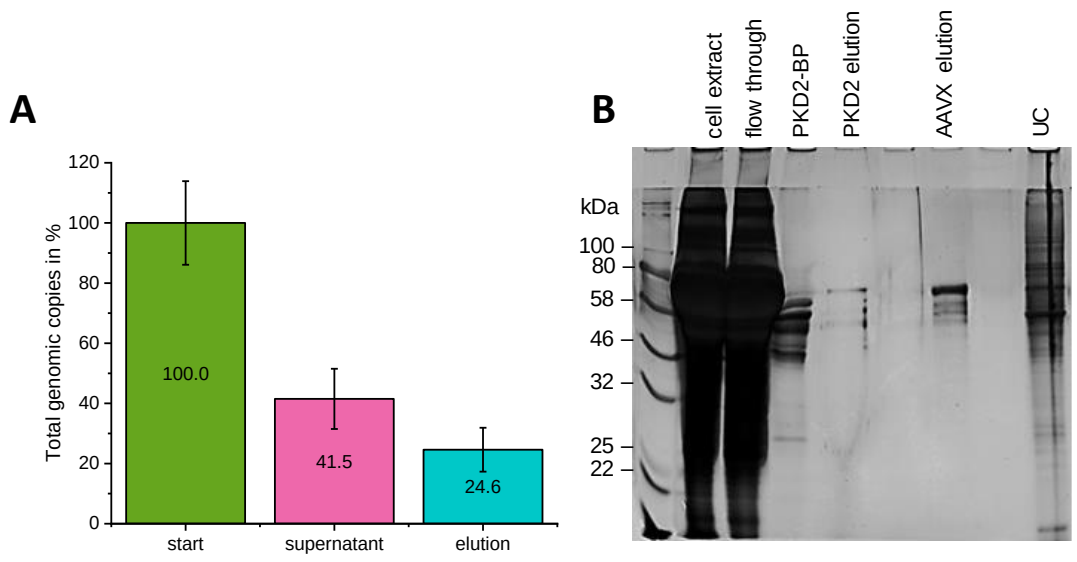

Figure 4: Characterization of rAAV2 binding to PKD2-BP from crude cell extract. (A) Distribution of rAAV2 in the respective fractions. Percentages were calculated by setting the genomic titer of starting material as 100 %. Genomic titer was quantified in crude cell extract after three freeze-thaw cycles for start value and for supernatant value after incubation with PKD2-BP by qPCR. For each column, standard deviation was calculated between two technical replicates. (B) Silver-stained SDS PAGE analysis of rAAV2 sample purity after purification with PKD2-BP, POROS AAVX or UC. Viral particles were produced in HEK293 cells seeded in two 100 mm dishes for each purification method and subsequently purified via PKD2-BP, POROS AAVX or iodixanol ultracentrifugation.

To compare the conventional UC method with a commercial affinity purification and the new PKD2 resin, two 10 cm dishes were purified either by PKD2, POROS CaptureSelect AAVX affinity resin (POROS AAVX) or UC, and the elution fractions were analyzed by qPCR **(Table 2).**

Table 33: Comparison of recovery rate for different purification approaches.

	vg loaded in total	**vg recovered total**	**Recovery rate in %**
PKD2	$8.32 \cdot 10^{11}$	$1.46 \cdot 10^{11}$	17.5 %
POROS AAVX	$8.32 \cdot 10^{11}$	$1.12 \cdot 10^{11}$	13.4 %
UC	$8.32 \cdot 10^{11}$	$3.2 \cdot 10^{11}$	38.0 %

For UC purified rAAV2 the highest recovery rate was reached, whereas for PKD2 and POROS AAVX with 17.5 % and 13.4 %, respectively a similar yield was obtained. In a SDS-PAGE using silver nitrate staining **(Figure 4B)**, many protein contaminants were observed for UC purified samples and, to a lower extent also for the POROS AAVX column material. Interestingly, the impurities in the POROS AAVX sample showed the same pattern as observed for the PKD2 sample. The most prominent contaminant was detected with a molecular weight of approximately 60 kDa, which may potentially be residual BSA or VP3. For the PKD2-BP some other proteins were bound to the material, indicating that a more rigid wash procedure may be necessary to diminish these.

Biological characteristics of PKD2 purified rAAV2

To analyze the biological activity of PKD2 purified rAAV2, a transducing titer assay on HT-1080 was performed and compared to UC purified rAAV2. Additionally, POROS AAVX was used in order to have a comparison to another affinity purification system. Here, 500 µl of slurry were used to purify rAAV2 from the clarified supernatant of a 10 cm dish, analogous to PKD2. Furthermore, the ratio of full to empty capsids was analyzed by a capsid ELISA. Therefore, a new capsid ELISA has been developed. While the standard capsid ELISA from PROGEN utilizes the A20 monoclonal antibody (mAB) to capture fully assembled AAV capsids, PKD2 was coupled to the surface of a microtiter plate. For detection of captured viral capsids, a recombinant A20 single-chain variant (A20 scFv-Fc) was cloned in our lab and produced in HEK-293 cells (for more details on this see Supplementary Method 1 and SI Figure 1).

For UC purified rAAV2 with 0.27, the highest ratio of full to empty capsids was determined, whereas for PKD2 and POROS AAVX the ratio is roughly the same.

Table 34: Biological characteristics of PKD2, POROS-AAVX and UC purified rAAV2 samples.

	TU/ml	**Capsids/ gc**	**full to empty ratio**
PKD2-BP	$1.6 \cdot 10^8$	7.07	0.14
POROS AAVX	n.D.	5.89	0.17
UC	$1.9 \cdot 10^8$	3.63	0.27

Transferring the method to AAV serotype 6 and 9

The optimization of the purification method to increase the yield and purity is still necessary, but is sufficient to transfer it to other AAV serotypes. Therefore, PKD1, as well as PKD3-PKD5 were subcloned into pet-24b expression vector as a fusion to maltose-binding protein starting from full AAVR (KIAA0319) cDNA as for PKD2 before. Protein expression was performed by IPTG induction of *E. coli* BL21(DE3) transformed with the individual plasmids and subsequent purification by (IMAC) via His-tag.

Individual PKD proteins were covalently coupled to blotting paper as before, and incubated with rAAV6 and rAAV9 containing HEK293 crude cell lysate from one 10 cm dish divided by five, so that for each domain the same amount of rAAV was secured. The elution fractions were then used for the determination of genomic titers by qPCR. rAAV6 showed a distinct affinity to PKD3 (**Figure 5A**), whereas for rAAV9, PKD2 and PKD5 gave a good result, with PKD5 giving a slightly higher genomic titer **(Figure 5B)**. As before, purity of the samples from PKD3 for AAV6, respectively PKD5 for AAV9, was confirmed by SDS PAGE and subsequent Coomassie brilliant blue staining **(Figure 5C)**. As concentrations of rAAV samples were too low to be detected by SDS PAGE analysis a western blot with B1 antibody was performed and confirmed the presence of VP3. The same samples were

also analyzed for the presence of PKD by anti-His-tag antibody to exclude leaching of PKD off BP during elution, but no PKD3, respectively PKD5 was observed in the elution fractions **(Figure 5D)**.

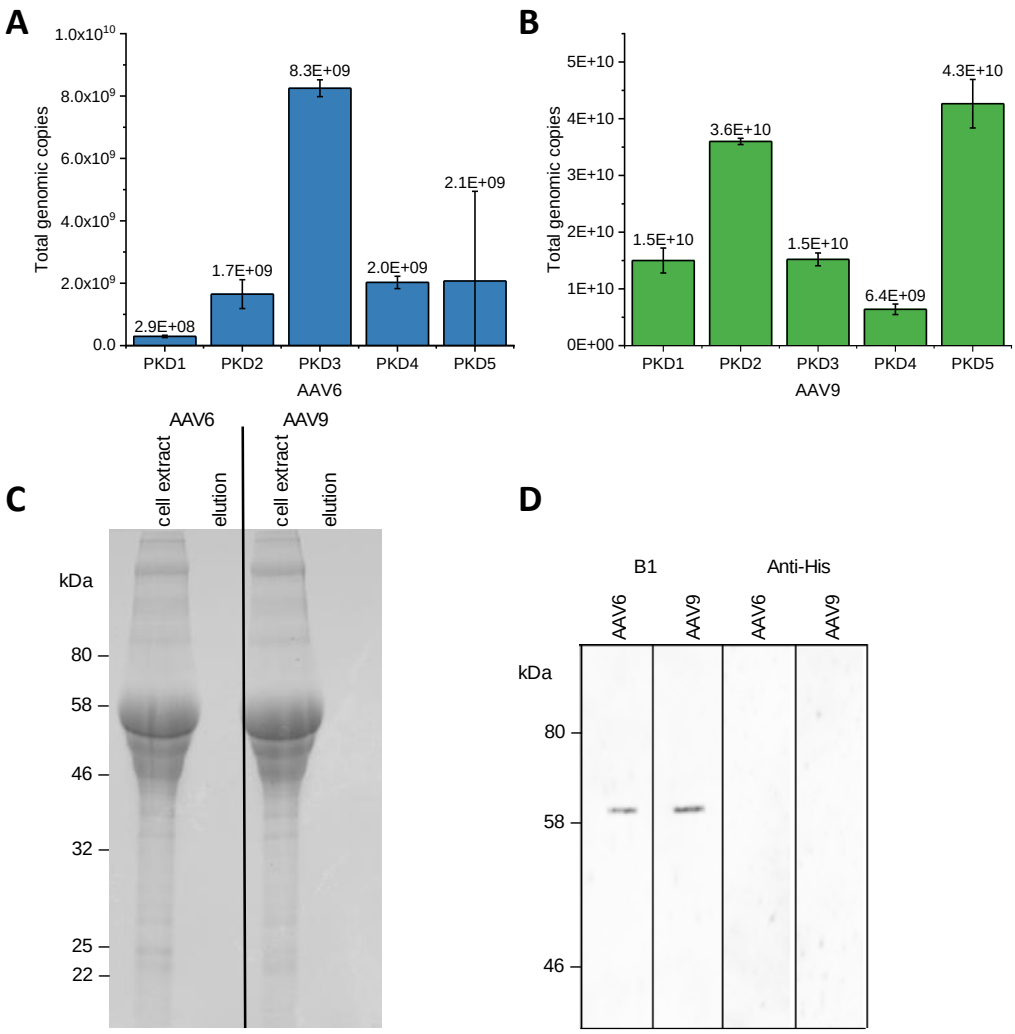

Figure 5: Summary of rAAV6 and rAAV9 purification. (A, B) Determination of suitable PKD domain for the purification of rAAV6 and rAAV9, respectively from crude cell extract by qPCR. For each column, standard deviation was calculated between two technical replicates. (C) Coomassie-stained SDS-PAGE protein analysis of PKD3 (rAAV6) or PKD5 (rAAV9) purified rAAV. (D) Western Blot analysis of rAAV6 and rAAV9 elution fractions for detection of VP proteins by B1 antibody (two left panels) or for detection of PKD by Anti-His-tag antibody (two right panels).

Discussion

As gene therapy utilizing AAV have become increasingly important with raising numbers of clinical trials worldwide, the demand for scalabale, user friendly purification strategies comes into focus.[17] Standard processes, relying on a cesium chloride (CsCl) or an iodixanol gradient ultracentrifugation are restricted in their potential to scale up.[18] Often, several chromatography steps are included into downstream processes like ion exchange, size exclusion and heparin column chromatography. These procedures are not only time intensive, but are accompanied by high costs and cumulative loss in yield. In this work a scalable affinity purification strategy, based on the natural AAV receptor AAVR, was developed which yields comparable rAAV titer as with commercial affinity chromatography resins. In a first step the method was evaluated for rAAV2 as for this, the most important interacting domain of the AAVR, namely PKD2 is well-known.[15] In order to avoid time-consuming and elaborate steps in the purification procedure, the method has been designed that it can be performed directly from the crude cell extract as concentration steps with ammonium sulfate or polyethylene glycol (PEG) precipitation interfere with upscaling due to the need for a centrifugation step.[19] As depicted in Figure 1, in contrast to a packed column the chosen cellulose material in form of blotting paper allows for a batch process in where the rAAV containing suspension is either stirred or shaken with the PKD functionalized paper. Thereafter, the column material can be transferred into a spin tube and by this, separation of the column material from the elution can easily be executed. As for commercial POROS CaptureSelect AAVX or AVB Sepharose High Performance, batch processes can also be conducted, but separation of the material from the sample is not easily realized as the small sized particles sticking to the vessels. PKD2 can be produced in high concentrations and purity in *E. coli* when fused to MBP (Figure 2 B) and thus inexpensive supply of the affinity ligand is possible. Covalent binding of the fusion protein to blotting paper by DVS activation does not impair the functionality of PKD2, so that the binding of rAAV2 to the blotting paper was proven by western blot analysis (Figure 3 A). Interestingly an increase in the amount of applied PKD2 did not decrease the quantity of rAAV2 found in the supernatant. Potentially, even if the amount of PKD2 was raised, no more functional protein was

covalently bound, as the method for coupling does not allow for quantification of bound protein as the blotting paper was just soaked with the protein without any protruding solution. After protein coupling SDS-PAGE analysis with subsequent determination of bound protein should be considered in the future. However, as the amount of affinity ligand exceeds applied viral capsids by far (Table 1), we hypothesize, that non bound rAAV2 may be in a structural conformation which does not allow for accurate binding and by this is not purified from crude cell lysate, but this hypothesis has yet to be substantiated. If this hypothesis could be confirmed, this method would primarily purify biologically relevant viruses and thus would have a substantial advantage over other systems. The purity of the samples was compared to ultracentrifugation and POROS CaptureSelect AAVX purified rAAV2 samples (Figure 4B). Many impurities were detected for the UC purified sample. By selecting non-contaminated fractions using an additional SDS PAGE analysis, these could potentially be minimized but also leads to a reduction in yield. For PKD2 nearly no contaminations were detected. Interestingly, for POROS CaptureSelect AAVX the protein pattern looked similar to those obtained for PKD2 but with a higher intensity indicating a higher protein contamination. The most prominent band on the heights of about 60 kDa may refer residual BSA contaminants. With the best elution conditions 17.5 % to 24.5 % of applied genomic copies were recovered. The $MgCl_2$ buffer does not only yielded the highest amount of rAAV but also offers the advantage of a neutral pH as other methods relying on elution conditions within a pH range of pH 2.0 - 3.0. AAV undergoes autolytic proteolysis at low pH which results in a decrease in VP1 and VP2 and in an increase in lower-molecular-mass bands.[20] For AAV serotype 8, amino acid side chain conformational rearrangements were observed at low pH values.[21] However, effects on viral preparation potency still need to be investigated. As expected, separation of full and empty capsids still needs a polishing step after affinity chromatography. Here, the UC purified rAAV sample showed highest proportion of full capsids with 27% in contrast to 14 % for PKD2-BP and 17 % for POROS CaptureSelect AAVX, respectively (Table 3). As empty capsids may cause serious side effects in patients, also for UC purified sample another polishing step is normally applied and by

this, UC offers only a slight advantage when used as a one-step purification strategy in the context of research, when the high purity of vector preparation is not needed.

As the affinity chromatography was successfully implemented for AAV serotype 2, the aim was to transfer the conditions to the other serotypes commonly used in our lab. Therefore, the other PKD domains were cloned into pet-24b expression vector and purified via IMAC from *E. coli* expression. Combinations of the domains 1 to 5 with AAV serotype 6 and 9 with subsequent elution and qPCR analysis revealed a high affinity of rAAV6 to PKD3 and for rAAV9 towards PKD2 and PKD5. SDS PAGE analysis showed the high purity of the vector preparations. This gives rise to the assumption that a transfer of the method will be possible for other AAV serotypes and needs to be evaluated in the future.

Conclusions

An affinity chromatography procedure was established for efficient AAV post-processing. Based on the natural cellular receptor AAVR, we could show that the covalent coupling of single PKD domains to the surface of blotting paper did not significantly affect the functionality, allowing purification from raw cell extract without further processing steps such as concentration or ultracentrifugation. This means not only a reduction in processing steps, but also the potential for scaling up in the future.

The simple production of the affinity ligand in *E. coli* as well as the easy accessibility of the carrier material in combination with the high purity of the end product shows the potential of the developed chromatography approach. We assume that this method can be adopted for other AAV serotypes by searching for the corresponding PKD domain, which makes the presented strategy a universal approach for the purification of AAVs by affinity chromatography with superior purity of the final product.

Materials and Methods

Construction of pET-24b_AAVR_PKDX-MBP-His6. The DNA sequence of individual PKD domains was amplified from a cDNA clone KIAA0319L (pCMV6_KIAA0319 (Myc_DDK-tagged, Origene). Starting from UniProt Q8IZA0 database, four amino acids to the left and to the right of the domain were included as proposed by Pillay *et al*. in order to ensure correct protein folding.[12] The PKD2 sequence was amplified with NdeI-PKD2-for (5'-AAAAACATAT GAATCGGCCC CCCATTGCTAT TG-3'), which introduced the underlined NdeI restriction site and at the same time contained the ATG start codon and KpnI-linker-BamHI-PKD2-rev (5'-TTTTTGGTAC CACCGCCTGA ACCACCACCA GAGCCACCAC CGGATCCGGG GTAATCCACA GCTTTGTTCA C-3'). The MBP was amplified from pMAL™-c5X Vector (NEB) with primer BamHI-linker-MBP-for (5'-AAAAAGGATC CGGTGGTGGC TCTGGTGGTG GTTCAGGCGG T*AAAATCGAA GAAGGTAAAC TGG*-3') which contained the underlined BamHI restriction site and the glycine-serine-linker sequence with the hybridizing region marked italic, and KpnI-linker-MBP-rev (5'-TTTTTGGTAC CACCGCTACC GCCACCTGAA CCACCAC-CGC TACC*AGTCTG CGCGTCTTTC AG*-3') with KpnI restriction site underlined and hybridizing region italicized. A third PCR was used to fuse PCR product 1 and 2 to KpnI-MBP-linker-BamHI-PKD2-NdeI. The oligonucleotides KpnI-His6-tag-XhoI-for (5'-ACCCATCATC ACCATCATCA TTAACTCGA-3') and XhoI-His6-tag-KpnI-rev (5'-GTTAATGATG ATGGTGATGA TGG-3') were hybridized and ligated to the KpnI and NdeI digested PCR product in order to add the His_6-tag and the XhoI restriction site. This product was then ligated into NdeI and XhoI opened pET-24b (+) (Novagen®).

For PKD3 to PKD5 following primers were used to amplify respective DNA sequence from cDNA clone KIAA0319L. PKD3-NdeI-for (5'-ATATACATAT GTACCCCCCT GTGGCCAACG CAGG-3') and PKD3-BamHI-rev (5'-CACCGGATCC CTTATTGTTT TCAGGTTGCA CAATAACAGT CAC-3'); PKD4-NdeI-for (5'-ATATACATAT GAATAAGCCT CCTCAGGCAG ATGCAGGC-3') and PKD4-BamHI-rev (5'-CACCG-GATCC TTTGTTTATT TCTTCTTTGA CAATGACATT CACAGA-3'); PKD5-NdeI-for (5'-ATATACATAT GAAACCACCT ATAGCCAAGA TAACTGGGAA T-3') and PKD5-BamHI-rev (5'-CACCGGATCC

GTTTTTCCTG GGATCAGGTT TCACCTCCAC-3'). They introduced underlined NdeI and BamHI restriction sites and allowed for subsequent cloning into previous generated pET-24b vector by removing PKD2 sequence via NdeI and BamHI. For PKD1 a second NdeI restriction site had to be removed before cloning into expression vector was performed. Therefore, the PCR product of PKD1-NdeI-for (5'-ATATACATAT GGTATCTGCT GGAGAGAGTG TC-3') and PKD1-Mut-rev (5'-AACATA**G**GCA TTTAATTGAA CTTCATTCTT AGGCA-3') as well as the PCR product of PKD1-Mut-for (5'-AATGC**C**TATG TTCTCCAAGA ACCACCTAA-3') and PKD1-BamHI-rev (5'-CACCGGATCC ACGGGGCTCT GGCTTGACTG TCAC-3') were used in a third PCR. After digestion with NdeI and BamHI it was introduced into the likewise opened pET-24b expression vector by removing PKD2. In bold the nucleotide was changed from A to C and thus did not alter the amino acid sequence. The restriction sites of NdeI and BamHI were underlined.

Plasmids for viral particle production. Plasmids were based on a pSB1C3 backbone and were assembled using the iGEM RFC10 BioBrick assembly standard.[22] pZMB0216_Rep_VP123_453_587wt_p5tataless contains a genetically modified *rep/cap* similar to one encoded in pAAV-RC (Genbank Accession number: AF369963.1). In the ITR containing plasmid pZMB0522_ITR_EXS_CMV_mVenus_hGHpA, a CMV promoter expresses the fluorescent protein mVenus. Plasmids are described in detail by Feiner et. al [submitted 2019].

Cell Culture. HEK-293 and HT-1080 (DSMZ) cells were cultured in Dulbecco's Modified Eagle Medium supplemented 10% (v/v) fetal calf serum and 1% (v/v) penicillin/streptomycin (Sigma Aldrich). Cells were maintained at 37 °C and 5% CO_2.

Viral particle production. HEK293 cells were seeded at a density of 3×10^6 cells per 100 mm dish the day before transfection. A total amount of 15 µg DNA per 100 mm dish was transfected using calcium phosphate. RepCap plasmid, ITR-containing plasmid and pHelper plasmid were used in a 1:1:1 molar ratio[23]. After 72 h of incubation at 37 °C, cells were harvested and pelleted by centrifugation (2000×g, 5 min).

Processing of viral particles for purification. Cells were resuspended in lysis buffer (50 mM Tris, 150 mM NaCl, 2mM $MgCl_2$, pH 7.5) and viral particles were released from cells with three freeze-thaw cycles. Remaining DNA contamination was degraded by incubation with benzonase nuclease (final 100 U/ml, Sigma Aldrich) at 37 °C prior to addition of CHAPS (3-[(3-cholamidopropyl)dimethylammonio]-1-propanesulfonate, 0.5% w/v final). The crude lysate was cleared from cell debris by centrifugation (3,000×g, 10 min). The supernatant was added to the virus containing spent media which was then used for affinity chromatography. For ultracentrifugation, precipitation of viral particles from spent media, 3.13 g ammonium sulfate per 10 ml volume were dissolved and incubated for 30 min on ice. After centrifugation at 8300 x g, 10 min, 4 °C the resulting pellet was resuspended with the supernatant from cell lysis. This crude viral stock was further purified by ultracentrifugation.

Purification by ultracentrifugation. The crude viral stock was used for a discontinuous iodixanol gradient[24]. Briefly, the lysate was transferred onto a gradient of 60%, 40%, 25% and 15% iodixanol in an open top polyallomer 16 x 76 mm tube (Science Services). Tubes were sealed and centrifuged in a T-880 rotor (Sorvall) at 340,000×g for 2 h at 18 °C. The rAAV containing fraction was collected with a 21G x 1 1/2” injection needle and the buffer was exchanged to 1× HBSS (Sigma Aldrich) via Amicon Ultra-4 100K centrifugal filter units (Merck Millipore).

Purification of viral particles by POROS CaptureSelect AAVX. For affinity purification a 5 ml empty lab column with Luer-lock connections (MoBiTec S10131) was filled with 500 µl of the POROS CaptureSelect AAVX suspension and equilibrated with 10 column volumes of PBS. The sample was loaded with 1 ml per min with a syringe pump. After washing with 10 CV with PBS-T (PBS + 0.05 % Tween20) rAAV2 were eluted three times with 250 µl 100 mM citric acid buffer pH 2.5 and neutralized with Tris-HCl pH 9.0.

PKD expression and purification. An overnight preculture (37 °C, 180 rpm) of *E. coli* transformed with pET-24b expression vector was used to inoculate a culture in 0.5 L LB medium containing 50

µg/mL kanamycin. This culture was grown (37 °C, 180 rpm) up to an OD_{600} of 0.5. Protein expression was then induced with isopropyl-β-D-thiogalactopyranoside (IPTG) (1 mM) and the cells were cultivated at 37 °C, 180 rpm for 4 h. Afterwards, cells were harvested by centrifugation (6000 × *g*, 4 °C, 15 min) and stored at -20 °C. For protein purification, cells from cultivation were thawed and suspended in 30 mL equilibration buffer (50 mM Na_2HPO_4, 300 NaCl, 10 mM imidazole pH 8). The cell membrane of bacteria was disrupted in three repeated French press cycles at a pressure of 1000 psi. Cell debris was separated from soluble protein by centrifugation at 11.600 × g for 20 min at 4°C. The supernatant was filtered and applied to a Protino Ni-NTA column (Macherey-Nagel) for purification. After washing with 10 CV buffer containing 20 mM imidazole in equilibration buffer, the protein was eluted with 5 CV of an elution buffer containing 250 mM imidazole. Finally, the buffer was adjusted to 1 × PBS using an Amicon Ultra centrifugal filter unit (MWCO 30 kDa).

Preparation of PKD affinity resin. Blotting paper (Rotilabo® Blotting Papers, Thickness 0.35 mm; Carl Roth) was cutted into 1 cm^2 large pieces and incubated in 2 ml DVS buffer (0.1 M Na_2CO_3, pH11) with 10 % DVS (Sigma Aldrich) for 2 h. Then, the blotting paper was washed five times with 10 ml MilliQ and dried for at least 2 h. Each blotting paper was incubated with 100 µl 5 µM PKD in PBS overnight in a water-saturated atmosphere. The remaining surface was blocked with 2 ml of PBS-T for 1 h before it was washed three times with PBS. Afterwards the material could be used for affinity purification or stored in PBS buffer at -20 °C.

Purification of viral particles by PKD affinity chromatography. For affinity purification from crude cell lysate, it was incubated with one 1 cm^2 of prepared PKD-blotting paper for 30 min in a suitable vessel under constant shaking. Afterwards the supernatant was removed and the resin was washed with PBS until no phenol red residues from the medium were seen (usually 5 to 6 wash steps with 10 ml PBS). Elution was performed by transferring the PKD-blotting paper into an empty spin column and adding 500 µl of elution buffer (2.5 M $MgCl_2$, 50 mM Tris, pH 7.0 or 100 mM citric acid pH 2.5). After 2 min incubation elution was performed by centrifugation (1000 × g, 2 min). The elution fractions were combined and the buffer was exchanged to 1× HBSS (Sigma

Aldrich) via Amicon Ultra-4 100K centrifugal filter units (Merck Millipore). For purification from UC purified rAAV 20 µl of UC purified rAAV were diluted with PBS to 100 µl and afterwards processed as for purification from cell lysate.

SDS-PAGE and Western blot analysis. Cell pellets from rAAV production (1× 100 mm dish) were resuspended in 100 µl PBS and 5× SDS loading buffer. Samples were incubated at 95 °C for 10 min, centrifuged and 20 µl per lane were loaded on a 10% SDS-polyacrylamide gel (Hoefer SE260). Samples were blotted onto a 0.45 µm nitrocellulose membrane (Thermo Fisher Scientific) using semi-dry electrophoretic transfer (V20-SDB, Sci Plas). After blocking the membrane with 10% (w/v) non-fat milk in TBS, the membrane was incubated simultaneously for 1.5 h with the B1 antibody (mouse monoclonal, supernatant, 1:100, Progen) and an anti β-Actin antibody (8H10D10, mouse monoclonal, 1:1000, Cell Signaling Technology). After incubation with an anti-mouse IgG, HRP-linked antibody (1:5000, Cell Signaling Technology), blots were imaged by luminescence detection (Pierce ECL Western Blot Substrate, Thermo Fisher Scientific).

Determination of genomic titers. Before determination of genomic titers via qPCR, samples were treated with 10 U DNase I (New England Biolabs) in 10× DNaseI buffer in a final volume of 50 µl at 37 °C for 30 min before heat inactivation of the DNase I (75 °C, 20 min). Crude lysate samples were additionally incubated with 0.8 U Proteinase K (New England Biolabs) for 50 min at 37 °C before heat inactivation (95 °C, 10 min). Dilutions of the DNase I digest were used as template in the qPCR reaction. The sample was mixed with 2.5 µl primer qPCR-hGH-for (5'-CTCCCCAGTG CCTCTCCT-3') and 2.5 µl primer qPCR-hGH-rev (5´-ACTTGCCCCT TGCTCCATAC-3´), each at a stock concentration of 4 µM, and 10 µl of 2× GoTaq qPCR Mastermix (Promega). The qPCR reaction was carried out as described in the manual (TM318 6/14, Promega) with an increased time interval for the first denaturation step (95 °C, 10 min) using a LightCycler 480 II (Roche). The genomic titer was calculated from a standard curve of 10 to 10^6 copies of the ITR plasmid (pZMB0522) with an efficiency between 90-110% and an R value less than 0.1. Genomic titres in crude lysates were estimated from a standard curve mixed with the same amount of a non-transfected cell lysate.

Transducing titer assay. 10,000 cells per well were seeded in 500 µl of the corresponding media on a 12-well plate and settled for 1 h before application of rAAV preparations. After 12 h incubation 500 µl of fresh media was added to the cells. Cells were incubated at 37 °C for further 72 h before detaching with 0.25% Trypsin/EDTA, resuspension in PBS and analysis of 10,000 events using a FACSCalibur. All experiments were performed as biological duplicates. Data sets were analyzed using FlowJo V10. Positive cells were gated above the 99 % interval of the negative control.

AAV Capsid ELISA. For the determination of viral capsid titer, a96-well cell culture plate was incubated overnight at 4 °C with purified PKD2 (200 ng in 100 µL per well) in 13 mM Na2CO3, 35 mM NaHCO3, pH 9.6. Afterwards, the plate was washed three times with PBS, 0.05% Tween-20 (wash buffer) and remaining sites were blocked with 200 µl blocking buffer (0.8 % BSA in PBS) per well for 1 h at RT. After three wash steps with wash buffer the A20 scFv was added with 100 ng per well in blocking buffer for 1 h at RT. The three times washed plate was then incubated with an anti-human IgG1 HRP antibody (AM08151HR-N, mouse monoclonal, 1:2000 in wash buffer with 0.8 % BSA, Acris antibodies**)** for 1 h. The detection was started, after three wash steps with wash buffer, with 150 µl ABTS buffer (3.25 mM BH_2NaO_4, 40 mM citric acid monohydrate, 60 mM Na_2HPO_4, pH 4.5) with 1 g L^{-1} ABTS (2,2'-azino-bis(3-ethylbenzothiazoline-6-sulphonic acid). The absorbance was measured at 405 nm with a microplate spectrophotometer (PowerWave HT, BioTek) after 30 min. Calculation of capsids was performed by a standard curve of a serial dilution of a known capsid concentration (Kit control/Standard, Progen)

List of abbreviation

Abbreviation	Meaning
rAAV	recombinant adeno-associated virus
PKD1-5	polycystic kidney disease domain 1-5
AAVR	adeno-associated virus receptor
AAV2	adeno-associated virus serotype 2

ITR	Inverted terminal repeat
qPCR	quantitative polymerase chain reaction

Declarations

Ethics approval and consent to participate

Not applicable

Consent for publication

Not applicable

Availability of data and material

All data generated or analyzed during this study are included in this published article and its supplementary information files.

Competing interests

The authors declare that they have no competing interests.

Funding

We acknowledge support of the publication fee by Deutsche Forschungsgemeinschaft and the Open Access Publication Funds of Bielefeld University. This work was supported by grants of Bielefeld University.

Authors' contributions

All authors were involved in the design of this study. KT and JT planned and performed the experiments to characterize the purification method for rAAV2. JT designed the plasmid construct and

optimized the protein production. KT optimized the protein binding to the column and purification parameters. ML performed the experiments to characterize the purification method for rAAV6 and rAAV9. KT, JT and KM wrote the manuscript. All authors read and approved the final manuscript.

Acknowledgements

We thank Philipp Borchert for experimental assistance.

References

1. Xiao, X., Li, J. & Samulski, R. J. Efficient long-term gene transfer into muscle tissue of immunocompetent mice by adeno-associated virus vector. *J. Virol.* **70**, 8098–108 (1996).

2. Russell, D. W., Miller, A. D. & Alexander, I. E. Adeno-associated virus vectors preferentially transduce cells in S phase. *Proc. Natl. Acad. Sci. U. S. A.* **91**, 8915–9 (1994).

3. Kaludov, N., Handelman, B. & Chiorini, J. A. Scalable Purification of Adeno-Associated Virus Type 2, 4, or 5 Using Ion-Exchange Chromatography. *Hum. Gene Ther.* **13**, 1235–1243 (2002).

4. GE Healthcare. AVB Sepharose™ High Performance - Datafile 28-9207-54 AB. (2007). Available at: https://www.gelifesciences.co.jp/catalog/pdf/28920754ab.pdf. (Accessed: 11th December 2018)

5. Oranje, P. *et al.* Isolation of an Adeno-Associated Virus (AAV)-Specific Camelid-Derived Single Chain Antibody Fragment: A Novel Tool for Purification of AAV Vectors of Different Serotypes. *Mol. Ther.* **9**, S162 (2004).

6. Toueille, M. *et al.* Development of purification steps for several AAV serotypes using POROS CaptureSelect AAVX affinity chromatography. *Cell Gene Ther. Insights* 637–646 (2017). doi:10.18609/cgti.2018.062

7. Nass, S. A. *et al.* Universal Method for the Purification of Recombinant AAV Vectors of Differing Serotypes. *Mol. Ther. - Methods Clin. Dev.* **9**, 33–46 (2018).

8. Eichhoff, A. M. Nanobodies als Werkzeuge zur Optimierung Adeno-assoziierter Viren für die Gen- und Tumortherapie. (2018).

9. Grimm, D., Kern, A., Rittner, K. & Kleinschmidt, J. A. Novel tools for production and purification of recombinant adenoassociated virus vectors. *Hum. Gene Ther.* **9**, 2745–60 (1998).

10. Srivastava, A. In vivo tissue-tropism of adeno-associated viral vectors. *Curr. Opin. Virol.* **21**, 75–80 (2016).

11. Herrmann, A. & Grimm, D. High-Throughput Dissection of AAV-Host Interactions: The Fast and the Curious. *J. Mol. Biol.* #pagerange# (2018). doi:10.1016/j.jmb.2018.05.022

12. Pillay, S. *et al.* An essential receptor for adeno-associated virus infection. *Nature* **530**, 108–112 (2016).

13. Mizukami, H., Young, N. S. & Brown, K. E. Adeno-associated virus type 2 binds to a 150-kilodalton cell membrane glycoprotein. *Virology* **217**, 124–130 (1996).

14. Dudek, A. M. *et al.* An Alternate Route for Adeno-associated Virus (AAV) Entry Independent of AAV Receptor. *J. Virol.* **92**, e02213-17 (2018).

15. Pillay, S. *et al.* AAV serotypes have distinctive interactions with domains of the cellular receptor AAVR. *J. Virol.* **91**, JVI.00391-17 (2017).

16. Yu, A. *et al.* Biofunctional paper via the covalent modification of cellulose. *Langmuir* **28**, 11265–73 (2012).

17. Ginn, S. L., Amaya, A. K., Alexander, I. E., Edelstein, M. & Abedi, M. R. Gene therapy clinical trials worldwide to 2017: An update. *J. Gene Med.* **20**, e3015 (2018).

18. Clément, N. & Grieger, J. C. Manufacturing of recombinant adeno-associated viral vectors

for clinical trials. *Mol. Ther. - Methods Clin. Dev.* **3**, 16002 (2016).

19. Vandenberghe, L. H. *et al.* Efficient serotype-dependent release of functional vector into the culture medium during adeno-associated virus manufacturing. *Hum. Gene Ther.* **21**, 1251–7 (2010).

20. Salganik, M. *et al.* Evidence for pH-Dependent Protease Activity in the Adeno-Associated Virus Capsid. *J. Virol.* **86**, 11877–11885 (2012).

21. Nam, H. *et al.* Structural Studies of Adeno-Associated Virus Serotype 8 Capsid Transitions Associated with Endosomal Trafficking . **85**, 11791–11799 (2011).

22. Shetty, R. P., Endy, D. & Knight, T. F. Engineering BioBrick vectors from BioBrick parts. *J. Biol. Eng.* **2**, 5 (2008).

23. Agilent Technologies. AAV Helper-Free System Instruction Manual. Available at: https://www.agilent.com/cs/library/usermanuals/Public/240071.pdf. (Accessed: 13th August 2019)

24. Zolotukhin, S. *et al.* Recombinant adeno-associated virus purification using novel methods improves infectious titer and yield. *Gene Ther.* **6**, 973–85 (1999).

Additional File

Generating a quick, easy and low-cost affinity purification method for rAAV based on adeno-associated virus receptor's PKD domain

Rebecca C. Feiner[1,†], Kathrin E. Teschner[1,†], Julian Teschner[1],Kristian M. Müller[1,*],

† Both authors contributed equally to this work.

[1] Cellular and Molecular Biotechnology, Faculty of Technology, Bielefeld University, Bielefeld, Germany

[*]Corresponding author information (Address; Email; Phone)

Kristian M. Müller, Cellular and Molecular Biotechnology, Faculty of Technology, Bielefeld University, Universitätsstraße 25, 33615 Bielefeld, Germany; Email: kristian@syntbio.net; Tel. +49-521-106-6323

SI Method 1:

On the basis of the Fab' fragment of the A20 antibody (PDB ID 3J1S), the A20 single chain variable fragment (scFv) was designed. For the light chain, all amino acids until position Lys107 were chosen. For variable heavy chain, the amino acid sequence ended with Thr124. A $(GGSG)_4$ linker was chosen to link the C-terminus of the light chain with the N-terminus of the heavy chain, where the last serine of the linker is also the first amino acid of the variable heavy chain. In order to enable secretory expression of the scFv, the protein construct was extended by the 22 amino acid long signal peptide sequence of the murine variants of the Ig-κ chain (UniProt: P01601) at its N-terminus. At the C-terminus it was extended by the sequence of the human IgG1-Fc part (the 232 C-terminal amino acids of the human Ig gamma-1 chain C region, including the hinge region and the C_H2 and C_H3 domains of the antibody (UniProt: P01857)) and a His_6-tag sequence. As an expression vector, pcDNA5/FRT (ThermoFisher Scientific) was chosen. The sequence was ordered as a gene synthesis and inserted into pCDNA5/FRT via restriction digest with NheI and ApaI of the gene synthesis and the vector. The insert sequence is shown below.

Sequence information for A20-scFv

Restriction sites are underlined

GCTAGCGCCACCATGGACATGAGAGTGCTGGCTCAGCTGCTGGGACTGCTGCTGTGTGTTTCCCTGGCGCTAGATGCGAC
ATCCAGATGACCCAGTCCTCCTCCAGCTTCTCCGTGTCTCTGGGCGACAGAGTGACCATCACATGCAAGGCCTCCGAGGA
CATCCACAACAGACTGGCCTGGTACAAGCAGAAGCCTGGCAACGCTCCCCGGCTGTTGATTTCTGGCGCTACCTCTCTGG
AAACCGGCGTGCCCAGTAGATTCTCCGGCTCTGGCTCTGGCAAGGACTACACCCTGTCTATCACCAGCCTCCAGAACGAG
GACGTGGCCACCTACTACTGCCAGCAGTATTGGATCGGCCCCTTCACCTTCGGCTCCGGCACCAACCTGGAAATCAAAGG
CGGAGGATCTGGCGGAGGAAGCGGTGGCGGATCAGGTGGTGGATCTGATGTCCAGCTGCAAGAGTCTGGCCCCGACCTGG
TTAAGCCCTCTCAGTCTCTGTCTCTGACCTGCACCGTGACCGGCTACTCTATCACCTCTGGCTACACCTGGCACTGGATC
AGACAGTTCCCCGGCAACAAGCAAGAGTGGATGGGCTACATCCACTTCAGCGGCTACA CCAACTACAACCCCAGCCTGA
AGTCCCGGGTGTCCATCACCAGAGATACCTCCAAGAACCAGTTCTTCCTGCACCTGAACTCCGTGACCACCGAGGATACC
GCTACCTACTATTGCGCCAGAGGCGACTACGGCTACGAGTGGTTTACCTATTGGGGCCAGGGCACCCTGGTCACCGTGTC
TGCTGCTAAAACAACCGGCGGTGGTAGTGGTGGTTCTGGTGGCGGAGGTACCGAACCTAAGTCTTGCGACAAGACCCACA
CCTGTCCCCCCTGTCCTGCTCCTGAACTGCTGGGCGGACCTTCCGTGTTCCTGTTCCCCCCAAAGCCCAAGGACACCCTG
ATGATCTCCCGGACCCCCGAAGTGACCTGCGTGGTGGTGGATGTGTCCCACGAGGACCCTGAAGTGAAGTTCAATTGGTA
CGTGGACGGCGTGGAAGTGCACAACGCCAAGACCAAGCCCAGAGAGGAACAGTACAACTCCACCTACCGGGTGGTGTCCG
TGCTGACCGTGCTGCACCAGGATTGGCTGAACGGCAAAGAGTACAAGTGCAAGGTGTCCAACAAGGCCCTGCCTGCCCCC
ATCGAAAAGACCATCTCCAAGGCCAAGGGCCAGCCCCGGGAACCTCAGGTGTACACCCTGCCCCCTAGCAGGGACGAGCT
GACCAAGAACCAGGTGTCCCTGACCTGTCTCGTGAAGGGCTTCTACCCCTCCGACATTGCCGTGGAATGGGAGTCCAACG
GCCAGCCTGAGAACAACTACAAGACCACCCCCCCTGTGCTGGACTCCGACGGCTCATTCTTCCTGTACTCCAAGCTGACA
GTGGACAAGTCCCGGTGGCAGCAGGGCAACGTGTTCTCCTGCTCCGTGATGCACGAGGCCCTGCACAACCACTACACCCA
GAAGTCCCTGTCCCTGAGCCCCGGCAAGACCGGTCATCACCACCACCATCACTGAGGGCCC

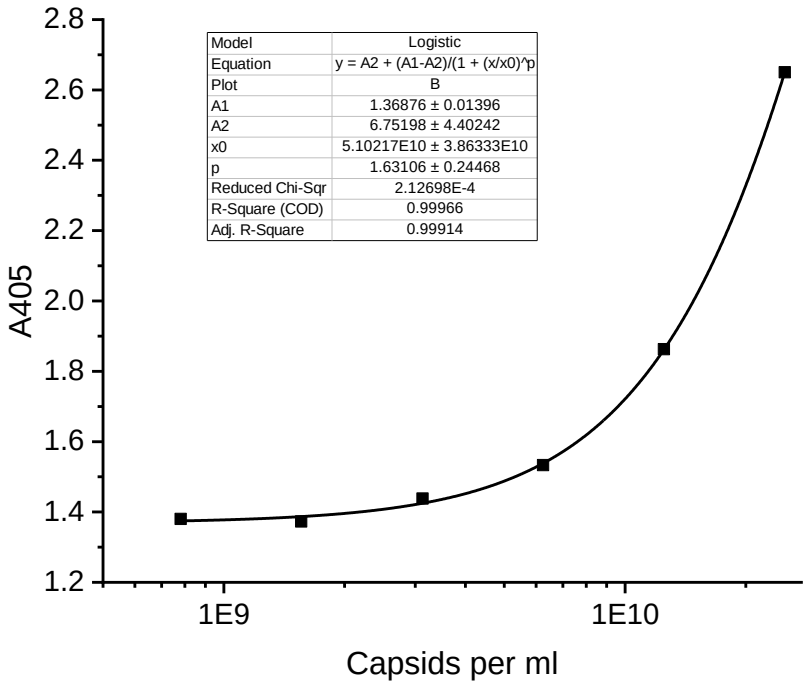

SI Figure 6: Standard curve for the determination of capsid titer. The kit control from AAV2 titration ELISA (Progen) was diluted as recommended in the kit instruction. The particle titer was calculated by a 4 parameter logistic fit with OriginPro 2018 software.

Comparison of viral mediated suicide gene therapy targeting by promoters and de-targeting by miRNA in tumor and primary cells

Kathrin E. Teschner[1], kathrin.schlicht@uni-bielefeld.de

Julian Teschner[1], julian.teschner@uni-bielefeld.de

Kristian M. Müller[1*], kristian@syntbio.net

Institutional Affiliation:

[1] Cellular and Molecular Biotechnology, Faculty of Technology, Bielefeld University, Bielefeld, Germany

* Corresponding author information (Address; Email; Phone)

Kristian M. Müller, Cellular and Molecular Biotechnology, Faculty of Technology, Bielefeld University, Universitätsstraße 25, 33615 Bielefeld, Germany; Email: kristian@syntbio.net; Tel. +49-521-106-6323

Abstract

Gene therapy for cancer offers the potential to of tailoring to specific cell types and thus overcome the lack of specificity of conventional non-invasive therapies. Targeting approaches limit the expression of a transgene to the tumor, thus avoiding normal tissue toxicity. This can be achieved at the transcriptional and translational level. Using recombinant adeno-associated virus (rAAV) for gene delivery in a virus-directed enzyme prodrug therapy (VDEPT), enables transcriptional control by tumor specific promoters and translational control mechanism by influencing the lifetime of mRNA transcripts. Here, we constructed rAAV2 vectors with thymidine-kinase (TK) under the control of survivin (SUR), cyclooxygenase-2 (COX-2) or the C-X-C motif chemokine receptor 4 (CXCR-4) promoter. Tumor specificity was compared to the strong cytomegalovirus immediate early promoter (CMV) driven gene expression. For an additional layer of tumor-specificity the let-7a microRNA (miRNA) target sequence was introduced into CMV- and SUR promoter driven expression cassettes. All promoters exhibited transcriptional activity in HT-1080, MDA-MB231, MDA-MB453 and A431 cancer cell lines as well as in primary HDFa and healthy M1FS fibroblast cells. In the presence of the prodrug ganciclovir (GCV) a cytotoxicity assay demonstrated dramatic repression of CMV promoter driven gene expression upon miRNA de-targeting, leading to the highest tumor-specificity among all investigated transgene expression cassettes. Contrary to expectations the CMV promoter may be a good candidate for tumor specific gene expression when combined with miRNA de-targeting strategies.

Introduction

Cancer is one of the leading causes of death in the world.[1] The clinical effectiveness of conventional chemo- and radiotherapy is limited due to a lack of specificity, which causes serious side effects. Gene therapy offers the possibility to target a therapeutic transgene to tumor cells in order to avoid tissue toxicity. Virus-directed enzyme prodrug therapy (VDEPT) is an emerging strategy in the treatment of cancer. By delivering of an enzyme, a prodrug is activated into a cytotoxic compound that leads to apoptosis of the cancer cell.[2] In this context, the herpes simplex virus type 1 thymidine kinase (HSV-tk) is most commonly used. By conversion of Ganciclovir (GCV) into the toxic metabolite GCV-triphosphate in cells expressing HSV-tk, fast dividing cells undergo apotosis.[3,4] To facilitate cell killing, a HSV-TK mutant (HSV-TK30) was developed which shows higher kinase activity and by this an increased GCV sensitivity [5]. For activation of the non-toxic prodrug ganciclovir to ganciclovir triphosphate it passes three phosphorylation steps in which endogenous guanylate kinases (GMK) catalyze the phosphorylation of ganciclovir monophosphate (GCV-MP) to GCV diphosphate (GCV-DP). To overcome limitations in this intracellular conversion, a fusion gene consisting of mouse guanylate kinase (mGMK) and HSV-TK30 (mGMK-TK30) was incorporated into our suicide gene construct.[6]

Recombinant adeno-associated viruses (rAAV) emerged as an outstanding option for gene therapy. rAAVs provide long-term target gene expression, are not associated with any disease and are unable to replicate autonomously resulting in a high safety profile. They transduce a wide range of dividing and non-dividing cells and are able to penetrate the stroma of solid tumors due to their small size, which ensures adequate distribution of the transgene throughout the tumor.[7,8] Systemic application of rAAV allows targeting of the primary tumor and metastases but requires a strict control of gene expression to prevent harm to normal tissue.[9] In general, tissue targeting with AAV can be attained by the use of different tissue specific serotypes. For example, AAV1 and AAV9 are able to transduce skeletal and cardiac muscle cells, whereas AAV8 delivers genes effectively to the liver of rodents and non-human primates.[10,11] By recombinant techniques, for instance directed evolution

or insertions of larger binding proteins, e.g. designed ankyrin repeat proteins (DARPins), variants of known AAV serotypes have been produced to ensure greater cell specificity.[12,13] Transcriptional control of transgene expression can further increase targeting efficiency and will be an essential part of systemic cancer therapy.[9,14] In the past a set of genes has been identified that are turned on or upregulated in certain types of tumors.[15–17]. The promoters of survivin (SUR), cyclooxygenase-2 (COX-2) and the C-X-C motif chemokine receptor 4 (CXCR-4) are potential candidates for directed cancer gene therapy. Survivin belongs to the inhibitor of apoptosis protein family (IAPs) with an important role in the regulation of apoptosis. It was found to be expressed in a variety of human cancers like brain, breast and ovarian tumors and to be absent in most normal tissue.[18,19] COX-2 expression is upregulated during inflammation and cancers like breast and colorectal cancer. It has been reported, that it is involved in tumor growth, invasion and metastasis and is rarely detected in most normal adult tissue.[17,20] Overexpression of CXCR-4 gene is typical for ovarian and breast cancer, as well as for human melanoma.[21,22] An additional layer of tumor specificity is advisable as residual activity of tumor-specific promoters in normal human cells was observed.[23,24] Post-transcriptional repression of transgene expression has been an emerging approach to improve vector targeting. MicroRNAs (miRNAs) are single-stranded, non-coding RNA molecules that anneal with complementary sequences in the 3`untranslated region (3'- UTR) of target mRNAs triggering either translational repression or mRNA degradation.[25]

The aim of this study was to develop a combined transcriptional and translational targeting strategy in for an increased tumor specificity in the context of VDEPT using rAAV serotype 2 (rAAV2). For this purpose, tumor-type specific promoters (TSPs) were used to drive the expression of the HSV-*tk* suicide gene rAAV2 upon transduction of various tumor cell lines. In the past, low promoter activity and by this insufficient expression of target proteins was observed.[14] Therefore, the tumor specific promotors (TSPs) were equipped with a strong Kozak sequence in front of the start codon. The Kozak consensus sequence 5'-GCCRCC**ATG**G-3' (R = purine A or G), is known to enhance the initiation of translation by improving the recognition of the AUG start codon through the pre-initiation complex (PIC) and recruitment of the large ribosomal subunit.[26,27] By this, potentially low transcription rate of chosen promoters should be compensated by improved translation. The early immediate cytomegalovirus promoter (CMV) in contrast shows high expression levels in a variety of mammalian cells without tumor specificity and by this leads to off-target effects in normal human tissue. This promoter was chosen as a positive control for transfection efficiency as well as for comparison of achieved protection of non-tumor cells using TSP. Furthermore, translational control of gene expression by addition of a let7a miRNA target sequence at the 3`UTR was included.

Results

Ganciclovir influences cell viability in a dose dependent manner

To determine the strength of TSPs, expression of HSV-TK was assessed by the conversion of GCV to GCV-TP. Previous data suggested, that a GCV concentration of 1 mM showed the greatest effect on cell viability after transduction of HT1080 cells with viral particles containing the mGMK-TK30 transgene.[28] Lower concentrations of GCV led to a weaker reduction in cell viability at a constant MOI. However higher concentrations were not tested in this previous study. To control whether even higher concentrations of ganciclovir were tolerated by the cells a cytotoxicity assay was performed on HT1080 cells. In **Fig. 1a**, a major drop in cell viability caused by the increasing GCV concentration was observed which remained relatively constant up to a concentration of 1 mM. Since healthy cells should be studied, the high impact of GCV in the absence of thymidine-kinase

is untenable. Therefore, the concentration of 1 mM GCV was retained and the effect on all other cell lines used was investigated. The decline in cell viability relative to untreated cells is comparable between chosen cells lines ranging between 80 % for MDA-MB231 and 100 % for A431 **(Fig. 1b)**.

rAAV2 transduction with bicistronic vector constructs lead to limited fluorescence signals

To correlate the effect of GCV on transduced cells with the transduction efficiency, the sequence of eGFP was introduced into the transgene expression cassette. However, flow cytometry analysis revealed, that the eGFP fluorescence signal was lower than expected, as at least for HT1080 transduction efficiencies of more than 90 % are known for rAAV2 when using the CMV promoter.[29] By this the eGFP fluorescence signal in the context of the bicistronic vector construct was not suitable for the determination of transduction efficiency **(SI Fig. 1)**. The T2A site in the bicistronic vector should mediate 'cleavage' of polypeptides during translation. The underlying mechanism relies on a steric hindrance during translation and ribosome skipping leading to two 'cleaved' proteins. More 2A sites exist, but T2A was reported to show the highest level of protein expression at the second gene position.[30] However, a decrease of up to 70 % compared to the first gene in a bicistronic vector construct was observed.[31] Additionally, it was found that cleavage efficiency differs widely between different cell lines.[32] Therefore, a drop in eGFP expression was to be expected, although a decrease of the fluorescence signal below the detection limit was unpredictable. To determine the transduction efficiency of rAAV2 wt on the cell lines despite missing GFP fluorescence, cells were transduced with a CMV-mVenus (rAAV2_mVenus) vector construct. Here, fluorescence gene expression was directly driven by CMV promoter without being influenced by the bicistronic vector conditions.

Successful transduction was detected by the expression of the delivered transgene mVenus using flow cytometry **(SI Fig. 2)**. Transduction efficiency ranged from 59.5 % for HDFa to 98 % for HT1080 cells **(Table 1).** This proved the functionality of the rAAV2 wt on HDFa, M1FS, MDA-MB453, MDA-MB231 and A431 cell lines and was therefore suitable as a test system for further investigations regarding the use of rAAV2 wt in combination with thymidine kinase to selectively kill tumor cells.

The efficiency of de-targeting is dramatically increased using a translational control mechanism

To access whether the chosen promoters are cancer-specific and to compare the cancer-specificity between the TSP and the commonly used CMV promoter, rAAV2 transduction with vector constructs listed in **SI Table 1** were used to determine the activity of the promoters in cancer and normal cell lines. A schematic picture of the bicistronic expression cassette used is shown in **Figure 2a**. As normal cell lines, HDFa and M1FS cells were chosen. HDFa are primary human dermal fibroblasts from adult skin. M1FS is a foreskin fibroblast culture from an apparently healthy individual and by this, both are not tumor derived. Cells were transduced with a multiplicity of infection (MOI) of 10'000 and after 24 h, 1 mM GCV was added for another 72 h and a cytotoxicity assay (Alamar Blue Assay) was performed by adding resazurin. As reference (negative control), cells transduced with rAAV2_mVenus **(Fig. 2b)** were used which were also incubated with GCV to exclude effects on cell viability resulting from transduction.

In Figure 3, results of the Alamar Blue assays for the two non-cancer cell lines HDFa and M1FS are shown. Additionally, the number of non-transduced cells is displayed via a horizontal line **(Fig. 3a, c)**. The conversion of GCV to its toxic metabolite was highest for the CXCR-4 promoter driven gene expression in HDFa **(Fig. 3a, sixth column)** and CMV promoter in M1FS **cells (Fig. 3c,** first column**)** indicated by the lowest relative fluorescence. The addition of the let-7a miRNA target

sequence (let-7aT) allowed for a strong protective effect for the CMV promoter construct, whereas the SUR promoter remained virtually unaffected by the translation control in both cell lines **(Fig. 3a, c** columns with banded pattern**)**. In **Fig. 3b, d**, only transduced cells were investigated and the proportion of dead cells in these populations were calculated from the relative fluorescence data. For HDFa and M1FS, the COX-2 promoter led to the lowest number of dead cells in the transduced population if only transcriptional targeting is considered. Overall, CMV promoter driven gene expression in combination with let-7aT, turned out to be the best combination for both non-cancer cell lines, and was able to rescue all transduced HDFa cells and only 12.8 % of M1FS cells died **(Fig. 3b, d** second columns**)**. Interestingly, even if the highest expression rate was achieved under the CMV promoter, many of the transduced cells were still viable (~ 40 % HDFa, ~30 % M1FS). Since we observed doubling times of up to 48 h for both cell lines, a higher effect of GCV-treatment can probably be achieved by longer exposure times, as cytotoxicity of GCV-TP is induced by its incorporation into the DNA of replicating cells and by this inhibiting DNA synthesis.

The results of the cytotoxicity assay for the four cancer cell lines were displayed in **Fig. 4**. On the left-hand side (Fig. 4a, c, e, g) an overview of the total transduced populations, and on the right-hand side **(Fig. 4b, d, f, h)** only the percentage of dead cells in the transduced fraction were shown. In the transduced population, for HT1080, MDA-MB231 and A431 almost all cells died under CMV promoter driven suicide gene expression **(Fig. 4b, d, h, first column)**. For MDA-MB453 **(Fig. 4f)** the high percentage of viable cells is expected to be a result of observed doubling times of approximately 48 h as before for HDFa and M1FS cells. HT1080 cells strongly responded to the treatment with ganciclovir regardless of the promoter and let-7aT and by this HT1080 were not well suited as a control cell line, since differences in targeting efficiency were not discernible **(Fig. 4a, b)**. De-targeting with let-7aT led to an increase in the relative fluorescence for all tumor cells **(Fig. 4a, c, e, g;** columns with banded pattern**)** indicating that let-7a target sequence may not be the best-possible sequence for selected cell.

De-targeting efficiency is highest for the CMV promoter in combination with the let-7a target sequence

To determine the individual tumor specificity of the promoters used alone, or in combination with the let-7aT, the percentage of dead cells for the given promoter in HDFa **(Fig. 5a)** or M1FS **(Fig. 5b)** cells was divided by the percentage of dead cells of the respective tumor cells with the corresponding promoters. By this a heat map was generated indicating a ratio of zero in green and a ratio of one and more in read. Combinations with a value close to zero or zero, show the highest tumor specificity. Here, no or low numbers of the non-cancer cells and high proportions of the cancer cells died. At a value of one and more at least the same proportion of dead cells was found in the cancer and non-cancer cell lines. For both reference cell lines (HDFa, M1FS) the same pattern can be seen, with MDA-MB453 showing the only exception for CMV_let-7a. Across all other cell lines, the highest tumor specificity was achieved with the combination of the CMV promoter with the let7a target sequence. The CXCR-4 promoter showed low tumor specificity in the investigated cell lines. On the contrary, in A431 and MDA-MB453 even more non-tumor than tumor cells died. For breast cancer cell lines MDA-MB231 and MDA-MB453 previous data suggested high survivin promoter activity.[33,34] At least for MDA-MB231 this was proven here as well. For MDA-MB453, both the COX-2 promoter and the SUR_let-7a combination achieve the highest tumor specificity.

Discussion

rAAV emerged as an outstanding option for gene therapy and systemic application allows targeting of the primary tumor and metastases. In order to prevent healthy cells from expressing a suicide gene, the integration of several target layers promises targeted gene expression limited to cancer cells. This work provides insights in the possibility of de-targeting of non-cancer cells in rAAV VDEPT approaches. Bicistronic vectors, with the sequence of HSV-*tk* and *eGFP* were constructed to correlate the effect of GCV on transduced cells with the transduction efficiency. To obtain two proteins from one promoter a T2A site was introduced in between the two genes. Upon transduction, low fluorescence for CMV promoter-driven gene expression and almost no eGFP fluorescence was detectable for the tumor-specific promoters. **(SI Fig. 1)**. The T2A site in the bicistronic vector should mediate 'cleavage' of polypeptides during translation. The underlying mechanism relies on a steric hindrance during translation and ribosome skipping leading to two 'cleaved' proteins. More 2A sites exist, but T2A was reported to show the highest level of protein expression at the second gene position.[30] However, a decrease of up to 70 % compared to the first gene in a bicistronic vector construct was observed.[31] Additionally, it was found that cleavage efficiency differs widely between different cell lines.[32] Therefore, a drop in *eGFP* expression was to be expected, although a decrease of the fluorescence signal near the detection limit was unpredictable. To determine the transduction efficiency of rAAV2 on the cell lines despite missing eGFP fluorescence, cells were transduced with rAAV2-CMV-mVenus and showed that rAAV2 represented a suitable vector for all investigated cell lines with transduction efficiencies ranging from 58.1 % for HDFa to 97.0 % for HT1080 **(Table 1)**. It was assumed, that this transduction ability should remain if the transgene is changed, since the capsid remains the same. Admittedly, it has been reported that about 10 % of undissolved polypeptides are produced by ribosome read-through.[31] This effect was not taken into account in the evaluations but should be aware, since individual activity of the two proteins in potentially present fusion proteins is unknown and may cause cells to show no thymidine kinase activity even though they were transduced.

By a cytotoxicity assay, cancer specific expression of HSV-*tk* was shown for all TSPs to varying degrees depending on the cell line. HT1080 cells strongly responded to treatment with ganciclovir regardless of the promoter **(Fig.4a, b)** and are therefore not well suited as a control cell line since differences in promoter strength are not apparent. For surviving, over-expression is well known in most human tumor types, including colon, breast, lung and melanoma cancer. For breast cancer cell lines MDA-MB231 and MDA-MB453 increased SUR promoter activity was reported in plasmid transfection approaches [35] or detection of survivin protein levels by western blot.[33] However, to our knowledge in the context of rAAV transduction, no data were available. This study demonstrates, that the survivin promoter in combination with a strong Kozak sequence can drive gene expression upon transduction in MDA-MB231 **(Fig. 4c, d)**, but not in MDA-MB453 **(Fig.4e, f)**, which was unexpected. The copy number of the transgene in plasmid transfection experiments is presumed to be much higher (up to 50,000 copies per nucleus) than in transduction approaches and by this may lead to this unsuspected result.[36] For MDA-MB453, both the COX-2 promoter and the SUR_let-7a combination achieve the highest tumor specificity. For the CXCR-4 promoter, high activity was detected in the two non-cancer cell lines and appears not to be an option in the context of rAAV2 based suicide gene therapy.

Surprisingly, the highest tumor-specific gene expression was reached with the CMV promoter driven gene expression in combination with let-7a miRNA translational repression. However, a reduced HSV-tk activity was observed in non-cancer as well as in cancer cells upon addition of the miRNA target sequence, indicating that even though aberrant miRNA expression is well known for

cancer cells,[37–39] a general statement about the expression profile cannot be made. For MDA-MB231 and MDA-MB453 cells, a high let-7a expression level was detected in miRNA microarrays, which fits to obtained results.[38] Though, for A431 and HT1080 no published data were found, but the experimental findings indicate that let-7a miRNA is also expressed in this both cell lines. To optimize the regulation of protein translation, other miRNA target sequences are possible or even the use of different targets in one transgene expression cassette to de-target various cells.[24]

In the HSV-*tk*/GCV prodrug system the occurrence of a bystander effect was frequently observed.[40–42] A drop of the relative fluorescence below the number of transduced cells **(horizontal line in Fig. 3a, c** and **4a, c, e, g)** may provide a good indicator for this effect, but was not observed in any investigated cell line. In previous *in vitro* studies, it was found that cell-cell contact is essential for most cell lines for an efficient bystander effect.[43,44] In this study low plating densities were used in order to circumvent an overgrowing of the culture during the four day long cultivation in 96-well plates which underlines this assumption.

In summary these results suggest, that no general statement can be made about the functionality of the individual promoters. Also, for let-7a upregulation rather than downregulation of the miRNA was reported for several types of cancer.[45] Regarding the bystander effect, higher plating densities could potentially lead to an increased killing and needs to be further evaluated. The addition of translational control by the introduction of miRNA target sequences showed to be a powerful tool. The most promising combination of the strong CMV promoter with the let-7a miRNA target sequence can serve as a good starting point for further optimization e.g. with other or even a combination of several miRNA target sequences in one transgene expression cassette. One optimal promoter and one miRNA target sequence for all types of cancer is unrealistic and a patient-specific adaptation of the transgene expression cassette is probably inevitable.

Methods

Construction of plasmids. Six different plasmids were constructed, harboring the bicistronic expression cassette (in parentheses the respective promotors): pZMB0588 (CMV); pZMB0589 (COX-2); pZMB0590 (SUR); pZMB0591 (CXCR-4); pZMB0639 (CMV_let-7a); pZMB0640 (SUR_let-7a). For the expression of the thymidine-kinase under the control of tumor-specific promoters, survivin (Sur), cyclooxygenase 2 (COX-2) and chemokine receptor type 4 (CXCR-4) gene syntheses (GeneArt, Thermo Fischer Scientific) were constructed. For human survivin promoter a 521-base-pair (bp) long fragment (nucleotides 2283 to 2804, GenBank Accession number U75285.1), for COX-2 a 904 bp (nucleotides 6249 to 7152, GenBank Accession Number AF044206.1) and for CXCR-4 a 936 bp (nucleotides 1165 to 2100, GenBank Accession Number AY728138.1) fragment was designed for idempotent cloning strategy according to RFC[10].[46] The CMV, hGHpA and mGMK-TK30 containing plasmids were from the iGEM parts registry (parts.igem.org). AAV plasmids listed in **SI Table 2** were cloned as described in **SI Method 1**. Resulting vectors were analyzed for their correctness by Sanger DNA-sequencing (Sequencing Core Facility, CeBiTec, Bielefeld, Germany).

Cell Culture. HDFa (Thermo Fisher Scientific), M1FS (HDZ), HT1080 and HEK293 (DSMZ) cells were cultured in Dulbecco's Modified Eagle Medium supplemented 10% (v/v) fetal calf serum and 1% (v/v) penicillin/streptomycin (Sigma Aldrich). A431, MDA-MB231 and MDA-MB-453 (DSMZ) were cultured in RPMI supplemented 10% (v/v) fetal calf serum and 1% (v/v) penicillin/streptomycin. Cells were maintained at 37°C and 5% CO_2.

Viral particle production. HEK293 cells were seeded at a density of 9×10^6 cells per 150 mm dish the day before transfection. A total amount of 30 µg DNA per 150 mm dish was transfected using calcium phosphate. RepCap (pZMB0216), ITR (pZMB0522) and pHelper (pZMB0088) plasmid were used in a 1:1:1 molar ratio.[47] After 72 h of incubation at 37 °C, cells were harvested and pelleted by centrifugation (2000×g, 5 min).

Purification of viral particles. Cells were resuspended in lysis buffer (50 mM Tris, 150 mM NaCl, 2 mM $MgCl_2$, pH 7.5) and viral particles were released from cells with three freeze-thaw cycles. Remaining DNA contamination was degraded by incubation with benzonase nuclease (final 100 U/ml, Sigma Aldrich) at 37 °C prior to addition of CHAPS (3-[(3-cholamidopropyl)dimethylammonio]-1-propanesulfonate, 0.5% w/v final). The crude lysate was cleared from cell debris by centrifugation (3,000×g, 10 min). This crude viral stock was further purified with a discontinuous iodixanol gradient[48]. Briefly, the lysate was transferred onto a gradient of 60%, 40%, 25% and 15% iodixanol in an open top polyallomer 16 x 76 mm tube (Science Services). Tubes were sealed and centrifuged in a T-880 rotor (Sorvall) at 340,000×g for 2 h at 18 °C. The rAAV containing fraction was collected with a 21G x 1 1/2" injection needle and the buffer was exchanged to 1× PBS (137 mM NaCl, 2.6 mM KCl, 10 mM Na_2HPO_4, 1.8 mM KH_2PO_4, pH 7.2) via Amicon Ultra-4 100K centrifugal filter units (Merck Millipore).

Determination of genomic titers. Before determination of genomic titers via qPCR, samples were treated with 10 U DNase I (New England Biolabs) in 10× DNaseI buffer in a final volume of 50 µl at 37 °C for 30 min before heat inactivation of the DNase I (75 °C, 20 min). 50-fold dilutions of the DNase I digest were used as template in the qPCR reaction. Samples were mixed with 2.5 µl primer qPCR-hGH-for (5'-CTCCCCAGTG CCTCTCCT-3') and 2.5 µl primer qPCR-hGH-rev (5´-ACTTGCCCCT TGCTCCATAC-3´), each at a stock concentration of 4 µM, and 10 µl of 2× GoTaq qPCR Mastermix (Promega). The qPCR reaction was carried out as described in the manual (TM318 6/14, Promega) with an increased time interval for the first denaturation step (95 °C, 10 min) using a LightCycler 480 II (Roche). The genomic titer was calculated from a standard curve of 10^2 to 10^7 copies of the ITR plasmid (CMV-mVenus) with an efficiency between 90-110% and an R value less than 0.1.

Transduction assay. The transducibility of the cell lines was analyzed by transduction of respective cells with a vector plasmid coding for the fluorescence reporter mVenus. 10′000 cells were seeded in biological duplicates on a 12-well plate and after cells had settled, they were transduced with a MOI of 10,000. After three days, cells were detached by trypsinization for flow cytometry analysis. 10′000 events were counted using a Becton-Dickenson FACSCalibur instrument. Data sets were analyzed using FlowJo V10. Positive cells were calculated by Overton cumulative histogram subtraction.

Alamar Blue Assay. Cell viability was assessed by a cytotoxicity assay. In case of transduction experiments, 10,000 cells with a cell density of 1,000 cells ml^{-1} of respective cell lines were mixed with rAAV_promoter_mGMK-TK30_T2A_eGFP were the expression is driven by different promoters. CMV, COX-2, Survivin and CXCR-4 were chosen and used with a MOI of 10′000 in biological duplicates. After careful mixing, 100 µl of the cell suspension was dispensed in 6-fold replicates in a 96-well plate. After 24 h, 1 mM ganciclovir (Sigma Aldrich) was added for another 72 h. After the incubation period, resazurin was added at a final concentration of 0.05 g L^{-1}. The plates were placed in an incubator at 37 °C, 5 % CO_2 and fluorescence intensity was measured at regular intervals in a PowerWave HT (BioTek) plate reader with an excitation wavelength of 545/30 nm and an 590/20 emission filter. Fluorescence data were normalized to the fluorescence signal of cells

transduced with rAAV2_mVenus with added ganciclovir. To study the effect of different GCV concentration on non-transduced cells, 1,000 HT1080 cells in 100 µl growth medium were seeded in 6-fold replicates in a 96-well plate and 0, 0.5, 1, 2 and 4 mM GCV was added. After 72 h Alamar Blue Assay was performed. The relative fluorescence of the samples was calculated by setting the fluorescence signal of cells without GCV as 100 % viable. For the other cell lines, only the working concentration of 1 mM GCV was tested as described.

References

1. Siegel, R. L., Miller, K. D. & Jemal, A. Cancer statistics, 2019. *CA. Cancer J. Clin.* **69**, 7–34 (2019).

2. Huber, B. E., Richards, C. A. & Austin, E. A. Virus-directed enzyme/prodrug therapy (VDEPT). Selectively engineering drug sensitivity into tumors. *Ann. N. Y. Acad. Sci.* **716**, 104–14; discussion 140-3 (1994).

3. Wang, Y., Canine, B. F. & Hatefi, A. HSV-TK/GCV cancer suicide gene therapy by a designed recombinant multifunctional vector. *Nanomedicine* **7**, 193–200 (2011).

4. Pan, J. G., Zhou, X., Luo, R. & Han, R. F. The adeno-associated virus-mediated HSV-TK/GCV suicide system: a potential strategy for the treatment of bladder carcinoma. *Med. Oncol.* **29**, 1938–1947 (2012).

5. Black, M. E., Newcomb, T. G., Wilson, H. M. & Loeb, L. A. Creation of drug-specific herpes simplex virus type 1 thymidine kinase mutants for gene therapy. *Proc. Natl. Acad. Sci. U. S. A.* **93**, 3525–9 (1996).

6. Willmon, C. L., Krabbenhoft, E. & Black, M. E. A guanylate kinase/HSV-1 thymidine kinase fusion protein enhances prodrug-mediated cell killing. *Gene Ther.* **13**, 1309–1312 (2006).

7. Clément, N. & Grieger, J. C. Manufacturing of recombinant adeno-associated viral vectors for clinical trials. *Mol. Ther. - Methods Clin. Dev.* **3**, 16002 (2016).

8. Grimm, D. & Kay, M. a. From virus evolution to vector revolution: use of naturally occurring serotypes of adeno-associated virus (AAV) as novel vectors for human gene therapy. *Curr. Gene Ther.* **3**, 281–304 (2003).

9. Robson, T. & Hirst, D. G. Transcriptional Targeting in Cancer Gene Therapy. *J. Biomed. Biotechnol.* **2003**, 110–137 (2003).

10. Halder, S. *et al.* Structure of neurotropic adeno-associated virus AAVrh.8. *J. Struct. Biol.* **192**, 21–36 (2015).

11. DiMattia, M. A. *et al.* Structural insight into the unique properties of adeno-associated virus serotype 9. *J. Virol.* **86**, 6947–58 (2012).

12. Grieger, J. C., Johnson, J. S., Gurda-Whitaker, B., Agbandje-McKenna, M. & Samulski, R. J. Surface-exposed adeno-associated virus Vp1-NLS capsid fusion protein rescues infectivity of noninfectious wild-type Vp2/Vp3 and Vp3-only capsids but not that of fivefold pore mutant virions. *J. Virol.* **81**, 7833–43 (2007).

13. Hagen, S. *et al.* Modular adeno-associated virus (rAAV) vectors used for cellular virus-directed enzyme prodrug therapy. *Sci. Rep.* **4**, 3759 (2014).

14. Chen, C. *et al.* Promoter-Operating Targeted Expression of Gene Therapy in Cancer: Current Stage and Prospect. *Mol. Ther. - Nucleic Acids* **11**, 508–514 (2018).

15. Qiu, Y. *et al.* Selective killing of lung cancer cells using carcinoembryonic antigen promoter and double suicide genes, thymidine kinase and cytosine deaminase (pCEA-TK/CD). *Cancer Lett.* **316**, 31–8 (2012).

16. Xu, C. *et al.* CEA promoter-regulated oncolytic adenovirus-mediated Hsp70 expression in immune gene therapy for pancreatic cancer. *Cancer Lett.* **319**, 154–163 (2012).

17. Wang, Z.-X., Bian, H.-B., Yang, J.-S., De, W. & Ji, X.-H. Adenovirus-mediated suicide gene therapy under the control of Cox-2 promoter for colorectal cancer. *Cancer Biol. Ther.* **8**, 1480–1488 (2009).

18. Garg, H., Suri, P., Gupta, J. C., Talwar, G. P. & Dubey, S. Survivin: a unique target for tumor therapy. *Cancer Cell Int.* **16**, 49 (2016).

19. Wang, K., Kievit, F. M. & Zhang, M. Evaluation of Four Tumor-Specific Promoters in Various Cancer Cell Lines. **6**, (2016).

20. Liu, B., Qu, L. & Yan, S. Cyclooxygenase-2 promotes tumor growth and suppresses tumor immunity. *Cancer Cell Int.* **15**, 106 (2015).

21. Rajendran, S. *et al.* Targeting of breast metastases using a viral gene vector with tumour-selective transcription. *Anticancer Res.* **31**, 1627–35 (2011).

22. Müller, A. *et al.* Involvement of chemokine receptors in breast cancer metastasis. *Nature* **410**, 50–56 (2001).

23. Adinolfi, B., Pellegrino, M. & Baldini, F. Human dermal fibroblasts HDFa can be used as an appropriate healthy control for PMMA nanoparticles-survivin molecular beacon cellular uptake studies. *Biomed. Pharmacother.* **69**, 228–232 (2015).

24. Geisler, A. & Fechner, H. MicroRNA-regulated viral vectors for gene therapy. *World J. Exp. Med.* **6**, 37–54 (2016).

25. Lee, H., Han, S., Kwon, C. S. & Lee, D. Biogenesis and regulation of the let-7 miRNAs and their functional implications. *Protein Cell* **7**, 100–13 (2016).

26. Grzegorski, S. J., Chiari, E. F., Robbins, A., Kish, P. E. & Kahana, A. Natural variability of Kozak sequences correlates with function in a zebrafish model. *PLoS One* **9**, e108475 (2014).

27. Acevedo, J. M., Hoermann, B., Schlimbach, T. & Teleman, A. A. Changes in global translation elongation or initiation rates shape the proteome via the Kozak sequence. *Sci. Rep.* **8**, 4018 (2018).

28. iGem_Freiburg. Virus Construction Kit for Therapy. (2010). Available at: http://2010.igem.org/Team:Freiburg_Bioware.

29. Feiner, R. C., Baumann, T. & Hannappel, Y. rAAV engineering for capsid-protein enzyme insertions and mosaicism reveals resilience to mutational , structural and thermal perturbations. *Sci. Rep.* 1–19

30. Szymczak, A. L. & Vignali, D. A. Development of 2A peptide-based strategies in the design of multicistronic vectors. *Expert Opin. Biol. Ther.* **5**, 627–638 (2005).

31. Liu, Z. *et al.* Systematic comparison of 2A peptides for cloning multi-genes in a polycistronic vector. *Sci. Rep.* **7**, 2193 (2017).

32. Kim, J. H. *et al.* High Cleavage Efficiency of a 2A Peptide Derived from PorcineTeschovirus-1 in Human Cell Lines, Zebrafish and Mice. *PLoS One* **6**, e18556 (2011).

33. Gong, Y., Li, Y., Abdolmaleky, H. M., Li, L. & Zhou, J. R. Tanshinones inhibit the growth of breast cancer cells through epigenetic modification of aurora a expression and function.

PLoS One **7**, (2012).

34. Yang, L. *et al.* Tumor-specific gene expression using the survivin promoter is further increased by hypoxia. *Gene Ther.* **11**, 1215–23 (2004).

35. Yang, L. *et al.* Tumor-specific gene expression using the survivin promoter is further increased by hypoxia. *Gene Ther.* **11**, 1215–1223 (2004).

36. Cohen, R. N. *et al.* Quantification of Plasmid DNA Copies in the Nucleus after Lipoplex and Polyplex Transfection. *J. Control. Release* **135**, 166 (2009).

37. Guo, J. *et al.* Differential microRNA expression profiles determined by next-generation sequencing in three fulvestrant-resistant human breast cancer cell lines. *Oncol. Lett.* **17**, 3765–3776 (2019).

38. Riaz, M. *et al.* miRNA expression profiling of 51 human breast cancer cell lines reveals subtype and driver mutation-specific miRNAs. *Breast Cancer Res.* **15**, R33 (2013).

39. Rabiau, N. *et al.* miRNAs differentially expressed in prostate cancer cell lines after soy treatment. *In Vivo* **25**, 917–21 (2011).

40. Drake, R. R. *et al.* Connexin-independent ganciclovir-mediated killing conferred on bystander effect-resistant cell lines by a herpes simplex virus-thymidine kinase-expressing colon cell line. *Mol. Ther.* **2**, 515–523 (2000).

41. Vrionis, F. D. *et al.* The bystander effect exerted by tumor cells expressing the herpes simplex virus thymidine kinase (HSVtk) gene is dependent on connexin expression and cell communication via gap junctions. *Gene Ther.* **4**, 577–585 (1997).

42. Qiao, J., Black, M. E. & Caruso, M. Enhanced ganciclovir killing and bystander effect of human tumor cells transduced with a retroviral vector carrying a herpes simplex virus thymidine kinase gene mutant. *Hum. Gene Ther.* **11**, 1569–1576 (2000).

43. Li Bi, W., Parysek, L. M., Warnick, R. & Stambrook, P. J. In Vitro Evidence That Metabolic Cooperation Is Responsible for the Bystander Effect Observed with HSV tk Retroviral Gene Therapy. *Hum. Gene Ther.* **4**, 725–731 (1993).

44. Kuriyama, S. *et al.* Bystander effect caused by suicide gene expression indicates the feasibility of gene therapy for hepatocellular carcinoma. *Hepatology* **22**, 1838–1846 (1995).

45. Nam, S., Kim, B., Shin, S. & Lee, S. miRGator: an integrated system for functional annotation of microRNAs. *Nucleic Acids Res.* **36**, D159 (2008).

46. Knight, T. Idempotent Vector Design for Standard Assembly of Biobricks Standard Biobrick Sequence Interface. *BBF RFC* (2007). Available at: http://hdl.handle.net/1721.1/45138. (Accessed: 24th January 2019)

47. Agilent Technologies. AAV Helper-Free System Instruction Manual. Available at: https://www.agilent.com/cs/library/usermanuals/Public/240071.pdf. (Accessed: 13th August 2019)

48. Zolotukhin, S. *et al.* Recombinant adeno-associated virus purification using novel methods improves infectious titer and yield. *Gene Ther.* **6**, 973–85 (1999).

Acknowledgements

We acknowledge support of the publication fee by Deutsche Forschungsgemeinschaft and the Open Access Publication Funds of Bielefeld University. We thank Philipp Borchert for experimental assistance.

Author contributions statement

KT, JT and KM conceived and designed the experiments. KT prepared the figures and wrote the manuscript. JT and KM helped with writing and edited the manuscript. KM secured funding and supervised all experiments. All authors critically read and approved the final manuscript.

Additional Information

Competing Interests: The authors declare that they have no competing interests.

Figures/ Figure Legends

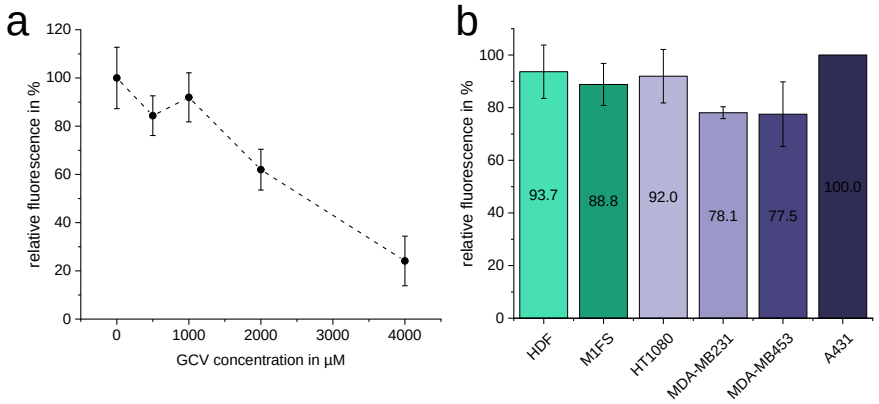

Figure 1: Effect of Ganciclovir on non-transduced cells. (a) Analysis of the effect of increasing GCV concentrations on the viability of HT1080 cells. Relative viability was determined to non-incubated HT1080 cells in biological duplicates and 6-fold technical replicates. For each spot, SD was calculated between biological samples. (b) Cytotoxicity assay to study the effect of 1 mM GCV on the cell viability of HDFa, M1FS, HT1080, MDA-MB231, MDA-MB453 and A431 cells. Relative viability was determined to non-incubated cells in biological duplicates and 6-fold technical replicates. For each column, SD was calculated between biological samples.

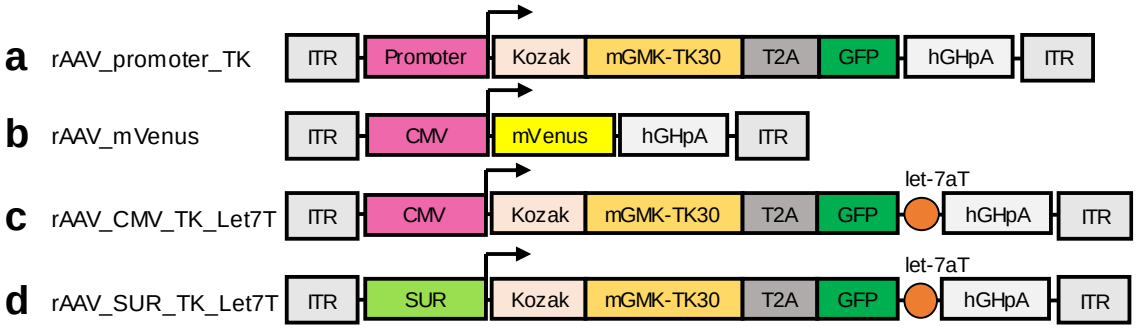

Figure 2: Schematic overview of the rAAV transgene expression cassettes. **a)** Vector plasmid for transcriptional targeting of cancer cells, with promoter as placeholder for CMV, COX-2, SUR or

CXCR-4 promoter, respectively. **b)** CMV_mVenus vector plasmid used as transduction control for the determination of transduction efficiency of rAAV2 and as negative control for the calculation of relative fluorescence. **c and d)** Vector plasmid for translational targeting of cancer cells, where transgene expression is driven by CMV and SUR promoter, respectively. In the 3' UTR of the transgene, a let-7a target sequence (let-7aT) was introduced.

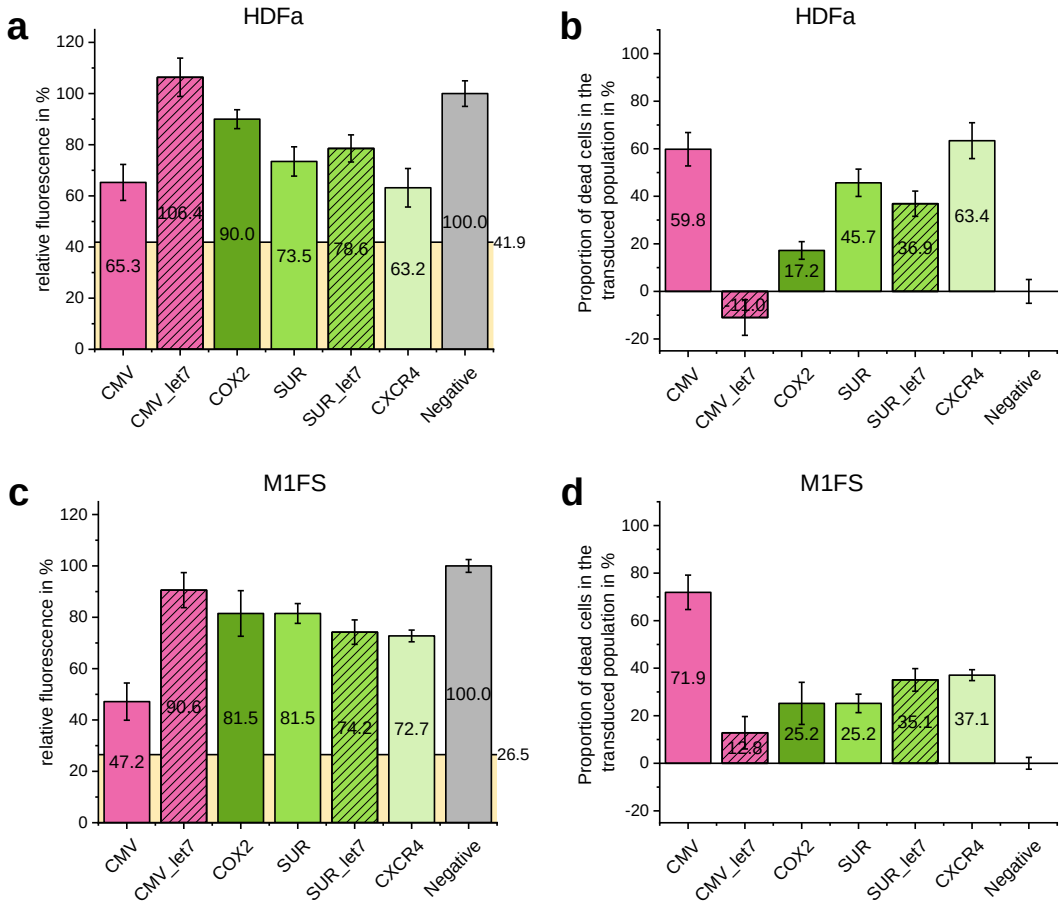

Figure 3: Alamar Blue Assay for determination of thymidine kinase activity in the context of TSPs. The transcriptional activity of CMV, COX-2, SUR and CXCR-4 promoters, driving the transgene expression upon rAAV transduction, was measured in the two non-cancer cell lines HDFa (a, b) and M1FS (c, c). Cells were transduced with a MOI of 10′000 and after 24 h treated with 1 mM GCV for another 72 h before performing the Alamar blue assay. Negative reference cells were transduced with rAAV2_mVenus and treated with 1 mM GCV. (a, c) Calculation of relative fluorescence was performed by normalization of the fluorescence for the different viral vectors to the fluorescence obtained from the rAAV-mVenus transduced reference (negative). The number of non-transduced cells is given as a horizontal line. (b, d) The proportion of dead cells in the transduced population was calculated from the relative fluorescence data and the transduction efficiency determined by rAAV_mVenus transduction of the respective cells. The data shown are the means of two biological duplicates with six technical replicates, with error bars indicating the standard deviation.

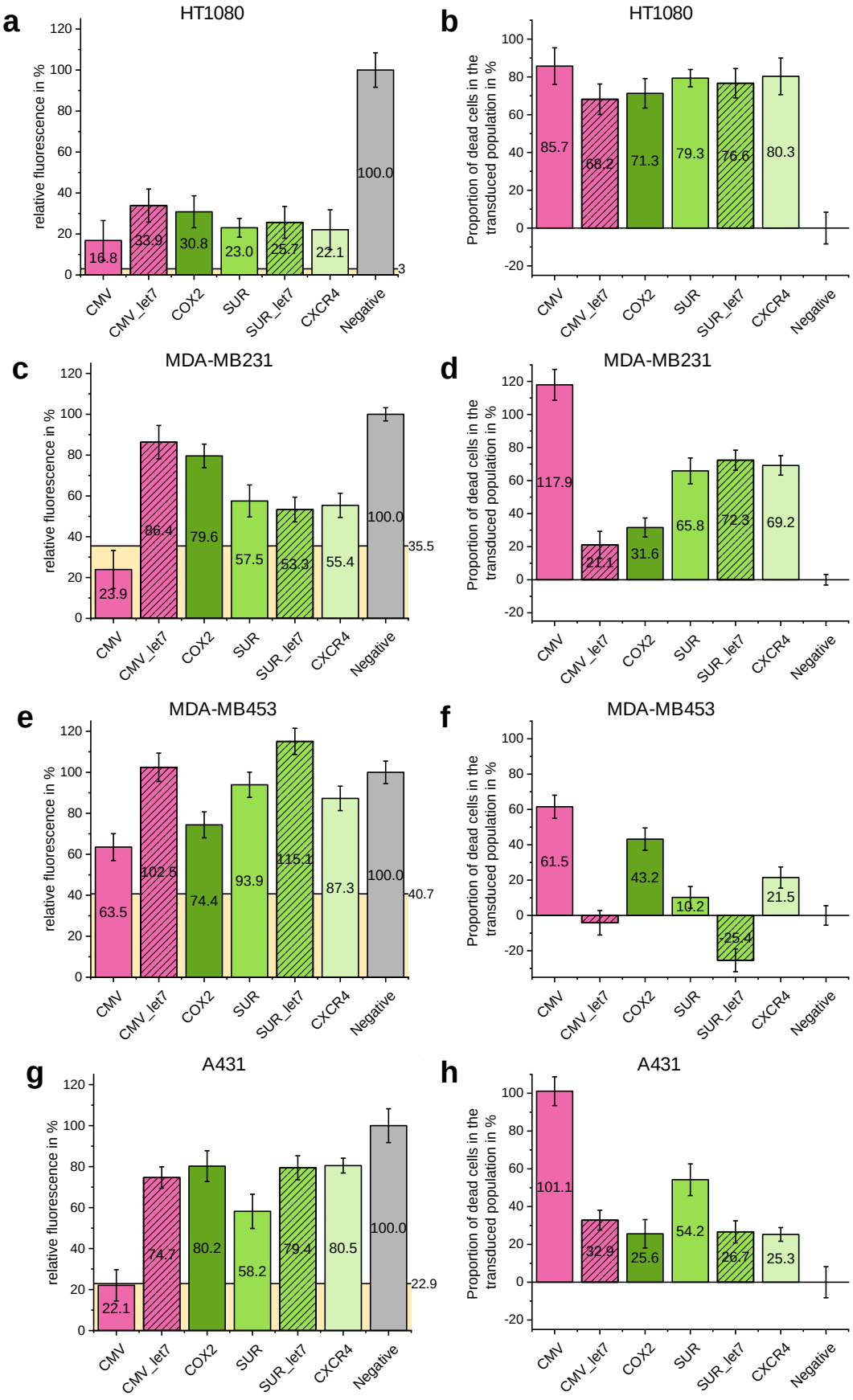

Figure 4: Alamar Blue Assay for determination of thymidine kinase activity in the context of TSPs. The transcriptional activity of CMV, COX-2, SUR and CXCR-4 promoters, driving the transgene expression upon rAAV transduction, was measured in two normal **(a, b)** and four cancer **(c-f)** cell

lines. As reference, respective cells were transduced with rAAV2_mVenus (negative). The data shown are the means of two biological duplicates with six technical replicates, with error bars indicating the standard deviation.

a

HDFa	A431	MDA-MB231	MDA-MB453	HT-1080
CMV	0.59	0.51	0.97	0.70
CMV_let7	0.00	0.00	2.65	0.00
COX2	0.67	0.55	0.40	0.24
SUR	0.84	0.69	4.46	0.58
SUR_let7	1.38	0.51	0.00	0.48
CXCR4	2.51	0.92	2.96	0.79

b

M1FS	A431	MDA-MB231	MDA-MB453	HT-1080
CMV	0.71	0.61	1.17	0.84
CMV_let7	0.39	0.61	0.00	0.19
COX2	0.98	0.80	0.58	0.35
SUR	0.46	0.38	2.46	0.32
SUR_let7	1.32	0.48	0.00	0.46
CXCR4	1.47	0.54	1.73	0.46

Figure 5: Alamar Blue Assay for determination of thymidine kinase activity in the context of TSPs. The transcriptional activity of CMV, COX-2, SUR and CXCR-4 promoters, driving the transgene expression upon rAAV transduction, was measured in four cancer cell lines HT1080 (a, b), MDA-MB231 (c, d), MDA-MB453 (e, f) and A431 (g, h). Cells were transduced with a MOI of 10′000 and after 24 h treated with 1 mM GCV for another 72 h before performing the Alamar blue assay. Negative reference cells were transduced with rAAV2_mVenus and treated with 1 mM GCV. (a, c, e, g) Calculation of relative fluorescence was per-formed by normalization of the fluorescence for the different viral vectors to the fluorescence obtained from the rAAV-mVenus transduced reference (negative). The number of non-transduced cells is given as a horizontal line. (b, d, f, h). The proportion of dead cells in the transduced population was calculated from the relative fluorescence data and the transduction efficiency determined by rAAV_mVenus transduction of the respective cells. The data shown are the means of two biological duplicates with six technical replicates, with error bars indicating the standard deviation.

Tables

Table 35*. Transduction efficiencies of rAAV2 with CMV_mVenus as reporter of different cell lines transduced with a MOI of 10.000. Mean and standard deviation (SD) of two biological duplicates are shown.*

Cell line	Transduction efficiency in %
HDFa	58.1 ± 1.5
M1FS	73.5 ± 1.4
HT1080	97.0 ± 1.0
MDA-MB231	64.5 ± 2.6
MDA-MB453	59.3 ± 2.3
A431	77.1 ± 2.3

Supplementary information

Comparison of viral mediated suicide gene therapy targeting by promoters and de-targeting by miRNA in tumor and primary cells

Kathrin E. Teschner[1], Julian Teschner[1], Kristian M. Müller[1*]

1 Methods

1.1 SI Method 1. Plasmid construction

1.1.1 Plasmids constructed for transcriptional targeting

pZMB0441_mGMK-TK30_T2A_eGFP_hGHpA. This plasmid was generated as a preconstruct, where in following steps all promotors could be inserted via RFC[10]. The coding sequence of mGMK-TK30 and eGFP were amplified via PCR. The oligonucleotide primers provided overhanging ends with RFC[10] restriction sites (lacking NotI) and overlapping nucleotides of the T2A site. The sequences of the primers for mGMK_TK30 amplification are as follows: mGMK-TK30_RFC10_for_new (5´-TGGAATTCTT CTAGATGGCC GGCGCAGGAC CTA) and mGMK-TK30_2A_rev (5´-CCTCTGCCCT CTCCACTGCC ACCGGTGTTA GCCTCCCCCA T). The coding sequence of eGFP was amplified from pSB1C3_001_eGFP (pZMB0398) which was a gene synthesis based on the pEGFP-C1 cloning vector (GenBank entry ACD99686.1) with primers T2A_eGFP_for_ new (5´-GGCAGTGGAG AGGGCAGAGG AAGTCTGCTA ACATGCGGTG ACGTCGAGGA GAATCCTGGC CCAATGGTGT CCAAGGGCGA GG and eGFP_RFC10_rev_new (5´-GGCATGGACG AGCTGTACAA GTAATACTAG TAGCGGCCGC TGCAGAAA). These two PCR products were used in a megaprimer PCR to generate mGMK-TK30_T2A_eGFP which subsequently was cloned into pSB1C3_001_hGHpA (pZMB0135). This plasmid was finally ligated with the different promoters using EcoRI, SpeI and XbaI, with CMV promoter coming from iGEM parts registry. The TSPs were planned as gene synthesis with overhangs according to RFC[10].

pZMB0588_ITR_EXS_CMV_Kozak_mGMK-TK30_T2A_eGFP_hGHpA. This vector was constructed in two steps, starting from pZMB0442_CMV_mGMK-TK30_T2A_eGFP_hGHpA. With primers Pr-for_CMV_MluI (5´-CCAGATATACGCGTTGACATTG) and Pr-rev_Kozak_CMV (5´-GGTGGCCTAG TAATTTCGAT AAGCCAGTAA GC) a part of the CMV promoter was amplified with the Kozak sequence as a 3´ extension. Pr-for_CMV_Kozak (5´-GAAATTACTA GGCCACCATG GCCGGCGCAG G) and Pr-rev_TK30_SalI (5´-CCTT-GTAGGT CGACATCTAG CAC) amplified a part of the mGMK-TK30 with the Kozak sequence as a 5´ extension. This to fragments were used in a megaprimer PCR and was finally ligated into the starting vector after restriction digest with MluI and SalI and by this generated pZMB0584_CMV_Kozak_mGMK-TK30_T2A_eGFP_hGHpA. In a second step, the insert sequence was introduced into pZMB0522_ITR_EXS_CMV_mVenus_hGHpA by restriction digest with EcoRI and SpeI.

pZMB0589_ITR_EXS_COX-2_Kozak_mGMK-TK30_T2A_eGFP_hGHpA. The Kozak sequence was introduced by hybridization of oligonucleotides COX-2-MfeI_Kozak-AvrII_for (5´-AATTGTCATA CTAGAGCCAC CATGGCCGGC GCAGGAC) and COX-2-MfeI_Kozak-AvrII_rev (5´-CTAGGTCCTGC GCCGGCCATG GTGGCTCTAG TATGAC) and ligation into pZMB0443_COX-2_mGMK-TK30_T2A_eGFP_hGHpA by restriction digest with MfeI. In a second step, this sequence was introduced into pZMB0522_ITR_EXS_CMV_mVenus_hGHpA by restriction digest with EcoRI and SpeI.

pZMB0590_ITR_EXS_SUR_Kozak_mGMK-TK30_T2A_eGFP_hGHpA. This vector was constructed in two steps, starting from pZMB0444_SUR_mGMK-TK30_T2A_eGFP_hGHpA. With primers Pr-for_Sur_MluI (5´-CTGCACGCGTTCTTTGAAA) and Pr-rev_Sur_Kozak (5´-GGTGGCCTAGTAGCCGCCACCTCTG) a part of the SUR promoter was amplified with the

Kozak sequence as a 3´ extension. Pr-for_Sur_Kozak (5´-GCGGCTACTAGGCCAC-CATGGCCGGCGCAGG) and Pr-rev_TK30_SalI (5´-CCTTGTAGGT CGACATCTAG CAC) amplified a part of the mGMK-TK30 with the Kozak sequence as a 5´ extension. This to fragments were used in a megaprimer PCR and was finally ligated into the starting vector after restriction digest with MluI and SalI and by this generated pZMB0586_SUR_Kozak_mGMK-TK30_T2A_eGFP_hGHpA. In a second step, the insert sequence was introduced into pZMB0522_ITR_EXS_CMV_mVenus_hGHpA by restriction digest with EcoRI and SpeI.

pZMB0591_ITR_EXS_CXCR-4_Kozak_mGMK-TK30_T2A_eGFP_hGHpA. This vector was constructed in two steps, starting from pZMB0474_CXCR-4_mGMK-TK30_T2A_eGFP_hGHpA. With primers Pr-for_MluI_CXCR-4 (5´-CACAGAGAGA CGCGTTCCTA G) and Pr-rev_CXCR-4_Kozak (5´-GGTGGCCTAG TAGACAAAGC AGGTT-GAAAC TG) a part of the CXCR-4 promoter was amplified with the Kozak sequence as a 3´ extension. Pr-for_CXCR-4_Kozak (5´-CTTTGTCTAC TAGGCCACCA TGGCCGGCGC AGG) and Pr-rev_TK30_SalI (5´-CCTTGTAGGT CGACATCTAG CAC) amplified a part of the mGMK-TK30 with the Kozak sequence as a 5´ extension. This to fragments were used in a mega-primer PCR and was finally ligated into the starting vector after restriction digest with MluI and SalI and by this generated pZMB0587_CXCR-4_Kozak_mGMK-TK30_T2A_eGFP_hGHpA. In a second step, the insert sequence was introduced into pZMB0522_ITR_EXS_CMV_mVe-nus_hGHpA by restriction digest with EcoRI and SpeI.

1.1.2 Plasmids constructed for translational targeting

For translational targeting a let-7a target sequence was introduced to plasmids pZMB0584_CMV_Kozak_mGMK-TK30_T2A_eGFP_hGHpA and pZMB0586_SUR_Kozak_mGMK-TK30_T2A_eGFP_hGHpA. Therefore, eGFP was amplified with following oligonucleotide primers: eGFP_ENX_for (5´-AAAGAATTCG CGGCCCTTCT AGATGGTGTC CAAGGGCGAG) and eGFP_let-7a_SNP_rev (5´-AAACTGCAGC GGCCGC-TACT AGTATGAGGT AGTAGGTTGT ATAGTTTACT TGTACAGCTC GTCCATGCC) which was cloned into pSB1C3_001 hGHpA. By restriction digest with SpeI and NdeI the sequence was introduced into mGMK-TK30_T2A_eGFP_hGHpA to generate pSB1C3_001_mGMK-TK30_T2A_eGFP_1xlet7a_hGHpA (pZMB0638). By restriction digest of pZMB0638, pZMB0588 and pZMB0590 with SalI and SpeI and subsequent ligation, CMV_mGMK-TK30_T2A_eGFP1xlet7a_hGHpA and SUR_mGMK-TK30_T2A_eGFP_1xlet7a_hGHpA where generated. For AAV production all constructs where transferred into (pZMB0522_ITR_EXS_CMV_mVenus_hGHpA), which serves as a final destination plasmid. By this, pZMB639_ITR_EXS_CMV_Kozak_mGMK-TK30_T2A_eGFP1xlet7a_hGHpA and pZMB0640_ITR_EXS_SUR_ Kozak_mGMK-TK30_T2A_eGFP1xlet7a_hGHpA were created.

1 Supplementary Information Figures

1.1 SI Figure 1

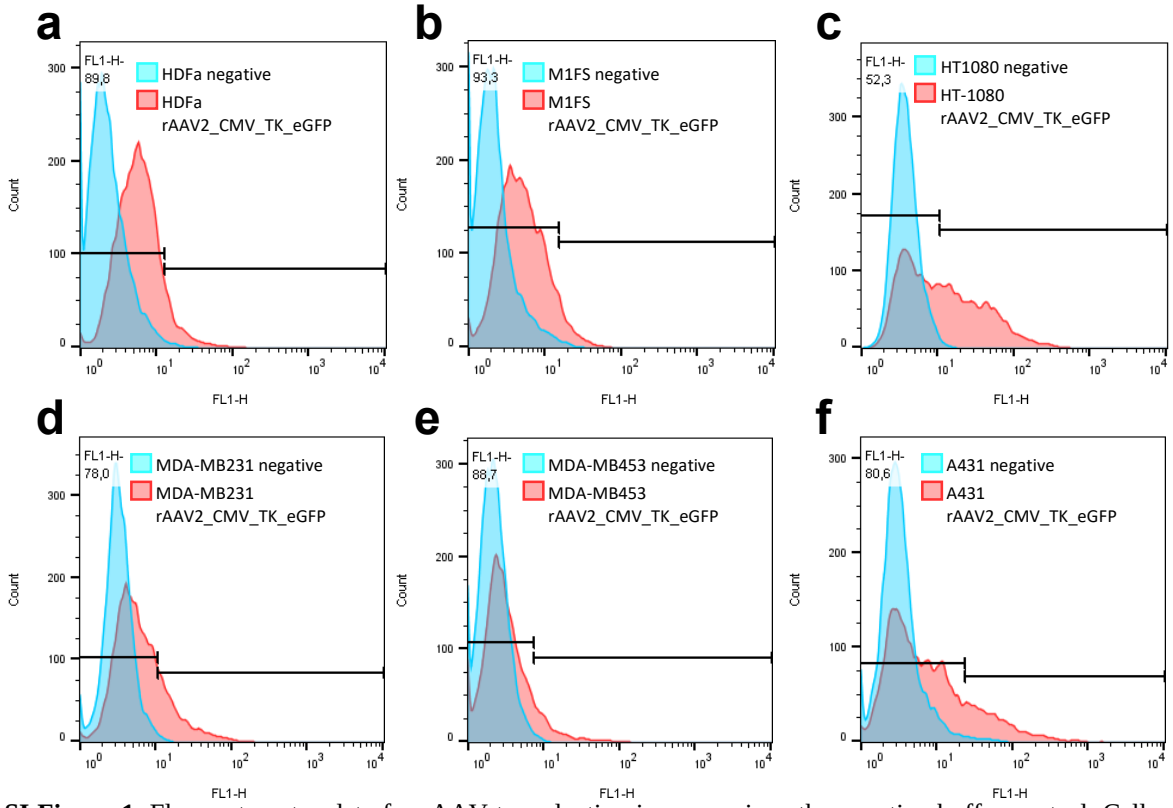

SI Figure 1. Flow cytometry data for rAAV transduction in comparison the negative buffer control. Cells were transduced with rAAV_CMV_Kozak_mGMK-TK30_T2A_eGFP_hGHpA at a MOI of 10,000 and analyzed via flow cytometry after incubation in biological duplicates. Data analysis was performed using FlowJo. A gate of 1% false positive cells was selected in the sample of the negative control. This gate is visualized in each diagram. Overlay histograms for the wild-type rAAV2 for **a)**, HT1080 **b)** HDFa **c)** M1FS **d)** MDA-MB453 **e)** MDA-MB231 **f)** A431 are shown.

1.2 SI Figure 2

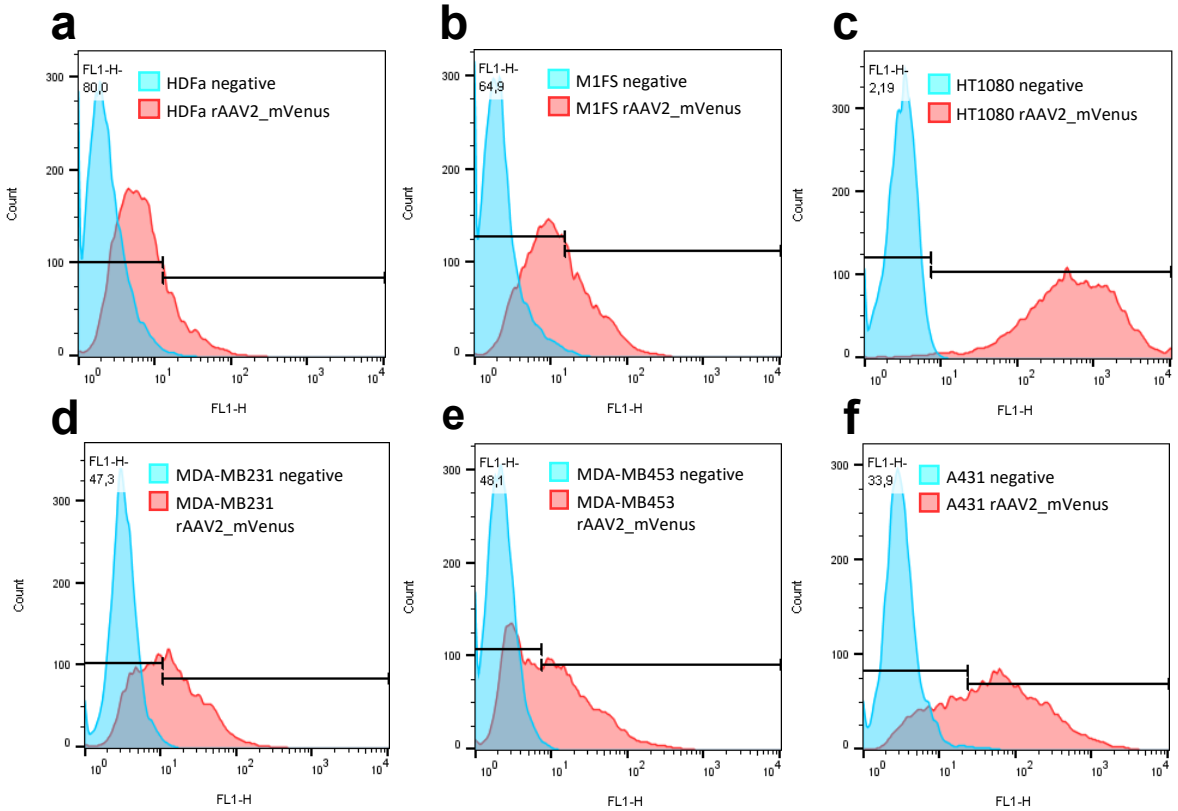

SI Figure 2. Flow cytometry data for rAAV variants in comparison the negative buffer control. Cells were transduced with rAAV2_mVenus at a MOI of 10,000 and analyzed via flow cytometry after incubation in biological duplicates. Data analysis was performed using FlowJo. A gate of 1% false positive cells was selected in the sample of the negative control. This gate is visualized in each diagram. Since the transduction efficiency was thus underestimated, the Overton algorhythm was used for the calculation in a subsequent step. Overlay histograms for the wild-type rAAV2 for **a)** HDFa **b)** M1FS **c)** HT1080 **d)** MDA-MB231 **e)** MDA-MB453 **f)** A431 are shown.

SI Table 1: Overview of plasmid vector constructs used as GOI for rAAV2 production

Plasmid name with description	Length
pZMB0522_ITR_EXS_CMV_mVenus_hGHpA AAV2 ITR flanking a CMV promoter expressing the fluorescent protein mVenus	4014 bp
pZMB0588_ITR_EXS_CMV_Kozak_mGMK-TK30_T2A_eGFP_hGHpA AAV2 ITR flanking a CMV promoter expressing the protein mGMK-TK30 and the fluorescent protein eGFP	5780 bp
pZMB0589_ITR_EXS_COX-2_Kozak_mGMK-TK30_T2A_eGFP_hGHpA AAV2 ITR flanking a COX-2 promoter expressing the protein mGMK-TK30 and the fluorescent protein eGFP	6027 bp
pZMB0590_ITR_EXS_SUR_Kozak_mGMK-TK30_T2A_eGFP_hGHpA AAV2 ITR flanking a SUR promoter expressing the protein mGMK-TK30 and the fluorescent protein eGFP	5647 bp
pZMB0591_ITR_EXS_CXCR-4_Kozak_mGMK-TK30_T2A_eGFP_hGHpA AAV2 ITR flanking a CXCR-4 promoter expressing the protein mGMK-TK30 and the fluorescent protein eGFP	6053 bp
pZMB0639_ITR_EXS_CMV_Kozak_mGMK-TK30_T2A_eGFP_1xlet7a_hGHpA AAV2 ITR flanking a CMV promoter expressing the protein mGMK-TK30 and the fluorescent protein eGFP with a 3'-let7a target sequence after the stop codon of the eGFP coding sequence	5801 bp
pZMB0640_ITR_EXS_SUR_Kozak_mGMK-TK30_T2A_eGFP_1xlet7a_hGHpA AAV2 ITR flanking a SUR promoter expressing the protein mGMK-TK30 and the fluorescent protein eGFP with a 3'-let7a target sequence after the stop codon of the eGFP coding sequence	5668 bp

BioMed Central

AAV production in suspension: Evaluation of different cell culture media and scale-up potential

Rebecca C Feiner[1], Kathrin Teschner[1], Irina Schierbaum[1], Julian Teschner[1], Kristian M Müller[1*]
[1] Cellular and Molecular Biotechnology, Bielefeld University, 33602 Bielefeld, Germany

*Email address of corresponding author: kristian@syntbio.net

Background
Recombinant adeno-associated virus (rAAV) approaches have an outstanding reputation in gene therapy and are evaluated for cancer therapy [1]. Advantages include long-term gene expression, targeting of dividing and non-dividing cells, and low immunogenicity. Established rAAV production utilizes triple transfection of adherent HEK 293 cells, which hardly meets product yield requirements for clinical applications. We transferred the AAV production system to HEK 293-F suspension cells. This process is scalable and uses serum-free media streamlining downstream procedures. After optimization of transfection efficiencies and shaker cultivations, we produced titers of 1×10^5 viral genomes per cell in a 2 l bioreactor.

Materials and methods
The suspension adapted HEK-FreeStyle 293-F cell line was used for the experiments in chemically defined animal component free media (HEK-TF, HEK-GM (Xell AG), Freestyle F17 (Thermo Fisher Scientific)). Samples for viable cell density and viabilities were taken daily and analyzed using an automated cell counting system (CEDEX, Roche Diagnostics). Transient transfection of 3×10^6 cells/ml was carried out with polyethylenimine Max in a 1:4 DNA-PEI ratio (w/w) with 2 µg DNA. Three plasmids (pGOI, pRepCap, pHelper) were applied in a molar 1:1:1 ratio (Figure 1 A). Pretests were performed in orbital shaking tube spin bioreactors. For scale-up, batch processes were carried out in 125 ml shake flasks as well as in 2 l stirred bioreactors at 30% air saturation and pH 7.1. Transfection efficiencies and rAAV production were quantified by flow cytometry using a GOI coding for a fluorescent protein and qPCR of genomic copies, respectively.

Results

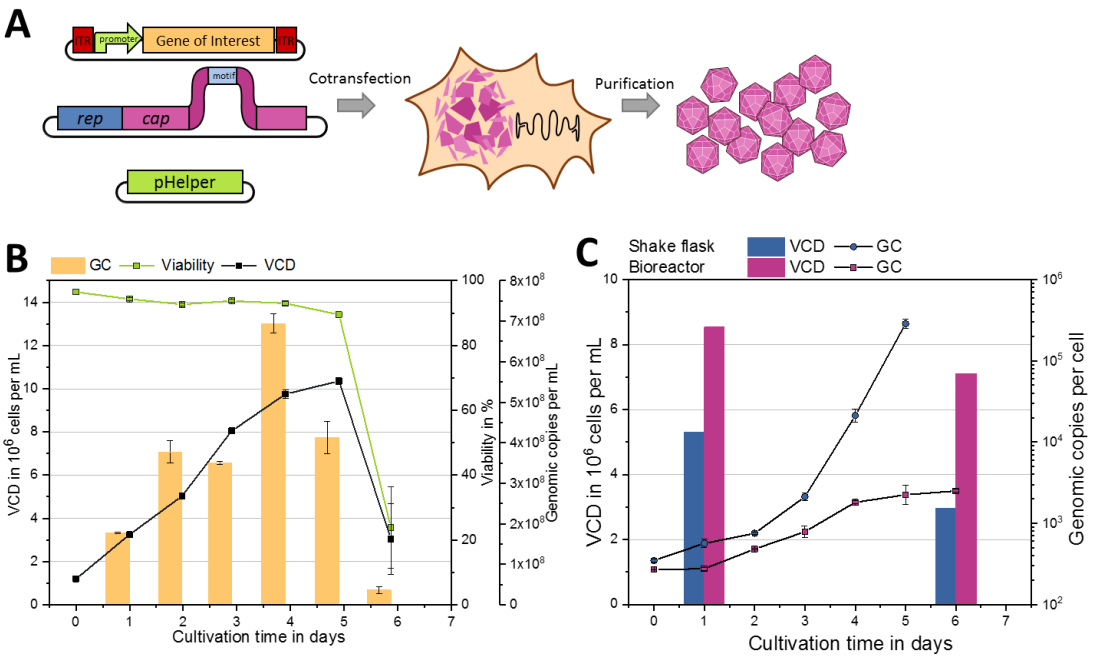

Figure 7: (A) Schematic overview of rAAV production in HEK293 cells with triple-transfection system. (B) Viable cell densities (VCD), viabilities and genomic copies per ml (GC) of a rAAV production with 293-F batch cultivations in shaker flasks. Genomic copies per ml refer to the titer determined in 1 ml culture volume. Error bars represent biological and technical duplicate measurements of samples. (C) Viable cell densities and genomic copies per cell of a rAAV production with 293-F batch cultivation in a 2 l bioreactor. For reasons of comparability between shaker and bioreactor data genomic copies are given per cell. Error bars represent technical duplicate measurements of samples.

By optimizing the DNA amount for transfection of 293-F cells more than 90 % of the cells were reproducibly transfected. Batch cultivations in shaker flasks revealed that rAAV were produced in the first 24-96 h after transfection. Figure 1 B shows viable cell densities and viabilities in relation to the genomic titer. Genomic titers were determined from raw cell extracts and up to 10^9 copies/ml were repetitively achievable. A decrease in viability marked the decline in genomic copies per ml showing that a prolongation of the process e.g. by addition of a feed would probably not increase yield. In a first scale-up, the rAAV production was transferred to a 2 l bioreactor (Figure 1 C). Transfection efficiencies in bioreactors of up to 55% were comparable to that obtained in a simultaneous shaker flask experiment. Transfection efficiencies were lower compared to prior experiments due to controlled conditions in the bioreactor. Nonetheless the titer with up to 1×10^5 genomic copies per cell was elevated compared to that of shaker flasks.

Conclusions

First experiments with 293-F cells in HEK TF medium showed promising results of transferring rAAV production from the adherent system to suspension. After improvement of transfections by the adjustment of DNA amounts in small scale experiments, AAV production was analyzed in shaker flasks. The batch process showed an expected increase in cell density with low variability between biological replicates (Figure 1 B). The genomic titer increased according to the viable cell density until day four where a sudden drop started. This observation was made for AAV productions in HEK-TF, HEK-GM and Freestyle F17 medium. For optimal yields, we assume that a slight decrease in viability marks the point in time for harvest. From optimized protocols, a batch process in a 2 l bioreactor was carried out. Interestingly the bioreactor cultivation resulted in lower overall viable cell densities but in higher genomic copies per cell compared to shaker flasks (Figure 1 C). These results are comparable to already published data for suspension cells [2]. Subsequent optimization of the bioreactor protocol will lead to further increase in rAAV yield.

Acknowledgements

The authors thank Xell AG, Bielefeld, for providing HEK serum-free media (HEK GM and HEK TF) and for fruitful discussions.

References

1. Hagen S, Baumann T, Wagner HJ, Morath V, Kaufmann B, Fischer A, et al. **Modular adeno-associated virus (rAAV) vectors used for cellular virus-directed enzyme prodrug therapy.** *Sci Rep*. 2014;**4**:3759.

2. Grieger JC, Soltys SM, Samulski RJ. **Production of Recombinant Adeno-associated Virus Vectors Using Suspension HEK293 Cells and Continuous Harvest of Vector From the Culture Media for GMP FIX and FLT1 Clinical Vector.** *Mol Ther*. 2016;**24**:287–97.